Ecological effects of turbidity variations in and around dredging areas in the Port of Tauranga

A thesis

submitted in fulfilment

of the requirements for the degree

of

Doctor of Philosophy in Earth Science

at

The University of Waikato

by

MARIANA COPPEDE CUSSIOLI

THE UNIVERSITY OF
WAIKATO
Te Whare Wānanga o Waikato

2018

ABSTRACT

Turbidity is the scattering of light in water bodies and is an important measurement for assessing water quality in coastal systems. Suspended particles in the water column can greatly impact on light penetration and measured turbidity levels. These suspended particles can originate from a range of natural and anthropogenic sources. This can include land use changes and soil erosion from surrounding catchment areas as well as resuspension from storms and dredging activities along coastlines. Although increased turbidity has the potential to affect coastal ecosystems, the interactions of different drivers have been poorly investigated. The objective of this study was to understand the sources, patterns and potential impacts of increased turbidity in a barrier-enclosed shallow lagoon. The study area, Tauranga Harbour (New Zealand) is a system affected by multiple stressors such as urban developments, industry, forestry, agricultural land use and a port facility. The Port of Tauranga is the largest export port in New Zealand and carries out regular maintenance dredging in the shipping channels. In this thesis, I focused on the effects of increased turbidity caused by the plumes generated during dredging activities and assessed the significance of these turbidity levels relative to background sediment inputs. The main body of this thesis covers three main areas: (1) the effects of turbidity on light attenuation (both light quantity and quality), (2) physiological response of sensitive species (*Paphies australis*) to increased turbidity, and (3) monitoring of dredging activity and plume footprints.

Benthic plants such as seagrasses depend on light availability, which is an important controlling factor for primary production and ecological health. To determine the drivers modulating the light attenuation coefficient K_d(PAR) in the harbour, I carried out low-frequency (bi-monthly) measurements of light irradiance, suspended sediment concentration (TSS), chlorophyll-a and coloured dissolved organic matter (CDOM). I also measured light irradiance before and after dredging activities. Using these measurements in a multiple regression analysis allowed the main contributor to light attenuation in the harbour to be determined. Correlating the light attenuation coefficients from field measurements to turbidity levels recorded by

turbidity sensors, I derived a regression model whereby turbidity data can be used as a proxy to estimate K_d(PAR). The turbidity records were collected by an array of six high-frequency sensors, deployed by the Port of Tauranga, which have been operating for approximately 3 years. The K_d(PAR) dataset derived from the turbidity measurements allowed the effect of storms and other relevant events such as dredging on light conditions to be assessed. The estimates of K_d(PAR) levels using this high-frequency dataset were considerably higher than those from the low-frequency dataset. Using these more representative K_d(PAR) values, I calculated thresholds of turbidity based on light requirements of New Zealand seagrass species, *Zostera muelleri*.

The influence of suspended material in the water column and its effect on light quality can largely depend on its origins (i.e. marine sources, such as dredging or terrestrial material from surrounding catchments). Terrestrial sediments usually differ in colour from marine sediments. Therefore, I investigated how different sediment colours (orange, grey and white), which were from different origins, affected underwater light quality. Results from a previous experiment using a modified water-holding tank and new spectrophotometer measurements showed that terrestrial based orange sediments changed the light quality more and filtered an exclusive range of wavelengths. The resultant wavelengths available were shown to be less effective for photosynthesis of some species, such as seagrasses. Among the sediments from marine sources, white sediments attenuated light more effectively compared to grey sediments; however, the spectral distribution of light was not modified by changes in suspended sediment concentration.

Based on the range of turbidity experienced in estuarine waters in New Zealand, considering both background values and maintenance dredging events, I tested six treatments containing different TSS on the bivalve *Paphies australis* (pipi). The aim was to predict the short-term effects of increased TSS on the feeding behaviour of pipis and to model these responses to estimate threshold values. Pipis, like other species of bivalves, responded to increased sediment concentrations by using adaptive mechanisms, such as reduction in clearance rates and productions of pseudofaeces. These mechanisms showed efficiencies in increasing the quality of

food ingested by pipis and thus regulating their energy acquisition in high turbidity treatments. However, above a threshold, responses in feeding rates indicated limitations of particle selection mechanisms. This suggests that further increases in sediment concentration could potentially constrain food acquisition and reduce pipi biomass. By including several feeding and digestion rates that have not been previously measured in pipis, this study contributes to modelling energetics of bivalves and in setting environmental limits for human activities in estuaries and harbours.

With a clearer understanding of the effect of TSS on light conditions and pipi condition, I then determined the spatial and temporal footprint of the dredging plume. To do this, I monitored the 2014 maintenance dredging in Tauranga Harbour and used a process-based numerical modelling system (Delft3D) to simulate dredging plumes. To acquire observational data in the field, a boat-mounted acoustic Doppler current profiler (ADCP) recorded backscatter signals. These were converted to suspended sediment concentrations (TSS) using calibrations developed with water samples. The ADCP transects were carried out before, during, and after dredging within the direct dredging area and along the plume. These transects provided information about plume development with time and distance from the dredging area and were used in the model calibration and validation. Based on the length and width of plume footprints, I proposed the use of an index of plume symmetry to define vulnerability zones around dredging areas. The index showed the main deposition paths and how dredging location affected the plume footprint. The primary and secondary axis lengths were used to define areas of vulnerability, which were then related to sensitive groups of species in the harbour. From ADCP transects and model results, TSS in plumes and its quick dissipation time characterized the maintenance dredging plumes as having a low impact on the two species that were identified as vulnerable to dredging in Tauranga Harbour: seagrass *Z. muelleri* and bivalve *P. Australis* (pipi). The maximum sediment deposition from dredging was restricted directly within the dredging areas. The thickness of deposits under plumes that might have reached seagrass meadows were below thresholds that were likely to impact growth rates of *Z.*

muelleri. However, plumes from terrestrial sources, due to its colour, can have a broader effect on seagrass photosynthesis compared with resuspended marine sediments.

This thesis attempts to provide a comprehensive understanding of turbidity variations and the associated ecological effects. It presents a number of important innovations in the field, including: (1) the development of a relationship between underwater light attenuation coefficients and turbidity; (2) the modelling of feeding and digestion rates of pipis, which have not been previously tested; (3) the development of a 'plume symmetry' index, and (4) the response of underwater light quality to sediment concentration and colour. It is recommended that future research adopts a greater and more regular sampling frequency in light and ecological measurements across coastal regions to better assess the interactions between natural and human induced changes.

ACKNOWLEDGEMENTS

TABLE OF CONTENTS

LIST OF FIGURES

LIST OF TABLES

CHAPTER 1

GENERAL INTRODUCTION

1.1 BACKGROUND

Turbidity is a key measurement for assessing water quality. It is a relative measurement of the scattering of light by particles in a liquid, which gives a "cloudy" appearance to the water (Kirk, 2011). The particles can originate from several sources (Figure 1.1). In the open ocean, particles are mainly of autochthone origin such as of phytoplankton (Durand and Olson, 1996). In coastal areas, the main source of particles is the erosion of soil from land, which is transported to water bodies, such as lakes, rivers and coastal areas, by wind, rain and storm runoff (Komar, 1996). In these environments, the influence of humans on turbidity becomes more apparent. Human activities such as mining, construction, forestry and agriculture can disturb the land, causing erosion or generating residues that can lead to high inputs of sediment in water bodies (Syvitski et al., 2005). Also, highly urbanized areas prevent water absorption by paved surfaces, leading to excess runoff that will carry excess particles (Brabec et al., 2002).

Estuaries naturally have a wide-range of variability in turbidity levels which depend on tidal currents and waves, surrounding land use, seasonal patterns associated with the rainfall regime, and large time-scale oscillations (e.g. El Niño) (Orpin et al., 2004). Estuaries worldwide are experiencing reduced water quality, caused by increasing sediment concentrations (Thrush et al., 2004). The changes are caused by increases in the frequency of storms and extreme weather events (Robins et al., 2016; Sheahan et al., 2013; Whitehead et al., 2009), human population growth and excessive changes in the catchment land use (GESAMP, 1990). Furthermore, some anthropogenic activities such as dredging are particularly effective at raising the levels of turbidity in coastal areas (Van Maren et al., 2015). Dredging activity is needed to maintain and deepen shipping lanes and navigation channels. A dredger can increase turbidity by disturbing sediments on

the seabed and by allowing overflow of surplus water on the surface. Whereas maintenance dredging programs are carried more often, capital dredging can have major impacts compared with maintenance dredging due to their larger time and spatial scales (EPA, 2011).

The increased concentrations of suspended particles in the water can impact on a number of ecosystem functions. The reduction in visual clarity can often affect detection of prey by fishes (Richmond et al., 2004) and decrease the light available for photosynthesis of submerged aquatic plants. This has ecosystem scale knock on effects by reducing primary productivity and impairing the flow of energy through the food web (Pauly and Christensen, 1995). In this context, a group of marine organisms that is sensitive to changes in water quality is seagrass, with its productivity being very dependent on light transmission through the water column (Dennison, 1987). Seagrasses provide habitat for a range of organisms, including shellfish, and play an import role in nutrient cycling and carbon sequestration. Nutrient cycling within seagrass meadows has been valued at around $2 trillion per year (Barbier, et al., 2011; Eyre and Ferguson, 2002; Fourqurean et al., 2012; Ruiz-Frau et al., 2017; Waycott et al., 2009).

High turbidity levels will also affect suspension feeders, clogging feeding structures (Newcombe and MacDonald, 1991). This reduces feeding activity and inhibits growth (Bricelj and Malouf, 1984; Bricelj et al., 1984). The sediment, once deposited, can accumulate on the seabed, smothering organisms, affecting burrowing activity (Cummings and Thrush, 2004; Schaffner et al., 2001), and altering the biogeochemistry of sediments originally present in the bottom (Woodin et al., 2012). Suspension-feeding bivalves are a key component in the benthic-pelagic coupling by removing particles from the water, thus increasing light availability for effective photosynthesis of aquatic plants (Newell, 2004; Newell and Koch, 2004) and contributing to fluxes of bio-deposits (Dame 1993).

Therefore, an understanding of patterns of natural and human-induced turbidity variation is of primary importance in managing suspended sediment concentrations to stay below acceptable thresholds based on species responses and detrimental effects. To understand those patterns, a range of techniques can

2

be used, such as field measurements and numerical modelling. Field measurements provide valuable information especially when instruments can be deployed for long-term field surveys. However, even when long datasets are available, the measurements only represent the time when they were collected and only a point or a small area. To fill spatial and temporal gaps, a numerical model can offer additional information and the possibility of isolating and quantifying the significance of different forcing conditions (Flaim, 2008; Flaim, 2012). For example, planning dredging operations could be accomplished through numerical modelling because each modelled scenario can reflect a specific dredging event. Multiple scenarios can be added to establish the combination of factors that will minimize the magnitude of turbidity and maximize the speed at which the dredging project is conducted (Clarke and Wilber, 2008).

The motivation for this work was based on two main factors: (1) the constant need for dredging in ports and harbours worldwide and its role as a potential source for elevated turbidity and (2) the necessity of a multidisciplinary approach to understanding the effects of elevated turbidity, focusing on the environmental management. The study area, Tauranga Harbour, is surrounded by various man-related influences, such as those cited above: urbanization, forestry, agriculture, etc., including port activities from the largest export port in New Zealand. Dredging at the port started in 1968. Maintenance dredging has been regularly carried out approximately every two years since 1992 (Sinner et al., 2011) and is currently carried out annually. In addition, the port recently carried out a capital dredging to accommodate larger ships to improve the country's economy (Port of Tauranga, 2013). Due to the dredging activities in the area, turbidity variations have been monitored to ensure that stressors stay below thresholds of adverse effects on the sensitive species around the area, such as the seagrass *Zostera muelleri* and the shellfish *Paphies australis* (pipi). Here, I propose the use of these turbidity datasets as a proxy to environmental indicators, to provide recommendations on acceptable levels of suspended material during dredging.
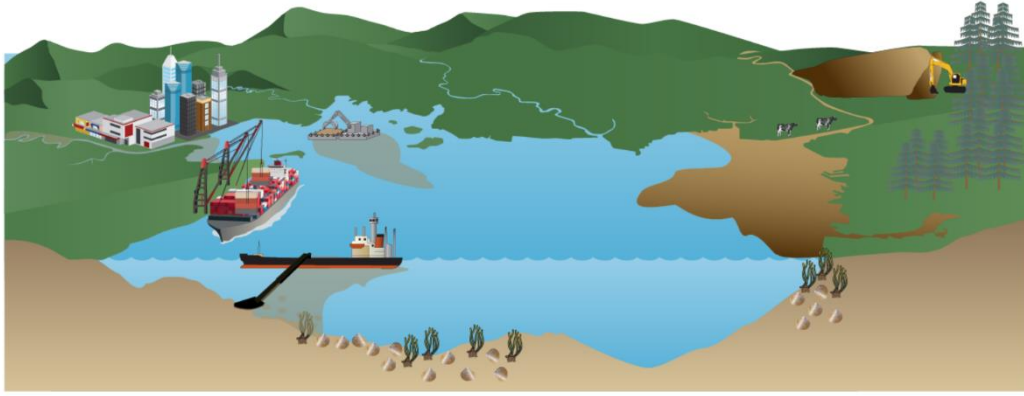
Figure 1.1: Conceptual diagram of potential sources of sediment plumes in Tauranga Harbour (e.g. dredging activities, urban land use, port activities, forestry, agriculture, and catchment land management) and sensitive species in the area (seagrass and shellfish bivalves).

1.2 QUESTIONS/AIMS

The over-arching objective of this thesis is to study the sources, patterns, and impacts of increased turbidity, in a barrier-enclosed shallow lagoon (Tauranga Harbour, NZ). This will be accomplished through (1) turbidity and light measurements, (2) manipulative experiments on the physiological response of species that are susceptible to water quality changes in this lagoon, (3) monitoring dredging activity, and (4) modelling dredging plume dynamics in the area.

1.3 THESIS OUTLINE

The first chapter of this thesis (Chapter 1) contains a general introduction providing the background for the present study. The core of this thesis comprises four research chapters (Chapter 2, 3, 4 and 5), which were written as papers for peer-reviewed publication. In addition to those chapters, the thesis contains a general discussion and conclusion (Chapter 5). A description of each chapter follows. A table of definitions of the key terms used in this thesis and their description is presented below (Table 1.1). A Venn diagram also explains the relationship between chapters in the thesis' context (Figure 1.2).

In Chapter 2, I assessed the annual variation in light irradiance, suspended particulate matter, chlorophyll-a and coloured dissolved organic matter (CDOM) in

Tauranga Harbour, which is subjected to dredging activity. The data were used to determine the drivers modulating the light attenuation coefficient, $K_d(PAR)$ in the harbour. Using a data set comprised of multiple turbidity sensors deployed in the shipping channels of Tauranga Harbour (about three years of high resolution data), and the low-frequency light measurements (bi-monthly), I derive a regression model from which we show that turbidity data can be used as a proxy to estimate $K_d(PAR)$. Using the regression model and values from literature, I recommend turbidity thresholds that would ensure that seagrass obtains sufficient light requirements for photosynthesis. Analysis of the high-resolution turbidity dataset is presented in Appendix A. Extra light and turbidity measurements are presented in Appendix B, as part of a deployment carried out for three weeks in one of the Port's beacon. Results from a pilot fieldwork carried out for this chapter were presented at the New Zealand Costal Society Conference, in Raglan (2014). Part of this chapter's data analysis and writing was carried out during a 3-month research stay at the Marine Botany Group, University of Bremen, Germany, under the supervision of Dr. Kai Bischof. The research stay was part of the INTERCOAST[1] collaboration.

The objectives of Chapter 3 were to (1) assess the effect of increased turbidity on the performance of a key species in the study area, *Paphies australis*, commonly known as pipi; and (2) to model those responses to estimate thresholds of impact to changes in estuarine suspended sediment concentrations. To accomplish this, a physiological laboratory experiment was designed using flow-through chambers and six treatments of target concentrations based on turbidity levels that occur in the area, both naturally and dredging-related (Chapter 2 and Chapter 4). The experiment included several feeding and digestion rates measurements. The results and main findings of this chapter were presented at the INTERCOAST Workshop (2017), in Bremen, Germany.

Chapter 4 covers several aspects of a maintenance dredging event in Tauranga Harbour, from sediment transport to environmental management. We tracked

---

[1] The INTERCOAST (Integrated Coastal Zone and Shelf-Sea Research) Research Training Group is a collaboration between the University of Bremen, Germany, and the University of Waikato, New Zealand, composed of international scientists with an interdisciplinary approach in the fields of marine geosciences and biology, social sciences and law. The research projects are of geoscientific, socio-economic, and legal interest.

dredging plumes using a combination of field monitoring and numerical modelling and described their development with time and distance from the dredged area. The plume footprint was used to define vulnerability zones and results were compared with thresholds for impacts for sensitive species of seagrass (Chapter 2) and shellfish (Chapter 3). Results from two monitored dredging plumes were presented at the Australasian Ports and Harbours Conference (2015) and published in their peer-reviewed proceedings (Appendix G). A modified version of this paper was published in the New Zealand Coastal Society Magazine, Coastal News (Issue 62, 2016, Appendix H). Those results were also presented at the INTERCOAST Workshop (2015), in Bremen, Germany, and at the INTERCOAST Workshop (2016), in Tauranga, NZ.

In Chapter 5, I investigated the changes in light quality (spectrum) in response to increased suspended sediment concentration of different colours (grey, white and orange), associated with their origin (marine or terrestrial). Terrestrial sediments are usually orange and marine sediments have a grey hue. They can generate highly visible plumes, especially after storms and dredging events, altering the underwater light regime and thus affecting the conditions needed for effective photosynthesis. This chapter includes results from a laboratory experiment I carried out during the stay at the Marine Botany Group, University of Bremen; and it also includes results from an experiment carried out by a former PhD candidate at the above cited department (Dr. Dorothea Kohlmeier), whom was also part of the INTERCOAST group.

Finally, Chapter 6 presents a summary of main findings and conclusions of this thesis. Informative maps of vulnerable areas in the harbour and suggestions for future work are presented.

Table 1.1: Definitions of key terms used in this thesis.

Term	Definition
Turbidity	Relative measurement of the scattering of light by particles in a liquid. It is usually used as a proxy for suspended sediment concentration and it is dependent on particle size and shape. The term is used here also to describe the concentration of suspended particles and its effects.
SSC	Suspended sediment concentration. The total dry weight of sediment present in a known volume of filtered water. It includes both inorganic and organic particles, unless specified in the text.
SPM	Suspended particulate matter, as described above for SSC. SSC and SPM are interchangeably used throughout the thesis.
Visual clarity	The distance an observer can see through the water.
Light penetration	The amount of light that reaches a certain depth and it is available for photosynthesis.
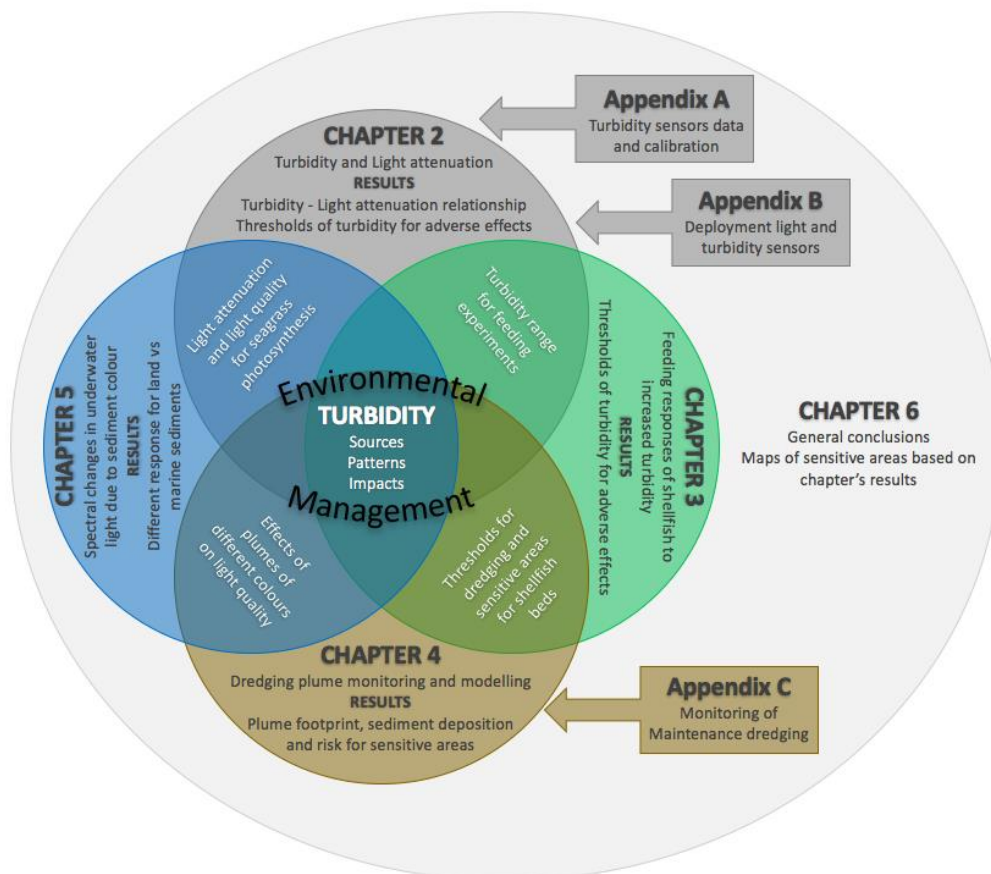
Figure 1.2: Venn diagram of associations between chapters.

CHAPTER 2

MODULATION OF PHOTOSYNTHETICALLY ACTIVE RADIATION (PAR) IN A WELL-FLUSHED CHANNELIZED TEMPERATE ESTUARY, TAURANGA HARBOUR, NEW ZEALAND: IMPLICATIONS FOR SEAGRASS GROWTH AND DREDGING

Mariana Coppede Cussioli[1], Karin R. Bryan[1], Conrad A. Pilditch[1], Willem P. de Lange[1], Kai Bischof[2] (submitted to *Ocean and Coastal Management* – status: in review)

1. School of Science, University of Waikato, Hamilton 3240, New Zealand
2. Marine Botany, University of Bremen, Leobener Str. NW2, 28359 Bremen, Germany

CONTRIBUTION OF AUTHORS:

ABSTRACT

Benthic plants such as seagrasses rely on light availability, which is affected by turbidity. Elevated turbidity inside habitats such as estuaries is governed by the recent history of natural events and human activities. To determine the drivers modulating the light attenuation coefficient, K_d(PAR), we assessed the annual variation in irradiance, suspended particulate matter, chlorophyll-a and coloured dissolved organic matter (CDOM) using measurements from a barrier-enclosed estuary in New Zealand, which is subjected to dredging activity. We derive a regression model from which we show that turbidity data can be used as a proxy to estimate K_d(PAR). K_d(PAR) calculated from light measurements ranged from 0.16 m^{-1} to 0.98 m^{-1} with overall average of 0.40 m^{-1}; post-dredging attenuation coefficients did not show a significant increase compared with background levels, which is consistent with continuous measurements of turbidity taken around the harbour dredging sites. Variations in K_d(PAR) were caused mostly by suspended particulate matter (explaining 38% to 50% of variance), chlorophyll-a (explaining 25% to 33%) and to a less extent by colour (CDOM explained 10% to 28%). Benthic light availability in the intertidal zone when immersed ranged from 28% to 76% of surface irradiance and so results indicate that even under high sediment load, light conditions in the intertidal zone are not limiting seagrass photosynthesis but may influence growth in deeper channels. Results demonstrate the critical importance in including storm events in monitoring to develop robust limits on light attenuation for management.

2.1 INTRODUCTION

Suspended particles make estuary waters turbid and can severely limit light penetration in shallow waters (Dennison et al., 1993), which is of significance as a limiting factor for photosynthesis (Kirk, 1977; Dennison, 1987), including aquatic plants (Lee and Rast, 1997) such as seagrasses. Incident light in water is attenuated through reflection, refraction, absorption, and scattering by the four constituents that determine the optical properties of the water body: the water itself, yellow pigments, organic particles and inorganic particulate matter (Davies-Colley and Smith, 2001; Dennison et al., 1993; Kirk, 2011; Vant, 1990). Among the constituents described above, the main contributor to light attenuation in estuaries is suspended material which is mainly composed of plankton and particles derived from soil erosion (Kirk, 1977; Vant, 1990). Yellow pigments, also known as coloured dissolved organic matter (CDOM), are products resulting from plant breakdown (Kirk, 1977) which affect the availability of blue light for photosynthesis (Kirk, 1976; Tian et al., 1994), and are usually a minor contributor to light attenuation in estuaries (Vant, 1990).

Estuaries naturally have wide-ranging variability in turbidity which depends on tide and wave generated currents (Green, 2006), land use in the surrounding areas, seasonal patterns associated with the rainfall regime, and large time-scale oscillations (e.g. El Niño). However, estuaries around the world are experiencing an increase in suspended sediment concentration (Thrush et al., 2004) because of population growth, catchment changes, agriculture, deforestation, marine farms, and dredging, all resulting in decreasing light penetration (GESAMP, 1990; Dennison et al., 1993; Gibbs and Hewitt, 2004). Predicting the potential impact of human induced turbidity and associated disturbances on marine ecosystem requires an understanding of the natural levels of turbidity i.e., distinguish anthropogenic disturbances from natural dynamics. A complete study of its spatial and temporal patterns is fundamental to ensure that levels are not been exceeded by potential turbidity sources, which will impact on marine fauna and flora through direct physical effects and indirectly through changes to light availability

(Erftemeijer and Lewis, 2006; James et al., 2009; Jones, 2008; Nightingale and Simenstad, 2001; Park, 1999).

In this context, a group of benthic primary producers that is considered as high-light adapted and thus sensitive to changes in water quality is seagrass (Duarte, 1991). Among estuaries worldwide, the decline in seagrass is correlated to reduced water quality (Erftemeijer and Lewis, 2006; Green and Short, 2003; Orth et al., 2006; Short et al., 2011; Short et al., 2014; Waycott et al., 2009). In New Zealand, seagrass has previously experienced a period of decline, from 1959 to 1996 (Matheson and Schwarz, 2007; Park, 1999), which is believed to be caused by the increase in turbidity levels related to human activities (Park, 1999); a recent study, however, shows stabilization of seagrass beds from 1996 to 2011 (Park, 2016). Although long-term elevations in turbidity can be detrimental to seagrass survival, short durations of elevated turbidity associated with dredging may have little impact on their physiology (Close et al., 2013; Nichols et al., 1990; Onuf, 1994); hence, the importance of detecting the duration of such events using continuous monitoring of turbidity. However, a long-term or high frequency dataset is not always available for turbidity analyses making it difficult to determine whether the impact is due to anthropogenic activities or only characterized by natural variations.

Recently, major ports in New Zealand, Australia, and Singapore, among others, have been developing management plans in relation to dredging effects through continuous turbidity monitoring (Bryan et al., 2014; Doorn-Groen, 2007; Environmetrics, 2007), seemingly a better alternative to low-frequency measurements which can be inconvenient due to ship traffic over sampling sites, short-term duration of turbidity plumes and poor weather conditions. The same improvements in turbidity monitoring strategy does not apply to light measurements because real-time high-frequency light measurements are not practical for long term monitoring water quality (Environmetrics, 2007). Therefore, the light data needed to detect relative changes in background in the long term are lacking. An alternative is to use turbidity as a proxy for other environmental indicators, such as light attenuation, since turbidity sensors are easier to install and

maintain relatively to light loggers. For this purpose, a relationship between NTU and K_d(PAR) is required.

There are few studies that establish a relationship between underwater light availability and turbidity needed to infer one from another, most of them focusing on the linear correlation between the two variables (Delvin et al., 2008; Hughes et al., 2015); although those models show a strong positive correlation between turbidity and K_d(PAR), they estimate average values rather than provide an upper limit with some certainty that K_d(PAR) or turbidity will not exceed a threshold (Environmetrics, 2007). Furthermore, until now, the conversion methods that exist for estuaries have been developed for a very limited range of conditions, with cases notably lacking for end members such as the volcanic catchments that characterise New Zealand's coast (Davis and Healy, 1993). This gap will be filled in this study using a data set, comprised of multiple turbidity sensors deployed in the shipping channels of Tauranga Harbour, one of the largest estuarine systems in New Zealand, providing about three years of high resolution data. In addition low-frequency in situ light and water constituents measurements were collected to determine the controls on light variation in a well-flushed barrier-enclosed estuarine lagoon in which ongoing dredging occurs. This nested sampling program allows us to assess the dominant forcing frequency, magnitude and duration of turbidity events.

Here we (1) assess the annual variation in light attenuation in an enclosed estuarine lagoon with a port facility surrounded by urban, industrial, forestry and agricultural land use and (2) determine relative contribution of water constituents to the light attenuation, in order to (3) establish a relationship between turbidity and light attenuation on which a turbidity-based management plan could be based, and, consequently, (4) set turbidity thresholds based on seagrass light requirements. Although our results are based around this case study, our methods are generally applicable, and specific results can be used for management and predictions for estuaries with catchments with similar geology and landuse practices. Moreover, methodologies for monitoring are often provided in unpublished reports, which hamper the design of robust programmes particular in

12

cases where funding is limited yet the greatest potential for optimising environmental outcomes exists.

2.2 METHODS

2.2.1 Study Area

Tauranga Harbour is an enclosed estuarine lagoon connected to the Pacific Ocean by a northern (not shown on Figure 2.1) and southern entrance, located on the east coast of New Zealand, comprising an area of about 200 km^2 (Park, 2004) (Figure 2.1). Intertidal flats separate the Harbour into two main areas, the northern and the southern basins. It is predominantly a shallow harbour, with an average depth at low tide of 3 m (Tay et al., 2012); the tides are semi-diurnal and have a tidal range of 1.62 m (spring) to 1.24 m (neap) (Heath, 1976). The harbour area is about 60% intertidal and the catchment covers an area of approximately 1,300 km^2, mainly characterized by agricultural land use (Park, 2004). The area receives multiple sources of sediment (Barker and Larcombe, 1976); the largest contributor of freshwater into the harbour is the Wairoa River, corresponding to 460 km^2 with an inflow of 17.6 m^3 s^{-1} (Park, 2004) and catchment sediment yields are 124 T y^{-1} km^{-2} (Matheson and Schwarz, 2007). The largest export port in New Zealand, the Port of Tauranga, is situated near the southern entrance of the Harbour. To maintain channel depths for navigation and increase its capacity to receive larger ships, the Port undertakes periodic dredging activities, during which there is an increased potential for elevated turbidity.
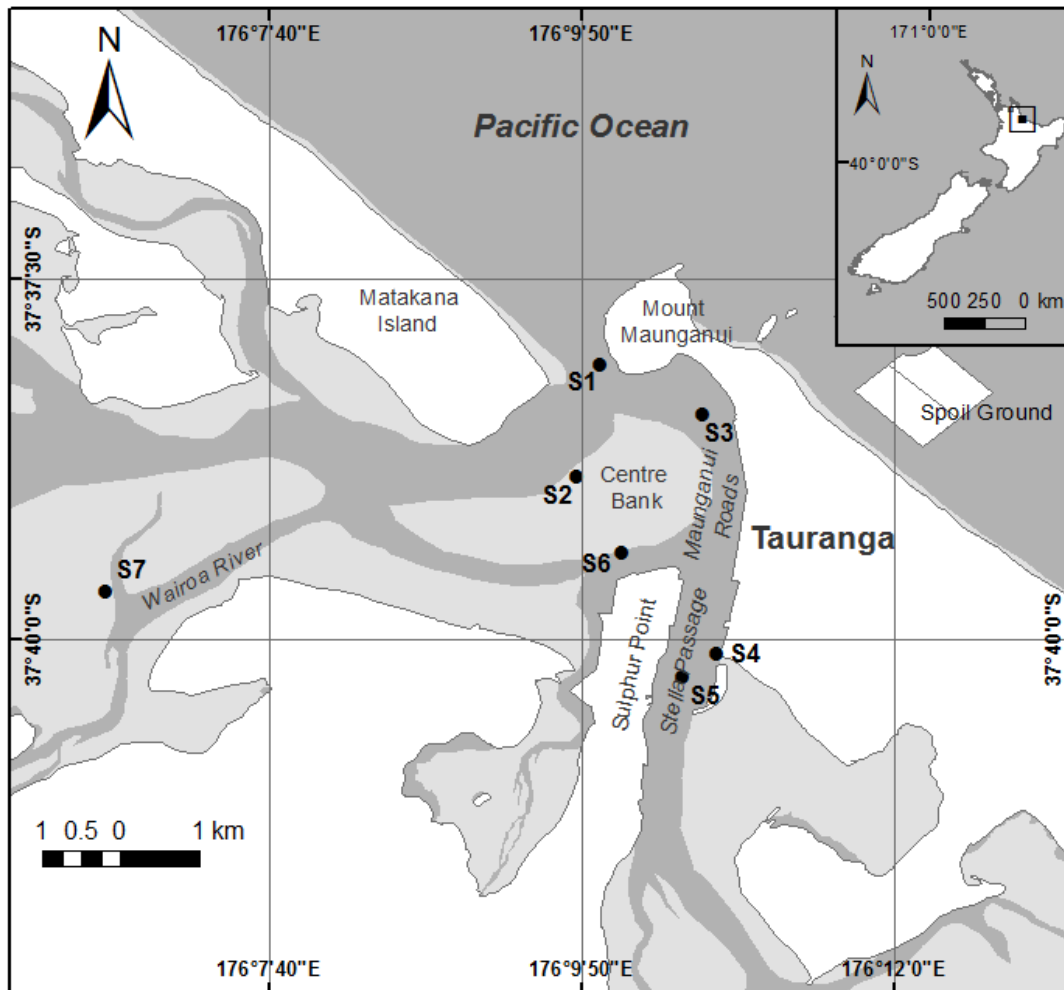
Figure 2.1: Study area and location of turbidity sensors (S1 to S6) and sampling sites (S1 – S7) (black dots). There was not a turbidity sensor deployed at S7. Light grey areas correspond to intertidal flats.

2.2.2 Field sampling and laboratory methods

To determine the drivers modulating the K_d(PAR), we used (1) bimonthly light measurements and water sampling, and (2) long-term turbidity records. Light measurements and water sampling were carried out approximately once every two months during 2014 to 2016; measurements were taken twice a day, at high and low tides, except for May 2014, and May and July 2015, when only measurements at high and low tide, respectively, could be carried out due to time constraints, and in March 2016, light measurements at low tide were not recorded due to technical problems (Table 2.4). Long-term turbidity data was recorded every minute by six turbidity sensors deployed by the Port of Tauranga at the southern harbour (sites

S1 to S6 - Figure 2.1). The dataset analysed in this study starts in January 2013 until late 2016 but sensors S3, S5, S2 and S4 were operational from January, October, November and December 2012, sensor S6 was operational from February 2013 and sensor S1 from January 2014.

To assess the variation in $K_d(PAR)$, a PAR sensor (LI-COR LI-192 Underwater Quantum Sensor) was lowered down from a boat at each of the six turbidity sensors sites (S1 to S6) and at a site in the Wairoa River (S7). Simultaneously, another PAR sensor (LI-COR LI-190R Quantum Sensor) measured changes in above water irradiance to correct data from shading effects of clouds. The light attenuation coefficient ($K_d(PAR)$, m^{-1}) was determined by fitting an exponential function (the Lambert-Beer equation) to the observations of PAR (Dennison, 1987; Dennison et al., 1993; Giesen et al., 1990; Kirk, 1977):

$$I = I_0 e^{-K_d(PAR)z}$$
Equation (1)

where I is the photosynthetically active radiation (PAR) measurement (µmol m^{-2} s^{-1}) at depth z (m), I_0 is the PAR measurement just below the water surface and z is the water depth (m). A total number of 88 profiles of PAR were fitted and the correlation coefficient in the regressions were high (average r^2 = 0.87).

Along with the light measurements, water samples were taken in duplicate at 1 m below surface for the determination of water constituents: chlorophyll-a concentrations (CHL, µg l^{-1}), suspended particulate matter (SPM, mg l^{-1}), and coloured dissolved organic matter (CDOM, m^{-1}). Water samples for SPM and CDOM determination were stored chilled in the dark immediately after sampling and filtered in less than 24 h after collection; CDOM analysis were carried out within 48 h after sampling. SPM was determined by filtering 1 L of water through pre-weighed 47 mm Whatman GF/C filters, which were dried at 105˚C for 18 hours and re-weighed. To determine the organic and inorganic content of samples, filters were combusted in a muffle furnace at 400˚C for 4 h and re-weighed; the weight loss corresponds to the weight of organic matter. Usually the organic content of samples was very low (<1%); therefore, SPM values considered in the analysis assume that samples were mainly composed of inorganic particles. CDOM was

determined following the method described in (Davies-Colley et al., 1993) which consisted of measuring the absorbance of water samples double-filtered using a Whatman GF/C followed by a 0.2 µm membrane filter. Samples were scanned from 250 to 800 nm with a resolution of 10 nm, using a double-beam spectrophotometer (Cary 100 Scan, Varian). The absorption coefficient of CDOM was calculated according to the formula:

$$g_{440} = \frac{2.303}{r}\left[D(440) - D(740)\frac{740}{440}\right]$$ Equation (2)

where D is absorbance, 440 is the wavelength proportional to CDOM concentrations, 740 is the IR wavelength used for scattering correction, r is the cuvette path length (0.01 m), and the constant 2.303 converts the logarithm with base 10 to the natural logarithm. For CHL determination, water samples were filtered onto 25 mm GF/C filters using a syringe immediately after water sampling and filters were stored frozen in the dark. Determination of CHL followed the standard procedures described in (Strickland and Parsons, 1972) with extraction in 90% buffered acetone and fluorescence signal converted into concentration.

To analyse the data recorded by the turbidity sensors (ANALITE NEP9500), spikes in the time series were removed using a de-spiking algorithm followed by manual removal; the data were then averaged using a 6-hour and a 2-week moving average. The spikes are usually caused by biofouling and periods of sensor cleaning and maintenance, which the Port carries out frequently, and are recognized as a sharp increase followed by a gap in the data. However, it is difficult to remove all the spikes in the records since natural turbidity events could be affected by the automatic removal. The long-term turbidity dataset will cover not only natural variations in turbidity but also variations caused by three dredging campaigns that occurred during the period here analysed: maintenance dredging in 2014 and 2015, and a capital dredging in 2015/2016.

To capture the short-term increases in turbidity related to dredging, we also carried out PAR profiles during maintenance dredging in the shipping channels of Tauranga Harbour, in October 2014 (Table 2.4), at Stella Passage, Sulphur Point,

Maunganui Roads, at the entrance, and at the dredging spoil ground location (all marked on Figure 2.1). More details regarding the dredging campaign and monitoring can be found in Cussioli et al. (2015).

In the laboratory, we calibrated an exemplar of the turbidity sensor the Port used in the deployments. The calibration procedure consisted of adding aliquots of known weight of sediment, from samples collected in the southern Tauranga Harbour, to a 40-liter bucket of distilled water. Sediment was kept in suspension by a stirrer, turbidity logged during 30 s and values averaged. Afterwards, water samples were collected for SPM analysis. Concentrations of sediment tested varied from 2 mg l^{-1} to approximately 200 mg l^{-1}. The slope and intercept (calibration coefficients) were 2.1041 and 0.1106, respectively with r^2 = 0.997.

2.2.3 Turbidity measurements and relationship K$_d$(PAR) - NTU

For the relationship between NTU and K$_d$(PAR), we followed the method described in Environmetrics (2007). The method is based on the joint probability distribution which describes the probabilistic distribution of a variable subject to the constraints imposed by other related variables. The bivariate normal distribution for NTU and K$_d$(PAR) is given by the equation below:

$$f_{X,Y}\big(x, y; \mu_x, \mu_y, \sigma_x^2, \sigma_y^2, \rho\big)$$

$$= \frac{1}{2\pi\sigma_x\sigma_y\sqrt{1-\rho^2}} \exp\left\{\frac{-1}{2(1-\rho^2)}\left[\left(\frac{x-\mu_x}{\sigma_x}\right)^2 \right.\right. \qquad \text{Equation (3)}$$

$$\left.\left. -2\rho\left(\frac{x-\mu_x}{\sigma_x}\right)\left(\frac{y-\mu_y}{\sigma_y}\right) + \left(\frac{y-\mu_y}{\sigma_y}\right)^2\right]\right\}$$

where X = turbidity (NTU), recorded by the sensors and Y = K$_d$(PAR), calculated using in situ light measurements. The conditional probability is given by the equation:

$$G_{Y|X}(t) = P[Y < \alpha | X < t] = \frac{\int_{-\infty}^{\alpha}\int_{-\infty}^{t} f_{X,Y}(x,y)\mathrm{d}x\,\mathrm{d}y}{F_X(t)} \qquad \text{Equation (4)}$$

where $F_X(t)$ is the cumulative distribution function of the marginal distribution for turbidity, α is a $K_d(PAR)$ value and t is a turbidity limit. We can solve the equation for some prescribed probability. This method is more suitable to our analysis than a simple fitted regression model because it provides an upper limit rather than an averaged value of NTU.

Using this relationship, we calculated: the most likely $K_d(PAR)$ to occur given a NTU value (obtained from the long-term turbidity time series), and the NTU thresholds relative to the $K_d(PAR)$ to meet 36% SI as a minimum light requirement for sustaining seagrass meadows of the species *Zostera muelleri* (Longstaff, 2003; Schwartz et al., 2006) which is the only species of seagrass in New Zealand (Turner and Schwarz, 2006).

2.2.4 Statistical Analysis

Multiple regression analysis was used to estimate the contribution of each one of the water constituents – SPM, CHL and CDOM – to the variability in the light attenuation coefficient $K_d(PAR)$. The constituents are additive (Kirk, 2011), expressed by $K_d(PAR) = K_{SPM} + K_{CHL} + K_{CDOM}$ (Equation 5). The analysis was carried out using MATLAB and the assumptions of independence of residuals, homoscedascity, multicollinearity, and normal distribution of residuals were tested beforehand.

All the results reported as seasons are averages of measurements/data pooled as: September, October and November (spring); December, January and February (summer); March, April and May (autumn); June, July and August (winter).

2.3 RESULTS

2.3.1 *In situ* spatial and temporal variation in $K_d(PAR)$

$K_d(PAR)$ calculated from our light measurements ranged from 0.16 m^{-1} to 0.98 m^{-1} with an overall (spatial and temporal) average ($\pm$ 1 SD) of 0.39 $\pm$ 0.15 m^{-1}. The

highest value of site-averaged $K_d(PAR)$ was at S5 and lowest average at S1 (Figure 2.2), resulting in a gradient with high values in the upper estuary decreasing towards the entrance of the harbour. S5 and S4 showed consistently higher coefficients (the high average values at S7 (0.41 ± 0.28 m^{-1}) result from one light profile in winter. Neglecting this anomaly, $K_d(PAR)$ had little seasonal variation, with 0.39 ± 0.14 m^{-1} in spring, 0.39 ± 0.08 m^{-1} in summer, and 0.38 ± 0.10 m^{-1} in autumn.
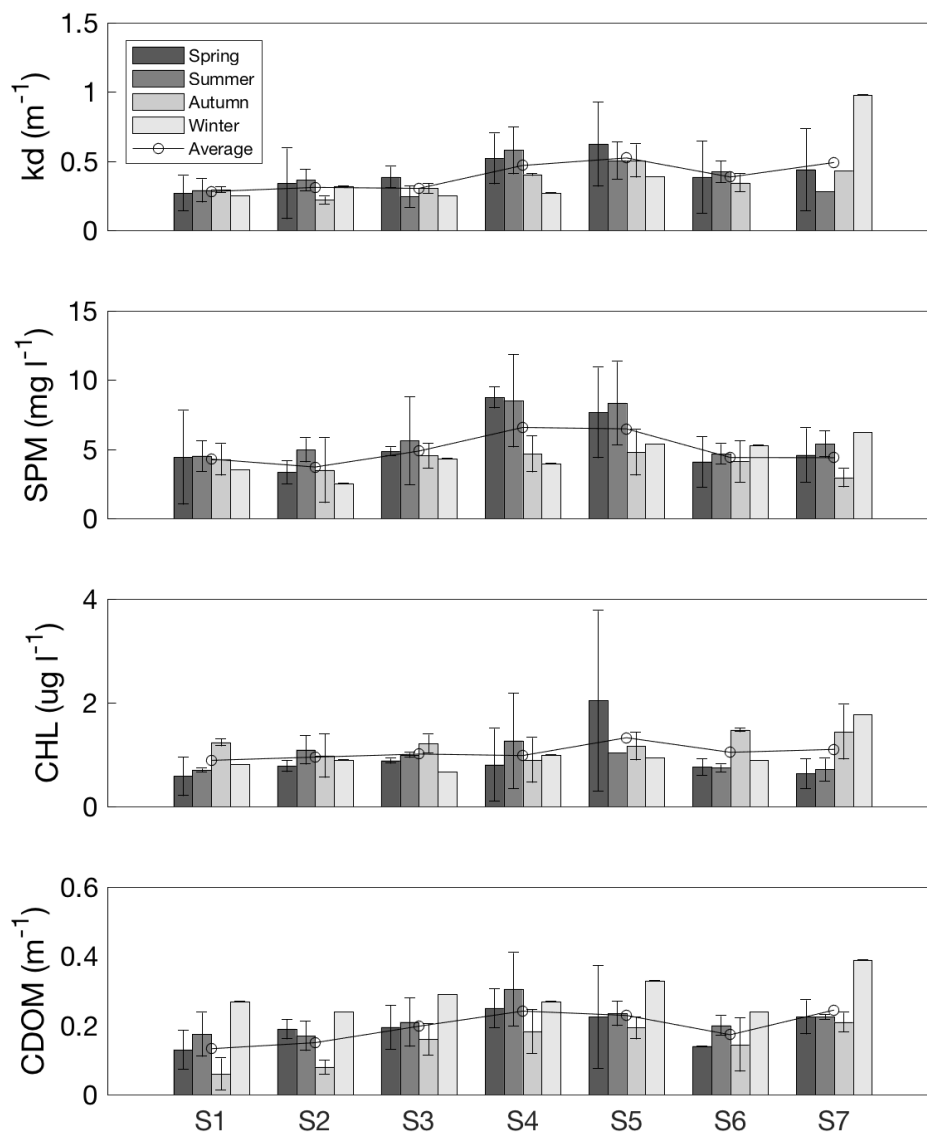
Figure 2.2: Seasonal variation of $K_d(PAR)$ and water constituents. Bars are the average data for each season (± 1 SD – thin bars) and thin black horizontal line is the seasonal average for each site. Season are calculated as averages carried out in the months: September, October and November (spring); December, January and February (summer); March, April and May (autumn); June, July and August (winter).

Graphs in Figure 2.3 compare measurements during high tide (HT) and low tide (LT). Maximum K_d(PAR) values (0.98 m^{-1}) occurred at LT at S7 in winter and minimum K_d(PAR) values (0.16 m^{-1}) occurred at HT at S2 in spring. The difference between averaged K_d(PAR) values for LT and HT was 0.12 ± 0.07 m^{-1}, and there were greater differences between HT and LT coefficients during spring and summer for most sites.
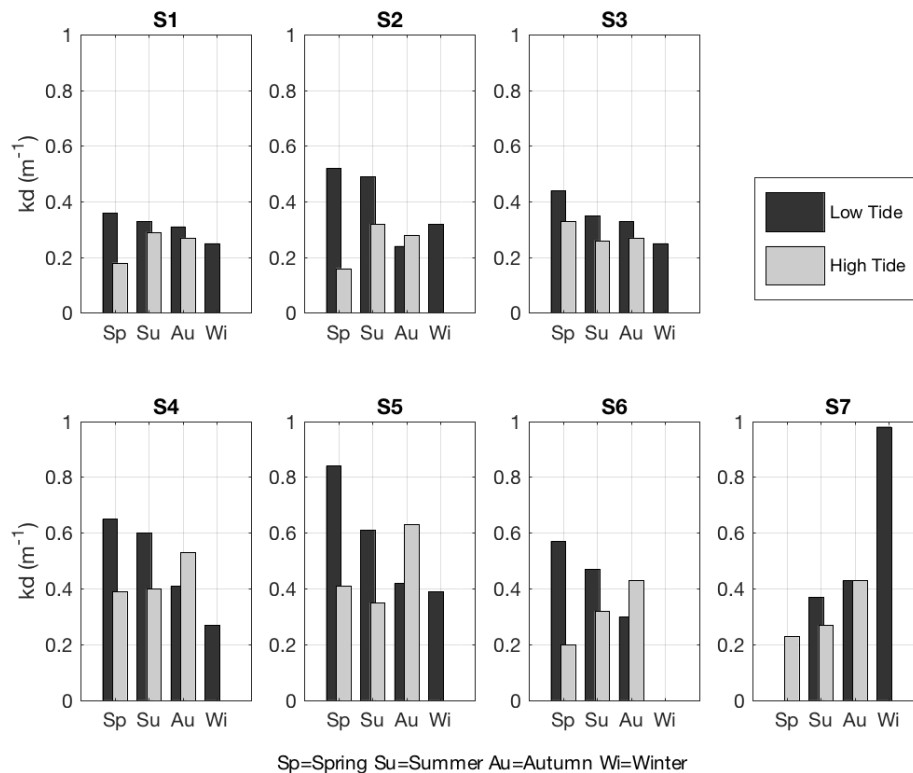
Figure 2.3: Average seasonal light attenuation coefficient (K_d(PAR)) at high and low tide for each site. Sp=spring, Su=summer, Au=autumn, and Wi=winter. Black shading refers to values for low tide and grey shading refers values for high tide.

During the 2014 maintenance dredging in the southern Tauranga harbour, our observations show ambient K_d(PAR) was higher in the Sulphur Point area, decreasing towards the entrance, and lower outside the harbour, at the spoil ground. After dredging, K_d(PAR) increased by approximately 0.1 m^{-1} (Table 2.4). This increase was most likely due to the dredging activity since most ambient and after dredging measurements were carried out during the same tidal state. The K_d(PAR) naturally increased from HT to LT and was greater than the increase in K_d(PAR) from

before to after dredging; on average, K_d(PAR) naturally increased 70% from HT to LT, whereas K_d(PAR) increased 46% during dredging.

2.3.2 Water constituents

We analysed the contribution of three main water constituents to the light attenuation: SPM, CHL and CDOM. SPM had an average over all measurements of 4.96 ± 2.04 mg l^{-1}, CHL of 1.04 ± 0.47 µg l^{-1} and CDOM of 0.19 ± 0.08 m^{-1} (Figure 2.2). Similar to K_d(PAR), constituents were higher in the upper harbour and lower near the entrance. Seasonally, SPM, CHL and CDOM had their maximum averages in summer, autumn and winter, respectively, and minimum SPM and CDOM averages in autumn, and in spring for CHL.

Results from the multiple regression analysis are shown in Table 2.1. Considering data from all sites resulted in relationship (1), which accounted for 60% of the variability in K_d(PAR) and all terms of the equation had p-value lower than 0.05 except for the intercept. Our results show that in general SPM contributed more than other constituents to the light attenuation. The dependence on CDOM is usually related to input from riverine waters containing relative higher proportion of degrading organic matter (Kirk, 2011). To test this hypothesis, we removed the site that is close to the river, S7, measurements from our multiple regression analysis that resulted in decreased % explained by CDOM and increased % explained by SPM. Relationship (2) had p-values greater than 0.05 for the intercept and CDOM terms.

Another potential source of yellow substances to the harbour is the logging area situated at Maunganui Wharf. The tannins from plants, especially the bark of the trees, are washed into the harbour waters during storms (Tian et al., 1994). The logging area is in the proximity of the S4 sensor, where we detected highest CDOM values on average (Figure 2.2 – bottom panel); removing S4 but retaining S7 resulted in relationship (3), with p-value for the intercept term greater than 0.05. Finally, relationship (4) resulted when both S4 and S7 data were removed from the analysis; in this case, p-values for the intercept and CDOM terms were greater than

0.05. New partitioning following relationship (3) show an increased contribution of CDOM whereas relationship (4) resulted in a similar partitioning of that for equation (2), with high % explained by SPM and low % explained by CDOM.

Table 2.1: Relationships derived from multiple regression analysis of light attenuation coefficient, $K_d(PAR)$ (m^{-1}), and the water constituents TPM $(mg\ l^{-1})$, CHL $(\mu g\ l^{-1})$, and CDOM (m^{-1}) considering (1) data from all sites, (2) excluding data from S7, (3) excluding data from S4, and (4) excluding data from both, S4 and S7. All equations were statistically significant (p-values << 0.01). Contribution of each water constituent (SPM, CHL and CDOM, in %) to $K_d(PAR)$, were calculated using average values.

Relationship	Adj-r^2	Partitioning (%)		
		SPM	CHL	CDOM
(1) $K_d(PAR) = 0.008 + 0.030$ SPM $+ 0.126$ CHL $+ 0.577$ CDOM	0.60	38	33	28
(2) $K_d(PAR) = 0.059 + 0.038$ SPM $+ 0.093$ CHL $+ 0.198$ CDOM	0.66	50	25	10
(3) $K_d(PAR) = -0.023 + 0.031$ SPM $+ 0.140$ CHL $+ 0.657$ CDOM	0.58	37	39	32
(4) $K_d(PAR) = 0.048 + 0.038$ SPM $+ 0.104$ CHL $+ 0.193$ CDOM	0.61	49	30	10

2.3.3 Establishing a relationship between $K_d(PAR)$ and turbidity

Given the importance of the suspended particles, and thus the turbidity, as a contributor to light attenuation in our observations, we used a conditional probabilistic approach to determine the light attenuation that would occur for the turbidity data recorded in each of the sensors S1 to S6.

The analysis of the 6-h moving average turbidity data showed that S4 had the highest turbidity, with a mean of 5.06 ± 2.66 NTU and S3 had the lowest turbidity, 2.93 ± 1.97 NTU (Figure 2.4 and Figure 2.5). Seventy-five percent of the values were below the 10 NTU level recommended by the ANZECC (2000) for south-east Australian estuaries, denoting general good water quality (Scholes, 2015). The highest average turbidity occurred in autumn, at S4, S5, S1 and S3 (Figure 2.6); S2 and S6 had highest turbidity in winter, and there was not an apparent seasonal trend at S6. Lowest average turbidity generally occurred in summer, except at S1, which lowest turbidity occurred in spring. Likewise, rainfall was highest in autumn and winter, and lowest during spring (Figure 2.7). Monthly mean turbidity at Site S4-S6 was correlated to monthly rainfall (r^2 ranged from 0.5 to 0.6). Spatial average

turbidity for the entire period and for periods of dredging, indicated in Figure 2.4 show that turbidity was 4 NTU for both periods analysed.
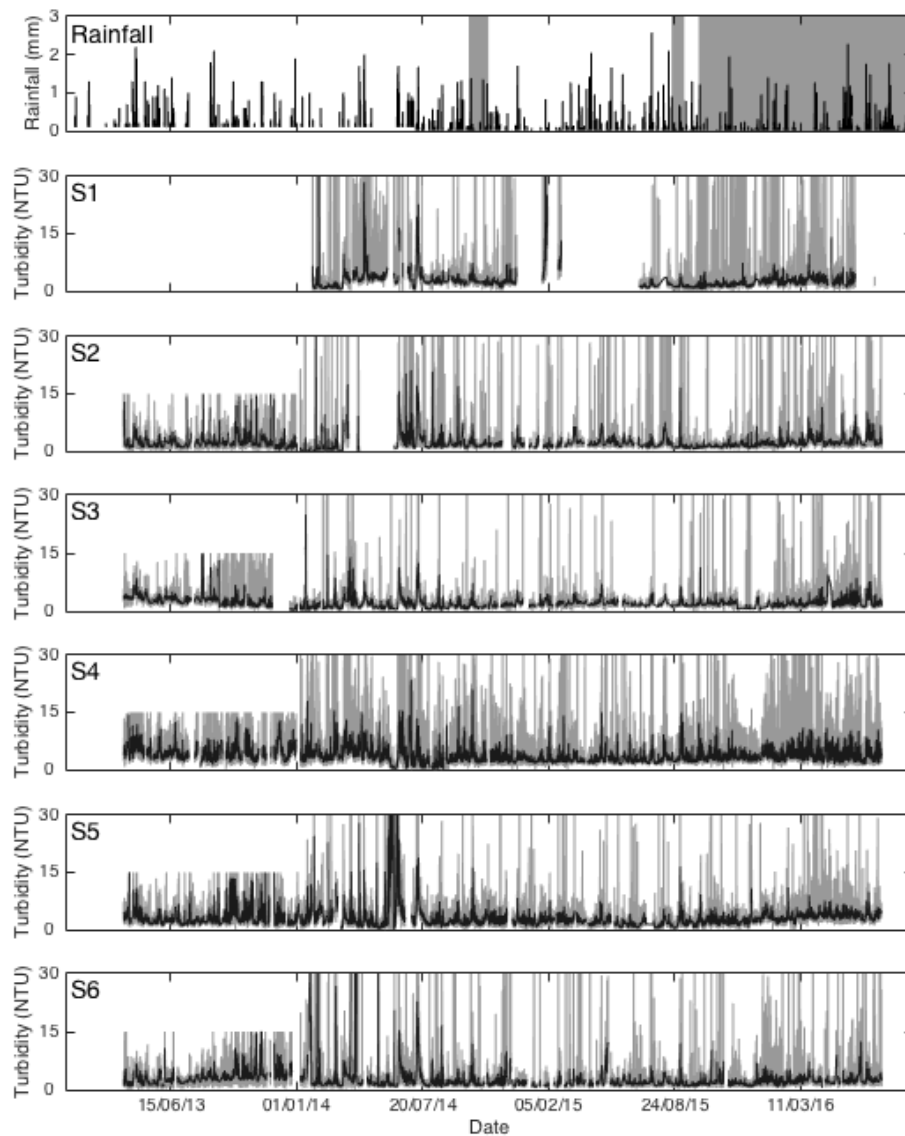
Figure 2.4: Time series of rainfall (mm, top panel) and turbidity (NTU, other panels) recorded every minute. Turbidity is recorded by the sensors located at S1 to S6 shown in Figure 2.1. Grey polygons on top panel indicates periods of dredging: maintenance dredging from 01/10/2014 to 01/11/2014, maintenance dredging from 19/08/2015 to 08/09/2015, and capital dredging from 01/10/2015 to 01/09/2016. Light grey lines represent raw turbidity data, spikes and biofouled data removed and black lines represents the 6-hour moving average data.
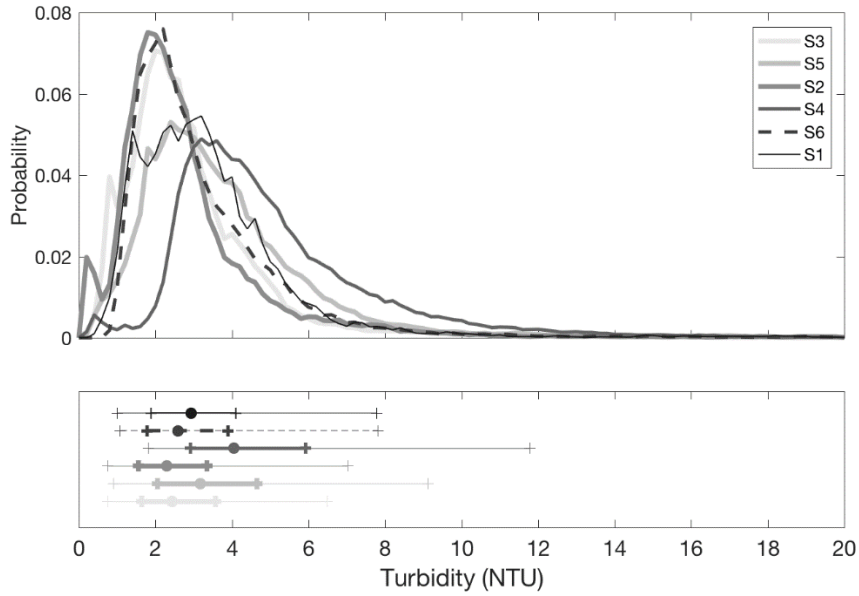
Figure 2.5: The probability of occurrence of turbidity calculated using the 6-hour average data for each sensor (top panel). Bottom panel shows the distribution of the data for each sensor; circles represent the average; thick lines represent the interval between 25% and 75% and thin lines represent the interval from 5% to 95%.
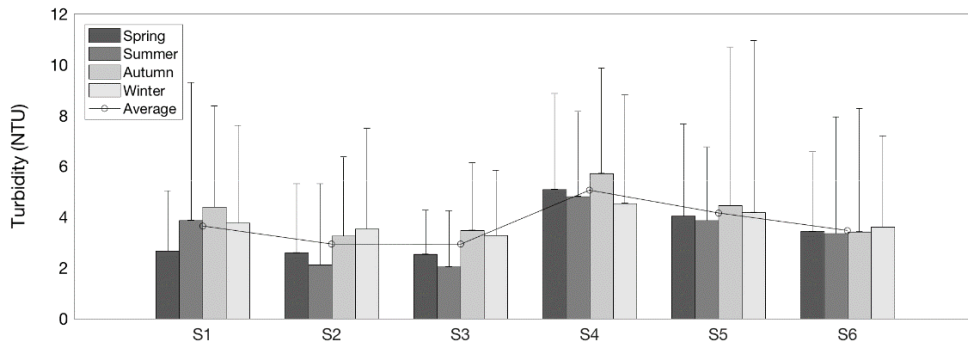
Figure 2.6: Seasonal variation of turbidity for each site, calculated using turbidity data recorded by the sensors from 2013 to 2016. Bars are the average data for each season (± 1 SD – thin bars) and think black line is the seasonal average for each site.
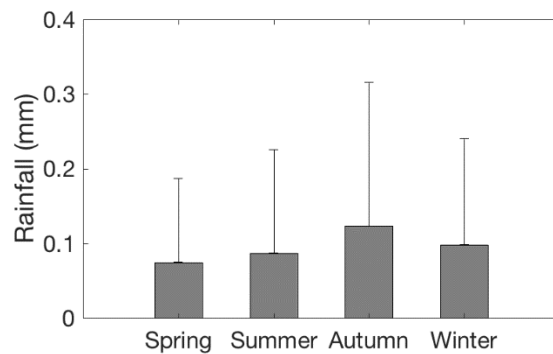
Figure 2.7: Seasonal variation of rainfall (± 1 SD, thin bars) from 2013 to 2016.

The 6-hour moving average turbidity was used in the conditional probability (Equation 4) to show that there was a 95% probability that K_d(PAR) derived from turbidity records will be less than or equal to 0.63 m^{-1}, on average, for the entire period analysed. This limit did not vary significantly between sites. Maximum K_d(PAR) at each site ranged from 0.75 to 0.97 m^{-1}, with average 0.85 m^{-1}. The average K_d(PAR) predicted using the 2-week moving average turbidity was similar to the 6-hour moving average values for all sites. However, the maximum values were lower: S5, 0.73 m^{-1}; S1 and S6, 0.68 m^{-1}; S4 and S2, 0.65 m^{-1}; and S3, 0.64 m^{-1}. No differences were observed between K_d(PAR) calculated for the entire dataset (background and dredging) and the non-dredging periods, which was also observed in the K_d(PAR) calculated before and after maintenance dredging (Table 2.4).

Maximum SPM measured in the dredging plume during the 2014 maintenance dredging in Tauranga Harbour was 70 mg l^{-1} (Cussioli et al., 2015), which corresponds to a turbidity of 33 NTU, calculated using the calibration coefficients for the turbidity sensor, and a predicted K_d(PAR) of approximately 0.8 m^{-1} in the dredging plume (using Equation 4).

2.4 DISCUSSION

The multiple regression analysis showed that, in general, SPM is the main contributor to the light attenuation in Tauranga Harbour, explaining 40% to 60% of variance, as expected for estuarine waters (Davies-Colley et al., 1993; Lund-Hansen, 2004). In Vant (1990), the suspended particulate component, mostly composed of inorganic particles, was also the main cause of light attenuation in northern New Zealand estuaries, contributing on average 56% (more in samples from the upper estuary). Tauranga sites S4 and S5 had the highest SPM concentrations and S4 also had the highest average turbidity. These sites are located in the dredged navigational channel of Stella Passage, in a busy berth area at depths between 5 and 7 m, which receives sediment input from the sub-catchments Waimapu, Kaitemako, Waitao, Papamoa and Mount Maunganui, together yielding approximately 25% of the sediment load to the southern Tauranga Harbour (Elliott

et al., 2010). Therefore, the higher SPM in Stella Passage is likely due to resuspended sediments from port activities such as ship traffic and manoeuvring, which can elevate the SPM in the short-term (Bryan et al., 2014) and runoff from the sub-catchments. In contrast, the more upper estuary site S7 is shallower, around 1 m deep, and it is comparatively more influenced by riverine characteristics as it is situated near the mouth of the Wairoa River. Although our results show that S4 and S5 have higher SPM compared with S7, Wairoa River is considered the largest contributor of freshwater (Park, 2004) and the main input of catchment sediment, approximately 45% of the sediment load (Elliott et al., 2010), into the harbour. Areas that are the first to receive river discharge and terrestrial runoff, especially after heavy rainfall, have higher concentrations of suspended particles causing reduction in light penetration (Bulmer et al., 2016, Davies-Colley et al., 1993). The impact of river discharge has been shown to affect benthic plants; for example, large loss of seagrass beds was recorded in Great Sandy Strait in Queensland, Australia, after a flooding period caused increased turbidity and nutrients (Campbell and McKenzie, 2004). In our case, Autumn SPM at S7 was lowest, whereas the autumn rainfall was generally highest (Figure 2.7). The in situ SPM measurements, conducted over fair weather conditions, might have not have included conditions when sediment loading from the Wairoa River was highest (during and after heavy rainfall). Although there was no continuous monitoring station directly at S7, in general, high-frequency, long-term turbidity measurements agree more with long-term rainfall patterns.

In Tauranga Harbour, tidal currents and waves are usually the main cause of resuspension and transport of suspended particles (Davies-Colley and Healy, 1978) and drive differences in the optical properties of the water between ebb and flood. In our study site, the sensors close to the Centre Bank, S1, S2 and S3, which are more exposed to open ocean conditions, had the lowest K_d(PAR), and small differences between tides, possibly due to the rapid flushing around those areas, especially at the harbour mouth (Davies-Colley and Healy, 1978, Tay et al., 2013). In the upper harbour, depending on wind direction and fetch, a combination of wave action resuspending bottom sediments in the tidal flat and tidal currents, are

likely to be the main controls on the transport of suspended particles (Green and Coco, 2007), which drive greater differences between ebb and flooding currents than near the entrance (Figure 2.3). Therefore, it is important to develop a sampling regime that recognises that tidal differences may cause sampling bias.

The variation in K_d(PAR) observed in the estuary is also linked to the presence of other water constituents, such as CHL and CDOM, which is similar to other estuaries (Kirk, 2011), where CHL contributed with 32% and 14 % (Lund-Hansen, 2004; Vant, 1990, respectively). Our results show somewhat higher concentrations in the upper harbour and lower values close to the entrance with a positive, but only a weak correlation ($r^2 = 0.3$) to K_d(PAR). Usually, maxima in CHL concentrations are found during spring, during the "spring bloom", when warmer temperatures increase phytoplankton growth (Kowalczuk, 1999; Matheson et al., 2017; Park, 1998; Scholes, 2015; Schwartz et al., 2006; Tay et al., 2012; Vant, 1990); however, phytoplankton blooms were not captured in our sampling. Highest values occurred in autumn and the lowest averages in spring, following rainfall patterns (potentially triggering nutrient pulses into the harbour). Variations can be also related to the seasonality of phytoplankton species, which can change the optical properties depending upon on their cell sizes and pigments (Fujiki and Taguchi, 2002).

CDOM was a minor contributor to the light attenuation, in accordance with other studies (Lund-Hansen, 2004; Vant, 1990) and in the range of estuarine values (Kirk, 1976; Lund-Hansen, 2004; Pfannkuche, 2002; Tian et al., 1994; Vant, 1990). The S4 site, together with S7, had the highest average CDOM; S4 is close to the site in the port where raw timber is processed for export, which could have contributed for the high coefficient (Brunschwiler, 2015), although site runoff occurs during and after rainfall, which was not the case when we carried out our sampling. Tian et al. (1994) studied the increase in CDOM in runoff plumes from log processing in Tauranga after rainfall; CDOM coefficients were 85 to 1280 times that of background values. However, storm runoff outside the processing area also presented high CDOM possibly due to pollution by surface dirt (Tian et al., 1994), which could also be the cause of high values at S4.

CDOM was higher in winter and lower in autumn, which is in contrast to some estuaries, which show higher CDOM in spring and low in autumn and winter (Kowalczuk, 1999); according to Carder et al. (1989), decaying CHL in offshore waters contributes to increased CDOM and, although measurements in our study were carried out in an estuary, not offshore, we had maximum CHL in autumn and maximum CDOM in the following season; therefore, the decaying CHL after high production in autumn may contribute to the increase in CDOM in winter.

CDOM is usually higher near river mouths and inland water sources, reducing towards the harbour entrance in more saline waters (Davies-Colley and Vant, 1987; Kirk, 1976, 1977; Pfannkuche, 2002; Schwarz et al., 2006). There was a gradient of decreasing CDOM down the estuary, likely due to the distance from riverine input that are sources of terrestrial CDOM. Moreover, yellow substances tend to precipitate as water is transported seaward (Sieburth and Jensen, 1968).

The range and the spatial variation of $K_d(PAR)$ calculated using the light measurements are similar to other estuarine and coastal waters around New Zealand (Kirk, 2011; Kohlmeier, 2016; Pfannkuche, 2002; Vant, 1990), but generally lower than overseas sites in Europe (Devlin et al, 2008; Giesen et al, 1990; Lund-Hansen, 2004) and in North America (Del Barrio et al., 2014; Dennison, 1987) where average $K_d(PAR)$ are approximately 1.5 m^{-1} and 2.7 m^{-1}, respectively. The seasons with highest and lowest averages of $K_d(PAR)$ calculated from NTU recordings did not agree with seasons of highest and lowest $K_d(PAR)$ calculated from the *in situ* light measurements. This dissimilarity is likely due to $K_d(PAR)$ derived from turbidity data characterizes turbidity variations related to a range of weather conditions, including storm events, whereas the measured seasonal variation in $K_d(PAR)$ accounts for much less variation related to the fair weather condition when the measurements were carried out. Other studies disagree on the timing of seasonal maxima in $K_d(PAR)$. For example, Vant (1990) observed highest coefficients in summer, and Pfannkuche (2002) observed highest in spring and lowest in winter, for the outer sites with $K_d(PAR)$ more stable in inner sites. In our study, overall (spatial and temporal) averages of $K_d(PAR)$ are not significantly different from the average of $K_d(PAR)$ for each season.

28

Light measurements during the maintenance dredging in October 2014 showed that the differences in K_d(PAR) before and after dredging were smaller than differences between tidal states, where dredging measurements were carried out after total dissipation of the plume from the dredged area (approximately 2 hours). We estimated a higher light attenuation coefficient during dredging using SPM concentrations measured inside the plume; however, the K_d(PAR) calculated from NTU recordings show that, in general, the turbidity levels during dredging and non-dredging periods are not substantially different. Onuf (1994) monitored a maintenance dredging project that occurred at Laguna Madre, Texas, USA, which has suffered severe loss of seagrass in the past. He found that K_d(PAR) after a dredging period (1 to 3 months after) had increased by 40%; however, he acknowledged the challenge of relating light reduction to the short-duration dredging plume. The increase in K_d(PAR) at the Laguna Madre could have been caused by the resuspension of sediments from the dumping areas which act as a point source of sediment as the excess of sediment above the bottom is eroded. Our observations show a return to ambient conditions indicating resuspension is minimal.

Table 2.2: Local depth (mean tide), percentage of surface irradiance (% SI) available at the bottom and depth relative to 36% SI (light requirement for photosynthesis of seagrass species *Zostera muelleri*) calculated using the average light attenuation coefficient, K_d(PAR), from light measurements in each site.

Site	Depth (m)	% SI bottom	Depth (m) 36% SI
S1	16.70	0.98	3.68
S2	3.70	31.04	3.24
S3	13.70	1.37	3.26
S4	6.70	4.62	2.22
S5	4.70	9.11	2.00
S6	6.70	7.99	2.72
S7	1.20	61.46	2.39

Table 2.3: Depth of seagrass colonization at mean tidal level (MT), at high tide (HT) and at high tide during spring tide (SHT), percentage of surface irradiance (% SI) available at the bottom considering two scenarios (1) average K_d(PAR) of 0.4 m^{-1} (calculated from the light measurements) and (2) average K_d(PAR) of 0.63 m^{-1} (converted from the 2-week averaged turbidity data recorded by the sensors). Thresholds of K_d(PAR) and calculated turbidity limits for seagrass growth which would possibly guarantee that the minimum light requirement is met at least 95% of the time. SPM converted using the turbidity sensor calibration coefficients.

| Tidal level | Depth (m) | Benthic light availability (% SI) | | Thresholds for 36% SI | | |
		Scenario 1 K_d(PAR) = 0.4 m^{-1}	Scenario 2 K_d(PAR) = 0.63 m^{-1}	K_d(PAR) (m^{-1})	Turbidity (NTU)	SPM (mg l^{-1})
MT	0.7	76	64	1.5	9.2	20
HT	1.4	57	41	0.7	8.2	17
SHT	2.0	45	28	0.5	7.9	17

2.4.1 Management Implications

Environmental limits which are set to regulate water quality during dredging are sensitive to the assumptions regarding the minimum light requirements of seagrass. Current response levels used in the Tauranga Harbour are based on a study carried out at Port Phillip Bay, in Australia, which considered a light requirement of 15% SI (PoMC, 2008), and were developed for subtidal seagrass, considered to have lower light requirements than intertidal seagrasses (Bulmer et al., 2016). Seagrasses of same genus worldwide have minimal light requirement of 20% in average (Dennison, 1993); however, *Z. muelleri* have usually higher light requirements, around 30% (Erftemeijer and Lewis, 2006). In this study, we have used the upper maximum of 36%. The derived relationships between K_d(PAR) and NTU are also very local (due to different contributions of water constituents), and so environmental limits are not necessarily transferable between sites. Moreover, the relationship varied with season and storm events, emphasising the necessity of basing estimates on a wide range of conditions. The probabilistic approach used here for the calculation of thresholds also assumes that sediment is well mixed in the water column and does not settle on seagrass leaves during emersion.

Setting limits for environmental effects also needs to accommodate the length of time over which conditions remain sub-optimal. In a review on the impacts of dredging activities on seagrass by Erftemeijer and Lewis (2006) the authors discuss that the reduction in seagrass could be more likely relate to natural

events like storms than to the dredging plume which are transitory and can be within background range. Seagrasses are resilient and can cope with short-term changes in light condition and some studies and monitoring programs (e.g. Chartrand et al., 2012 and PoMC, 2008) suggest averaging light condition over a two-week period would more reflect the conditions needed to maintain growth of seagrass beds. Although seagrass is adapted to tolerate periods of low light condition for weeks or months (Erftemeijer and Lewis, 2006; Onuf, 1994), as evidenced by seagrass survival after high turbidity caused by storm events, other species might not perform well in shorter period of elevated turbidity. For example, intertidal seagrass, like *Z. muelleri* in Tauranga Harbour, will not necessarily compensate for reduced clarity when photosynthesizing during emersion periods. The same species of seagrass in Australia showed negative effects on photosynthesis when exposed (Chartrand et al, 2012), whereas relative gain in photosynthesis occurred during emersion in Whangapoua Harbour, in New Zealand (Schwarz, 2004).

Seagrass experience seasonal variations in their physiological state. For example, seagrass can be more sensitive during its growing period, which usually occurs in spring and summer (Chartrand et al., 2012), which would cause seasonal variations in the potential impacts from dredging. On the other hand, poor seagrass condition detected during dredging might reflect a natural period of no growth, and so monitoring seagrass condition should be integrated over the year (Dennison, 1987).

Reducing or ceasing dredging during flood and high tide, especially during daylight, will reduced impacts on intertidal meadows. Dredging at low tide should be carried out with caution, since it is the time when the natural component of light attenuation coefficient is the highest (although intertidal beds would be largely emerged over that period).

2.5 CONCLUSION

Our assessment shows how critical it is to have longer-term measurements of light conditions, including measurements from poor weather to set environmental limits on activities in estuaries and harbours. Inferring light conditions from turbidity measurements can reduce costs of data collection in which case, establishing a relationship between underwater light availability and turbidity is essential. We proposed the application of a probabilistic approach using turbidity data as a proxy for $K_d(PAR)$, as a complement to the turbidity-based management plan. Estimates of light availability from turbidity measurements enabled us to include storm conditions in our assessment of average light conditions, the inclusion of which caused an average increase in the light attenuation coefficient of 45% on the intertidal. Our study shows that estuarine and coastal monitoring programs and monitoring programs surrounding port and dredging activities should continuously monitor background conditions to distinguish effectively between anthropogenic versus natural elevation in turbidity, in cases where turbidity varies seasonally and episodically.

Our results in Tauranga Harbour indicate substantially reduced benthic light availability in subtidal channels caused by increased turbidity. Levels were well below those needed to sustain seagrass, possibly explaining loss of subtidal seagrass in the harbour. Conversely, light is not limiting seagrass photosynthesis on the intertidal for *Zostera muelleri*, likely explaining the modern day distribution of seagrass. More continuous monitoring over multiple dredging events allowed us to conclude that $K_d(PAR)$ during dredging periods did not show significant increase compared with background levels.

2.A APPENDIX

Table 2.4: Light attenuation coefficient (K_d(PAR)) and water quality parameters (suspended particulate matter concentration (SPM), turbidity (TURB), chlorophyll-a (CHL) concentration, coloured dissolved organic matter (CDOM)) collected in the period of 2014 to 2016, including measurements during the maintenance dredging in Tauranga Harbour (13/10/2014 to 16/10/2014), which were carried out around the areas described in the name, also shown in Figure 2.1. * represents measurements carried out after dredging (or after dumping, at the Spoil Ground).

Date	Season	Tide	Site	K_d (PAR) (m^{-1})	SPM (mg l^{-1})	TURB (NTU)	CHL (µg l^{-1})	CDOM (λ_440) (m^{-1})
02/05/14	autumn	high	S1	0.25	–	3.18	–	–
02/05/14	autumn	high	S2	0.35	–	–	–	–
02/05/14	autumn	high	S3	0.26	–	0.67	–	–
02/05/14	autumn	high	S6	0.46	–	3.77	–	–
02/05/14	autumn	high	S4	0.66	–	5.23	–	–
02/05/14	autumn	high	S5	0.67	–	4.48	–	–
13/10/14	spring	ebb	Off Entrance	0.22	–	–	–	–
13/10/14	spring	ebb	Off Entrance	0.32*	–	–	–	–
14/10/14	spring	ebb	Sulphur Point	0.39	–	–	–	–
14/10/14	spring	ebb	Sulphur Point	0.43*	–	–	–	–
15/10/14	spring	flood	Maunganui Roads	0.33	–	–	–	–
15/10/14	spring	flood	Maunganui Roads	0.22*	–	–	–	–
15/10/14	spring	high	Stella Passage	0.27	–	–	–	–
15/10/14	spring	ebb	Stella Passage	0.37*	–	–	–	–
16/10/14	spring	flood	Spoil Ground	0.11	–	–	–	–
16/10/14	spring	flood	Spoil Ground	0.21*	–	–	–	–
10/12/14	summer	high	S3	0.32	–	1.49	–	–
10/12/14	summer	high	S2	0.33	–	1.02	–	–
10/12/14	summer	high	S1	0.35	–	2.84	–	–
10/12/14	summer	high	S4	0.31	–	1.85	–	–
10/12/14	summer	high	S5	0.30	–	0.94	–	–
10/12/14	summer	high	S6	0.33	–	1.29	–	–
10/12/14	summer	high	S7	0.26	–	–	–	–
10/12/14	summer	low	S7	0.37	–	–	–	–
10/12/14	summer	low	S1	0.21	–	3.46	–	–
10/12/14	summer	low	S2	0.48	–	2.19	–	–
10/12/14	summer	low	S3	0.41	–	2.51	–	–
10/12/14	summer	low	S4	0.54	–	3.85	–	–
10/12/14	summer	low	S5	0.57	–	2.80	–	–
10/12/14	summer	low	S6	0.34	–	1.72	–	–
26/02/15	summer	low	S6	0.61	–	2.75	–	–
26/02/15	summer	low	S3	0.34	–	2.90	–	–
26/02/15	summer	low	S1	0.44	–	8.69	–	–
26/02/15	summer	low	S2	0.58	–	4.04	–	–
26/02/15	summer	low	S7	0.51	–	–	–	–
26/02/15	summer	low	S5	0.66	–	4.19	–	–
26/02/15	summer	low	S4	0.56	–	5.69	–	–
26/02/15	summer	high	S1	0.30	–	12.60	–	–
26/02/15	summer	high	S3	0.27	–	3.62	–	–
26/02/15	summer	high	S2	0.30	–	3.91	–	–
26/02/15	summer	high	S7	0.28	–	–	–	–
26/02/15	summer	high	S7	0.42	–	–	–	–
26/02/15	summer	high	S6	0.27	–	2.70	–	–
26/02/15	summer	high	S5	0.34	–	2.14	–	–
26/02/15	summer	high	S4	0.44	–	2.88	–	–
06/05/15	autumn	low	S1	0.31	3.00	–	1.17	0.05
06/05/15	autumn	low	S2	0.24	1.35	2.06	0.59	0.08
06/05/15	autumn	low	S3	0.33	4.03	3.43	1.03	0.20
06/05/15	autumn	low	S4	0.41	3.19	2.64	0.47	0.22

06/05/15	autumn	low	S5	0.42	3.49	2.93	0.86	0.18
06/05/15	autumn	low	S6	0.30	2.41	15.61	1.49	–
06/05/15	autumn	low	S7	0.43	2.32	–	1.91	–
01/07/15	winter	low	S1	0.25	3.52	2.01	0.81	0.27
01/07/15	winter	low	S2	0.32	2.55	1.47	0.90	0.24
01/07/15	winter	low	S3	0.25	4.32	2.52	0.67	0.29
01/07/15	winter	low	S4	0.27	3.97	5.66	1.00	0.27
01/07/15	winter	low	S5	0.39	5.39	1.28	0.94	0.33
01/07/15	winter	low	S6	–	5.29	2.23	0.89	0.24
01/07/15	winter	low	S7	0.98	6.23	–	1.77	0.39
28/10/15	spring	high	S1	0.18	2.04	1.53	0.32	0.17
28/10/15	spring	low	S1	0.36	6.83	3.46	0.85	0.09
28/10/15	spring	high	S2	0.16	2.75	1.31	0.71	0.17
28/10/15	spring	low	S2	0.52	3.94	2.88	0.86	0.21
28/10/15	spring	high	S3	0.33	4.63	3.14	0.85	0.15
28/10/15	spring	low	S3	0.44	5.08	3.79	0.92	0.24
28/10/15	spring	high	S4	0.39	8.21	3.07	0.31	0.21
28/10/15	spring	low	S4	0.65	9.31	12.38	1.30	0.29
28/10/15	spring	high	S5	0.41	5.36	2.94	0.81	0.12
28/10/15	spring	low	S5	0.84	9.99	7.44	3.27	0.33
28/10/15	spring	high	S6	0.20	2.80	2.28	0.65	0.14
28/10/15	spring	low	S6	0.57	5.40	3.03	0.88	0.14
28/10/15	spring	high	S7	0.23	3.19	–	0.43	0.19
28/10/15	spring	low	S7	0.65	5.97	–	0.84	0.26
14/12/15	summer	high	S1	0.23	3.73	1.58	0.73	0.13
14/12/15	summer	low	S1	0.35	5.31	2.81	0.68	0.22
14/12/15	summer	high	S2	0.31	4.35	1.53	0.90	0.20
14/12/15	summer	low	S2	0.42	5.59	2.00	1.29	0.14
14/12/15	summer	high	S3	0.19	3.37	0.69	0.96	0.16
14/12/15	summer	low	S3	0.30	7.88	0.86	1.03	0.26
14/12/15	summer	high	S4	0.46	6.16	3.95	0.62	0.23
14/12/15	summer	low	S4	0.70	10.88	4.83	1.92	0.38
14/12/15	summer	high	S5	0.41	6.22	3.42	1.04	0.21
14/12/15	summer	low	S5	0.60	10.47	3.57	1.04	0.26
14/12/15	summer	high	S6	0.37	4.15	1.87	0.80	0.18
14/12/15	summer	low	S6	0.48	5.19	2.26	0.69	0.22
14/12/15	summer	high	S7	–	6.07	–	0.56	0.22
14/12/15	summer	low	S7	0.28	4.73	–	0.87	0.23
02/03/16	autumn	high	S1	0.28	4.62	4.94	1.31	0.02
02/03/16	autumn	low	S1	–	5.22	4.30	1.24	0.11
02/03/16	autumn	high	S2	0.20	3.17	1.92	0.93	0.10
02/03/16	autumn	low	S2	–	5.99	3.46	1.43	0.06
02/03/16	autumn	high	S3	0.28	4.03	2.20	1.23	0.11
02/03/16	autumn	low	S3	–	5.58	3.47	1.39	0.17
02/03/16	autumn	high	S4	0.40	5.64	3.84	0.89	0.11
02/03/16	autumn	low	S4	–	5.21	5.50	1.34	0.22
02/03/16	autumn	high	S5	0.59	6.63	2.70	1.30	0.17
02/03/16	autumn	low	S5	–	4.21	3.55	1.34	0.23
02/03/16	autumn	high	S6	0.39	4.69	2.66	1.51	0.09
02/03/16	autumn	low	S6	–	5.27	2.73	1.44	0.20
02/03/16	autumn	high	S7	0.43	3.64	–	0.87	0.19
02/03/16	autumn	low	S7	0.43	2.92	–	1.55	0.23

34

CHAPTER 3

FEEDING RESPONSES OF *Paphies australis* TO INCREASES IN SUSPENDED SEDIMENT CONCENTRATIONS

Mariana Coppede Cussioli[1], Conrad A. Pilditch[1], Karin R. Bryan[1], Daniel R. Pratt[2], Kai Bischof[3] (to be submitted to *Journal of Experimental Marine Biology and Ecology*)

1. School of Science, University of Waikato, Hamilton 3240, New Zealand

2. East Coast Ecology, Old Post Office, Castle Road, Offton, Ipswich IP8 4RG United Kingdom

3. Marine Botany, University of Bremen, Leobener Str. NW2, 28359 Bremen, Germany

CONTRIBUTION OF AUTHORS:

Fieldwork campaigns and physiological experiments were planned and organized by MCC and carried out by MCC with contribution of DRP and technical help of the University's field technicians. Two volunteers helped with pipi collection. All laboratory work was carried out by MCC with technical help of the University's laboratory technicians. CAP provided helpful guidance with experiment planning and data interpretation. MCC analysed all data and wrote the initial and subsequent drafts, and co-authors contributed with valuable comments.

ABSTRACT

Bivalves are likely to experience variable conditions in the quantity and quality of suspended material, altering their diet, and use adaptive mechanisms to provide an optimal food supply. We tested six laboratory treatments of target concentrations of 0, 10, 30, 70, 100 and 300 mg l^{-1} to predict the short-term effects of increased suspended sediment concentrations on the feeding behaviour of the mesodesmatidae bivalve *Paphies australis*, commonly known as pipi. Pipis responded to increases in seston concentration by reducing clearance rate and by using rejected inorganic particles though pseudofaeces production to select for organic material. In this way, they were able to increase by a factor of two the organic content of ingested matter compared with organic fraction present in treatments provided. Our results suggest optimal condition for pipis are when seston concentration is below 30 mg l^{-1} and thresholds for adverse effects on feeding rates are between 30 and 70 mg l^{-1}. Stabilization of feeding rates when conditions were above 70 mg l^{-1} indicate potential physical constraints that could limit food acquisition.

3.1 INTRODUCTION

Coastal areas are characterised by diverse and dense populations of benthic macrofauna organisms and a significant group of these organisms is represented by suspension-feeding bivalves (Asmus and Asmus, 1993; Smaal and Prins). Suspension feeding bivalves, play an important role in the complex interactive processes between benthos and water column of coastal ecosystems. It is recognized their importance in reducing turbidity by removing both organic and inorganic particles from the water (Newell, 2004). Consequently, light availability at the benthos increases, therefore improving photosynthesis of benthic plants (e.g. seagrasses and microphytobenthos; Newell and Koch, 2004). They also produce biodeposits (faeces and pseudofaeces) which contribute to the flux of materials in the benthic-pelagic coupling, and nutrient processing and regeneration (Dame 1993). By filtering large quantities of water, they are directly affected by variations in suspended sediment (Bayne, 1993; Bayne and Newell, 1983) and thus, a good indicator of changes to water quality.

Bivalves are likely to experience variable environmental conditions such as temperature, salinity and food quality/quantity over a range of spatial and temporal scales (Bayne, 1993). The quantity and quality of suspended material (seston) can also be affected by natural fluctuations (tides, seasonal, wind-wave current resuspension) (Urrutia et al., 1997) and/or by human activities such as dredging and port activities (Healy et al., 1996), which will increase the turbidity in the water column (Thrush et al., 2004; Norkko et al., 2006). Increasing the proportion of inorganic matter in the suspended load will, thus, decrease the organic content of seston, diluting the food and altering its nutritional quality (Navarro and Widdows, 1997; Urrutia et al., 1997). To have an optimal food supply in areas of high variability of turbidity, adaptive mechanisms must operate in filter feeders (Urrutia et al., 1997). These mechanisms include the closure of valves and the reduction of clearance rate or selection of organic material by rejecting inorganic particles though pseudofaeces (Bricelj and Malouf, 1984; Navarro et al., 1992; Hawkins et al., 1996; Navarro and Widdows, 1997; Newell and Shumway, 1993; Urrutia et al., 1997; Macdonald et al., 1998).

Paphies australis, commonly known as pipi in New Zealand, is considered to be sensitive to turbidity variability (Norkko et al., 2005; Hewitt and Norkko, 2007), thus being a good indicator species for detecting environmental change. Pipis are burrowing suspension-feeding bivalve of the Family Mesodesmatidae found at mid-intertidal depths (juveniles) to shallow subtidal (adults), usually forming dense beds (Cook, 2010). Therefore, they likely play an important role in benthic-pelagic coupling and food web structure (Dame, 1993). They are also an important food source for higher trophic groups including humans (Hooker, 1997) and have potential for aquaculture (Mamat and Alfaro, 2014). They normally inhabit relatively coarse sediments, shows a strong sand preference and is abundant in sediments where the mud ranges from 0 to 5% (Gibbs and Hewitt, 2004) and is common near the mouths of estuaries, harbour channels and sand banks (Cook, 2010; Cummings and Thrush, 2004; Hooker, 1997). According to Mamat (2010), mature stages of pipi occur during early winter to June and spawning occurs during late winter/early spring, continued through to late summer.

As far as we are aware of, only one study documented response in feeding behaviour of pipis to increased turbidity. In laboratory, short-term (2 days) responses of pipis presented an initial increase in clearance and filtration rates in concentrations up to 30 mg l^{-1} and 250 mg l^{-1}, respectively. The increase was followed by a decline in these rates in seston concentrations above these thresholds (Hewitt and Norkko, 2007). A decrease in biomass occurred in concentrations above 30 mg l^{-1}.

Different from the study cited above, where only clearance and filtration rates were considered to estimate thresholds of feeding response, our study considers several feeding and digestion rates (clearance, filtration, ingestion, rejection and absorption rates, and selection efficiencies). Given that, the objectives of this study were to (1) examine the short-term response of pipi feeding behaviour to increases in seston concentration and (2) model those responses to estimate thresholds of impact to changes in estuarine suspended sediment loading.

Given the importance of suspension-feeding bivalves in coastal ecosystem processes and their role within food webs, it is important to understand how

changes in water quality parameters affect their behaviour. This is particularly pertinent in complex systems with multiple drivers, such as estuaries, where human activities take place. In this context, this study is a valuable contribution for energetic modelling studies of bivalves and in setting environmental limits for human activities in estuaries and harbours. Keeping water quality levels below environmental limits will ensure maintenance of population dynamics and survival.

3.2 METHODS

We had a total of five experimental days and ran two experiments per day, except on the first day when we ran only one experiment. Ten to eleven replicates of six treatments were used to test the feeding behaviour of *Paphies australis* at target concentrations of 0, 10, 30, 70, 100 and 300 mg l^{-1}. These concentrations represent the range of turbidity experienced in estuarine waters in New Zealand, where pipi are commonly found, considering background values and maintenance dredging events (Cussioli et al., submitted; Fahey and Coker, 1992). The treatments were prepared by mixing natural seawater and sediment in a slurry. Seawater was pumped from a location near to where pipis were collected (Figure 3.1), on the days preceding each day of experiments, 2 hours before high tide, and temperature and salinity were recorded. The sediment slurry was prepared on the day prior to the start of the experiments, using scraped surface sediment (top 1 cm) from the Welcome Bay sandflat (south of study area, not shown in the map and sieved through a 53-μm mesh. This resulted in a mixture where 90% of the volume distribution included grain sizes below 50 μm, 50% below 13 μm, and 10% below 3 μm. The slurry was kept in refrigerator (4 ˚C) and treatments were prepared just before each experimental run. On the day prior to each set of experimental runs, pipis of 50 to 60 mm shell length were collected from opposite sulphur point (Figure 3.1) at low tide, brought to the laboratory, the shells cleaned, and kept in aerated aquaria with filtered seawater and starved overnight, which ensured that feeding behaviour and biodeposit production was a result of the treatments only.
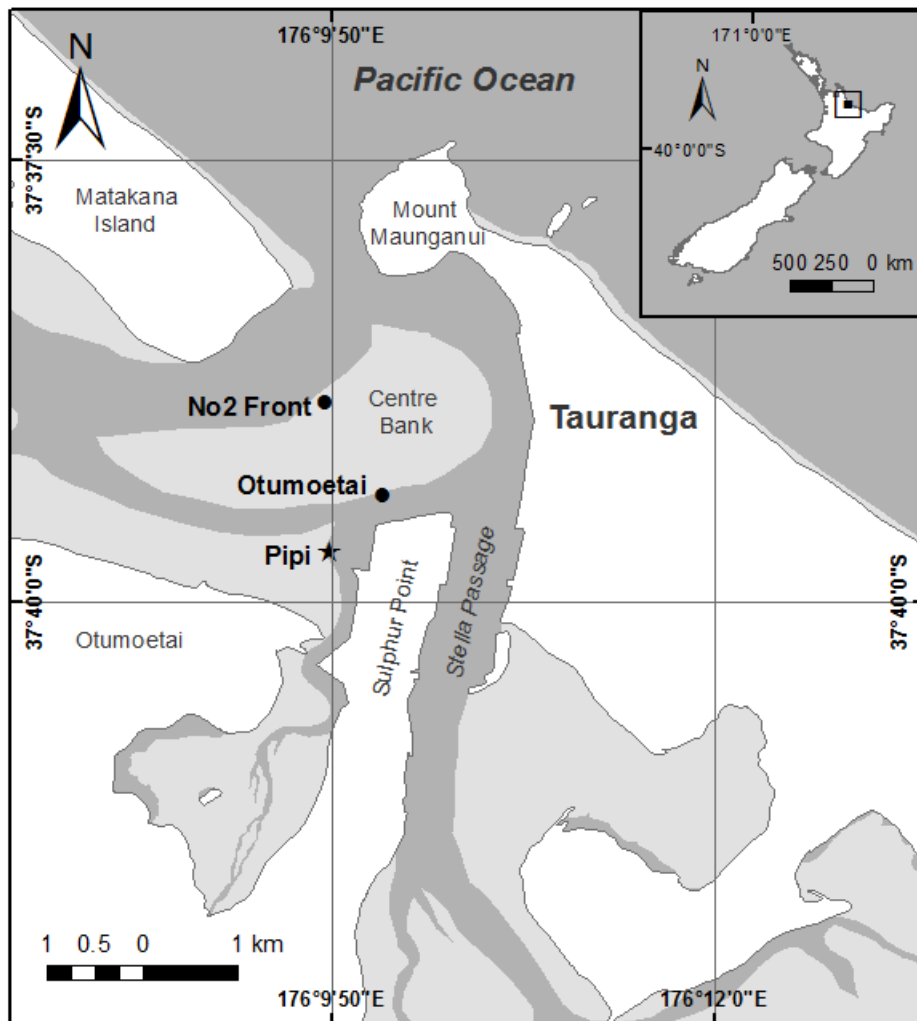
Figure 3.1: Map showing the location where pipis (*Paphies australis*) were collected for laboratory experiments (star marker). Dots represent the location of turbidity sensors near pipi beds which were used to estimate background turbidity and suspended sediment concentration (details in APPENDIX A). Light grey areas represent intertidal flats. Inset shows the map of New Zealand.

We used eight flow-through chambers: six chambers for treatments, one duplicate treatment and one control. Target concentrations in the duplicate chamber and control chamber changed in each run.

The chambers were 18.5 cm long, 13.0 cm wide and held a volume of approximately 1.6 l. They were designed whereby turbulence could be minimized and avoid an outflow of biodeposits through the outlet. This was achieved by mounting an upward curved plastic tube at the inflow port and placing a slot near the outflow port (Teaioro, 1999).

Approximately two hours before each experiment run, 'active' pipis identified by shell gaping and feeding activity were randomly selected and two pipis were placed in each one of the seven flow-through chambers for acclimation, and all biodeposits produced prior experiment started were removed while making sure pipis were not disturbed. Each treatment (natural seawater + aliquots of sediment slurry to reach target concentrations) was placed in an input bucket and kept in suspension using aquarium stone aerators and pumped into the corresponding chamber using peristaltic pump at about 30 ml min^{-1}. Each experiment run lasted two hours and observations of pipi behaviour, when possible, were made every 20 or 30 minutes. According to our preliminary experiments, pipis were very responsive to treatments and produced biodeposits (faeces and pseudofaeces, depending on the sediment concentration) during this time frame.

Water samples were taken from input buckets at the beginning of each experiment. At the end of each experiment, output buckets were spun to stir and mix the water and water samples were collected for following analysis. The samples were filtered onto pre-ashed (450 ˚C for 2 hours) and pre-weighed 47-mm GF/C filters, and dried at 105 ˚C until constant weight (for about 18 hours) and the weight recorded for calculation of total particulate concentration (TPM, mg l^{-1}). Afterwards, filters were combusted at 400 ˚C for 5.5 hours and the weight recorded. Inorganic matter of the TPM was calculated from the weight after combustion (PIM, mg l^{-1}) and the organic matter was calculated from the weight loss (POM, mg l^{-1}).

At the end of each experiment, pipis were frozen for posterior analysis: measurements of shell length and width and their flesh removed and dried at 60 ˚C until constant weight (for about 48 hours). Also at the end of experiments, the biodeposits were collected by passing the water from inside the chambers through a 76-μm mesh; the deposits retained on the mesh were preserved in saline solution and kept in refrigerator until examined under the microscope. Pipis biodeposits were separated in faeces and pseudofaeces (when present) using a stereo microscope and dried onto pre-ashed and pre-weighed 25-mm GF/C filters at 105 ˚C until constant weight (about 48 hours). After, filters were combusted at 400 ˚C for 5.5 hours and organic and inorganic fractions were calculated.

3.2.1 Feeding rates

Calculation of feeding and digestion rates is based on the formulations described in Hawkins et al., (1996; 1998a) and Hewitt and Pilditch, (2004) (Table 3.1). This method considers the quantity and quality of the treatments and biodeposits. The feeding and digestion rates were converted to a standard 1 g of pipi flesh dry weight to account for the differences in the responses that could be caused by differences in biomass, using the following formula:

$$R_s = \left(\frac{TDW_s}{TDW_{obs}} \right)^b R_{obs}$$

where R_s is the standardised rate, TDW_s is the standard weight of 1 g, TDW_{obs} is the average dry tissue weights (g) of pipis, R_{obs} is the rate per animal, and b is the average weight exponent of 0.66 for feeding rate to body weight relationships for a variety of suspension feeding bivalves (Bayne and Newell 1983; Macdonald 2006).

Table 3.1: Parameters and calculation of the feeding rates (after Hawkins et al., 1996, 1998b; Hewitt and Pilditch, 2004). PIM = particulate inorganic matter, POM = particulate organic matter, f = fraction, (-) = dimensionless.

Symbol	Parameter	Units	Calculation
FR	Filtration rate	$mg\,h^{-1}$	$\left(PIM_{faeces} + PIM_{pseudofaeces} \right) / \left(fPIM_{treatment} \right)$
CR	Clearance rate	$ml\,h^{-1}$	$FR / PIM_{treatment}$
RR	Rejection rate	$mg\,h^{-1}$	$mg\ pseudofaeces\ h^{-1}$
fRR	Fraction rejected	fraction	RR / FR
IR	Ingestion rate	$mg\,h^{-1}$	$FR - RR$
NOIR	Net organic ingestion rate	$mg\,h^{-1}$	$\left(FR \times fPOM_{treatment} \right) - \left(RR \times fPOM_{pseudofaeces} \right)$
OCI	Organic content of ingested matter	fraction	$NOIR / IR$
NOSE	Net organic selection efficiency	fraction	$\left(OCI - fPOM_{treatment} \right) / fPOM_{treatment}$
NOAR	Net organic absorption rate	$mg\,h^{-1}$	$NOIR - \left(mg\ faeces\ h^{-1} \times fPOM_{faeces} \right)$
NAEIO	Net absorption efficiency from ingested organics	fraction	$NOAR / NOIR$

3.2.2 Statistical Analysis

To establish functional relationships between feeding response of pipis to suspended sediment concentrations in the treatments a variety of regression equations were fitted to the data. We first tested data for normality using Shapiro-Wilk test; however, data generally violated this assumption, and logarithmic transformation did not usually increase data normality. Therefore, we used regression analysis based on the curve estimation procedure using IBM SPSS Statistics Software and functional relationships were selected based on coefficient of determination and significance and F values.

3.3 RESULTS

3.3.1 Ambient variables and *Paphies australis* measurements

Seawater was collected on four different days around the same time relative to the tide. Therefore, temperature and salinity did not vary greatly during the experiment period; temperature ranged from 19.3 ˚C to 19.8 ˚C and salinity ranged from 28.23 to 29.7, averages were 19.5 ˚C and 28.7 for temperature and salinity, respectively. Shell length of *P. australis* used in the experiments (total = 118 shells) varied from 46.32 mm to 58.78 mm with an average of 51.84 mm (SD = 2.84). Shell width varied from 26.62 mm to 35.51 mm with an average of 30.28 mm (SD = 1.97); and flesh dry weight varied from 442.0 mg to 989.7 mg with mean weight of 681.9 mg (SD = 112.3). This resulted in a length-width ratio of around 1.7 (SD = 0.07) and an average condition index (CI) of 1.3 (SD = 0.16).

3.3.2 Treatments and feeding rates

The feeding rates were calculated using the values of SPM, POM and PIM measured from the input buckets; however, those values were overestimated due to sampling after resuspension of slurry, which does not represent the amount of

sediment that was pumped into the chambers and available for pipis. Therefore, input values of SPM, POM and PIM of treatments were corrected considering the difference between input and output concentrations measured for the control chamber in each experiment run. The target concentration of the control chamber changed in each run, however, there was not a control chamber for the treatment of 10 mg l^{-1}; therefore, the averages of variables measured for treatments of 0 mg l^{-1} and 30 mg l^{-1} was used in the calculations of feeding rates for the treatment of 10 mg l^{-1}.

The relationship between quantity and quality of treatments show the dilution of organic rich particles as SPM concentration increases. SPM and POM varied from approximately 1.3 mg l^{-1} to 360.0 mg l^{-1} and 0.4 mg l^{-1} to 32.0 mg l^{-1}, respectively; and fPOM ranged from around 0.1 to 0.3. POM was positively correlated with SPM according to a linear equation; however, fPOM decreased rapidly according to an inverse function (Table 3.2), with significant decrease of organic content between treatments of 0 mg l^{-1} and 10 mg l^{-1} and following an asymptotic tendency above 70 mg l^{-1} (Figure 3.2).

Table 3.2: Functional relationships between feeding rates of *Paphies australis* and suspended sediment concentration.

Regression	r^2	p-value
POM $= 0.287 + 0.086 \times$ SPM	1.00	0.00
fPOM $= 0.092 + 0.316 /$ SPM	0.97	0.00
FR $= 2.320 \times$ SPM$^{0.374}$	0.98	0.00
RR $= -1.877 + 2.427 \times \log(SPM)$	0.93	0.00
fRR $= 0.656 + -0.872 /$ SPM	0.92	0.00
CR $= 2353.832 \times$ SPM$^\wedge - 0.599$	0.99	0.00
IR $= 3.249 + 0.011 \times$ SPM	0.89	0.01
OCI	(no relationship)	
NOIR $= 0.567 \times$ SPM$^{\wedge}0.182$	0.88	0.01
NOSE $= -0.092 + 0.436 \times \log(SPM)$	0.90	0.00
NOAR $= 0.002 \times$ SPM $+ 0.598$	0.77	0.02
NAEIO $= 0.587 + 0.289 /$ SPM	0.53	0.10
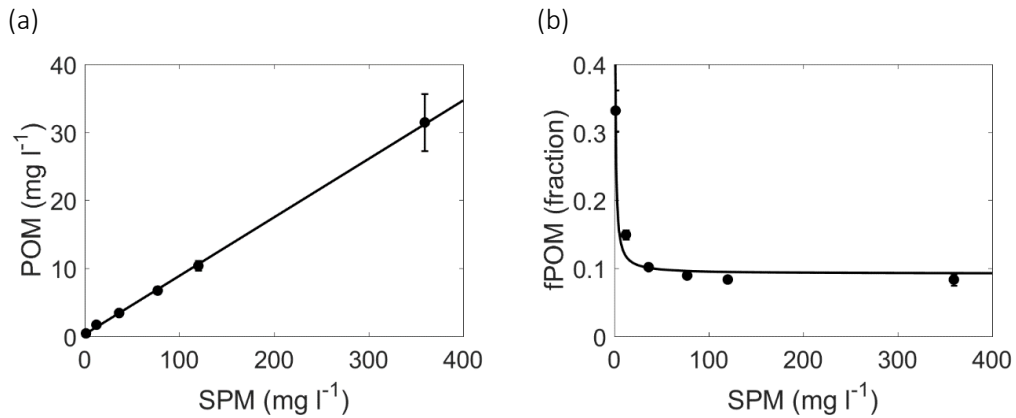
Figure 3.2: Correlation between (a) particulate organic matter (POM, mg l-1) and (b) fraction POM to total suspended particulate matter (SPM, mg l-1). See Table 3.2 for fitted line statistics. Dots represent the mean of 3 to 11 replicates of individual determinations. Error bars are 1 SE.

Feeding rates of pipis changed according to treatment (Figure 3.3); pipis cleared less particles and produced more pseudofaeces in accordance to the reduction in food quality and increase in quantity. Clearance rate declined from around 2000 ml h^{-1} to 500 ml h^{-1} between treatments of 0 mg l^{-1} and 10 mg l^{-1} and, likewise to fPOM, CR tend to stabilize above 70 mg l^{-1} at 191 ml h^{-1}. An inverse function explained 98% of the variance of this rate to SPM. Pipi rejected more pseudofaeces as suspended particulate concentration increased, with a pronounced increase in RR from background concentrations of SPM up to 70 mg l^{-1}, followed by a less change in RR with further increases in SPM, and was best explained by a logarithmic function. There was no pseudofaeces production in ambient concentrations and a maximum rejection rate of 15 mg h^{-1} was observed at the highest concentration treatment.

The proportion between particles filtered (FR) and particles rejected (RR), show high quantity of filtered material rejected as pseudofaeces above 30 mg l^{-1}, approximately 75% (fRR, Figure 3.3d). Filtration rate ranged from around 3 mg h^{-1} to 22 mg h^{-1} and correlated positively to increases in suspended particulates with response of FR best explained by a power function. Ingestion rate ranged from 2.6 mg h^{-1} to 6.5 mg h^{-1}, with rates nearly constant at around 3.5 mg l^{-1} from treatments 10 mg l^{-1} to 100 mg l^{-1}, as a result of increasing rates of filtered particles being rejected as pseudofaeces.

(a) (b) (c) (d) (e)
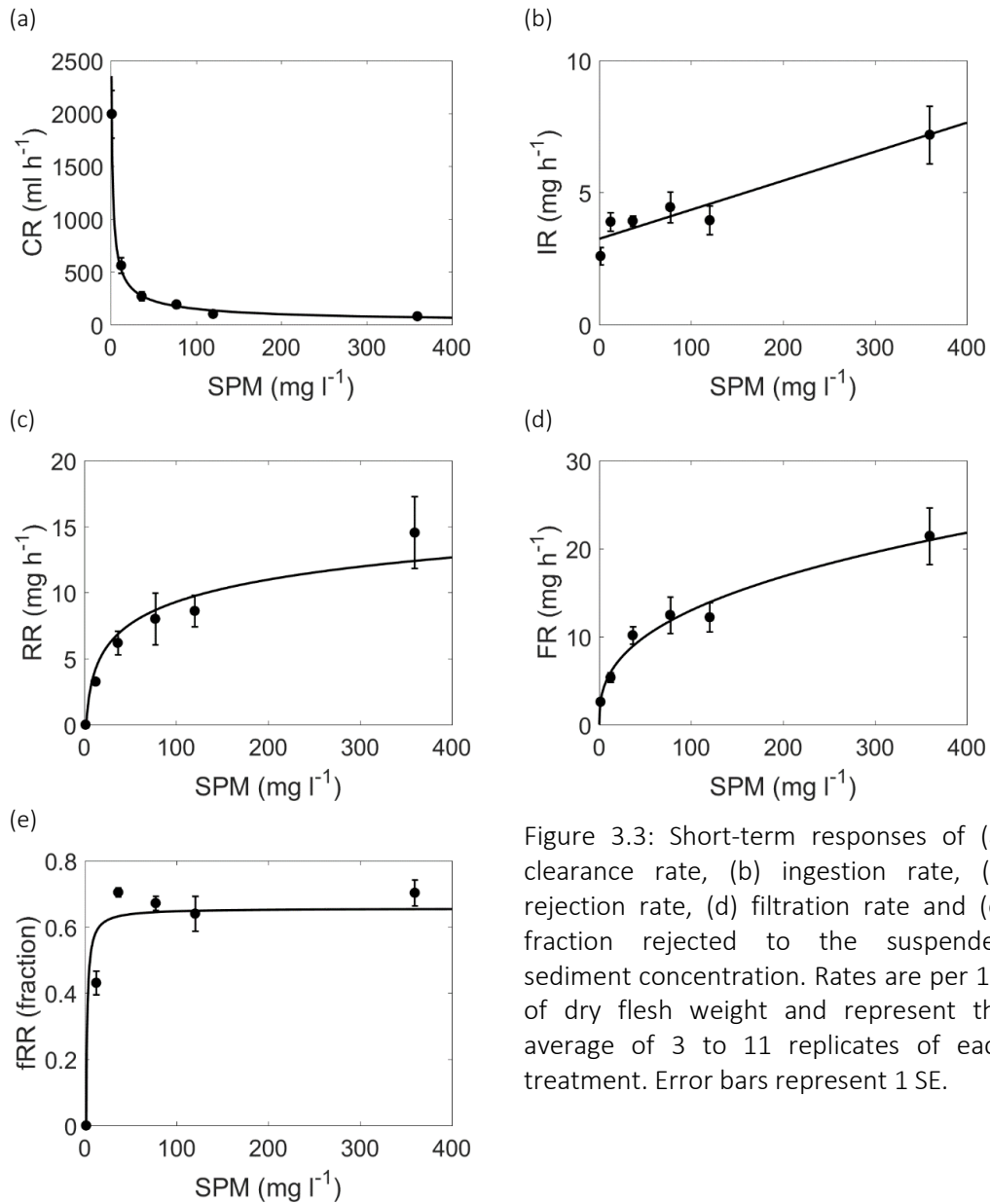
Figure 3.3: Short-term responses of (a) clearance rate, (b) ingestion rate, (c) rejection rate, (d) filtration rate and (e) fraction rejected to the suspended sediment concentration. Rates are per 1 g of dry flesh weight and represent the average of 3 to 11 replicates of each treatment. Error bars represent 1 SE.

Even though the organic content of the treatment decreased with increases in SPM concentration, the ingestion of organic particles increased as a result of the enrichment of ingested food through selective processes (Figure 3.4). Net organic ingestion rate (NOIR) was lower at treatments of 0 mg l^{-1} and 10 mg l^{-1}, but increased at concentrations above 30 mg l^{-1} and followed an asymptotic tendency. NOAR tend to increase linearly with SPM from 0.7 to 1.3 mg h^{-1} except at treatment of 10 mg l^{-1} when it reduced to 0.3 mg h^{-1}.

46

The organic content of ingested matter (OCI) was similar to the organic content (fPOM) for treatments 0 mg l^{-1} and 10 mg l^{-1} but higher than fPOM for concentrations above those limits. OCI was comparatively lower at 10 mg l^{-1}, probably because of low CR together with low production of pseudofaeces, so selective process did not substantially increase the organics ingested and absorbed compared with background concentrations. The higher proportion of organic particles present in the ingested matter compared to the fraction present in the treatments was confirmed by positive net organic selection efficiencies (NOSE); except for ambient concentrations when no selection occurred. Also for NOSE, treatment of 10 mg l^{-1} had a relatively lower efficiency in selecting organic particles, compared to efficiencies for treatments above that concentration, which tend to stabilize at around 2. Net absorption efficiency of ingested organics (NAEIO), calculated as the fraction between the organic absorption rates (NOAR) and the organic ingestion rates (NOIR) show that pipis absorbed organics more efficiently when feeding in suspended sediment concentrations at background levels (1.3 mg l^{-1}), and, following a decrease in NAEIO at 10 mg l^{-1}, efficiencies increased up to around 0.7 at 70 mg l^{-1} and showed an asymptotic tendency related to further increases in SPM concentrations.

(a)

(b)

(c)

(d)

(e)
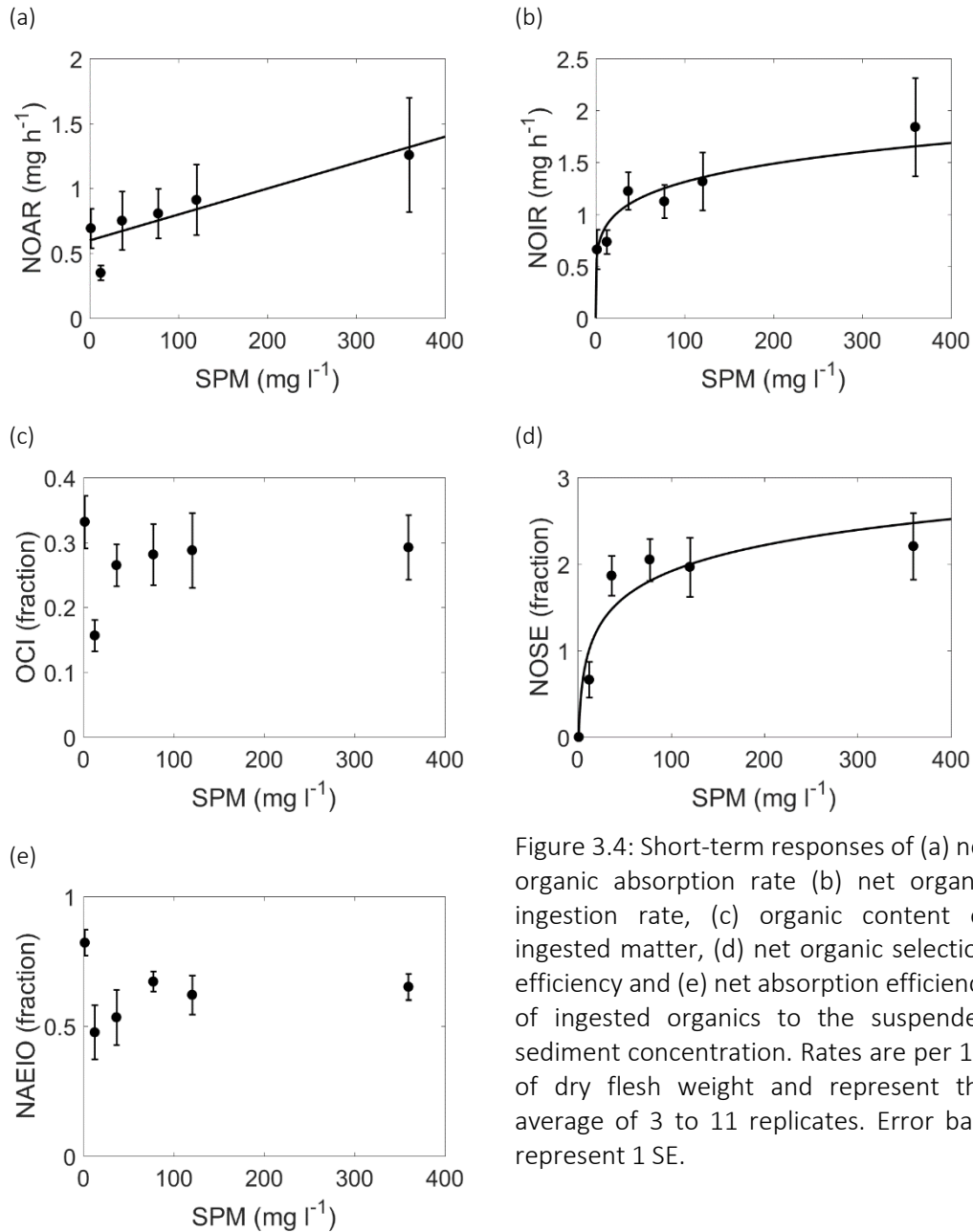
Figure 3.4: Short-term responses of (a) net organic absorption rate (b) net organic ingestion rate, (c) organic content of ingested matter, (d) net organic selection efficiency and (e) net absorption efficiency of ingested organics to the suspended sediment concentration. Rates are per 1 g of dry flesh weight and represent the average of 3 to 11 replicates. Error bars represent 1 SE.

3.4 DISCUSSION

This study aims to investigate the response of feeding behaviour of pipis (*Paphies australis*) to increases in suspended sediment concentration, from ambient (background) concentrations up to concentrations likely to be reached during dredging operations in ports and harbours. Pipis responded to increases in suspended sediment concentration by using two mechanisms, which are (1) the

reduction in clearance rates (CR) and (2) the increase in the rejection rate (RR). CR decreased sharply from background concentrations up to concentrations of 30 mg l^{-1} and did not change significantly with further increases in SPM, following the same curve pattern as for the variations in seston quality. Several species use the same strategy such as the infaunal bivalve *Mercenaria mercenaria* and *Cerastoderma edule*; however, higher thresholds were observed for those species. For example, CR reduced by around 50% at concentration of 40 mg l^{-1} for *M. mercenaria* and at 50 mg l^{-1} for *C. edule* (Bricelj and Malouf, 1984; Navarro and Widdows, 1997), while CR of pipis reduced by 75% at 10 mg l^{-1}. One study carried out with pipis and cockles (*Austrovenus stutchburyi*) (Hewitt and Norkko, 2007), show similar responses of CR for both species, but pipis were more sensitive to increases in SPM comparatively, and thresholds were higher than this study; for example, the reduction of 75% in CR was observed at an SPM around 500 mg l^{-1}. The higher thresholds could be due to the use of suspensions of sediment and algal monocultures (one single species of algae, *Isochrysis galbana*) which tend to show slightly different and higher responses in CR compared with natural seston (Jorgensen, 1996), and limit particle selection and consequently organic enrichment (Winter 1978).

Rejection rate (RR) followed a classic response described by a logarithmic curve (Bayne et al., 1993; Barillé et al., 1997) and is proportional to the rate of pseudofaeces production. Pseudofaeces were present in the chambers containing treatments of 10 mg l^{-1} and above, but were not observed at the low ambient concentrations, indicating that the threshold for pseudofaeces production occurs between those concentrations. This is similar to the range of 3 to 5 mg l^{-1} observed for some suspension-feeding bivalves feeding on natural seston, such as *Mytilus edulis* and *Crassostrea virginica* summarized in Bayne and Newell (1983) and around 10 mg l^{-1} for mussels in Maine, USA (Newell and Shumway, 1993). Similar pattern was observed for C. edule which did not produce pseudofaeces at the lowest experimental diet, about the same SPM as the zero-added sediment treatment in this study, and pseudofaeces were observed above concentrations of around 5 mg l^{-1} (Navarro and Widdows 1997).

Together with CR and RR, filtration rate (FR) altered to regulate ingestion rate (IR). FR increased with decreasing quality of suspended sediment, which kept IR near constant, at around 4 mg h^{-1}, operating to balance the particle intake independent of sediment concentration (Iglesias et al., 1998; Urrutia et al, 1997). There was an increase in IR for highest treatment related with increases in filtration rate at that concentration (Navarro and Widdows, 1997).

The reduction in clearance rates and production of pseudofaeces are correlated to the reduction in food quality (Gardner, 2002; Urrutia et al., 1997). Those mechanisms are commonly observed in bivalves feeding upon natural seston with low organic content (Hawkins et al 1998b; 1999). The fraction of organic particles decreased as seston concentration increased, from approximately 30% to 10%, as a result of resuspension of inorganic sediment causing the dilution of organic particles, described as a classic negative relationship for seston in coastal environments (Barillé et al, 1997; Hawkins et al 1996; 1998b; 1999; Navarro and Iglesias, 1993; Navarro and Widdows, 1997; Navarro et al, 1991; Ren et al, 2000; Wong and Cheung, 2001). While some species show preference for one of those mechanisms (Bricelj and Malouf, 1984), several others, such as the epifaunal *Placopecten magellanicus* and infaunal *Mya arenaria* bivalves (Bacon et al., 1998) and the infaunal *C. edule*, can regulate ingestion using both mechanisms (Navarro and Widdows, 1997), usually reflecting the treatment composition, i.e., regulation in CR when seston composition is of high organic content, and pseudofaeces production when exposed to low quality treatments (Iglesias et al, 1992; Navarro et al., 1992).

Pipis had optimal organic intake at low background concentrations but showed a capability of using adaptive mechanisms to increase the proportion of organic matter ingested comparable to the organic content in the treatments provided. The fraction of filtered particles rejected as pseudofaeces increased with decreasing organic content of treatments and tended to stabilize at around 60%, indicating relevant differential rejection of filtered particles by pipis. As a result, the organic content of ingested matter (OCI) increased up to approximately two-fold compared with the organic content of treatment (fPOM). Such enrichment of

ingested particles has been observed in several species of bivalves such as *P. magellanicus* and *M. arenaria* (Bacon et al, 1998), *Perna canaliculus* (Hawkins et al., 1999), *A. zelandica* (Hewitt and Pilditch, 2004) and *C. edule* (Navarro and Widdows, 1997; Urrutia et al., 1997) and results in positive selection efficiency (NOSE); except for ambient concentrations, when no selection occurred (organic content of treatment equals organic content of ingested particles). The fraction of material rejected observed for pipis was comparable to cockles *C. edule* (Navarro et al., 1994) and in the range found for *M. edulis* and *C. gigas* (Hawkins et al., 1998a).

The linear increase in NOAR with SPM suggests that pipis may be still gaining energy from the treatments even at the highest concentration tested. Since NOAR represents, ultimately, the energy available for bivalve physiological functions (Hawkins et al., 1998b), pipis may withstand higher suspended sediment loads. Similar trend in NOAR was reported in *Crassostrea belchen*, and it would possibly result in increased ingestion and faster growth (Hawkins et al., 1998b); however, increases in NOAR for *C. belchen* were in combination with no decline in CR, differently from CR of pipis in this study.

No major difference was observed in NOIR between ambient concentration and 10 mg l^{-1} and, similar to IR, NOIR tend to be stable at concentrations above thresholds for pseudofaeces production indicating also that ingestion of organics was balanced by filtration and rejection of organics. According to Navarro et al. (1992), the benefit of the selective process, which regulates ingestion of organics, is of keeping absorption rate proportional to the filtration rate of organics.

The rate of organics absorbed compared with the organics ingested are represented by NAEIO. Although NAEIO tends to balance the absorption efficiencies with increasing in SPM and dilution of food, it indicates that pipis were not as efficient in absorbing organics in treatments of concentrations above threshold for pseudofaeces production, as they were at background concentrations, which tends to be close to 100% (Møhlenberg and Riisgård, 1978). At treatments above 70 mg l^{-1}, NAEIO is kept nearly constant at around 60 to 70%, which is inside the range described for *M. edulis* (40% to 80%; Bayne and Newell, 1983; Navarro

et al., 1991) but considerably high compared with clam *M. mercenaria* (~20%; Bricelj and Malouf, 1984).

Despite being able to compensate for low organic content available in treatments of high SPM, asymptotic responses indicate limitation of benefits. Studies suggest that further increases in the duration and/or the seston concentration would result in overloading of the feeding apparatus limiting food acquisition and it is usually indicated by a sharp reduction in filtration and rejection rates (Barillé et al., 1997; Hawkins et al., 1999; Hewitt and Norkko, 2007; Navarro and Widdows, 1997; Wong and Cheung, 1999). Our study did not capture this overloading; however, stabilization of rates is indicative of such trend (Hawkins et al., 1998a). Thresholds occurred between concentrations of 30 mg l^{-1} and 70 mg l^{-1}, and, in general, levelled off above 70 mg l^{-1}, which suggested that pipis are not benefiting from the selective process above those limits, potentially resulting in reduced condition and biomass. The previous study on pipis shows a negative response in biomass at concentrations between 28 and 58 mg l^{-1}, for median and upper quartile concentrations, respectively (Hewitt and Norkko, 2007). For species of oyster, the optimal range is below 100 mg l^{-1} (Barillé et al., 1997), and between 300 and 350 mg l^{-1} for cockles (Hewitt and Norkko, 2007; Navarro and Widdows, 1997). Thresholds for mussels can vary from 150-200 mg l^{-1} (Hewitt and Pilditch, 2004) to 1000 mg l^{-1} (Hawkins et al 1999).

SPM from water samples (Cussioli et al., submitted) and turbidity records (converted to suspended sediment concentration using calibration coefficients, Table A.2), show that average SPM nearby pipi beds (No2 Front and Otumoetai sites - Figure 3.1) is approximately 5 mg l^{-1}. This concentration is in between the background concentration we tested in this study (~ 1.3 mg l^{-1}) and the concentration at which pipis produced pseudofaeces (~ 12.3 mg l^{-1}).

Suspended sediment concentration measured during maintenance dredging in 2014 reached 70 mg l^{-1} but decreased after two hours (Cussioli et al., 2015), which was the duration of our experiment. It is important to note that sediment from resuspension has more labile material, which is preferred over refractory

matter, usually present in dredging plumes, which is of low nutritional value (Hawkins et al, 1999).

Our findings suggest that *Paphies australis* is adapted to cope with short-term increases in suspended sediment concentration, which reduce the organic fraction available as food. By means of particle selection and rejection processes, organic content ingested was higher than available in treatments. Treatment concentrations from approximately 1 mg l^{-1} to 300 mg l^{-1} did not result in feeding constraints, usually resultant of overloading of feeding apparatus. However, absorption efficiencies of organics are lower for high SPM compared with low background concentrations. Furthermore, asymptote of rates indicate that pipis might not perform very well if concentrations and/or time of exposure to high SPM increase.

CHAPTER 4

USING PLUME FOOTPRINT SHAPE AS A VULNERABILITY INDEX FOR DREDGING IMPACTS IN A MESOTIDAL WELL-MIXED ESTUARY

Mariana Coppede Cussioli[1], Karin R. Bryan[1], Conrad A. Pilditch[1], Willem P. de Lange[1], Kai Bischof[2] (in preparation)

1. School of Science, University of Waikato, Hamilton 3240, New Zealand
2. Marine Botany, University of Bremen, Leobener Str. NW2, 28359 Bremen, Germany

ABSTRACT

Dredging is a recurrent activity in ports and harbours, which has the potential to generate turbid sediment plumes. These plumes can reduce light penetration and increase rates of sedimentation, affecting the surrounding marine flora and fauna. The scale of these plume footprints and its potential impacts can vary spatially and temporally in coastal systems. Here, we used a combination of field monitoring and numerical modelling to track the sediment plumes generated during the 2014 maintenance dredging in Tauranga Harbour, New Zealand. We proposed the use of an index of 'plume symmetry', which compares the length and width of plume footprints in defining vulnerability zones around dredging areas. The index showed that sediment deposition occurred predominately in the main direction of tidal currents. However, depending on the location of dredging, the secondary axis also had a relatively extended reach. Suspended sediment concentrations (TSS) in plumes was $\leq$ 70 mg l^{-1} and dissipated quickly. Soon after dredging ceased, concentrations decayed to ambient levels in less than two hours around dredging areas and within six hours further afield. Two groups of marine organisms were considered in the vulnerability zones that could be affected by dredging in Tauranga Harbour: seagrass *Zostera muelleri* and bivalve *Paphies Australis* (pipi). The Pipi showed indication of adverse effects in concentrations > 70 mg l^{-1}, whereas the seagrass may be affected in TSS > 20 mg l^{-1} in the intertidal zones if sustained over a two-week period. The maximum sediment deposition from dredging was 10 mm, which was restricted to the nearby dredging areas. For *Z. muelleri*, burial of 5 mm over a month did not reduce growth rates significantly. However, burial depths $\geq$ 10 mm combined with long-term exposure periods may reduce growth rates. A few studies address the decaying rates in perpendicular cross-sections of dredging plumes; however, this study shows that plume footprint can develop in different patterns, which have implications on ecological communities and sensitive ecosystems. This study filled the research gaps by providing an index, which can be used to determine vulnerability risk in estuaries.

4.1 INTRODUCTION

In ports and harbours, routine dredging activity is needed to maintain and deepen navigation channels. This can improve their economic viability by allowing larger ships (e.g. bulk cargo carriers) to transit safely and more frequently (Nichols et al 1990). Two forms of dredging campaigns are in use: capital dredging, which is the initial excavation and deepening of an area in a channel or harbour and maintenance dredging, which is carried out to remove material that is deposited over previously dredged areas, such as material transported by river flow, tidal currents and waves. Maintenance dredging is carried out periodically, the timescale of which varies depending on the location and local conditions (often from yearly to every five or ten years) (MEMG, 2003). Large-scale dredging programs, such as capital dredging, can have major impacts compared with maintenance dredging due to their increased time frame of disturbance and/or area covered (Lewis, 1976; Ridley Thomas et al., 1998).

Dredging can resuspend bed material in the water column and generate turbid plumes or 'plume footprints'. These footprints are governed by the surrounding hydrodynamics and water conditions, such as depth, temperature, salinity and sediment characteristics (Hitchcock and Bell, 2004). For example, the plume path is unidirectional in canals compared to oscillatory in coastal waters and estuaries (HR Wallingford Ltd and Dredging Research Ltd, 2003). These differences in flow direction will determine the footprint 'shape', which can be symmetric, i.e. the plume footprint and the dispersion/deposition characteristics are similar along the main and lateral axis directions. Alternatively, the plume can have one axis that is significantly more elongated (an asymmetrical plume).

The dredging footprint can change substantially with the type of dredging method. For example, the backhoe, clamshell, bucket, cutter suction and/or trailing suction hopper. For example, a trailing suction hopper dredge (TSHD) can increase turbidity by (1) disturbing sediments on the seabed around the draghead; (2) causing an overflow of surplus water at the surface to increase hopper capacity and (3) scouring the seabed with the main propellers and bow thrusters. Among these

56

mechanisms, the sediment released from overflow may be the most significant in creating plumes (HR Wallingford Ltd and Dredging Research Ltd, 2003).

The dynamics of dredging plumes can be characterized by three zones ('dredging', 'near field' and 'far field') and two phases ('dynamic' and 'passive'). The dredging zone is the area adjacent and immediately below the dredger where sediments and water are strongly mixed. This creates turbulence in the surrounding area and is known as the 'dynamic phase'. The near-field zone is where coarser particles settle to the bottom and fine particles form a passive plume that is advected by currents. This stage generally occurs within ten minutes after the overflow from the hopper enters the water. The second 'passive phase' occurs in the far-field zone, where only fine particles remain in suspension and are transported by currents until critical sedimentation thresholds are reached. Dredging-induced sediment plumes are usually of short duration after dredging ceases. High total suspended sediment (TSS) is mostly confined to the immediate area around the dredging vessel, which can range from 200 to 500 m and decay rapidly with time and distance (Close et al., 2013; Healy et al., 1999; Hitchcock and Drucker, 1996; Newell et al., 1998). The decay of (TSS) concentrations to background levels in the passive zone usually occurs within two to three hours (HR Wallingford Ltd and Dredging Research Ltd, 2003; Newell et al., 1998).

Suspended sediments caused by dredging and their potential impacts are a key concern for environmental managers. Increased concentrations of suspended matter can temporarily reduce water transparency (Davies-Colley and Smith, 2001) and increased rates of sedimentation (Wilber et al., 2005). This can affect marine flora and fauna, such as benthic populations (Newell et al., 1998), various fish species (Wilber and Clarke, 2001) and seagrasses (Erftemeijer and Lewis, 2006; Onuf, 1994). For example, the deposition of suspended sediment can also change the seabed sediment characteristics and smother benthic biota (Cooper et al., 2011; Hendrick et al., 2016; Newell et al., 1998). A significant group of benthic macrofauna organisms that can be impacted by dredging is represented by suspension-feeding bivalves (Asmus and Asmus, 1993). These organisms play an important role in the processes between benthos and the water column by

removing particles from the water, increasing light availability for effective photosynthesis of benthic plants (e.g. seagrasses and microphytobenthos) (Newell, 2004; Newell and Koch, 2004) and producing fluxes of bio-deposits for benthic - pelagic coupling (Dame 1993). They are directly affected by variations in suspended sediment concentration (see reviews by Bayne, 1993; Bayne and Newell, 1983) and use adaptive mechanisms as a response to increased turbidity to maintain their feeding activity (e.g. closure of valves, reduction of clearance rate or selection of organic material by rejecting inorganic particles) (Hawkins et al., 1996; Navarro and Widdows, 1997; Urrutia et al., 1997).

Probably the most sensitive plant to dredging is marine seagrasses, and so maintaining water quality is vital for their health and productivity. They provide a range of ecosystem services, including a habitat for a range of organisms, carbon sequestration, nitrogen fixation and have been valued at $1.9 trillion per year in the form of nutrient cycling (Barbier, et al., 2011; Eyre and Ferguson, 2002; Fourqurean et al., 2012; Ruiz-Frau et al., 2017; Waycott et al., 2009). Seagrass areas are being lost worldwide mainly due to the reduction in water quality (Duarte, 2002). Elevated suspended sediment concentration can alter growth, morphology and below ground biomass (Longstaff et al., 1999; Waycott et al., 2005), increase patchiness of meadows (Abal et al., 1994) and if persistent, cause mortality Longstaff, 2003). Smothering of seagrass beds due to sediment deposition after dredging is also of concern. Although an overview of critical thresholds for sedimentation is presented in Erftemeijer and Lewis (2006), general thresholds and tipping points are still hard to define due to species and environmental variability.

Whether dredging impacts on estuarine ecosystems depends on the spatial and temporal scale of the plume, and so improving our understanding of dredge plume dynamics and dispersal will facilitate improvements to predictive models for dredge operation planning and thus reduce environmental impacts. Several analytical models have been developed to predict the spatial extent and concentration of sediment plumes: 2D models which assume sediment settling velocity based on Stokes' law (Kuo et al., 1985; Kuo and Hayes, 1991) and refinements of these models which adopt flocculation settling formulations (Je and

Hayes, 2004; Je et al., 2007), usually based on the assumption of plume steady state. More recently, a transient version has been developed, although still incorporating only a mean tidal current velocity (Shao et al., 2015). These simplified analytical models can be used to simulate worst-case scenarios when dredging operation requires a rapid assessment on potential impacts; however, in terms of environmental implication, variations in tidal current velocity and tide induced fluctuations in turbidity are critical for assessing impacts on sensitive areas (Shao et al., 2015) and thus, the use of more complex models has become necessary in applied environmental management approaches.

Various published studies on monitoring of dredging plumes (Duclos et al., 2013; Kuo and Hayes, 1991; Kuo et al., 1985; Nichols et al., 1990) have focused on plume fate and decay in the main direction of plume transport, assuming that the dominant plume path causes the main threat to the local ecosystem. However, depending on tidal currents (e.g. low velocities during slack tide), water column stratification (e.g. gradient of temperature and density between surface and bottom) and location of dredged area (e.g. at the divergence point of two perpendicular channels) plume footprint can develop in a less elongated, circular or elliptic pattern (Goodwin and Michaelis, 1984; Seo et al., 2018). The change in plume footprint has implications on ecological communities and sensitive ecosystems susceptible to adverse impact located around the dredging area, increasing the relevance of considering the plume area as whole. Extensive measurements of plume dispersal can only be found in unpublished reports or documents of restricted access and little is known about decaying rates in perpendicular cross-sections of plume for different types of estuaries.

Here, we propose the development of an index of plume symmetry which quantifies the relative length and width of plume footprint with the aim of defining vulnerability zones (e.g. areas in proximity to a slow decay (far field) plume vs. a high decay (near field) plume). Given the high frequency of maintenance dredging globally and the similarities of dredging methods, our methodology of plume monitoring and plume analysis is applicable to a variety of vulnerable estuaries.

To meet our objectives, we used a combination of field monitoring and numerical modelling to track sediment plumes created during maintenance dredging in Tauranga Harbour, New Zealand, to describe their development with time and distance from the dredging area. We used field data to calibrate and validate a numerical model and simulated scenarios of dredging activities in different hydrodynamics conditions. We used model results of sediment deposition to calculate decay rates and plume footprint symmetry to identify critical areas inside the harbour. Finally, results of suspended sediment concentration and sediment deposition were compared with thresholds for impacts for sensitive species of seagrass and shellfish.

4.2 METHODS

4.2.1 Study Area

Tauranga Harbour is located at 37˚40'S and 176˚10'E, on the east coast of New Zealand's North Island. This estuarine lagoon comprises an area of about 200 km^2 (Park, 2004), mainly characterised by intertidal sandflats (Park, 2004), with an average depth at low tide of 3 m (Tay et al., 2012). Tides in the Harbour are semi-diurnal with amplitudes of 1.62 m and 1.24 m for spring and neap tide, respectively (Heath, 1985). The harbour is separated into two main areas, the northern and the southern basins and has two tidal inlets, one at each end of Matakana Island. The southern inlet (shown in Figure 4.1) is important for navigation, characterized by shipping channels and adjacent to the rocky headland of Mt. Maunganui, where it is also the entrance to the Port of Tauranga (Davies-Colley and Healy, 1978).

The Port of Tauranga is the largest export port in New Zealand. It was officially established in 1873 and dredging activities at the port occurred from 1968 until 1978, restarting in 1991, aiming at deepening and widening of the shipping channels. Channels inside the harbour were deepened from 10.0 m to 12.9 m during capital dredging in 1992 and from 12.9 m to 16.0 m in the 2015/2016 capital dredging campaign. The entrance channel was deepened to 14.1 m and to 17.4 m during those capital dredging campaigns (Ramli, 2016). Maintenance dredging was

60

carried out approximately every two years since 1992 (Sinner et al., 2011) and annually more recently.
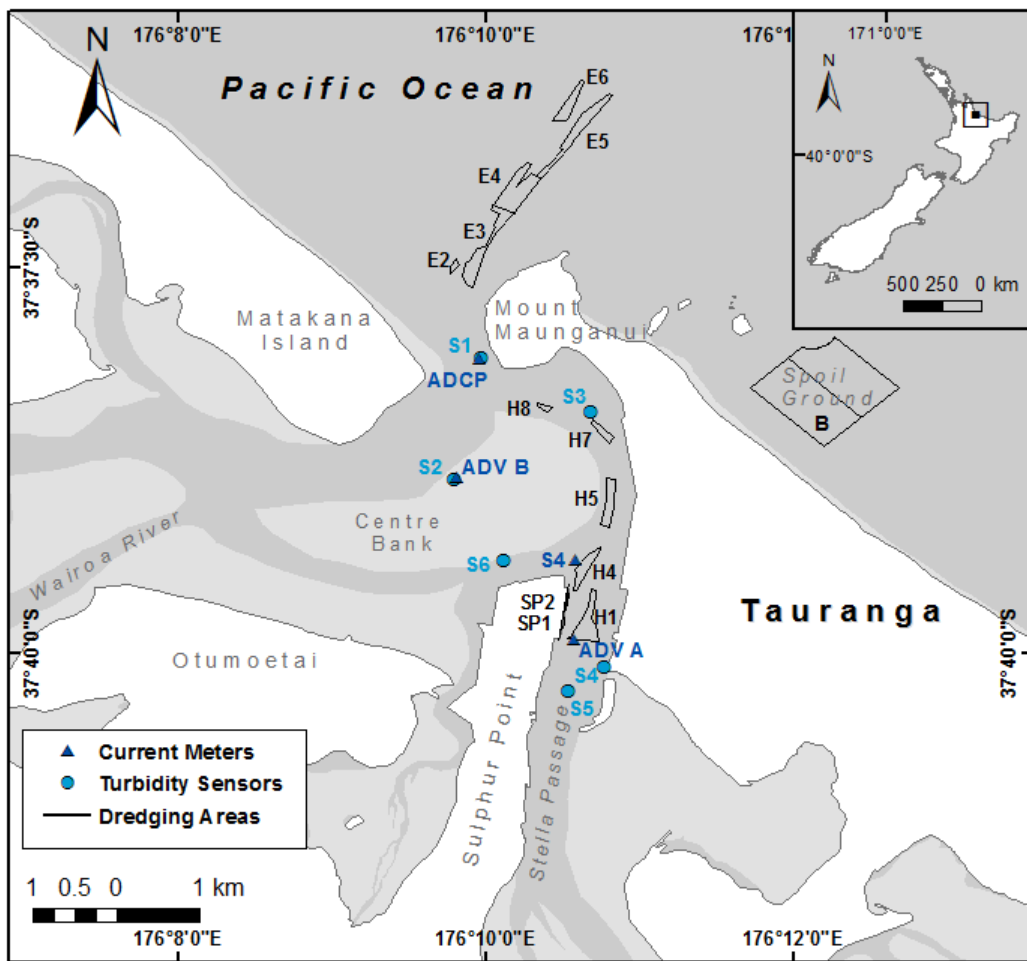
Figure 4.1: Map of study area, Tauranga Harbour, and position of current meters and turbidity sensors. Dredging and dumping (Spoil Ground) areas outlined with black polygons correspond to the location of dredging/dumping cycles monitored in this study. Light grey areas correspond to the intertidal zone.

4.2.2 Tracking the plumes generated during dredging activities

We monitored the sediment plumes caused by maintenance dredging in Tauranga Harbour, New Zealand, between 13th and 16th October 2014. Dredging was carried out using the trailing suction hopper dredge (TSHD) "Pelican" (Van Oord) which is 63 m long, 11 m wide and the draft is 3.7 m when loaded. It has a hopper capacity of 965 m³.

Each dredging cycle is divided in four steps: sailing empty (from disposal area), loading, sailing loaded (to disposal area), and dumping. The sailing time to and from the discharge sites was usually between 20 and 50 minutes, loading times ranged from 25 to 70 minutes, and dumping duration was usually 5 minutes. We tracked six plumes generated during the loading phase of the dredging cycle and one plume generated during dumping. An average of 630 m^3 of material was dredged in monitored loads and sediment was mainly composed of sand. Dredging and dumping sampling times are listed in Table 4.1. Monitored dredged areas are located at the entrance of the harbour (E5), Sulphur Point (H4 and SP1), Stella Passage (H1), Maunganui Roads (H7), and dumping area is at the polygon labelled B (Figure 4.1).

Table 4.1: Sampling times and dredging/dumping specifications. Sampling was carried out before (background), during and after dredging. Times are in New Zealand Standard Time (NZST).

Date	13/10/2014	14/10/2014	14/10/2014	15/10/2014	15/10/2014	15/10/2014	16/10/2014
Dredging/Dumping Areas	E5	H4	SP1	H1_1	H7	H1_2	Dump B
Background Sampling							
CTD	14:11	07:03	12:50	07:13	09:45	12:16	10:33
Water surface	14:23	07:07	12:54	07:25	09:52	12:17	10:37
Water mid-depth	14:19	07:01	12:52	07:22	09:50	12:16	10:33
Water bottom	14:15	07:00	12:49	07:20	09:48	12:14	10:31
ADCP Transects	14:32–14:46	7:11–7:14	12:44–13:52	07:21–07:59	09:49–10:10	12:18–12:33	10:34–10:43
Plume Sampling							
Tide during sampling	ebb	flood	ebb	flood	flood	high/ebb	flood
ADCP Transects	14:48–15:33	07:19–09:10	13:52–15:04	08:15–09:36	10:11–11:42	12:34–14:28	10:45–11:56
Water surface	15:03	07:31 / 08:12[a]	13:50	08:30	10:28	12:45	10:50
Water mid-depth	15:00	07:32 / 08:14[a]	13:53	08:31	10:30	12:43	10:52
Water bottom	14:59	07:34 / 08:16[a]	14:03	08:35 / 08:48[a]	10:35	12:41	10:54
CTD	15:33	09:04	14:58	09:37	11:27	14:28	11:52
Dredging/Dumping Specifications							
Dredging/Dumping times	14:25–15:15	07:00–08:10	13:50–14:15	08:15–08:45	10:05–11:05	12:25–13:15[b]	10:45–10:50
Volume dredged/dumped [c]	560 m³	600 m³	1116 t (587 m³)	1283 t (675 m³)	720 m³	625 m³	751 m³

a: Second sampling
b: Dredging time was reduced to 30 minutes following an operational delay of 20 minutes
c: Volume in brackets were calculated using hopper density of 1900 kg m^{-3}

Given the transient nature of dredge plumes (which can disperse rapidly both vertically in the water column, and transversely across the harbour), past sampling technologies for suspended sediments, such as pump and bottle samples, are limited in their ability to provide high spatial and temporal resolution data (Puckette, 1998; Reine et al., 2002). The use of acoustic technologies to measure suspended sediment concentration is an advance over the use of point sample measurements (Gartner, 2004; Hoitink and Hoekstra, 2005; Holdaway et al., 1999; Smith and Friedrichs, 2011), improving understanding of dredging plume dynamics (Cutroneo et al 2012; Cutroneo et al., 2013; Hitchcock and Bell, 2004; HR Wallingford Ltd and Dredging Research Ltd, 2003; Puckette, 1998; Reine et al., 2002; Tubman and Corson, 2000), and providing reliable validation data for numerical models (Shao et al., 2015).

We measured backscatter signals using a boat-mounted acoustic Doppler current profiler – ADCP (Workhorse Teledyne RD Instruments 1200 kHz) based on the method developed in Flaim (2012). Acoustic backscatter is proportional to the concentration of suspended particles in the water and so can be used to detect the plumes. A total of 318 transects were carried out during monitoring. Transects along and across the main current direction were made immediately before each dredging monitoring to determine background values, and during and after dredging until the plume signal declined to background levels or until time or technical limits were imposed. Temperature and salinity were measured using a CTD (SBE 19plus V2 SeaCAT) and casts carried out before dredging and at the end of each monitoring period. Water samples for total suspended solids (TSS) analysis were collected at the surface, mid-depth and bottom using a Schindler-Patalas trap. TSS was determined by filtering known volumes of water onto pre-rinsed and pre-weighed 47-mm GF/C filters, and dried at 105 ˚C until constant weight (minimum 18 hours) and weight recorded. The total TSS (mg l^{-1}) is given by the difference between the weight of the filter after and before filtering (APHA, 1997). Additionally, we pumped water directly from the dredging plumes into 20-l buckets and where sediments were naturally settled in laboratory until enough

accumulated to estimate particle size distribution using MALVERN Mastersizer 2000. Grain size class was described according to Wentworth (1922).

4.2.3 Calibration of ADCP using TSS samples

ADCP data were processed using WinRiver software and MATLAB. For conversion of ADCP backscatter to TSS, we extracted the maximum signal at each depth (since this should be the signal of the plume) along each transects, where water sampling was concurrently conducted (selected by date and time). This resulted in a depth-varying profile of maximum backscatter signal, corresponding to the plume. ADCP record at depths corresponding to the depths of TSS sampling were paired and plotted. Due to the ephemeral and patchy nature of dredging plumes, it was difficult to match water sampling depths and times with peak ADCP signals; therefore, outliers were selected by visual inspection and excluded manually, based on field notes on plume position and differences in sampling time. Calibration coefficients were determined by selecting the best-fit curve (Figure 4.2) and backscatter data (dB) was converted to suspended sediment concentration (TSS) using the resulting equation (r^2 = 0.72, n=23):

$$TSS = 0.0376 \times \exp(0.0622 \times ADCP_{db}) \qquad \text{Equation (1)}$$
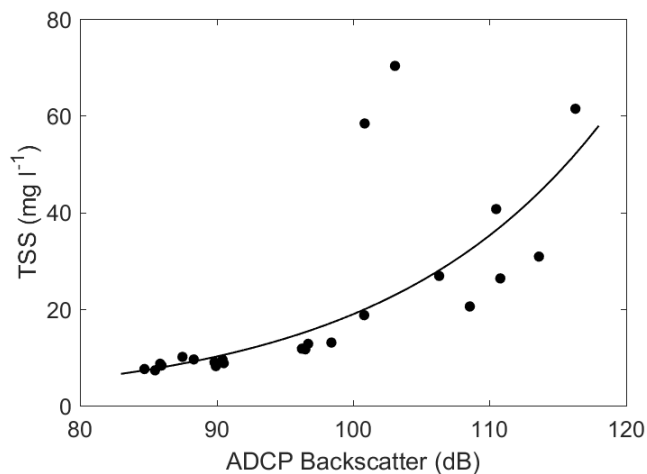
Figure 4.2: Correlation between ADCP backscatter signal (dB) and TSS (mg l^{-1}). Solid line represents the line of best fit.

4.2.4 Numerical model

Model Description

We modelled the hydrodynamics and the transport of suspended sediment plumes in the southern Tauranga Harbour using Delft3D (modules FLOW and SED) developed by Deltares. Delft3D-FLOW simulates the hydrodynamics by solving the non-steady shallow water flow and transport equations on a rectilinear or a curvilinear grid, forced by tide and meteorological conditions at the open boundaries. Delft3D-SED simulates the transport of cohesive and non-cohesive sediments. Transport of sediments is calculated similarly to the transport of other conservative constituents, by solving the three-dimensional advection-diffusion equation for the suspended sediment, considering sediment-type specific formulation of settling velocity, sedimentation and erosion parameters. The sediment transport simulation uses the Delft3D-FLOW module results as input and accounts for processes of critical importance such as the exchange of sediment at the bed-flow boundary layer, including the feedback on hydrodynamics from changes in bathymetry and vice-versa.

Domain, Bathymetry and Boundary Conditions

Simulations were carried out using an existing calibrated hydrodynamic model setup (Watson, 2016) and validated for the period of field campaign carried out in this study. The model used a depth averaged (2D), 20 x 20 m grid, with bathymetry prepared using a combination of data from multiple sources: multibeam, LiDAR (Light Detection and Ranging), LINZ hydrological charts NZ 5411 and NZ 5412. Depths were then compared with field data (water levels recording using the ADV deployments described below) and corrected accordingly.

The hydrodynamic model was forced by water levels at two open ocean boundaries outside the harbour (north and east). Water levels were determined by amplitude and phase of major tidal constituents extracted from field data (Table D.1). The model setup also included ten discharge points representing the main rivers and freshwater input into southern Tauranga Harbour (Table D.2). Discharge volumes were constant throughout simulations. A summary of model parameters

66

used in the hydrodynamic simulations are listed in Table D.3. More detailed description of model setup in Watson (2016).

Validation of hydrodynamic model for period of study

During the fieldwork campaign, we deployed two ADVs (SonTek Triton) and a S4 current meter (InterOcean Inc) at three locations around the study area (Figure 4.1) from the 13th to the 17th October 2014. Current speed and direction and water level were used to validate the hydrodynamic model prepared by Watson (2016) for the dates of our field campaign. We also used data measured by an ADCP deployed in the entrance of the harbour, provided by the Port of Tauranga. The ADVs sampled data every 5 minutes, the S4 sampled at 2 Hz for 2 minutes every 10 minutes, and the ADCP (at the entrance channel) sampled every 2 minutes. We calculated current speed and direction from U and V velocities, and direction was corrected for magnetic declination, which was 20˚13' for Tauranga Harbour in 2014 (calculated using the Magnetic Field Calculator tool at https://www.ngdc.noaa.gov/geomag-web/#declination). Pressure was converted to water depth using MATLAB Seawater toolbox (SW_DPTH).

We simulated the hydrodynamics over the period of field campaign and compared model results against field data, visually and statistically, to validate the model. Statistical analyses (bias, accuracy and skill) were based on Sutherland et al. (2004) (APPENDIX E).

Dredging plume model setup for calibration

To simulate the dredging plumes in Delft3D, we used input plume sediments using discharge points located in the dredging areas shown in Figure 4.1. We assumed zero initial sediment layer thickness at the bed and no initial suspended sediments, and no input sediments at boundaries and from rivers/streams; therefore, dredging provides the only source of suspended sediments into the model.

The 2014 maintenance dredging was carried out using a trailing suction hopper dredge (TSHD). This dredger can generate sediment plumes through two main mechanisms: resuspending bottom sediments during excavation and suction

caused by the draghead, and caused by the overflow, which consists in the excess of water discarded to increase hopper capacity, usually at the surface and composed mostly of fine sediments. Because the draghead is at the seabed when dredging, a large proportion of resuspended material deposits in the immediate surroundings, particularly when sediment is mostly sandy, which was the case in the plumes monitored here. Therefore, we did not consider this source of sediment in the model. We considered the overflow as the main source of plumes in the model setup and chose cohesive as the type of sediment to be modelled, with specific density of 2650 kg m^{-3} and settling velocity of 0.3 mm s^{-1}, for silt settling velocity in saline water.

Discharge flow (m^3 s^{-1}) was calculated based on loading time, total volume dredged and concentration of sediments in the overflow. Loading time and volumes are presented in Table 4.1. For total dredged in tons, we used a density in the hopper of 1900 kg m^{-3} based on the main sediment type present in the hopper (Vlasblom, 2007) and estimated volumes (values in brackets, Table 4.1). We considered that 30% of the total volume dredged would be in the overflow. Concentration at the discharge point was set to 300 kg m^{-3} based on model calibration (detailed below).

TSS calibration/validation of sediment model

We simulated the loading cycles of monitored dredging activities and compared modelled suspended sediment concentration to TSS (converted from ADCP backscatter data). Due to limitation in the grid size, we simulated only dredging activities inside the harbour (H4, SP1, H1_1, H7, and H1_2, Table 4.1). Representative transects carried out during monitoring of the plumes generated during the above dredging cycles were selected to represent plumes at the beginning, during and after dredging. A description of other transects is provided in APPENDIX C.

ADCP transects were integrated over depth resulting in a 2D length/time-varying TSS line. Model results were extracted at the same position and time of ADCP transects and maximum concentration of predictions and observations were calculated and plotted (Figure 4.3). Bias, accuracy and skill (based on Sutherland et

68

al. (2004)) were also calculated to verify model results (Table 4.4).

Dredging Simulations Scenarios

A total of six dredging scenarios were carried out: (1) dredging during flood tide and (2) during ebb tide, both in area H1; (3) dredging during flood tide and (4) during ebb tide, both in area H4; (5) All loading cycles that occurred in the time frame of field campaign, inside the harbour and at the entrance channel (including cycles not monitored); and (6) loading cycles that occurred in the time frame of field campaign, inside the harbour (excluding dredging at the entrance channel).

Dredging events (1) to (4) were given a hypothetical flow rate of 0.2 m^3 s^{-1} based on a 1-hour loading time of a dredger with hopper capacity of around 2000 m^3, similar to the TSHD used during the 2015/2016 capital dredging campaign in Tauranga Harbour. Those simulations were set up to provide insights into dredging under different tidal conditions in terms of the effect on plume footprint and dispersal time. Due to the proximity of seagrass and shellfish beds, dredging activities in both areas (H1 and H4) could be of potential pressure to those ecosystems. Scenarios (5) and (6) were chosen to investigate the plume footprint and sediment deposition of successive dredging activities (e.g. cumulative effects). Flow rates at each dredging area simulated in scenarios (5) and (6) are listed in APPENDIX F. Initial concentration at the discharge point for all scenarios was 300 kg m^{-3}.

4.2.5 Decay coefficients and Index of plume symmetry

The decay coefficients of plume footprint were calculated fitting an exponential curve to sediment deposition results from model simulation (1) to (4); using the exponential equation:

$$D = Ds \times \exp^{-kx}$$
<div align="right">Equation (2)</div>

where D is the sediment deposition (mm), Ds is the sediment deposition in a longitudinal or cross-section, -k is the decay coefficient and x is the section length (m). The position of each section is shown in Figure 4.6a. These transects were

chosen in order to quantify deposition along the main and secondary plume axis. The index of symmetry was then calculated as the ratio between the main axis decay coefficient (N-S) and secondary decay coefficients (W-E1, W-E2 and W-E3):

4.3 RESULTS

4.3.1 Tracking the plumes

Temperature, salinity and suspended sediment concentration

Temperature and salinity were in average 15.3 °C and 34.3, respectively (n=28, SD=0.7). There was usually no vertical gradient in temperature and salinity, and no marked difference between casts carried out before and after dredging. Occasionally, temperature was slightly higher at the surface (by approx. 1 °C) and salinity slightly higher at the bottom (by 1 ppt) (Table 4.2).

Table 4.2: Temperature and salinity recorded before (and after) dredging/dumping at each area monitored.

Date Dredging/ Dumping Areas	13/10/14 E5	14/10/14 H4	14/10/14 SP1	15/10/14 H1_1	15/10/14 H7	15/10/14 H1_2	16/10/14 Dump B
Temperature (°C)							
Surface	14.83 (14.93)	16.79 (15.96)	14.95 (16.43)	16.61 (16.01)	14.87 (14.63)	15.23 (15.44)	15.24 (15.61)
Bottom	14.77 (14.75)	15.81 (14.77)	14.8 (15.7)	15.65 (15.42)	14.36 (14.4)	14.56 (15.19)	14.75 (14.82)
Salinity							
Surface	34.83 (34.77)	32.2 (33.62)	34.67 (33.77)	32.34 (33.32)	34.54 (34.81)	34.38 (34.54)	34.74 (34.77)
Bottom	34.84 (34.84)	34.02 (34.68)	34.77 (34.28)	33.98 (33.78)	34.77 (34.97)	34.9 (34.62)	34.93 (34.9)

Background concentrations inside the harbour determined by water samples ranged from 7 to 9 mg l^{-1} at the surface, 7 to 9.5 mg l^{-1} at mid-depth and 8 to 13 mg l^{-1} at the bottom. Outside the harbour, at the Dump B, background TSS was lower, 4 mg l^{-1} at the surface and 6 mg l^{-1} at mid-depth and bottom. According to the

dredging reports (*pers. comm.* Port Engineering) all dredged material was classified as sand. Grain size analysis of the sediment deposited in the buckets (and three samples from plume collected in water bottles) usually had a bimodal distribution. A potential source of secondary peaks is the growth of organic material in buckets that were settling for a long period. The results indicate that 90% of the material in background samples and plume samples was finer than medium sand and 10% finer than medium silt (background) and fine silt (plume) (Table 4.3). The sand fraction could potentially be underestimated due to rapid settling and not being collected by sampler.

Table 4.3: Particle size (µm) distribution from samples collected before (background) and during/after (plume) dredging for each dredging/dumping cycle monitored. Sediment samples are from water pumped into buckets or from water samples stored in bottles for TSS analysis. d(0.1) represents the fraction of 10% of the cumulative curve of sediment distribution, d(0.5) represents 50% and d(0.9) represents 90%.

Date Dredging/Dumping Areas	Sample	d(0.1)	d(0.5)	d(0.9)
13/10/2014 – E5	Background (bucket)	7.95	71.98	213.31
	Plume (bucket)	9.97	90.61	224.17
14/10/2014 – H4	Background (bucket)	6.03	26.08	115.13
	Plume (bucket)	5.93	35.82	184.00
	Plume (Water Sample - bottle)	4.93	29.50	148.72
	Plume (Water Sample - bottle)	4.88	37.04	207.92
15/10/2014 – H1_1	Background (bucket)	9.74	143.18	412.95
	Plume (bucket)	5.55	35.64	277.64
	Plume (Water Sample - bottle)	4.93	41.02	334.58
15/10/2014 – H7	Background (bucket)	27.74	126.07	324.14
	Plume (bucket)	10.61	118.59	300.14
15/10/2014 – H1_2	Background (bucket)	21.50	215.44	457.29
	Plume (bucket)	5.67	27.56	185.16
16/10/2014 – Dump B	Background (bucket)	8.33	70.24	341.11
	Plume (bucket)	5.99	31.31	232.59

During dredging, TSS was slightly higher than background, however, plumes generated during dredging in H1 and H4 show a significant increase in TSS comparted with background, reaching concentrations up to 70 mg l^{-1}; e.g. in H4, TSS increased from approximately 8, 7 and 8 to 61, 31 and 27 mg l^{-1} at the surface, mid-depth and the bottom, respectively. After 45 minutes, plume signal is still

present in the TSS results, but higher concentration at mid-depths possibly show plume descending movement; concentration decreased to 26 mg l^{-1} at the surface, but increased to 58 mg l^{-1} at mid-depth and was slightly lower, 21 mg l^{-1}, at the bottom. Particle size analysis of suspended sediment of plumes monitored also had bimodal distribution with d(0.5) ranging from 22 μm and 119 μm. Samples from H7 and E5 were classified as very fine sand and other samples were between medium and coarse silt.

ADCP transects (TSS)

We carried out from one to eleven transects to determine background conditions before each monitoring. Those transects were averaged in length/time resulting in one depth-varying profile of background TSS for each dredging event which was subtracted from TSS of transects carried out during and after dredging. Background TSS from transects was in average 7 mg l^{-1} and usually highest at the surface (<2 m depth). Lowest background TSS was at the dumping ground, Dump B (5 mg l^{-1}) and highest at E5 (10 mg l^{-1}), possibly because dredging had already commenced when measurements took place; although transects to measure background signal were carried out upstream of dredging area.

In general, transects during and after dredging could detect an initial plume, with highest concentrations at the surface (< 3 m). Highest TSS (from ADCP backscatter signal) was 61 mg l^{-1} above background at Dump B site, but subsequent transects show that peak of TSS had a short duration; H4 also presented one of the highest TSS, max of ~ 55 mg l^{-1} above background with TSS decreasing gradually to background. Following transects in all areas monitored showed sediment settling as evidenced by the gradient of decreasing TSS toward the bottom. When possible to collect them, transects carried out one to two hours after dredging ceased show that TSS had reduced to background levels within dredging areas and surroundings. Detailed description of relevant transects for each dredging area monitored is in Appendix I.

4.3.2 Model validation (hydrodynamics)

Plots of measured versus modelled current speed, direction and water level are shown in Figure E.1 to Figure E.4 (APPENDIX E). Locations of validations points are provided in Figure 4.1. Water level was only measured at ADV A and ADV B. Comparing plots visually, model satisfactorily predicted those parameters. Water levels were accurately predicted, presenting a minor over prediction in the ebb tide, more pronounced in ADV A. Modelled current speed was under predicted at the location of the ADCP, but the model was able to predict the difference between tidal currents (ebb vs flood current speed). Currents at ADV B presented only a slight over prediction of minimum values and there was a phase lag in currents during flood tide at ADV A. The S4 current meter showed the largest divergences in current speed with model under predicting magnitudes.

Evaluation of model predictions using statistical analyses are shown in Table 4.4. The model showed high level of skill (except for speed recorded by the S4 and level at ADV B). Values were above 0.5, which is classified as 'excellent' in the scheme proposed by Sutherland et al. (2004). BSS for water level at ADV B was just slight below that threshold, 0.48, which is considered 'good'. Therefore, the model predicts the hydrodynamic conditions around those locations with confidence. The lowest BSS was for S4 current speed (0.03) considered to be 'poor'. Because S4 was deployed at the divergence of two navigational channels (Stella Passage and towards S6), it is more likely to present larger discrepancies in current speed and direction. Also, the 2D model may not represent the vertical structure of currents governed by the changes in bathymetry.

Model predictions usually underestimated current speed and water level, indicated by negative bias. The exception was at ADV A where model over predicted current speed by 0.06 m. The highest bias in the mean between modelled and observed current speed was 0.23 m s^{-1} at ADCP. MAE ranged from 0.04 m s^{-1} to 0.23 m s^{-1} for current speed, 16° to 40° for current direction and it was below 0.2 m for water level. RMSE was higher than MAE as expected since the presence of outliers is increased in RMSE calculations.

Table 4.4: Statistical parameters calculated to evaluate the hydrodynamic model at location of current meters deployed during field campaign, and the maximum suspended sediment concentrations (TSS) of measured and simulated dredging plumes at several transect locations.

		Bias	MAE	RMSE	BSS
Speed		**(m s^{-1})**	**(m s^{-1})**	**(m s^{-1})**	
	ADCP	-0.23	0.23	0.27	0.76
	ADV B	-0.01	0.04	0.05	0.91
	S4	-0.08	0.11	0.13	0.03
	ADV A	0.06	0.07	0.09	0.67
Direction		**(˚)**	**(˚)**	**(˚)**	
	ADCP	10.30	21.11	32.58	0.81
	ADV B	9.25	16.03	50.71	0.64
	S4	12.46	40.06	64.66	0.59
	ADV A	10.01	27.63	56.85	0.64
Level		**(m)**	**(m)**	**(m)**	
	ADV B	-0.05	0.14	0.42	0.48
	ADV A	-0.17	0.17	0.18	0.87
TSS		**(mg l^{-1})**	**(mg l^{-1})**	**(mg l^{-1})**	
	Plume	0.23	3.02	4.00	0.66

4.3.3 Model validation (dredging plumes)

A total of 66 transects carried out during and after dredging at H4, SP1, H1, H7, and H12 were chosen to verify the dredging plume simulations. Figure 4.3 show a good agreement between maxima of modelled and observed data. Best fit line ($\text{TSS}_{\text{modelled}} = 0.7032 \times \text{TSS}_{\text{measured}} + 2.663$, $r^2 = 0.67$) compared with 1:1 line show that model probably simulates plumes in the far field better compared with near field, as expected, since simulations considered a fixed source point of sediments whereas in the field, the dredger was moving while dredging. Statistical analysis show that, in average, model predictions over estimated TSS by 0.23 mg l^{-1}, indicated by positive bias, and errors were below 4 mg l^{-1} (Table 4.4). Considering those parameters, the model is well suited for representing plume fate, concentration and resultant sediment deposition.
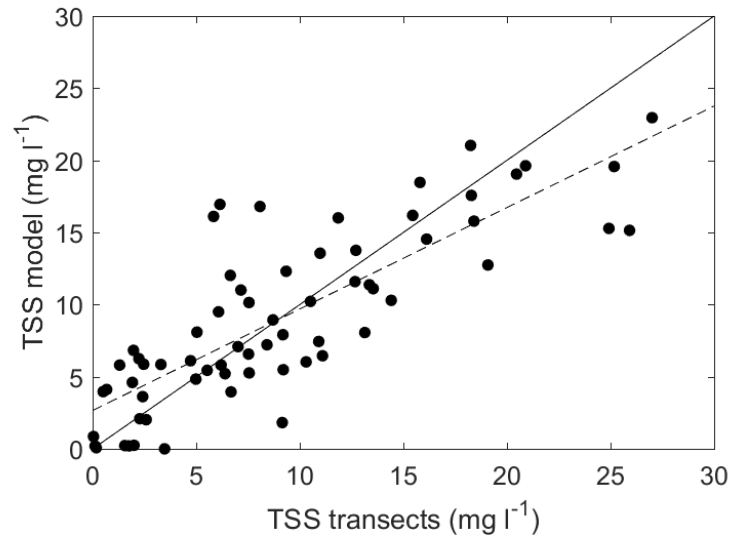
Figure 4.3: Correlation of maximum suspended sediment concentration (TSS, mg l^{-1}) of simulated (Delft3D) and measured (depth-integrated ADCP transects) plumes. Black dashed line is the best-fit line and black solid line is the 1:1 line.

4.3.4 Model Results

The monitored plumes generated during maintenance dredging were simulated for TSS calibration purposes. Differently from the TSHD, that moves while dredging causing the plume to have a meandering pattern, simulated dredging had a fixed point as a sediment source. Therefore, modelled near field plume footprint differed from observed. However, after dredging, plumes had similar dispersion time and decrease in TSS as observed in the field and revealed by ADCP transects. The plume dispersion pattern at H1 (H1_1) is presented in Figure 4.4; times refer to minutes after dredging activity ceased. Suspended sediment plume dispersion is consistent with current direction at the time of dredging (flood tide) and is transported south of dredging area. Thirty minutes after dredging, maximum TSS decreased to approximately 50% of its initial level with further decreases afterwards. After 2 hours, TSS had reduced to background levels around the dredging area, consistent with ADCP transects, and TSS was in the order of 5 mg l^{-1} above background south of monitored area. The advantage of using numerical model in plume dispersion studies is the possibility of inspecting plume fate and concentration beyond monitored area and time. Hence, it is possible to verify that TSS associated to dredging had reduced to background levels after 6 hours.
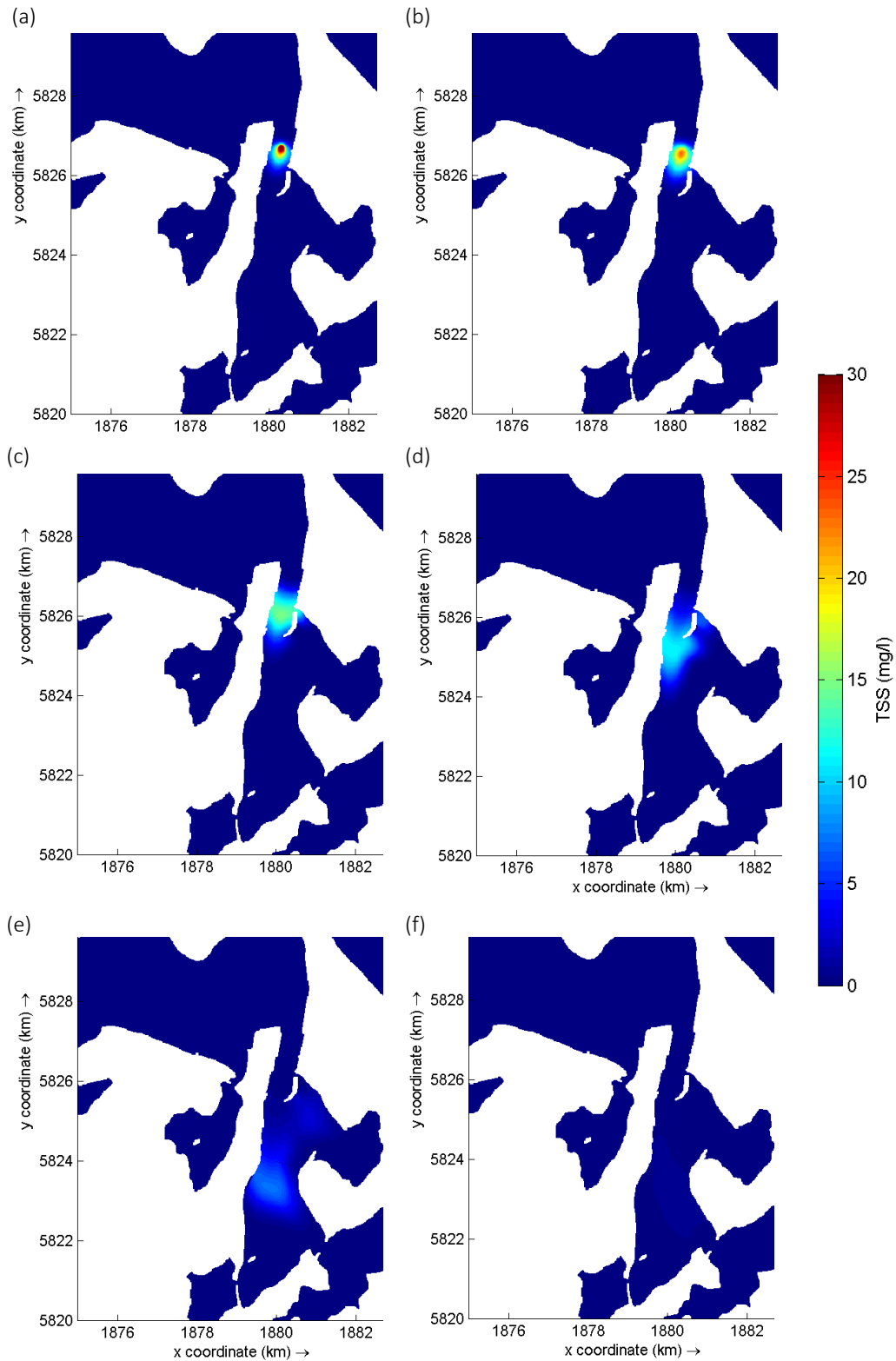
Figure 4.4: Results of simulation of dredging plume at H1. Shading represents the concentration of suspended sediments (TSS, mg l^{-1}) above background TSS at (a) the end of dredging and at (b) 10 min, (c) 30 min, (d) 60 min, (e) 120 min and (f) 360 minutes after dredging finished.

In the context of ecological impact assessment, it is important to evaluate the percentage of time a given TSS level is exceeded based on a threshold. We used two thresholds, 30 and 70 mg l^{-1}, based on environmental limits used by the Port of Tauranga to monitor dredging activities (Bryan et al., 2014) and based on results from a laboratory experiment to test effects of increased TSS on the feeding behaviour of a key species of shellfish bivalve in the harbour, *Paphies australis* (Cussioli et al., in prep.). Those limits suggest changes in the energy acquisition that could affect their health. Calculating the exceedance time percentage for one dredging loading cycle only, (e.g. H1_1), TSS exceeded both thresholds 7.3% of time (total time corresponds to dredging time length plus six hours after dredging ceased), which correspond to 30 minutes. This was the length of dredging, i.e., limits were only exceeded during dredging. The difference between the two thresholds were the spatial limits where concentrations were exceeded: threshold of 70 mg l^{-1} was exceeded only at the discharge point, whereas 30 mg l^{-1} level was exceeded within a radius of approximately 75 m around the discharge point.

Simulations (1) to (4) show that TSS at the discharge point decreased exponentially after dredging ceased within 1 to 1:30 h (Figure 4.5). TSS was higher at H4 at the end of dredging but similar between tides, whereas for plumes at H1, a difference in concentration at the end of dredging can be observed. Plume during flood tide presented higher TSS and slower decaying rate (Table 4.5).
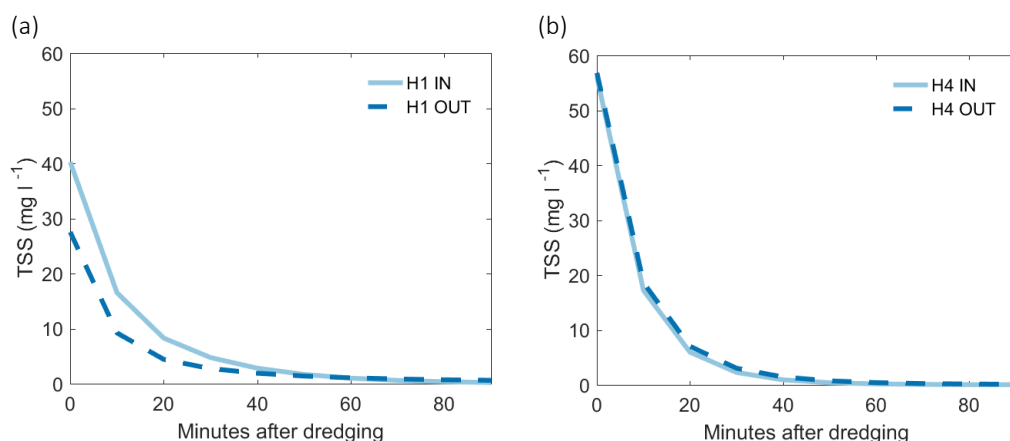
Figure 4.5: Suspended sediment concentration (TSS) decay after dredging ceased at areas (a) H1 and (b) H4 for hypothetical plumes (same flow rate and concentration for both simulations – see methods). Solid light blue line represents results of simulation during flood tides (IN) and dashed dark blue solid line represents results of simulation during ebb tide (OUT).

Table 4.5: Decay coefficients calculated from exponential decrease in TSS (total suspended sediments), sediment mass and sediment deposition based on our model results and from literature available. * denotes that outliers were removed from original data before exponential curve fitting.

Type of decay	Plume Reference (as in source paper)	Decay coeff. -k (N, r^2)	Estuary type	Source
TSS vs time after dredging ceased	H1 IN	0.080 (37, 0.99)	Mesotidal	This work
TSS vs time after dredging ceased	H1 OUT	0.095 (37, 0.93)	Mesotidal	This work
TSS vs time after dredging ceased	H4 IN	0.115 (37, 0.99)	Mesotidal	This work
TSS vs time after dredging ceased	H4 OUT	0.108 (37, 0.99)	Mesotidal	This work
TSS vs time after dredge passage	mid-depth (7 m) Chesapeake Bay, USA	0.053 (7, 0.98)	Microtidal	Nichols et al. (1990)
TSS vs time after overflow	dredging at Bay of Seine, France	0.032 (8, 0.94)	Macrotidal	Duclos et al. (2013)
Sediment mass vs time after overflow	dredging at Bay of Seine, France	0.030 (8, 0.97)	Macrotidal	Duclos et al. (2013)
TSS vs distance from dredging point source	9/7/78 (Elizabeth River, Virginia, USA)	0.006 (6, 0.97)*	Microtidal	Kuo et al. (1985)
TSS vs distance from dredging point source	Model results	0.016 (7, 0.98)	-	Kuo et al. (1985)
TSS vs distance from dredging point source	St. Johns River, USA	0.016 (4, 0.98)*	Microtidal	Kuo and Hayes (1991)
TSS vs distance from dredging point source	Black Rock Harbour, USA	0.010 (5, 0.80)	Mesotidal	Kuo and Hayes (1991)
TSS vs distance from dredging point source	Thames River, USA (Bohlen 1978)	0.022 (6, 0.98)	Microtidal	Kuo and Hayes (1991)
TSS vs distance from dredging point source	Thames River, USA (Cundy and Bohlen 1980)	0.017 (7, 0.99)	Microtidal	Kuo and Hayes (1991)
TSS vs distance from overflow point source	mid-depth (7 m) – average 6 cycles	0.014 (7, 1.00)	Microtidal	Nichols et al. (1990)
Deposition vs distance from channel axis	Northeast Side	0.002 (3, 0.84)*	Microtidal	Nichols et al. (1990)
Deposition vs distance from channel axis	Southwest Side	0.003 (4, 0.99)	Microtidal	Nichols et al. (1990)

Figure 4.6 shows contours of sediment deposition resultant from dredging simulations at H1 and H4, comparing deposition footprint during flood and ebb tide. Simulations for both areas show that sediments settle mainly within navigational channels. Due to its location, sediments from dredging at H4 were deposited west of dredging area, off Otumoetai, also extending through the entrance channel. The flow rate of sediments and initial concentration resulted in deposition of less than 1 mm within those contours and reaching maximum thickness of approximately 2 mm in close proximity to the discharge points. Sediment deposition also increased because of cumulative plumes over the period simulated (simulations 5 and 6). At the discharge points, thickness was slightly above 2 cm, decreasing according to the distance from those areas (Figure 4.7). Including dredging areas at the entrance channel (Figure 4.7a) contributed to increase plume dispersion and deposition around Centre Bank, and increased sediment deposition thickness in the areas simulated in Figure 4.7b.
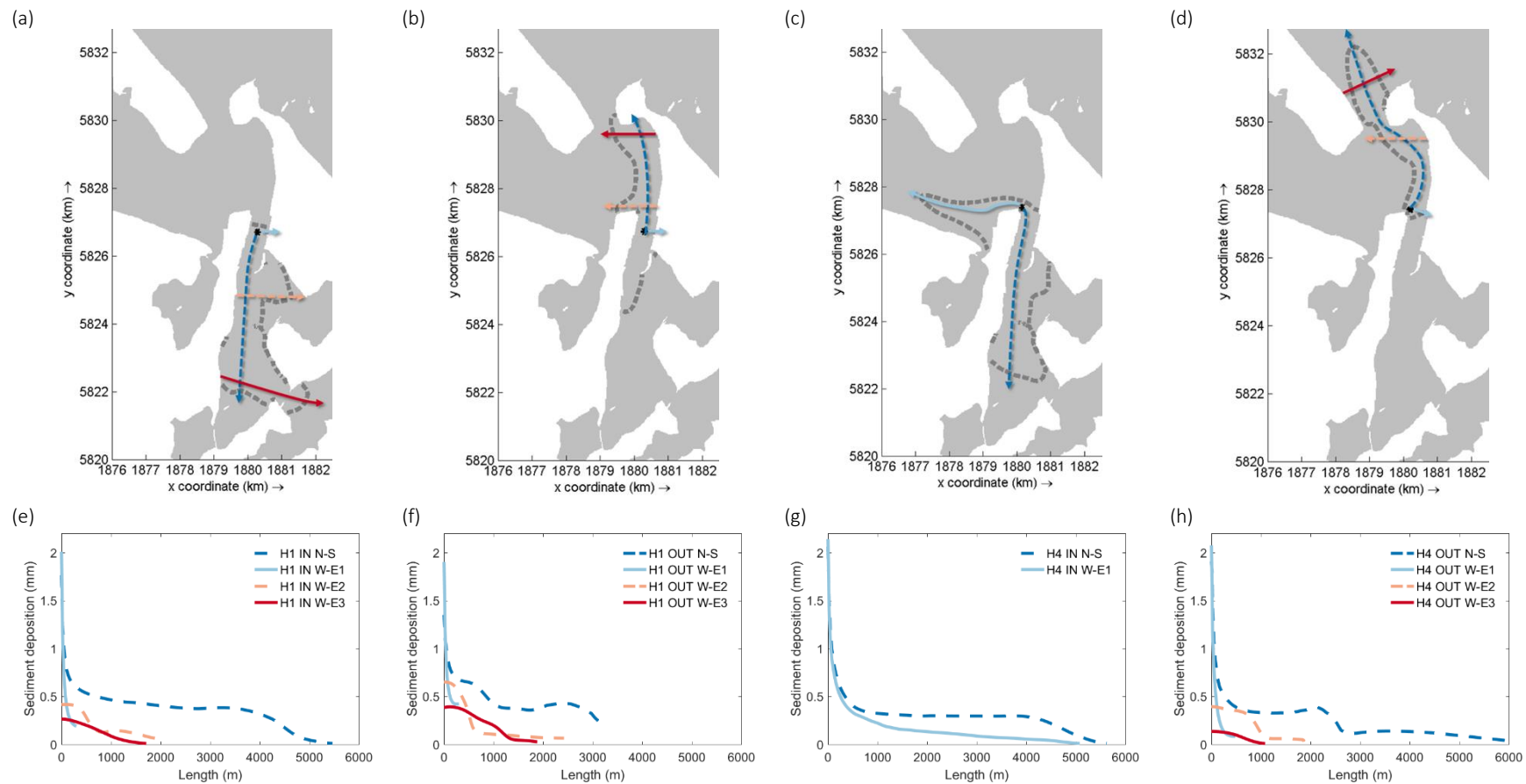
Figure 4.6: Contour of sediment deposition (mm) generated by dredging simulations (a) H1 IN, (b) H1 OUT, (c) H4 IN, and (d) H4 OUT, and respective sediment deposition decay plots (e to h). Maps (a) to (d) show the 0.1 mm deposition contour (grey dashed line), location of dredging point source and 1 mm deposition contour (black dot), longitudinal ('N-S' dark blue dashed lines) and cross-sections ('W-E1' light blue solid lines, 'W-E2' yellow dashed lines, and 'W-E3' red solid lines) lines from where the results of sediment deposition, presented in plots (e) to (h) were extracted. All four dredging simulations had same setup (sediment type, flow rates and initial concentrations).
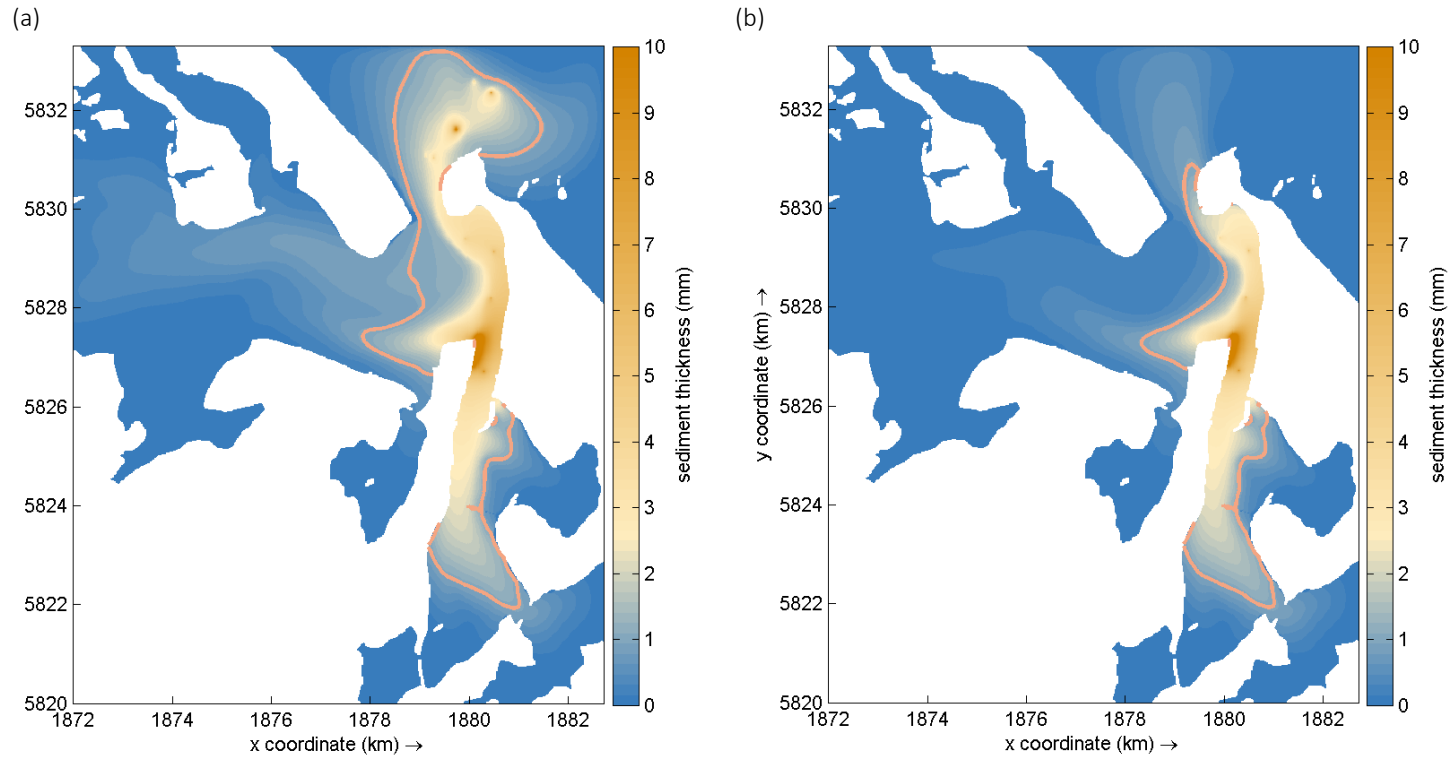
Figure 4.7: Sediment deposition/thickness (mm) at the end of (a) dredging simulation (5) and (b) dredging simulation (6). Simulation (5) included all dredging points, whereas simulation (6) did not include dredging points at the entrance. Waves were not considered in the simulations. Orange line represents the 0.1 mm contour.

4.3.5 Plume Footprint – Index of Plume Symmetry

Decay coefficients for sediment deposition were usually lower for sections extracted along the main plume axis, N-S (Table 4.6). Comparing the N-S decay coefficient with those of cross-sections W-E1, which are located across the dredging area, the difference is an order of magnitude greater for the cross-section, except for the case of H4 IN. Secondary cross-sections W-E2 and W-E3 usually show slower decay, hence the extended width; however, deposition depths were below 1 mm. The plume footprint was usually asymmetric for N-S/W-E1, with index of symmetry around 0.06-0.07. Cross-sections W-E2 and W-E3 for H1 IN simulation presented high index of 0.90, considerably higher than in H1 OUT. The deposition footprint in H4 shows that N-S and W-E1 had similar decay patterns and extended to similar distances from the dredging area to the point where deposition dropped to zero (Figure 4.6c). This resulted in a high index of symmetry. A high index was also calculated for H4 OUT W-E2; although lengths of those sections were different, decaying of deposition thickness had similar pattern.

Table 4.6: Decay coefficients for sediment deposition in longitudinal and cross-sections from results of model simulation (1) to (4). Index of symmetry is calculated as a ratio of depositions in N-S and W-E sections.

Plume Reference	Decay coefficient (N, r^2)	Index of Symmetry N-S $\div$ W-E
H1 IN N-S	0.0009 (8, 0.80)	-
H1 IN W-E1	0.016 (8, 0.94)	0.06
H1 IN W-E2	0.001 (10, 0.90)	0.90
H1 IN W-E3	0.001 (10, 0.92)	0.90
H1 OUT N-S	0.0006 (10, 0.71)	-
H1 OUT W-E1	0.009 (8, 0.81)	0.07
H1 OUT W-E2	0.001 (7, 0.94)	0.60
H1 OUT W-E3	0.001 (10, 0.91)	0.60
H4 IN N-S	0.002 (11, 0.82)	-
H4 IN W-E1	0.002 (9, 0.98)	1.00
H4 OUT N-S	0.001 (8, 0.92)	-
H4 OUT W-E1	0.015 (8, 0.98)	0.07
H4 OUT W-E2	0.001 (9, 0.86)	1.00
H4 OUT W-E3	0.003 (7, 0.95)	0.33

4.4 DISCUSSION

4.4.1 Plume footprint dynamics

The footprint shape of dredging plumes and subsequent sediment deposition may be used to define risk of vulnerability zones for estuaries. The model results for sediment deposition showed a longer dispersion zone in the north-south (N-S) direction than in the east-west width (W-E) (Figure 4.6, Figure 4.7 and Table 4.6). This suggests the main dredging plume dispersion pattern was in the N-S direction. Considering an ideal symmetric plume footprint (N-S ÷ W-E = 1); the simulations which were run during a flood and ebb tide, in H1 and H4, had low ratio of N-S ÷ W-E1 around 0.07 (except for H4 IN). This asymmetry between longitudinal and lateral dispersion may be modulated by the subsequent hydrodynamics from the deeper, faster flowing main shipping channels in the harbour. This pattern has also been observed in Baltic waters (Gajewski and Uscinowicz, 1993) and off Southern U.K. (Hitchcock and Bell, 2004), where the sediment deposits from dredging vessels followed a narrow band (100m either side of the dredger track) in the direction of the currents. A much higher ratio was calculated for N-S ÷ W-E1 for H4 IN and for other cross-sections W-E2 and W-E3. Although initial deposition thickness for those sections were smaller compared with N-S and W-E1, the decay coefficient was similar. Therefore using this indicator of plume footprint shows that sensitive areas located in the N-S direction could be exposed to plumes for longer periods of time than areas located east and west of dredging areas; however, away from the dredging area, attention should be taken in areas of high index, such as in H4, where plume dispersal and deposition in the east-west direction is of similar length and/or of similar decay coefficients of north-south.

The plume footprint depends on dominant tidal flow and current speed at the location where the dredging occurred. In a simplified analytical model developed by Shao et al. (2015), the levels of suspended sediment were shown to be primarily influenced by the tidal current velocities. This impacted significantly on the turbidity profile of the dredging plumes. Lower speeds (~ 0.1 m s^{-1}) extended the duration of turbidity build-up causing an increase in the steady-state SSC. The

opposite trend was shown to occur when current velocities were increased (up to ~ 1 m s^{-1}). However, assessing risk vulnerability for sensitive areas using simple models assume tide averaged velocities, which neglect tide-induced changes in the stressor and greatly underestimate the plume footprint. (Shao et al., 2015). To better understand the dynamics of plume footprints, a model including tidal variations is needed.

The tide regime in different estuary types (microtidal, mesotidal and macrotidal) will influence the plume asymmetry. Tauranga harbour is a well-mixed mesotidal tidally-dominated estuarine lagoon (de Lange and Healy, 1990). The maximum current speeds recorded was approximately 2 m s^{-1} at the entrance (ADCP – Figure 4.1) and 0.5 m s^{-1} around dredged areas (ADVA, ADVB and S4 – Figure 4.1) with a tidal amplitude of approximately 2 m. The plume footprint, as observed in our model results, show asymmetry linked to the main tidal current patterns (Figure 4.6). The processes occurring in microtidal estuaries are different and would be more dominated by wind and wave effects (Hayes, 1975). Therefore, the plume footprint would be governed more by these unpredictable forces and may present a more variable deposition pattern. Macrotidal estuaries on the other hand are systems that are most dominated by tidal currents (Hayes, 1975). This would likely present the most asymmetric plume, with the longitudinal component stretched in the main direction of current flow. This large asymmetry has been reported by Duclos et al., 2013, from a study in the Bay of Seine, France. The region experiences a 7 m tidal range and associated current speeds in the order of 1.5 m s^{-1}, with the reported plume length from 5 to 10 times greater than plume width. The estimated deposits of fine sand calculated for that study show length just over two times deposit width, however fine particles would settle up to 6.5 km from dredging area.

4.4.2 Environmental implications of dredging induced sediment deposition and suspended sediments

The estuarine plume footprint can be estimated from many different modelled parameters such as suspended sediment concentration and sediment deposition. In this study, the index of plume symmetry was calculated using sediment deposition thickness. Deposited sediments from dredging plumes can accumulate and have impacts on the surrounding ecosystem. For example, sensitive seagrass meadows can suffer from increased burial rates from the additional sediment availability (Campbell, 2016). This can cause a decline in seagrass density, biomass and productivity (Cabaço et al., 2008). Some species of seagrass (e.g. *Cymodocea nodosa*) can modify their vertical growth to place their meristems above the new level after sedimentation, however, within certain limits (Marbà and Duarte, 1994). Depending on the species and level of sedimentation, burial can lead to mortality. In several experiments to test the effects of burial on seagrasses, low burial levels of 2 to 4 cm caused at least 50% mortality in all species studied (Cabaço et al., 2008).

Our model results show maximum cumulative deposition of 10 mm, restricted to the dredging areas, when all plumes were considered in the simulation. However, deposition decreases rapidly a few meters outside the dredging areas. When only one dredging cycle was considered (H1 or H4), maximum deposition was 1 mm. A risk indicator rating was proposed by the National Estuary Monitoring Protocol for shallow, intertidally-dominated, estuarine systems in New Zealand (Robertson et al., 2002). This established that sedimentation rates between 1 and 2 mm yr^{-1} have low risk of adversely affect estuary condition, whereas sedimentation between 5 to 10 mm yr^{-1} causes a high risk.

Dredging activities are usually small relative to the spectrum of natural disturbances. In a review on the impacts of sediment burial on seagrasses, burial caused by natural disturbances are divided in small scale, such as bioturbation, and large scale, such as hurricanes. These disturbances have resulted in sedimentation of around 6 cm to 70 cm, respectively, around seagrass meadows in the USA and

Mexico (Cabaço et al., 2008). In comparison to natural sedimentation rates, the potential maximum sediment deposition derived from sediment traps during dredging at Chameis Bay (Namibia), was in the order of 4 mm (SD = 2 mm) (Smith et al., 2008). Simulations demonstrated a short duration of those deposits (hours or days). This was likely due to the highly dynamic, wave-dominated environment (Smith et al., 2008). At Lough Foyle (Ireland), sedimentation was in the order of 10 mm and mainly restricted to the disposal site, where background sedimentation was around 5 mm yr^{-1} (Close et al., 2013). It was expected that after one year, few patches of that magnitude would be present, as most patches would be in a range of only a few millimetres (Close et al., 2013).

Comparisons between sedimentation rates must be done with caution because of limitations on the length of monitoring periods. The sedimentation rates cited above were per year, whereas the sediment deposition from model simulations of the maintenance dredging in Tauranga Harbour was a result of a short simulation (few days). Although resuspension was included in the model, our results do not consider the contribution of background suspended sediment (which was low), but which will also contribute to settling. The simulations also neglect the stirring and resuspension by waves the dredging cycles of the maintenance dredging campaign outside the monitoring period and re-dredging over the same areas, which removes recently deposited sediments. Moreover, as it was a short simulation, it does not consider the resuspension and transport of sediments after the dredging campaign ceased (> a month). It is therefore unable to represent the absolute final deposition, or the rate per year.

A review on the environmental impacts of dredging on different species of seagrasses showed critical thresholds for sedimentation levels. Values range from 2 cm yr^{-1} (e.g. *Halophila ovalis* and *Zostera noltii*) to 13 cm yr^{-1} (e.g. *Cymodocea serrulata*) (Erftemeijer and Lewis, 2006). Burial of seagrass seedlings and propagules in depths of approximately 4 cm caused a 100% mortality rate in seedlings after ~ 42 days in mesocosm experiments that simulated periodic and prolonged burial events. Propagules, on the other hand, performed well in periodic burial, although they could not survive in prolonged burial experiments (Campbell,

2016). In a burial experiment using seagrass species *Z. muelleri*, New Zealand endemic species of seagrass (Turner and Schwarz, 2006), burial of 5 mm over a month or less did not reduce rhizome growth rates significantly (Benham et al., 2016). However, longer periods of shading combined with greater burial depths (≥ 10 mm) notably reduced the growth rates. In studies done in a < 2 month experimental period by Cabaço et al., 2008, a burial of 4 cm caused 50% mortality in *Z. marina* and 12 cm caused 100% mortality. The species *Z. noltii* presented lower thresholds with a burial of 2cm and 8cm causing 50 to 100% mortality rates respectively. (Cabaço et al., 2008). Species of genera Zostera have a slow response to sedimentation, reducing its survival rate in burial events (Campbell, 2016). The post-impact recovery time should also be taken into consideration for the management of dredging campaigns (Van Raalte et al., 2007). This is especially important for maintenance dredging, which usually occurs more frequently compared with capital dredging. At dredging spoil grounds, seagrass recovery was evident after 2 to 3 years after deposition of dredged sediments (Cabaço et al., 2008). However, a thick sediment layer (10 cm burial depth) dumped on a single occasion was shown to have a longer recovery time of five years for the intertidal seagrass *Z. noltii* (Do et al., 2012). In Hervey Bay (Australia), the same 5 year recovery period was observed for intertidal seagrasses to start to recover after major flood events, whereas subtidal seagrasses started to recover much faster within two years (Coles et al., 2003). These varying factors and recovery rates can make universal thresholds of deposited sediment and its impact difficult to define. In a review by Smith et al (2006), submillimetre thick sediment deposition occurring over hours to days in the high wave energy environment of Southern Africa was suggested as having a low or neutral impact (Smith et al., 2008).

Ecological effects caused by increased levels of suspended sediments associated with dredging plumes need to be compared against the levels experienced naturally in that area (for example, catchment runoff after storm events, wave action and river discharges (Aarninkhof, 2008; Erftemeijer and Lewis, 2006; Netzband and Adnitt, 2009; Pennekamp et al., 1996)). As an essential element in environmental management, monitoring the background turbidity

levels before dredging is one approach that can help distinguish between natural and anthropogenic turbidity variations (Luger et al., 1998; Sofonia and Unsworth, 2009). Long-term monitoring of background variations was used to define acceptable limits around coral reefs in Australia and has shown that a comparatively short-term increase in turbidity which is within background range will not affect corals considerably (Orpin et al, 2004). Turbidity caused by major storms in the Thames River estuary, USA, were observed to be an order of magnitude greater than caused by dredging, occur more frequently (one to three times per year) and affect a broader area compared to a more restricted region affected by dredging (Bohlen et al. 1979). Similarly, Luger at al. (1998) concluded that turbidity caused by dredging in Saldanha Bay, South Africa, would have same order of magnitude of naturally occurring during storms and dredging would have a local effect whereas storms would have a widespread effect. Understanding the spatial and temporal variation of suspended sediments and turbidity occurring naturally in a region, it is possible to properly address the causes of increased values and predict ideal conditions for dredging or any other related activity, aiming to avoid scenarios that could cause adverse effects.

Far-field plumes, both monitored and modelled, predicted suspended sediment concentrations ≤ 70 mg l^{-1}. Suspended sediment concentration from other reported dredging programs in the USA are 190 mg l^{-1} to 600 mg l^{-1} (reviewed in Cutroneo et al., 2012) and 5.5.g l^{-1} to 450 mg l^{-1} in the UK (Hitchcock and Bell, 2004). The range of TSS during the 2014 maintenance dredging is comparable to the work of Healy and Tian (1999) at Pine Harbour Marina where dredging TSS also reached 70 mg l^{-1}.

The plumes and associated turbidity dissipated quickly as indicated by ADCP transects and rapidly-decaying TSS during the first 10 minutes of dredging (Figure 4.4, Figure 4.5, and APPENDIX C). This behaviour has also been observed in other dredging studies (Bohlen et al., 1979; Smith et al., 2008). A decrease in TSS of up to three orders of magnitude has also been measured within 3 minutes of deposition close to a dredge zone (Nichols et al., 1990). In Tauranga Harbour, the TSS declined to background levels around the dredged area and a low-concentration plume (<

10 mg l^{-1}) was detected 1 km away from the dredged area in the H1_1 cycle, 35 minutes after dredging ceased. For that same dredging cycle, our model simulation shows that plume drifted 3-4 km south of dredged area and TSS decreased to values close to background levels 2 hours after dredging ceased (Figure 4.4). The dredging plume dispersion time (i.e. time for plume TSS to reduce to background level) has also been reported in several other studies to be in the similar range of 0.5 to 2.5 hours (Duclos et al., 2013; Luger et al., 1998; Pennekamp et al., 1996).

Based on modelled estimates for maximum TSS (~70 mg l-1) and dissipation time (~ 2 h), the potential effects on biota were evaluated according to thresholds for species found in the literature and in laboratory experiments. Wilber and Clarke (2001) found that sub-lethal effects (e.g. reduced gap width, pumping rates, and growth) in adult bivalves occur in concentrations > 100 mg l^{-1} in a 3-day exposure period and mortality can occur in concentrations above 1000 mg l^{-1} if exposure extend to 10 days. Critical thresholds for oysters *Ostrea edulis*, mussels *Mytilus edulis*, and larval bivalves are between 750 and 1000 mg l^{-1} for short-duration exposure (2 to 3 days) (Close et al., 2013; Wilber and Clarke, 2001). In short term laboratory experiments (~2 hours of exposure), Tauranga species of bivalve *Paphies australis* (pipi) exhibited optimal conditions when seston concentration was below 30 mg l^{-1}. However, stabilization of feeding rates occurred in concentrations of 70 mg l^{-1}, which may indicate potential physical constraints that limiting food acquisition for concentration above that threshold (Cussioli et al., in prep.).

Impacts on seagrass can occur at TSS levels above 75 mg l^{-1} (Doorn-Groen, 2007). However, whether impact can take place or not depend on how long a turbid plume is sustained above seagrass meadows. Dredging plume tend to dissipate quickly, unlikely to be long enough to adversely affect seagrass condition (Doorn-Groen, 2007). Nevertheless, in Tauranga Harbour, TSS level should be maintained below 20 mg l^{-1} in the intertidal zones over a two-week moving average period (Cussioli et al., submitted) to sustain the upper maximum light requirement of 36% surface irradiance for the New Zealand species *Zostera muelleri* (Longstaff, 2003; Schwartz et al., 2006).

4.5 CONCLUSIONS

The occurrence of impacts caused by dredging plumes are largely dependent on their spatial and temporal scales. By using an index of 'plume symmetry', which compares the length and width of plume footprints, this study shows the importance of considering plume shape and decaying rates over distances in assessing the potential dredging impacts on coastal ecological communities. This index allowed us to define vulnerability zones in proximity to the dredging areas.

Results showed that sediments from dredging plumes were deposited predominately in the main channels, presenting an elongated shape in the north-south direction. However, depending on the location of dredging, dispersion in the east-west direction was also significant, highlighting the importance of surrounding physical forces and environmental setting.

Two groups of marine organisms were considered in the vulnerability zones that could be affected by dredging in Tauranga Harbour (seagrass *Zostera muelleri* and bivalve *Paphies australis* (pipi)). However, the suspended sediment concentrations, exposure duration and sediment deposition of plumes generated during the 2014 maintenance dredging were below thresholds for adverse impacts on those species. This demonstrated that combining both the surrounding physical characteristics through the use of models with biological thresholds are powerful tools in assessing the impacts of dredging activities within coastal systems.

CHAPTER 5

SPECTRAL CHANGES IN UNDERWATER LIGHT REGIME CAUSED BY SEDIMENT COLOUR: IMPLICATIONS FOR SEAGRASS PHOTOSYNTHESIS

Order of co-authors are presented in alphabetical order and does not represent the contribution of each author. Order of authors to be defined for paper submission.

Mariana Coppede Cussioli, Conrad Pilditch, Daniel R. Pratt, Dorothea Kohlmeier, Janet F. Bornman, Kai Bischof, Karin Bryan, and Willem de Lange (in preparation)

CONTRIBUTION OF AUTHORS:

Data and results of tank experiment were provided by DK. Sediment samples used in the spectrophotometer experiments were kindly provided by WDL and David McPherson. Laboratory experiments were planned and carried out by MCC with guidance of KB and the Marine Botany's laboratory technicians. MCC prepared plots and wrote the manuscript, and KB contributed with valuable comments.

ABSTRACT

The underwater light regime is fundamental to the ecological health of aquatic systems because it is a limiting factor for photosynthesis in marine plants such as seagrasses. Although seagrass meadows are a key component of coastal systems, their survival has been challenged by increased turbidity levels. Both resuspension of marine sediments and input of terrestrial material contribute to increase light attenuation. Terrestrial sediments usually have a yellow-orange colour, whereas marine sediments can range from white to grey hues. Given the different sediment colours and sources, the objective of this study was to investigate how those sediments affect underwater light quality. We carried out two experiments including (1) in a tank and (2) using a spectrophotometer, using natural sediment samples from New Zealand. Within the marine cases, white sediments caused lower transmittances compared to grey sediments, however increases in concentration did not modify the spectral distribution of light. High concentrations of marine mud reduced transmittance considerably, particularly below 400 nm. Although marine sediments contribute to broad-band light attenuation, terrestrial orange sediments completely depleted light below 500 nm, which is the light band most relevant to aquatic vegetation. Marine sediments also shifted light transmittance maxima towards the upper end of the spectrum, which is not suitable for seagrass photosynthesis.

5.1 INTRODUCTION

Coastal zones and estuaries are experiencing increased turbidity levels (Lotze et al., 2006; Thrush et al., 2004), caused by human population growth and changes in catchment land use (GESAMP, 1990; Dennison et al., 1993). The sediment levels contributing to the elevated turbidity are determined by natural land based and marine events (i.e. sediment runoff after rainfall; Wheatcroft et al., 1997) and human activities (i.e. resuspended sediments during dredging; Erftemeijer and Lewis, 2006). Both the resuspension of marine sediments and the input of terrestrial material of different sediment concentrations and types (grain size and colour) affect the underwater light regime (Davies-Colley and Vant, 1987; Kirk, 1976; Kirk, 2011). Smaller particles will preferably scatter wavelengths in the blue range of the spectrum, while larger particles scatter red wavelengths more strongly (Hach et al., 1982).

The underwater light regime is a vital factor for the ecology of aquatic systems and is a limiting factor for photosynthesis in marine organisms such as phytoplankton and macrophytes, including seagrasses (Dennison, 1987; Matheson and Schwarz, 2007). Seagrasses have high light requirements (Dennison et al., 1993) and do not present accessory pigments, which limits the effective spectral range for photosynthesis (Frost-Christensen and Sand-Jensen, 1992). A reduction in underwater light penetration and changes in light quality (spectral composition) can affect seagrasses pigment content (Maxwell et al., 2014; Silva et al., 2013), decrease biomass (Abal et al., 1994; Longstaff et al., 1999), increase meadow patchiness or canopy thinning (Abal et al., 1994; Ruiz and Romero, 2003) and change population genetics (Waycott et al., 2005).

This study investigates the variations in underwater light transmittance and spectral composition in response to increased suspended sediment concentration of different sediment colours (grey, white and orange). Terrestrial sediments usually have a yellow-orange colour, due to the presence of iron rich-minerals (Thrush et al., 2004) and humic-type material (Davies-Colley and Vant, 1987), which is distinctly different from the colour of marine sediments. Yellow hues will mainly absorb light at the ultraviolet and blue part of the spectrum (Kirk, 1976), which is

significant for photosynthesis of aquatic plants. Therefore, we hypothesise that orange sediments of terrestrial origin will affect most significantly the underwater light quality available for aquatic plants relative to grey and white marine sediments.

5.2 METHODS

This study is based on two experiments carried out to test the changes in light spectra due to sediment concentration, type and colour. Experiments were carried out in different locations and on separate occasions which involved (1) a tank experiment, over two consecutive days in April 2011 in Hamilton, New Zealand and (2) a laboratory experiment using a spectrophotometer, in September 2016, at the Marine Botany Centre, University of Bremen, Germany.

5.2.1 Tank experiment

Three types of sediments were used in the tank experiment: fine marine sand, marine mud, and terrestrial clay. These were representative of the main types of sediment input into estuarine and coastal areas, including ambient marine sediment, re-suspended and/or dredged marine material, and very fine sediments from river discharge and catchment run-off. Fine marine sand and marine mud were collected in Whangamata Harbour, New Zealand and terrestrial clay was obtained from the National Institute of Water and Atmospheric Research (NIWA), in Hamilton. Terrestrial clay had an orange colour whereas marine sediments were grey or grey/tan.

For each sediment type a range of sediment quantities was added to a 170-liter tank (built by NIWA), filled with artificial seawater. The tank was fitted with a recirculation pump, light sensors and a hose for water sampling (Figure 5.1a, b and c). Light spectra were recorded with a spectroradiometer (RAMSES-ACC-UV/Vis, TriOS) at 0.5 m depth around noon (between 11:00 and 15:00 h) and water samples were collected after light measurements for each sediment treatment tested.

Total suspended solids were determined by filtering a known volume of water sample through pre-combusted and pre-weighed filters. The filters were oven-dried until no further weight loss and re-weighed. The concentration of sediments was calculated as the weight of dry sediment (minus the weight of filter) per volume of water filtered. The treatments tested were divided in low, intermediate and high concentration, which varied for each type of sediment: sand (low: 3.65 mg l^{-1}, intermediate: 3.72 mg l^{-1}, high: 600 mg l^{-1}); mud (low: 1.25 mg l^{-1}, intermediate: 6.5 mg l^{-1}, high: 1400 mg l^{-1}); clay (low: 1.25 mg l^{-1}, intermediate: 15 mg l^{-1}, high: 500 mg l^{-1}).

To determine wavelength-specific attenuation, percentage transmittance of energy was calculated for the UV-B (280-319 nm) and UV-A (320-399 nm) bands and in the photosynthetically active radiation (PAR) interval (400 to 700 nm), using the equation below. The lowest concentration tested for each sediment type was considered as a reference, i.e., to have 100% transmittance.

$$\% \, T = \frac{I}{I_0} \times 100$$

where I is the light energy transmitted through the water and I_0 is the energy transmitted through the reference, which was the lowest concentration in I.

(a) (b) (c)

(d) (e)
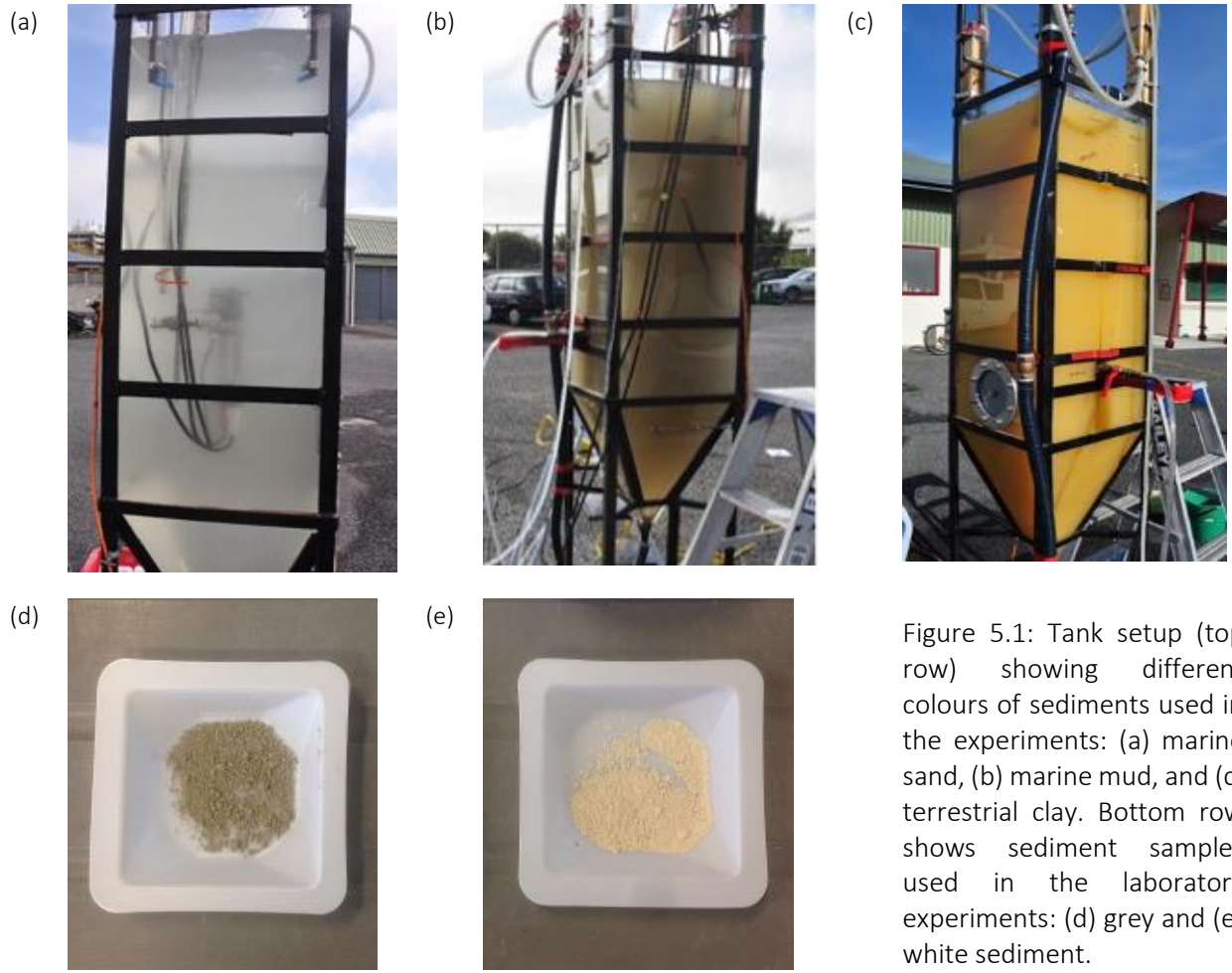
Figure 5.1: Tank setup (top row) showing different colours of sediments used in the experiments: (a) marine sand, (b) marine mud, and (c) terrestrial clay. Bottom row shows sediment samples used in the laboratory experiments: (d) grey and (e) white sediment.

5.2.2 Laboratory experiment - Spectrophotometer

We used two samples from a sediment core (core n. 78) collected by the Port of Tauranga at the Stella Passage, Tauranga Harbour, New Zealand. The sediment cores were part of a survey that aimed to characterize the sediment layers in the shipping channels to meet the requirements of dredging consent prior to the 2015/2016 capital dredging. Details of sample location and textural analysis results are provided in de Lange et al (2014). The samples were chosen based on the sediment colour, grey and white (Figure 5.1d and e). Grey sediment sample was taken from depth of 75 cm (depths are relative to the sea floor) and is composed of 54.5% sand and 45.5% fines (42% silt and 3.5% clay) and white sediment is from layer 136 cm, composed of 54% sand and 46% fines (43% silt and 3% clay).

In the laboratory, a slurry was prepared with each sample and diluted to get the concentrations desired: grey (low: 0.5 g l^{-1}, intermediate: 3.0 g l^{-1}, high: 9 g l^{-1}); white (low: 0.5 g l^{-1}, intermediate: 3.0 g l^{-1}, high: 6 g l^{-1}). We added samples in a 1-cm path cuvette and measured absorbance using a spectrophotometer with an integrated sphere to reduce effects of scattering. Absorbance was recorded every 2 minutes for 10 minutes to check for differences in absorbance response due to settling. The initial measurements at zero minute were used for our results. Absorbance was converted to percentage transmittance of energy using the formula:

$$\% \, T = \ 10^{(-A \times 100)}$$

where I is the light energy transmitted through the sample and I_0 is the energy transmitted through the reference blank, which was artificial seawater.

5.3 RESULTS

Spectral composition of underwater light in low (3.65 mg l^{-1}) and intermediate (3.72 mg l^{-1}) concentrations of marine sand was similar, with all wavelengths evenly transmitted. The results for the intermediate treatment show that, except for UV-B range, which show a higher percentage, transmittance is

approximately 90% throughout the spectrum. The increase in suspended sediment concentration to 600 mg l^{-1} at the high treatment reduced light energy over all wavelengths, particularly in the UV-A range, which decreased to the minimum of 10% (Figure 5.2a).

The treatments using marine mud show a relatively homogeneous reduction in transmittance, indicating that all wavelengths were attenuated similarly. From low to intermediate concentrations (1.25 to 6.5 mg l^{-1}), transmittance is clearly reduced. Transmittance percentages in the intermediate treatment were similar and ranged from approximately 70 to 80%, with highest value for UV-A. In the treatment using highest marine mud concentration, virtually no light was transmitted below 400 nm, and only less than 10% of light was transmitted between 450 and 700 nm (Figure 5.2b).

Results from terrestrial clay treatments show substantial reduction of transmittance. At intermediate concentrations (~15 mg l^{-1}), maximum and minimum transmittance is approximately 80% and 20%, respectively. Noticeable reduction occurred in wavelengths below 400 nm. Similarly to marine mud, high concentrations of terrestrial clay (~700 mg l^{-1}) led to no light transmission between 280 and 450 nm and only 1 to 14% transmittance between 500 and 700 nm (Figure 5.2c).
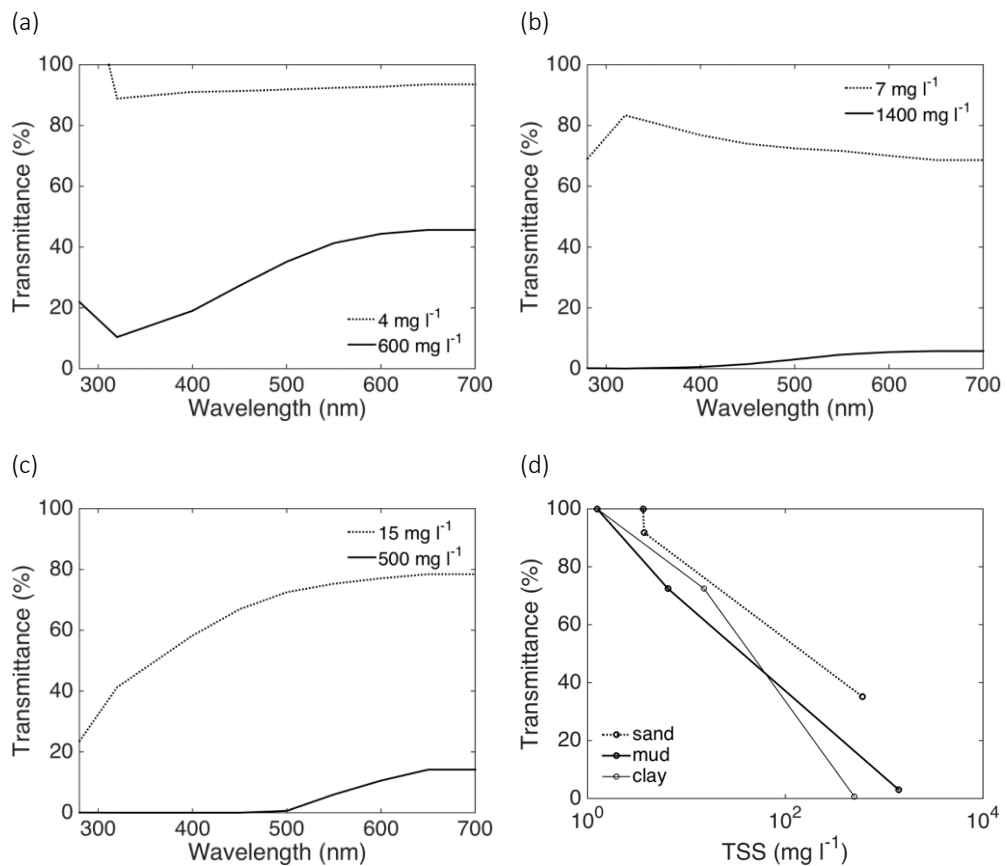
Figure 5.2: Percentage transmittance for ultraviolet (UV = 280-400 nm) and photosynthetically active radiation (PAR = 400-700 nm) obtained in the tank experiment for (a) marine sand, (b) marine mud, and (c) terrestrial clay. Dashed and solid line represent intermediate and high concentrations, respectively. Plot (d) shows variations in transmittance caused by various suspended sediment concentration (TSS) among sediment types at 500 nm.

Transmittance for grey and white sediment in low concentration treatment was approximately 100% over the spectrum (data not shown). Likewise, treatments using intermediate concentrations of grey sediment showed high values; however, they were slightly lower for treatments using white sediment. In general, transmittance was lower in the UV and increased in the PAR range, with peaks at around 350 nm, levelling off in the visible range. White sediments showed lower values compared to grey sediments, with a difference of 20%. Increases in concentration by a factor of two decreased overall transmittances by 20-30%. However, it did not alter the spectral distribution of light (Figure 5.3).

(a)

(b)

(c)
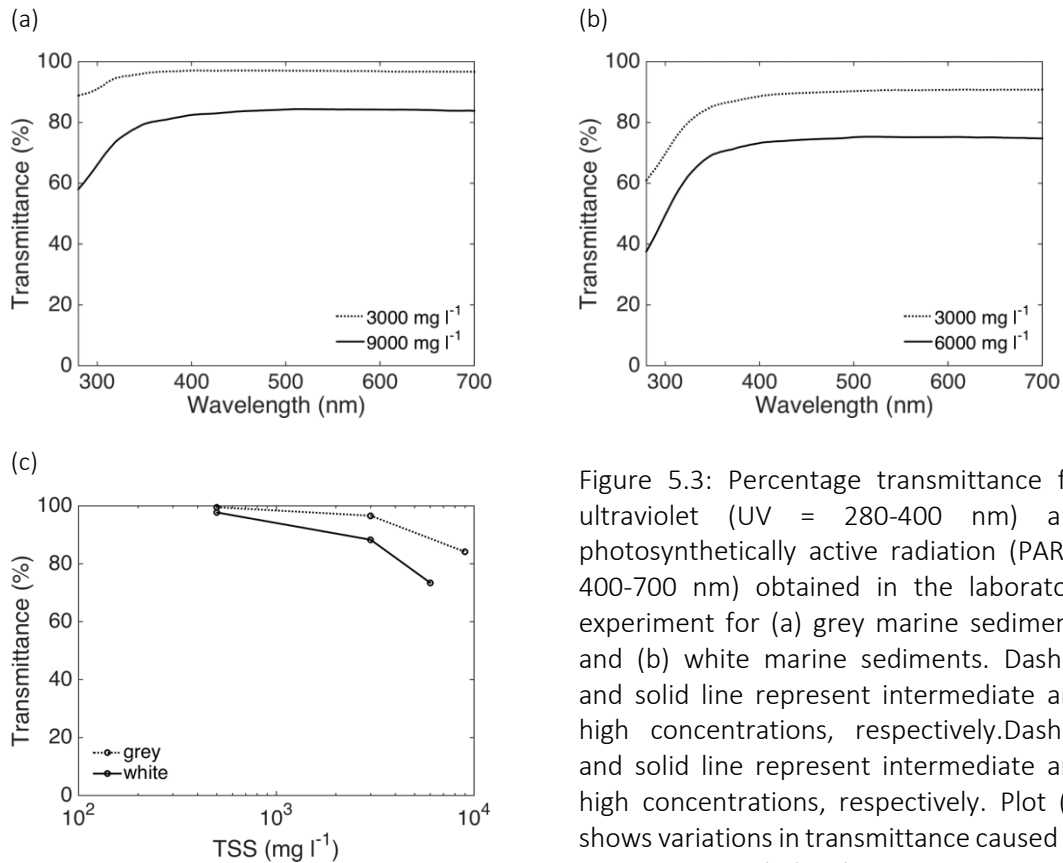
Figure 5.3: Percentage transmittance for ultraviolet (UV = 280-400 nm) and photosynthetically active radiation (PAR = 400-700 nm) obtained in the laboratory experiment for (a) grey marine sediments and (b) white marine sediments. Dashed and solid line represent intermediate and high concentrations, respectively.Dashed and solid line represent intermediate and high concentrations, respectively. Plot (d) shows variations in transmittance caused by various suspended sediment concentration (TSS) among sediment types at 500 nm.

5.4 DISCUSSION AND CONCLUSIONS

The results from both experiments show that terrestrial clay had the largest effect on light quality among all treatments. Light was selectively attenuated over the spectrum with pronounced decrease in transmittance in the blue and green wavelength bands. The highly-coloured water treatment using terrestrial clay, characterized by yellow-red hues is a result of the organic and mineral particulate content and is expected to contribute to the absorption of blue light (Davies-Colley and Close, 1990). The yellow substances may also significantly attenuate light in the overall photosynthetically active radiation (PAR) range (Storlazzi et al., 2015).

Intermediate concentrations of marine sand, marine mud, grey and white marine sediments showed similar responses in spectral distribution of light transmittance. The results show that all wavelengths were attenuated similarly, and there was no marked difference in light quality between grey and white.

100

Treatments using white sediment transmitted slightly less light compared with grey sediments, noticeably in the UV-A range. These two sediment colours may be released from deeper sediment deposits during dredging operations causing visual impact, particularly light-coloured plumes. For example, during the 1992 capital dredging in Tauranga Harbour, New Zealand, excavation by a cutter suction dredge in Stella Passage generated a highly visible plume, which was light in colour. This was a result of resuspension of Pleistocene sediments containing high percentage of silt (de Lange et al., 2014). However, only grey sediments were visible in dredging plumes during the 2014 maintenance dredging in the same area (Cussioli et al., in prep.). Since there was no change in the transmittance over the spectrum between these two colours, resuspension of these sediments will cause a similar impact to the water quality.

The concentration used in treatments also played an import role in light quality attenuation. Whereas it is possible to detect differences in light quality between low and intermediate concentrations, those differences were more pronounced in higher concentrations. An excessive increase in concentration of marine mud between intermediate and high treatments explains the near complete light extinction at the higher mud concentrations (Figure 5.2b). The difference in light transmittance response at high concentrations may be due to two factors: (1) increased concentrations will make the colour darker, therefore increasing the effect of selective absorption (Udelhoven and Symader, 1995) and (2) increased number of particles for a given suspended sediment concentration can absorb more light (Storlazzi et al., 2015). Darker colours also attenuated more light than light-coloured sediments in a tank experiment in Storlazzi et al. (2015). Increased number of particles will also increase the scattering effect. The results from spectrophotometer had scattering effects reduced by an integrated sphere, whereas the scattering effect was not addressed in the tank experiment. Higher attenuation in the results obtained in the tank experiment could be explained by the less controlled experimental environment.

The selective light absorbance of specific wavebands can cause a stress on the ecosystem because photosynthetic processes and growth of aquatic plants will

be greatly affected by the attenuation of blue light (Kirk, 1976). Figure 5.4 summarizes the effect of sediment plumes in altering light quality. Shifts in transmittance maxima from blue and green bands to longer wavelengths toward the red end of the spectrum reduces photosynthesis efficiency (Davies-Colley and Vant, 1987). These wavelength bands are rapidly attenuated by the water itself and are not suitable for marine angiosperms due to the absence of accessory pigments (Frost-Christensen and Sand-Jensen, 1992).

Overall, the results indicate that input of orange coloured sediments, which are specifically from terrestrial sources (Thrush et al., 2004) leads to shifts in light transmittance maxima which is intensified by increased concentrations. Although resuspended marine sediments contribute to the overall broad-band light attenuation, changes in specific bands of the spectrum are of more concern in relation to photosynthesis. Therefore, our results emphasise the importance of larger scale catchment and land-use management to minimize excessive sediment erosion and runoff from land to sea.
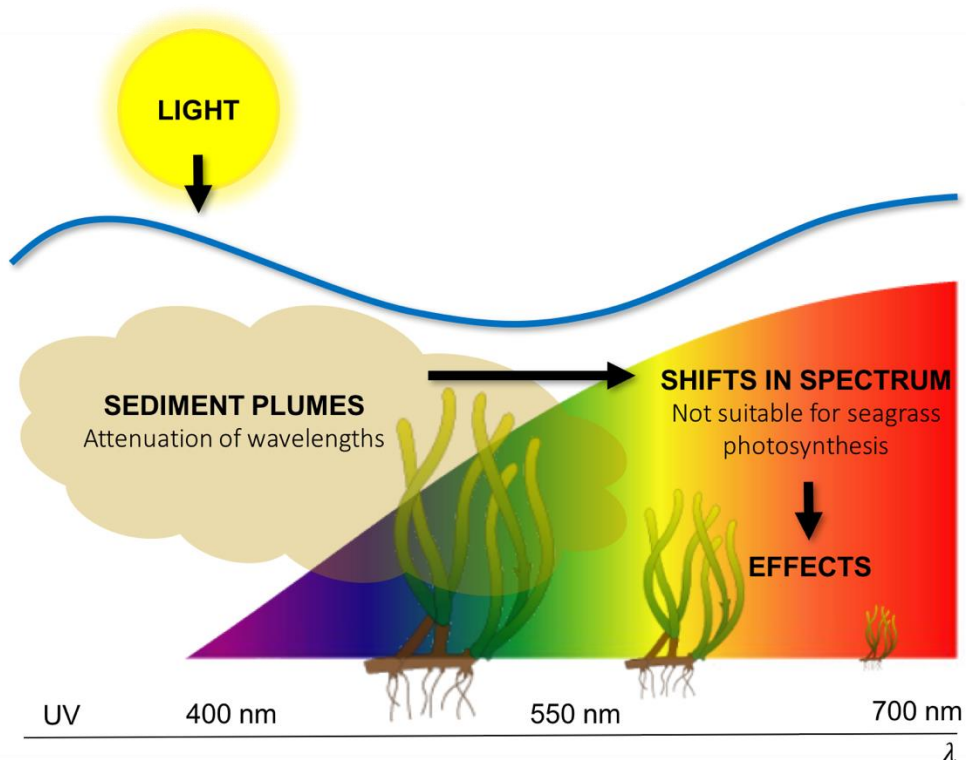
Figure 5.4: Schematic diagram showing changes in the spectrum caused by sediment plumes and implications for seagrass photosynthesis.

CHAPTER 6

GENERAL DISCUSSION

6.1 SUMMARY OF FINDINGS

In this study, I explored turbidity in coastal areas, which is an issue gaining more attention with future changes in land use practices, population growth and climate change. Increases in population also means a growing need for goods, which leads to enlargement of ports and harbours to accommodate larger ships to facilitate the import/export processes. In this context, this thesis aimed to understand the sources, patterns and potential impacts of increased turbidity in a barrier-enclosed shallow lagoon in Tauranga Harbour (north island of New Zealand). The area is surrounded by urban developments, industry, forestry and agricultural land use. Also, the presence of a major port in the study area, the port of Tauranga, is of significance because it is the largest export port in New Zealand and maintenance dredging is conducted regularly. Therefore, I focused on the effects of increased turbidity due to the resuspension of marine sediments during dredging. I have also considered some aspects of catchment scale terrestrial sediment inputs in our study (in Chapter 2 and Chapter 5).

The topic of this study was divided into three main areas: (1) turbidity and light attenuation (both quantity and quality), (2) physiological response of sensitive species to increased turbidity, and (3) monitoring of dredging activity.

According to the results in Chapter 2, among the water constituents that attenuate light (inorganic and organic suspended particles and colour), turbidity caused by suspended particles is the main contributor to light attenuation in Tauranga Harbour (40-50%) (Table 2.1). This result was found using low-frequency (bi-monthly) measurements which did not include adverse weather conditions. By using the low-frequency light measurements in a regression model, I show that turbidity data can be used as a proxy to estimate the light attenuation coefficient, K_d(PAR). Hence, I could combine low-frequency with long-term, high-frequency

turbidity measurements to estimate variations in light attenuation. The high-frequency measurements are derived from an array of six sensors, deployed by the Port of Tauranga, which have been monitoring turbidity every minute for about 3 years. Thus, storms and other relevant events such as dredging were included in the analysis of K_d(PAR). The K_d(PAR) levels increased 45% on the intertidal when using the high frequency turbidity data, showing the relevance of long-term measurements which may include turbidity variation related to a variety of weather conditions and port activities (Macdonald et al., 2013). For management plans based on turbidity monitoring, this was an important finding since for aquatic plants, K_d(PAR) is a more relevant measurement than turbidity.

I found that light conditions in the intertidal zone are not limiting seagrass photosynthesis when immersed, but may affect growth in deeper channels. Therefore, turbidity thresholds for seagrass photosynthesis were revised. Currently, the turbidity limits used in Tauranga Harbour are based on a study which considered a light requirement of 15% surface irradiance for subtidal seagrasses (PoMC, 2008). Although that study is based on the same seagrass species (*Zostera muelleri*), intertidal seagrass, such as in Tauranga Harbour, is considered to have higher light requirements than subtidal seagrasses (Bulmer et al., 2016). I used the upper limit of 36% light requirement in our calculations for a conservative approach (Longstaff, 2003; Schwartz et al., 2006).

Turbidity can also be used as a proxy for suspended sediment concentration. Therefore, this can be used to estimate the effects of increased levels on suspension-feeders such as shellfish bivalves. In Chapter 3, I present results of experiments that tested the short-term effects of increased levels of suspended sediment concentrations on the feeding behaviour of the bivalve *Paphies australis*, commonly known as pipi. The concentrations tested were based on the range of turbidity generally experienced in the study area, including dredging events, which ranged from approximately 1 mg l^{-1} to 300 mg l^{-1}.

Pipis, like other species of bivalves, used adaptive mechanisms as a response to increases in suspended sediment (seston) concentrations, such as reduction in clearance rates and productions of pseudofaeces. Thus, they could control the

organic intake and regulate their energy acquisition. By fitting simple models to those results, it was possible to estimate thresholds of impacts. My results suggest that stabilization of feeding rates, in treatments ≥ 70 mg l^{-1} (Figure 3.3 and Figure 3.4), could impair food acquisition and therefore potentially impact pipi's biomass. Despite the recognized relevance of pipis in the area, both ecologically and culturally (Sinner et al., 2011), just a few studies have addressed the effects of increased turbidity in their feeding behaviour. My study brings progress in this field by adding several feeding and digestion rates that have not been previously measured, and thus, improving prediction models.

In Chapter 4, I used a combination of field monitoring and numerical modelling to track sediment plumes created during maintenance dredging in 2014, in Tauranga Harbour, New Zealand. A boat mounted ADCP recorded backscatter signals and was calibrated for suspended sediment concentration from water samples. The ADCP transects were used to describe plume development with time and distance from the dredging area and to calibrate and validate a numerical model. With that model, I simulated all monitored plumes and other scenarios of dredging activities in different hydrodynamics conditions. From ADCP transects and model results, monitored plumes presented maximum suspended sediment concentration of 70 mg l^{-1} and concentrations at dredging areas decayed to ambient levels in less than two hours after dredging ceased and in about six hours elsewhere. ADCP transects showed a stronger backscatter signal at the surface which fitted the hypothesis that overflow in TSHD is more critical than resuspension at the draghead for the far field plume.

Simulations of dredging cycles during flood and ebb tide in two different locations in the harbour were used to assess plume effects. Given the response levels and environmental limits used in Tauranga Harbour to monitor dredging activities, 30 and 70 mg l^{-1} (converted from turbidity), I found that concentrations exceeded thresholds only during dredging time, which was approximately 30 minutes, and the area in which exceedances occurred was limited to a narrow radius around the dredging area. Suspended sediment concentration at the dredging point decreased quickly after dredging ceased. I also found that the decay

time of the plume during flood tide presented higher concentrations and slower decaying rates for the time simulated (i.e. for specific hydrodynamics conditions). These results suggest that dredging during flood tide should be avoided.

Deposition of sediment plumes occurred mainly within navigational channels, in the order of 1 mm, and maximum thickness of approximately 2 mm were restricted to the dredging points. Sediment deposition thickness and area increased in simulations of cumulative plumes. I used sediment deposition to calculate the plume's footprint symmetry, which compares both length and width of plume, to identify vulnerability zones inside the harbour. The deposition in the main direction of tidal currents usually presented slower decay rates, which means that plumes will stay in suspension for longer, affecting light penetration and reaching further areas. However, depending on the location of dredging, the secondary axis might also be of a concern. This is usually neglected in simple models for worst-case scenarios; however the lateral dispersion can be relevant because it can cause low initial values, but have the same decaying rates as the main axis.

Throughout the study, I considered resuspension of marine sediments on turbidity. However, a large contribution of increased turbidity in harbours is the input of terrestrial sediments. In Chapter 5, I compared the effects of these two types of sediments and their colours - grey and white from marine sources, and yellow, from terrestrial sources - in the selective light attenuation, i.e., the change the spectral composition of underwater light. I analysed results from experiments using a tank and a spectrophotometer. Both marine and terrestrial sediments contribute to reduce light transmittance. However, terrestrial sediments caused extinction of light in the blue-green range and shifted light transmittance maxima towards wavelength bands that are not suitable for seagrass photosynthesis.

Sediment plumes from either dredging or catchment runoff will impact on light penetration, light quality, suspended sediment concentration in relation to background/ambient levels and in sediment deposition. The modelled plume footprint was put in perspective in relation to the location and thresholds of seagrass and pipi beds in Tauranga harbour (Figure 6.1).

With the relationship between sediment concentration, NTU and light attenuation, a conversion between the results from the numerical model and the turbidity data was possible, extending the model output to many applications. These include defining sensitive areas in the harbour during normal and storm conditions and during different dredging operations. Areas of concern in Tauranga Harbour are the pipi beds, particularly on the Centre Bank, where they are more densely populated (Ellis et al., 2013), and seagrass meadows south of Stella Passage and around Otumoetai.

Figure 6.1 illustrates that seagrass meadows around the harbour are located predominately on the intertidal flats. Our results indicated light levels in the channels were below those needed to sustain important seagrass communities, possibly explaining a loss of subtidal seagrass in the harbour. The light attenuation coefficient calculated from the long-term turbidity dataset shows the light requirements of seagrass *Z muelleri*, with the depth limit of colonization in the harbour at 1.62 m (Figure 6.1, solid white contour). This is the tidal range (spring tide) in the area (Heath, 1976). Light is not limiting seagrass photosynthesis in the intertidal areas for *Z. muelleri*, possibly explaining the current distribution of seagrass. Turbidity monitoring and dredging simulations over multiple dredging events allowed us to conclude that $K_d(PAR)$ during dredging periods did not show significant increase compared with background levels. Furthermore, results from model simulation of dredging cycles show that a 20 mg l^{-1} contour of plume concentration, which is the concentration threshold to guarantee minimum light requirements for *Z. muelleri* (Cussioli et al., submitted), do not generally extend over seagrass meadows. The exception for this is over a few small patches east and south of Stella Passage (Figure 6.1, dotted red contour).

The 30 mg l^{-1} and 70 mg l^{-1} contours of dredging plume concentrations are also presented in Figure 6.1 (solid red contours). These concentrations were determined in laboratory experiments as thresholds of potential feeding limitation on pipis (Cussioli et al, in prep), and are approximately the current limits used in Tauranga Harbour for monitoring dredging activities (converted from NTU values using the calibration equations in Appendix A). The contours of threshold

concentrations do not reach areas of concern. The upper threshold of 70 mg l^{-1}, is exclusively restricted to a small region around the dredging points used in the simulation.

The sediment deposition footprint from the model results show sediment layers of 1mm extend to areas of seagrass and pipis, however, sedimentation of 1mm thickness have not demonstrated negative impacts in *Z. muelleri* and pipi (Benham et al., 2016, Norkko et al., 2006). Deposition of 10 mm can potentially impact seagrass growth (Benham et al., 2016) but is still below the impact thresholds for pipis (Norkko et al., 2002). This was restricted to just a very small and immediate area around Sulphur Point.
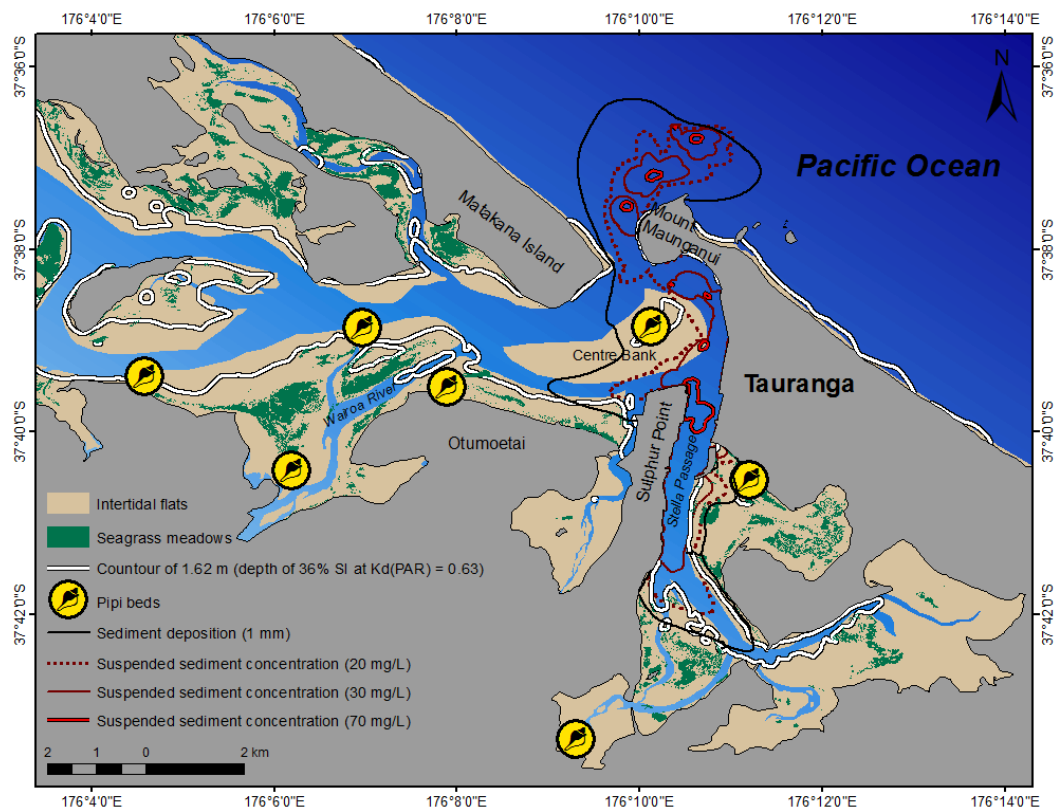
Figure 6.1: Illustration of the dredging plume footprint in relation to surrounding biological communities (seagrass meadows and Pipi beds). Seagrass meadows were mapped in 2011 (Park, 2016). Pipi beds are from an ecological survey conducted in the harbor between 2011/2012 (Ellis et al., 2013). The dredging plume footprint is represented by sediment deposition contour line and suspended sediment concentration contour lines, which were calculated as the maximum concentrations over the simulation period.

6.2 CONCLUSIONS

The research chapters described above provided a comprehensive, multidisciplinary understanding of the spatial and temporal variations of turbidity, particularly during dredging, and the effects on underwater light quantity and quality as well as the health of shellfish. The main thesis outcome was to predict whether negative impacts of a turbidity event on key species are likely to occur and to help manage conditions for dredging or any other port-related activity with monitoring and threshold suggestions.

We used a combination of different methods to improve understanding of the dominant forcing frequency, magnitude and duration of turbidity events as well as to track the sources, paths and impacts of turbidity plumes in Tauranga harbour. The key innovations and findings from this were:

- The development of a relationship between underwater light attenuation coefficient and turbidity in an estuarine lagoon system (New Zealand). Currently, there are few studies in the literature and very few studies for New Zealand estuaries that establish a relationship between underwater light availability and turbidity. This is an important controlling factor for primary production and ecological health. Until now, the conversion methods between light and turbidity that exist for estuaries have been developed for a very limited range of conditions.

- The estimates of light availability from turbidity measurements also enabled including both storm conditions and dredging periods in our assessment of average light conditions, which has not been previously investigated elsewhere.

- Modelling of several feeding and digestion rates of pipis, which have not been previously tested. There are only a few studies on the effects of increased turbidity on pipis and only one published study documenting the effects on pipi feeding behaviour. This study considered several feeding and digestion rates: clearance, filtration, ingestion, rejection and absorption rates, and selection efficiencies.

- The development of an index of plume symmetry, which contributed to identify sensitive areas around Tauranga Harbour. Most published studies on monitoring of dredging plumes have not considered both length and width of plume footprint, only focusing on the sediment transport in the main direction of currents. However, changes in plume footprint may have implications on ecological communities located around dredging areas. Furthermore, much of the information on plume dispersal can only be found in unpublished reports or are of restricted access (private companies).

- The effects of various types of sediment on the underwater light quality. There are currently very limited published papers on the effects of sediment colour on light quality. Previous studies have only documented effects of increased turbidity on the broad-band PAR. They have not, however, tested the changes in the energy distribution over waveband intervals. The underwater light quality is a vital factor for photosynthesis of seagrasses because they do not have accessory pigments and the efficiency of their photosynthetic processes is limited to a narrow spectral range. Therefore, shifts in light transmittance maxima related to suspended sediment concentrations can affect seagrass productivity.

- The methods used in this study are generally applicable, and specific results can be used for management and predictions for other similar systems.

Overall, the results indicated that sediment plumes generated during maintenance dredging caused suspended sediment concentrations and exposure duration that were below thresholds for adverse impacts for the two main groups of species in the harbour, seagrass and pipis. Plume deposition also caused low disturbance, but increased when multiple plumes were considered in the model simulation. On the other hand, Terrestrial sediment inputs are suggested to be of higher concern when compared with resuspended marine sediments. This is due to the reddish-coloured sediments, which can enhance the reduction in the wavelengths needed for seagrass photosynthesis.

6.3 SUGGESTIONS FOR FUTURE RESEARCH

In Chapter 2, results show the critical importance of long-term datasets to capture events of increased turbidity levels. Those events are essential to develop robust limits on light attenuation for environmental management. A higher frequency of *in situ* light measurements, would be beneficial to the relationship between turbidity and light attenuation and improve the statistical analysis used for establishing that relationship. Measurements of light during poor weather conditions would provide a valuable addition to the model. Since fieldwork is challenging during poor weather, and even hazardous, this could be achieved by deployment of sensors. For example, in Appendix B, I described results from a deployment of turbidity and light sensors. The measurements display a rainfall period that affected both light and turbidity records. The instruments recorded data for 3 weeks without interferences, including biofouling, due to a wiper system that kept sensors clean of incrustations. The site was visited once during deployment to check for any other source of error, such as detached seagrass, ulva, etc. Therefore, future work should consider sensor deployment to cover a wet season, and locate sensors in strategic sites near major rivers (Wairoa), on seagrass beds, in the shipping channels and in the southern estuaries and bays. That would cover most of the areas that influence seagrass beds and includes the main sources of plumes in the harbour.

Another suggestion is to measure light attenuation and sediment deposition in the boundary layers, sediment-canopy and canopy-water column. When I calculate light attenuation coefficient, I infer values from the water column which is considered more 'stable' compared with the benthic-pelagic layer. The resuspension and turbulence at the fringe of seagrass meadows can decrease light penetration several fold (Pedersen et al., 2012). Also in this context, measurements of light spectra on seagrass beds would add valued information on the thresholds for turbidity in relation to seagrass, as shown in Chapter 5.

The turbidity sensors deployed in the harbour by the Port offer a unique dataset, comprising (in some of the sensors) more than 3 years of high-frequency data. The sensors are cleaned and maintained on a regular basis; however,

biofouling and interruptions usually occur. Some of those signals are easily detected in the dataset, and so affected data can be removed manually. However, as shown in Appendix A, after using those methods, the data still contains some spikes and noise. Perhaps an improvement would be the use of wipers to maintain sensors clean of incrustations, as these were shown to be effective in the shorter-term deployment.

In Chapter 3, improvements could be done in terms of increasing time and concentrations tested. The length of experimental runs was chosen based on a pilot study that indicated pipis responded to treatments in about 2 h. It was also the length of time for dredging plumes to dissipate, according to the ADCP results. Therefore, I could compare the experiments results to the turbidity generated during maintenance dredging campaign. The short time frame had the advantage of allowing us to carry out several replicates which improved our analysis. However, an increase in the time of experimental run could have shown different results (Hewitt and Norkko, 2007) and represented other more extensive dredging programs, such as capital dredging. The maximum concentration tested did not show an overload of the feeding apparatus, only an indication of it (Barillé et al., 1997; Hawkins et al., 1999). Therefore, for future work, it would be beneficial to increase length and concentrations tested to reach the ultimate overload. It would also be of interest to test the effects of marine and terrestrial sediments on pipi feeding behaviour and smothering.

During dredging monitoring, the ADCP was a very useful instrument to track plumes. It could capture the plume in the far field and distinguish between different layers of turbidity. The sequence of transects, both in time and distance, showed sediment settling and dispersal. I calibrated the ADCP using suspended sediment concentrations from water samples. However, it was difficult to sample the plume given their transient nature. The time of water samples did not always match the position and time of maximum concentrations as indicated in the ADCP backscatter profile, which compromised calibration. Also, I did not account for differences in particle size which may have large influence in the in the calibration process. A simultaneous sampling approach using several sensors would improve the

calibration process considerably. An example of this method is described in (Gartner, 2004). A frame containing several instruments (ADCP, particle size analyser, turbidity sensors, water bottles, CTD and light sensors), would record simultaneous data and permit a more reliable calibration. Also, such a set up would allow measurements inside the plume and closer to the dredging vessel, which was very challenging during fieldwork.

Regarding model simulations, the implementation of a 3D model could reveal the differences in turbidity within the water column, as shown in the ADCP transects. This depth-distribution of suspended sediments is relevant when several processes are responsible for the generation of plumes. Testing the outcome of different overflow methods, for instance, could be tested. Also, in the case of a stratified estuary, the gradient in density would separate suspended sediment layers and trap plume at one depth, extending the plume footprint while being transported by currents.

Working together with the dredging company for more information in the dredging cycles, a simulation of a complete month of maintenance dredging, with grain size analysis, volumes, and exact time and percentage of overflow, would give a realistic view of maintenance dredging effects. Although monitored and modelled plumes dissipated and deposited quickly, plume decay and footprint may be different in other hydrodynamic conditions.

The model did not include salinity, rainfall, wind, or waves, which are all important contributors to the hydrodynamic conditions and therefore sediment transport. Sediment plumes transported to shallow areas might be more susceptible to be resuspended by strong winds and be transported elsewhere. The same is valid for sediment deposited near areas affected by waves. Therefore, future projects could apply a more complex 3D model setup, including wind and waves. Additionally, models could include background sediment concentrations and inputs from rivers to compute the overall budget of sediment in the system.

APPENDIX A

TURBIDITY (ANALYTE SENSORS)

METHODS

The Port of Tauranga deployed six turbidity sensors (ANALITE NEP9500) at the southern harbour (sites S1 to S6 - Figure 2.1) which records turbidity every minute and were operational from January, October, November and December 2012 (S3, S5, S2 and S4, respectively), from February 2013 (S6), and from January 2014 (S1). Here I present data from January 2013 until October 2016.

I removed spikes in the dataset using a de-spiking algorithm and smoothed data using a 6-hour moving average (see Chapter 2 for detailed methods and timeseries plot). The turbidity dataset includes three dredging events: maintenance dredging from 01/10/2014 to 01/11/2014 (M1), maintenance dredging from 19/08/2015 to 08/09/2015 (M2), and a capital dredging from 01/10/2015 to 01/09/2016 (CP).

Calibration of turbidity sensors

I calibrated an exemplar of the ANALITE NEP9500 turbidity sensor in laboratory using two sediment samples in the calibration, grey and white, same samples used in the spectrophotometer experiment in Chapter 5. Details of sample location and textural analysis are in de Lange et al (2014). Grey sediment sample is composed of 54.5% sand and 45.5% fines (42% silt and 3.5% clay) and white is composed of 54% sand and 46% fines (43% silt and 3% clay). Photos of sediment samples are shown in Figure 5.1d and Figure 5.1e. I added aliquots of sediment to a 40-liter bucket of distilled water (concentrations of sediment tested varied from 2 mg l^{-1} to approximately 200 mg l^{-1}) and sediment was kept in suspension using a stirrer while turbidity was logged during 30 s. Afterwards, water samples were collected for total suspended sediment concentration analysis (TSS). Turbidity

values used in the linear regression were the average over the 30-seconds recording time for each concentration tested. The equations and correlation coefficients are presented below.

Table A.1: Calibration equation and correlation coefficient for turbidity sensors ANALITE. Grey and white refer to sediment colour used in the calibration procedure.

Turbidity sensor	Sediment	Equation	r^2 (n)
ANALITE	grey	TSS = 2.104 × NTU + 0.111	0.997 (10)
	white	TSS = 3.887 × NTU − 3.782	0.997 (7)

Here I present the mean and median of turbidity records and TSS for each site (S1, S2, S3, S4, S5 and S6) and period (ALL, NO, M1, M2, and CP). ALL represents all records in the dataset from the period analysed and NO is the ALL dataset excluding M1, M2 and CP periods. I also present plots of probability of occurrence, duration of turbidity events, and percentage exceedance curves.

RESULTS AND DISCUSSION

Mean and median values showed that S4 presented highest turbidity and thus TSS (Table A.2). For all periods analysed, S4 had mean turbidity of approximately 5 NTU and median 4 NTU (Table A.2 and Figure A.1). The highest mean and median value was calculated for the CP period. However, comparison between datasets must be done with caution because it could be biased by rainfall and seasonal patterns. The dataset excluding some dredging events (NO) presented highest averages when compared with dredging periods M1 and M2. NO was also of similar mean as CP periods. NO and CP had the highest number of records. Instead, M1 and M2 had lowest averages and lowest number of points. Therefore, NO and CP included relatively larger number of rainfall events that may have contributed to the increased turbidity (Figure 2.4).

Highest averages were also calculated for S5. S4 and S5 are in the southern region of the shipping channels in the harbour. Additional to the dredging, the area is close to an inlet which flows from an intertidal flat. It is also close to a marina and the Port's berthing wharves, therefore, experiences ship traffic and water flowing from adjacent bays.

Lowest average turbidity ranged from 2 to 3 NTU and was typically recorded in S2 and S3. The fast-flowing currents around those areas, which are close to the entrance of the harbour, contributed for a rapid flush of suspended material. At the entrance (S1), although presenting strong currents (APPENDIX E) and therefore rapid flushing periods, elevated turbidity could be related to dredging carried out in the area and peaks of turbidity related to the transport of plumes flowing outside the harbour from other dredging areas.

Table A.2: Statistics of turbidity data recorded by ANALITE sensors from January 2013 until October 2016. Periods analysed are all dataset (ALL, n~106), excluding dredging periods M1, M2 and CP (NO, n~106), maintenance dredging 1 (M1, n~104), maintenance dredging 2 (M2, n~104) and capital dredging (CP, n~104).

Site	Period	Turbidity (NTU) Mean	Turbidity (NTU) Median	Grey sediment (mg l⁻¹) Mean	Grey sediment (mg l⁻¹) Median	White sediment (mg l⁻¹) Mean	White sediment (mg l⁻¹) Median
	ALL	3.6	3.1	7.8	6.6	10.4	8.1
	NO	4.1	3.2	8.7	6.8	12.0	8.6
S1	M1	3.7	3.4	8.0	7.2	10.7	9.3
	M2	2.0	1.7	4.4	3.7	4.1	2.8
	CP	3.2	2.9	6.8	6.3	8.7	7.7
	ALL	2.9	2.4	6.3	5.1	7.6	5.4
	NO	2.9	2.3	6.3	4.9	7.7	5.1
S2	M1	2.6	2.3	5.5	4.9	6.2	5.1
	M2	2.2	1.5	4.7	3.3	4.6	2.1
	CP	3.0	2.6	6.4	5.5	7.9	6.2
	ALL	2.9	2.5	6.3	5.4	7.6	6.0
	NO	3.0	2.6	6.4	5.5	7.9	6.1
S3	M1	2.1	1.7	4.5	3.6	4.3	2.7
	M2	2.6	2.1	5.6	4.5	6.4	4.4
	CP	2.8	2.5	6.1	5.4	7.2	6.0
	ALL	5.1	4.4	10.8	9.4	15.9	13.4
	NO	5.0	4.3	10.7	9.2	15.7	13.0
S4	M1	4.8	3.8	10.3	8.1	15.0	11.0
	M2	4.8	3.8	10.2	8.1	14.9	10.9
	CP	5.2	4.7	11.0	10.1	16.4	14.6
	ALL	4.2	3.3	8.9	7.1	12.4	9.1
	NO	4.1	3.0	8.8	6.4	12.3	7.8
S5	M1	4.0	3.2	8.6	6.9	11.9	8.8
	M2	2.9	1.8	6.3	3.9	7.6	3.3
	CP	4.3	4.1	9.2	8.8	13.1	12.3
	ALL	3.5	2.7	7.4	5.8	9.7	6.7
	NO	3.7	2.7	7.8	5.8	10.4	6.8
S6	M1	3.0	2.3	6.5	5.0	8.0	5.3
	M2	2.6	2.0	5.7	4.4	6.5	4.2
	CP	3.1	2.7	6.5	5.8	8.1	6.8
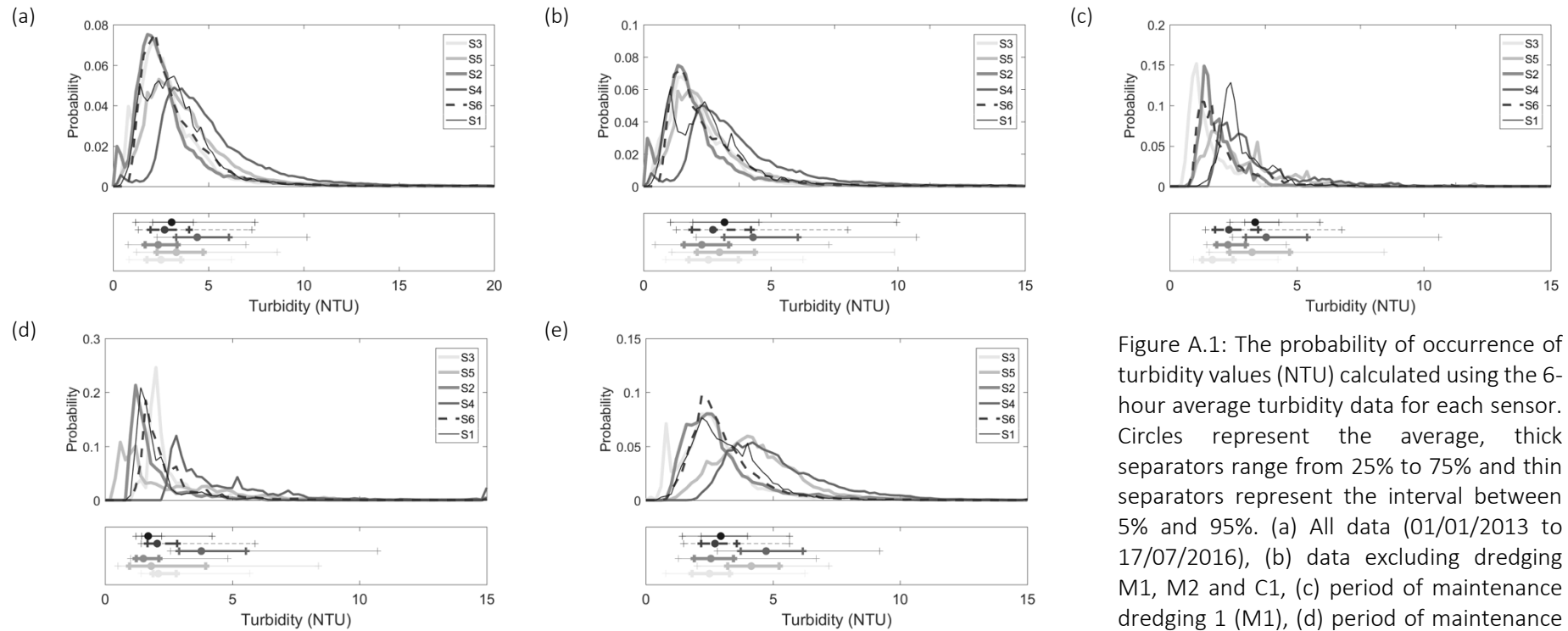
Figure A.1: The probability of occurrence of turbidity values (NTU) calculated using the 6-hour average turbidity data for each sensor. Circles represent the average, thick separators range from 25% to 75% and thin separators represent the interval between 5% and 95%. (a) All data (01/01/2013 to 17/07/2016), (b) data excluding dredging M1, M2 and C1, (c) period of maintenance dredging 1 (M1), (d) period of maintenance dredging 2 (M2) and (e) capital dredging (CP).

Figure A.2 shows the mean duration of turbidity events of certain magnitude at all sites. As cited above, the highest average turbidity, approximately 5 NTU, occurred at S4. Turbidity events of that magnitude were also of the longest duration at same site (10 h). Therefore, S4 presented not only the highest average turbidity, but the highest average was also the value of longest duration. Turbidity events greater than 5 NTU (at S2, S3 and S6) and greater than 8 NTU (at all sites except S4) had a duration of about six hours, which is the related to the tides. It is important to note that this duration may be slightly biased by the 6-hour window used in the moving average process.
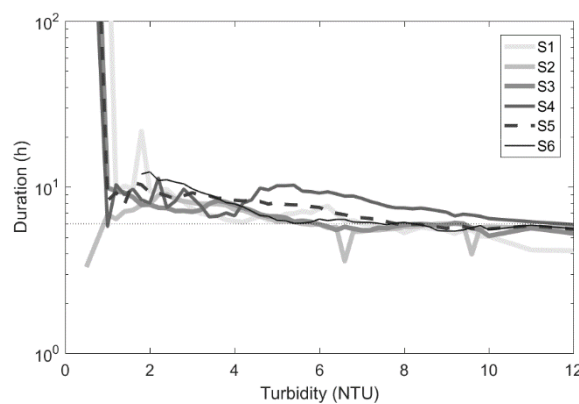
Figure A.2: Mean duration of turbidity events at each site. Dotted line shows the duration of 6 hours for reference.

The exceedance curves were calculated at all sites for different periods (ALL, NO, M1, M2 and CP). In Figure A.3, horizontal dotted lines highlight 10, 50 and 90% exceedance and vertical dotted lines represent several thresholds: 9 NTU (optimal conditions for seagrass, Chapter 2), 12 NTU (threshold for seagrass currently used in Tauranga Harbour), 14 NTU (lower threshold baseline for pipis feeding response, calculated from TSS (30 mg l^{-1}, Chapter 3) using calibration coefficients for grey sediment), 15 NTU (threshold for shellfish currently used in Tauranga Harbour), and 33 NTU (upper threshold baseline for pipis feeding response, calculated from TSS (70 mg l^{-1}, Chapter 3) using calibration coefficients for grey sediment).Except for S4, all sites presented less than 5% of records exceeding lowest threshold (9 NTU). At S4, 10% of measurements exceeded lowest threshold. Similarly, 10% of turbidity values exceeded thresholds at S4 and less than 5% at other sites during dredging periods. The sites with lowest turbidity, S2 and S3, presented less than 2% of data exceeding thresholds.

(a)

(b)

(c)

(d)

(e)
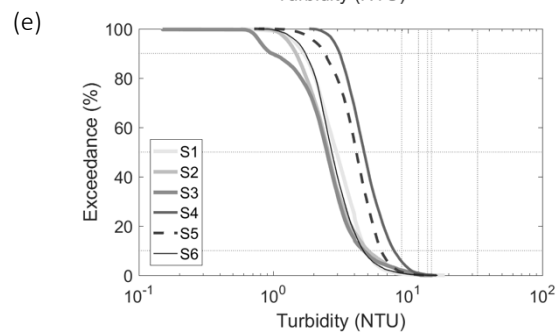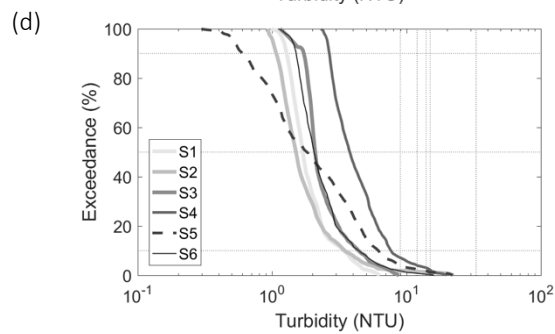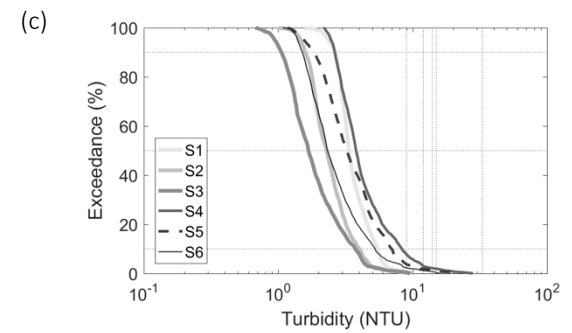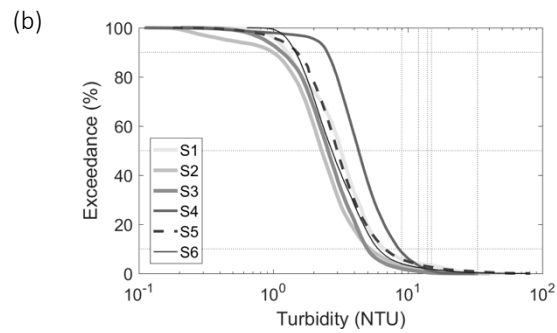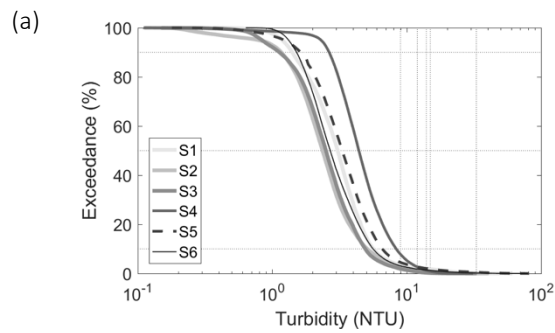
Figure A.3: Exceedance curves at all sites for turbidity measurements. Plots are for different periods: (a) All data (01/01/2013 to 17/07/2016), (b) data excluding dredging M1, M2 and C1, (c) period of maintenance dredging 1 (M1), (d) period of maintenance dredging 2 (M2) and (e) capital dredging (CP).

APPENDIX B
TURBIDITY AND LIGHT SENSORS DEPLOYMENT

METHODS

I deployed turbidity and light sensors at S6 (Figure 2.1) for three weeks in March 2016 (09/03/2016 – 01/04/2016). The deployment period was simultaneously to the capital dredging (CP, Appendix A). Two sets composed of one light sensor (Licor) and one turbidity sensor (Seapoint) were attached 1.2 m apart to a frame (Figure B.1), with bottom set extending out from the frame to avoid being obscured by top sensors. The frame was attached to one pole at the Otumoetai A beacon, below chart datum, therefore it was constant submerged during deployment. All sensors were connected to a connected to a RBR Concerto logger. Wipers kept the sensors clean of biofouling and the site was visited once to check if sensors were clean. I calculated the light attenuation coefficient (K_d(PAR), m^{-1}) using the equation described in Davies-Colley, Vant and Smith (1993). PAR is the photosynthetically active radiation.

$$K_d(PAR) = \frac{\ln[I_{z_1}/I_{z_2}]}{z_2 - z_1}$$

Equation (2)

where I_{z1} and I_{z2} are the irradiances (PAR, μmol m-2 s-1) measured at depths $z1$ and $z2$ (m). z_2–z_1 equals the distance between sensors, 1.2 m.

The deployment was carried out to measure variations in turbidity and irradiance due to the ongoing capital dredging near seagrass meadows in the harbour, at Otumoetai (Figure 4.1).
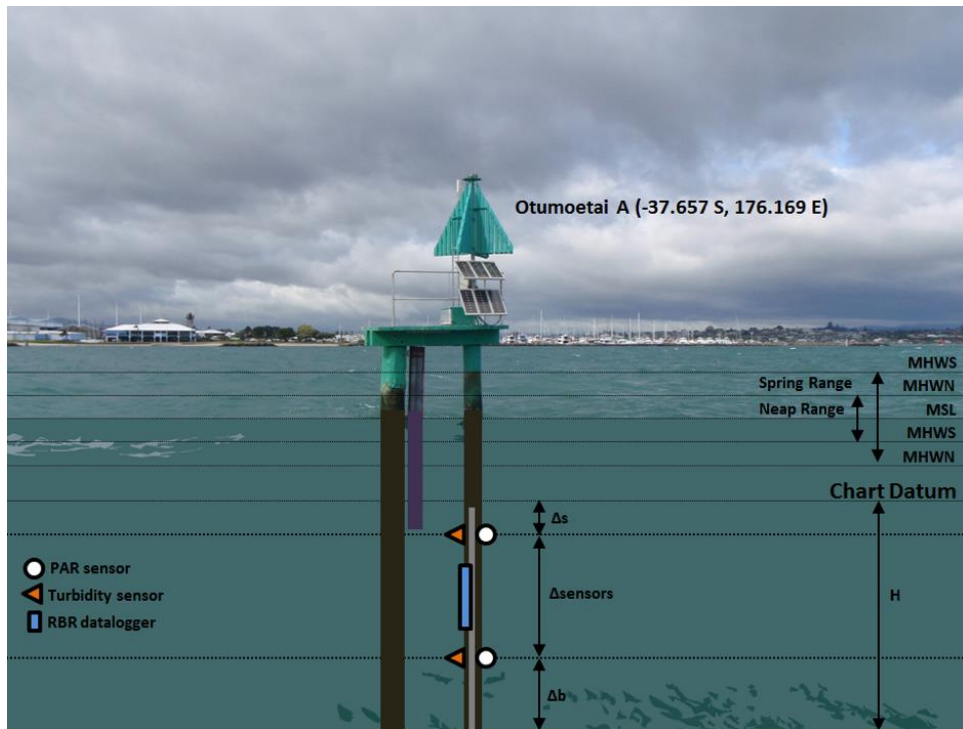
Figure B.1: Diagram of deployment at S6 (Otumoetai A beacon). Light and turbidity sensors are represented by a white circle and an orange triangle, respectively, and data logger is represented by a blue rectangle. ΔSensors was 1.2 m. The purple bar is the turbidity sensors at S6 described in Appendix A.

Calibration of turbidity sensors

I calibrated the turbidity sensor Seapoint for suspended sediment concentration (TSS, mg l^{-1}) simultaneously to the turbidity sensor ANALITE, as described in Appendix A, for both grey and white sediment. The resultant equations are presented in Table B.1.

Table B.1: Calibration equation and correlation coefficient for turbidity sensors ANALITE (deployed by the Port of Tauranga) and Seapoint (part of the 3-week deployment carried out in this study using turbidity sensors and PAR at S6 (Figure 2.1)). Grey and White refer to sediment colour used in the calibration procedure.

Turbidity sensor	Sediment	Equation	r2 (n)
Seapoint	Grey	TSS = 1.412 × NTU + 9.637	0.993 (12)
	white	TSS = 3.012 × NTU + 2.594	0.999 (7)

RESULTS

Figure B.2 presents time series of rainfall, average solar radiation, photosynthetically active radiation, turbidity recorded by Seapoint sensors, total suspended sediment concentration, turbidity recorded by ANALITE, and water level.

Photosynthetic active radiation (PAR) was maximum at around noon and during low tides. Top sensor had slightly higher values than bottom sensor, reaching approximately 1000 µmol s^{-1} m^{-2}. Variations in PAR occurred with changes in average solar radiation (Kdown) related to rainfall events. Although both, Kdown and rainfall, were not recorded at the same location as turbidity and PAR, it is possible to observe concurrent changes in those parameters in the timeseries. On the 17th March, there is a peak in rainfall followed by a peak in turbidity and decrease in Kdown; however, PAR is not notably affected. Similarly, rainfall peaks on the 18th and Kdown decreases from 18th to 24th in Omokoroa, but those variations do not cause a significant change in light availability at Otumoetai. Towards the end of the deployment, a weaker but longer rainfall period recorded from 24th to 25th is marked by a low Kdown, increased turbidity and the lowest PAR recorded in the period of deployment.

Both turbidity sensors (Seapoint – this deployment and ANALITE – deployed by the Port) recorded similar turbidity variations, particularly turbidity sensor at the bottom set. Differently from the sensors I deployed, which were fixed at a depth, the ANALITE sensor is attached to a floating device which keeps sensor at 1 m depth below water level, i.e., it moves up and down following tidal variations. Various peaks in turbidity data can be seen in both records, however top Seapoint sensors presented several spikes which could be related to the sensors being exposed at times. Biofouling might have occurred for short periods; however, sensors were clean when retrieved. Although planned to be at least 70 cm below lowest water level, strong winds or the passage of a fast boat could have caused the water level to locally drop below depth of sensors, exposing them to the air. Peaks in turbidity could also be related to the ongoing capital dredging at the time of deployment. According to our results of Chapter 4, if dredging took place around Sulphur Point, as shown in area H4, dredging plumes could have dispersed towards Otumoetai

122

during flood tides. Nevertheless, runoff after heavy rainfall from Omokoroa sites towards Otumoetai during ebb tides, could also bring suspended sediments which would be recorded by turbidity sensors at the surface.
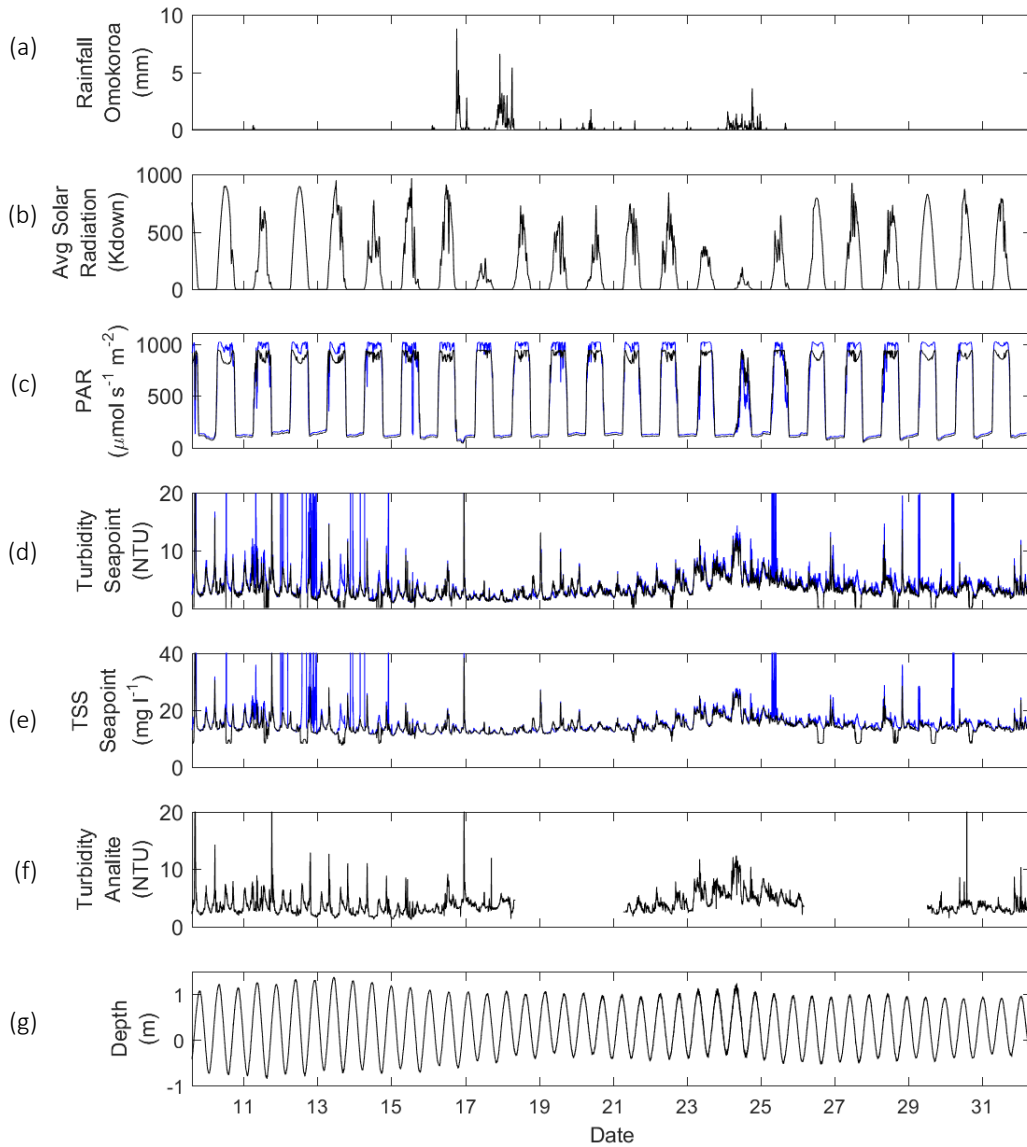
Figure B.2: Time series of (a) rainfall, (b) average solar radiation, (c) photosynthetically active radiation, (d) turbidity recorded by Seapoint, (e) total suspended sediment concentration, (f) turbidity recorded by ANALITE, and (g) water level. Photosynthetically active radiation (PAR), turbidity (Seapoint) and water levels were recorded from 09/03/2016 to 01/04/2016, at site S6. Total suspended sediment concentration (TSS) was calculated from turbidity data (recorded by sensors Seapoint). Blue line indicates values recorded by sensors at surface and black line by sensors placed 1.2 m down from surface sensors. ANALITE sensor is deployed since February 2013 and data was provided by the Port of Tauranga. Rainfall and average solar radiation were recorded at a nearby weather station at Omokoroa (site not shown in map) and are the average value over preceding 10 minutes.

Comparing the mean and median for recorded data, median was usually considerably lower than the mean, except for turbidity recorded by bottom sensors (and thus TSS for that layer). Differences between surface and bottom values were larger for turbidity and lower for PAR (Table B.2). Mean surface turbidity had high values compared with mean bottom and median, likely biased by spikes, as discussed above.

Table B.2: Statistics of PAR and turbidity data recorded by Seapoint and Licor sensors at S6 from 09/03/2016 to 01/04/2016 (n=37621). TSS is calculated using calibration coefficients and K_d(PAR) calculated using PAR data.

	Mean	Median
PAR surface (μmol s^{-1} m^{-2})	487.3	169.3
PAR bottom (μmol s^{-1} m^{-2})	464.8	167.7
Turbidity surface (NTU)	20.0	3.4
Turbidity bottom (NTU)	3.2	2.9
TSS grey surface (mg l^{-1})	37.9	14.5
TSS grey bottom (mg l^{-1})	14.1	13.7
K_d(PAR) (m^{-1})	0.1	0.1

The probability density function of turbidity compares median values for surface and bottom. Thin lines, which extend from the 5th to the 95th percentile, show that 95% of data records were below 10 NTU, and 75% (thick lines) were below 5 NTU. The distribution of K_d(PAR) calculated from PAR records show 95% of values below 0.2 m^{-1}. Those values of K_d(PAR) were lower compared with values measured at S6 in different periods and elsewhere in southern Tauranga Harbour (Chapter 2, Appendix I). They were also lower than values measured during dredging in a nearby area (Sulphur Point) in the 2014 maintenance dredging campaign (Chapter 2, Appendix I).
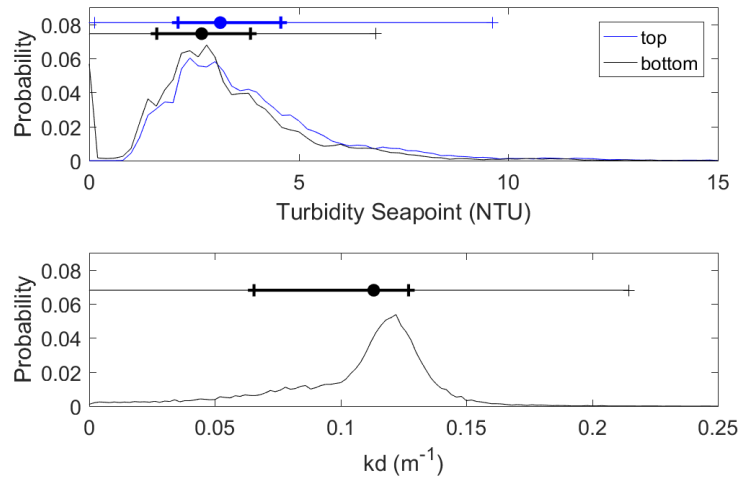
Figure B.3: Probability density functions of turbidity and K_d(PAR). Kd was calculated using 6-hour averaged PAR data. Circles represent 50% (median), thick lines represent the interval between 25% and 75% and thin lines represent the interval from 5% to 95%.

The exceedance curves for surface and bottom turbidity are plotted against environmental thresholds for reference (Figure B.4, vertical dotted lines): 9 NTU (optimal conditions for seagrass, Chapter 2), 12 NTU (threshold for seagrass currently used in Tauranga Harbour), 14 NTU (lower threshold baseline for pipis feeding response, calculated from TSS (30 mg l^{-1}, Chapter 3) using calibration coefficients for grey sediment), 15 NTU (threshold for shellfish currently used in Tauranga Harbour), and 33 NTU (upper threshold baseline for pipis feeding response, calculated from TSS (70 mg l^{-1}, Chapter 3) using calibration coefficients for grey sediment). Horizontal dotted lines represent 10, 50 and 90% exceedance limits. The results show that surface turbidity had approximately 6% of its records exceeding the lowest threshold of 9 NTU and bottom turbidity had less than 2% of values exceeding that threshold.
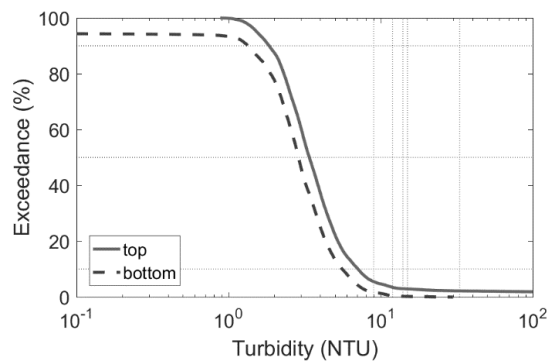
Figure B.4: Exceedance curves for turbidity measurements at surface and 1.2 m below surface sensor.

APPENDIX C

ADCP TRANSECTS – DREDGING

Dredging 13/10/2014 – Area E5

ADCP measurements after 25 minutes of the start of dredging activity detected a surface plume approximately 150 m long with a vertical gradient of TSS ranging from around 40 mg l^{-1} at the surface and decreasing towards the bottom (Figure C.1a). Following transect downstream of the tidal flow (ebb) show plume at surface, shorter (~60 m long) and lower in TSS (~20 mg l^{-1}, Figure C.1b). Transects carried out 10 to 15 minutes after dredging finished depicted settling of sediments and consequent reduction in TSS (Figure C.1c and d).

DATA_017_ASC.TXT [13/10/2014 14:50-14:53]
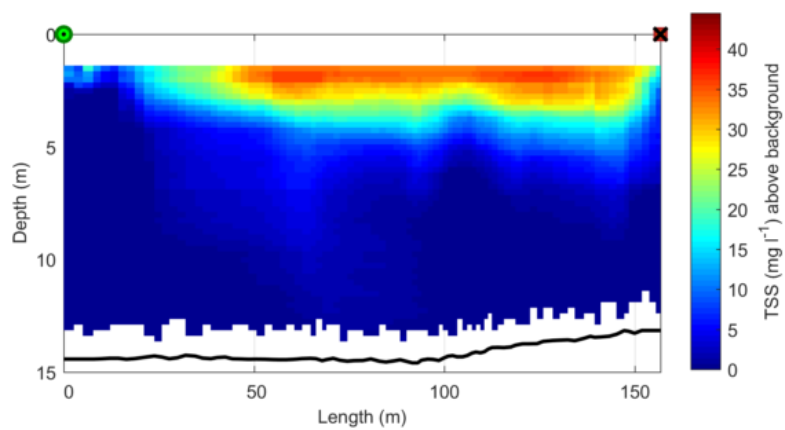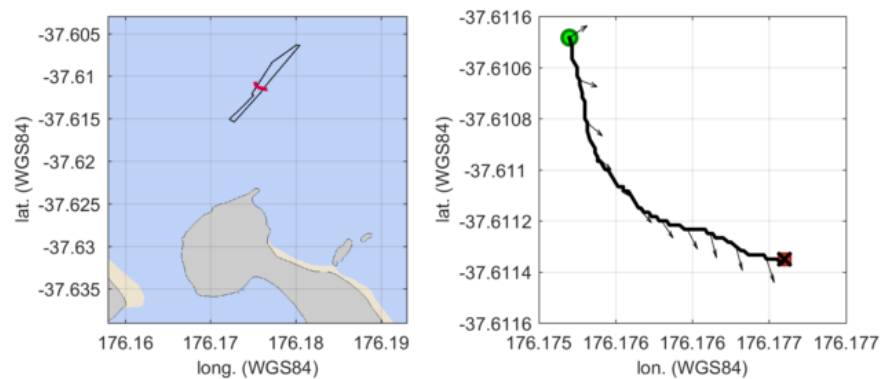
DATA_019_ASC.TXT [13/10/2014 14:55-14:57]

(a)

(b)
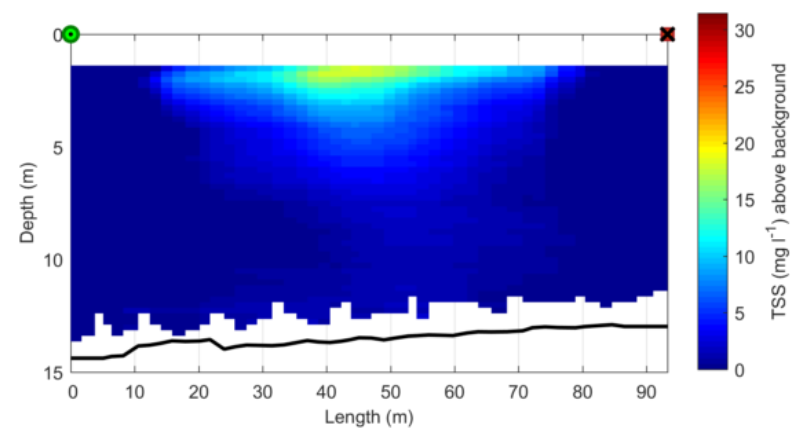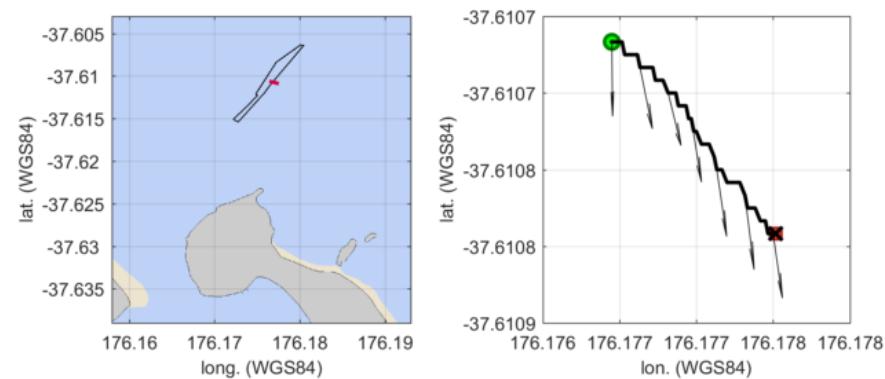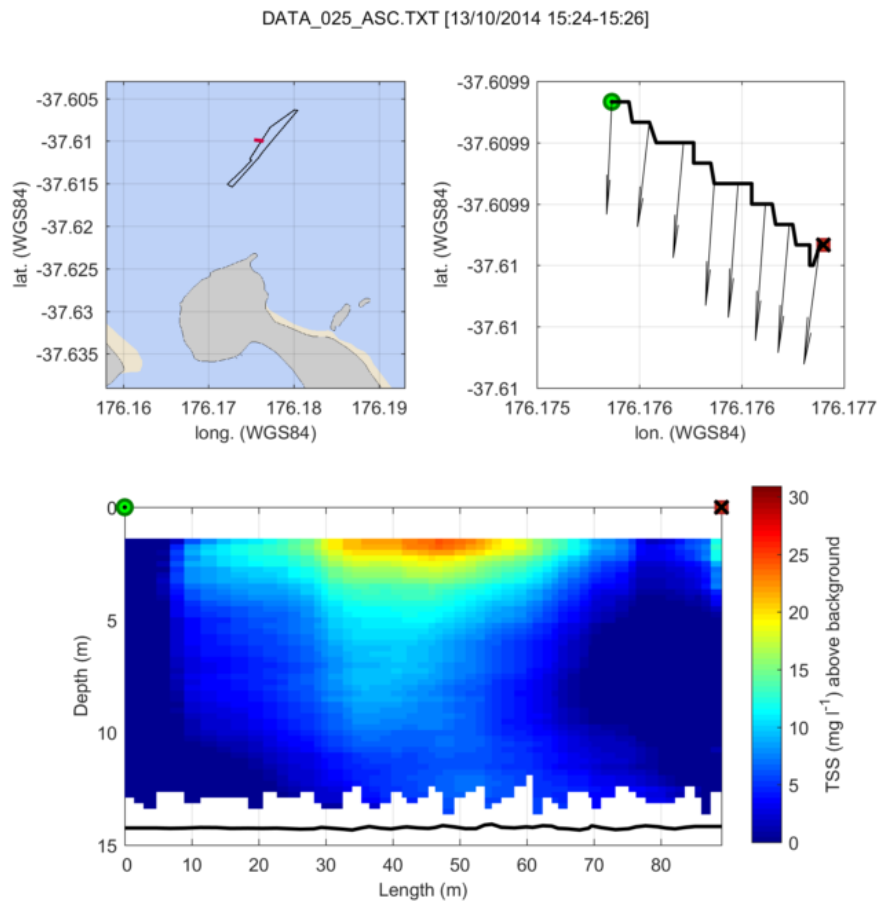
Figure C.1: Transects carried out during and after maintenance dredging at E5 on the 13th October 2014. Top left map shows the location of transects (red line) and dredging area (black line) and top right map shows detailed transect position. Green circle is the start point and red square is the end point. Bottom profile shows TSS above background; white areas represent the bottom and bins not measured by the ADCP.

Dredging 14/10/2014 – Area H4

TSS during monitoring of dredging at H4 reached 55 mg l^{-1} above background. A transect carried out 26 minutes after dredging started show high TSS at the surface down to 4 m depth, with TSS decreasing gradually to background TSS at 8 m depth (Figure C.2a). Given the dredging at H4 was carried out during flood tide, a series of transects were performed to identify main pathway of plume, to Stella Passage or Otumoetai. Two transects carried out towards Stella Passage after 42 and 54 minutes (Figure C.2c and d) show that part of the plume is transported to the channel and has low TSS (~ 8 mg l^{-1}) compared with TSS shown in transect carried out towards Otumoetai (Figure C.2e), after 68 minutes (~ 36 mg l^{-1}). This indicate that main plume was likely transported towards Otumoetai. One transect carried out nearly 2 hours after dredging (46 minutes after dredging ceased) at the dredging area, show TSS decreased to background level.

130
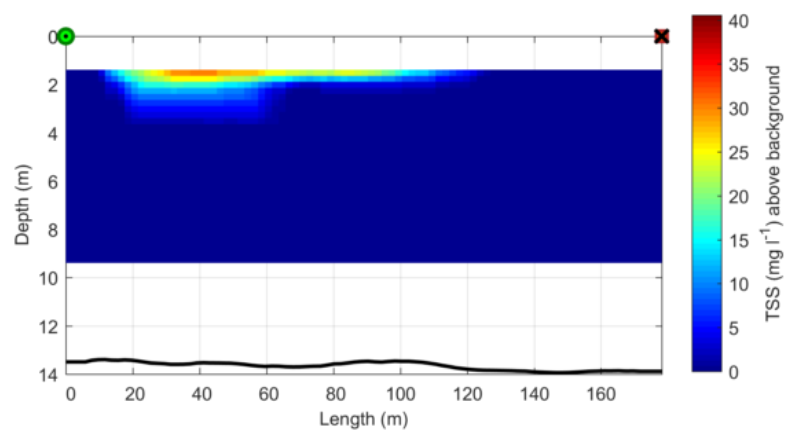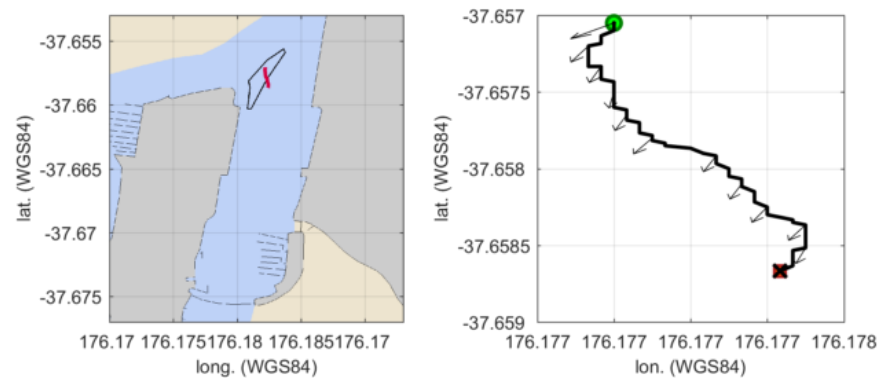
(c) DATA_039_ASC.TXT [14/10/2014 07:42-07:43]
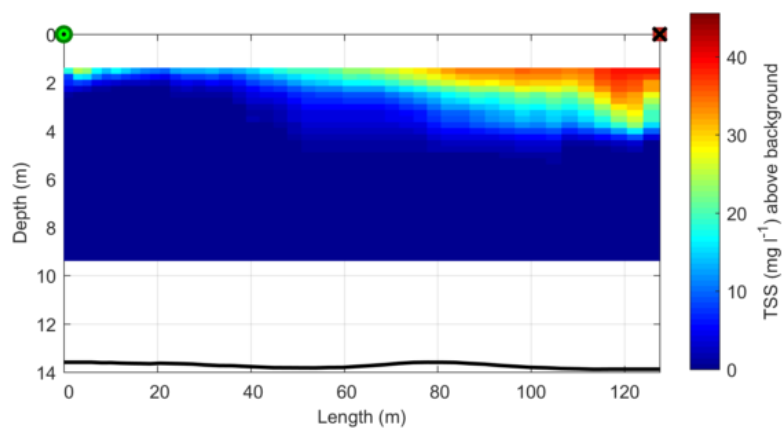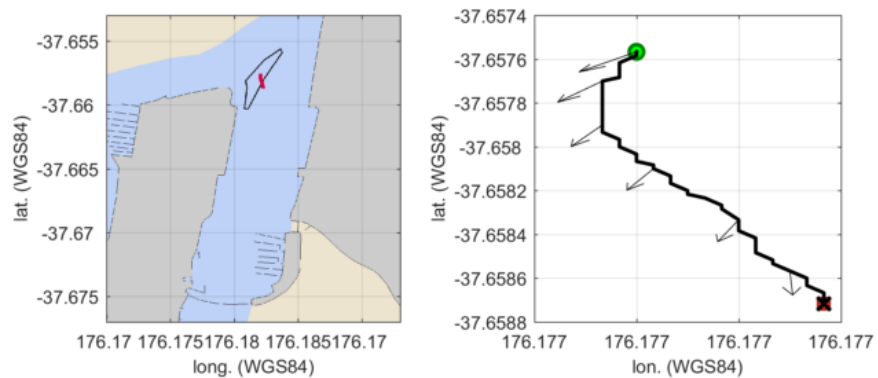
(d) DATA_045_ASC.TXT [14/10/2014 07:54-07:56]

131
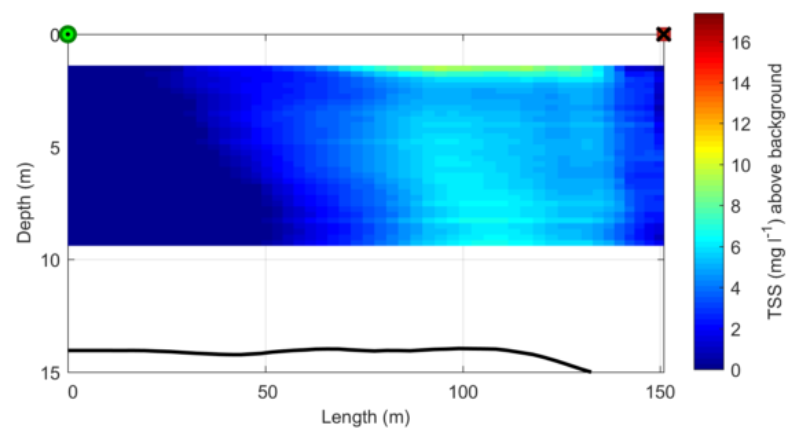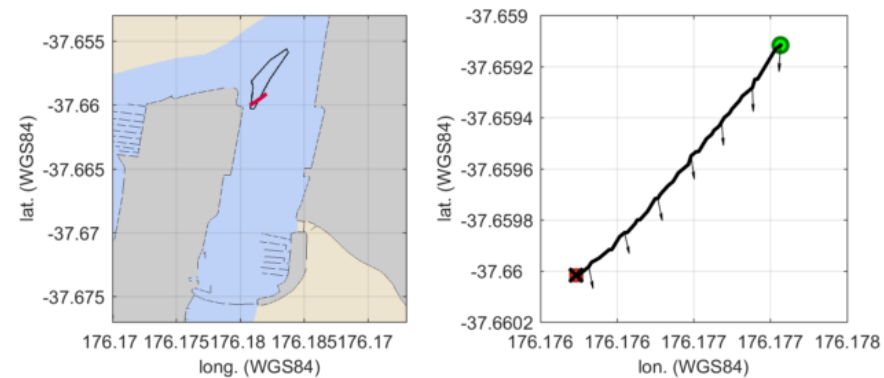
Figure C.2: Transects carried out during and after maintenance dredging at H4 on the 14th October 2014. Top left map shows the location of transects (red line) and dredging area (black line) and top right map shows detailed transect position. Green circle is the start point and red square is the end point. Bottom profile shows TSS above background; white areas represent the bottom and bins not measured by the ADCP.

Dredging 14/10/2014 – Area SP1

Plume detected during dredging at SP1 was usually restricted to the Sulphur Point berthing area. Maximum TSS during dredging was 49 mg l^{-1} above background level. Transect at the end of dredging show plume of around 30 mg l^{-1}, at the surface, with TSS decreasing to the bottom, depicting the settling of sediments (Figure C.3a). Following transect at 10 minutes after dredging ceased show plume of similar characteristics slightly higher in TSS (Figure C.3b). Approximately 15 minutes after dredging finished, a transect carried out in the channel show background TSS (Figure C.3c) and 25 minutes after dredging, a transect north of dredging area (downstream - ebb tide) show a descending plume with maximum TSS at mid-depth between 3 and 5 mg l^{-1} and low concentrations around 2.5 mg l^{-1} reaching the bottom (Figure C.3d).

(a) DATA_109_ASC.TXT [14/10/2014 14:13-14:16]
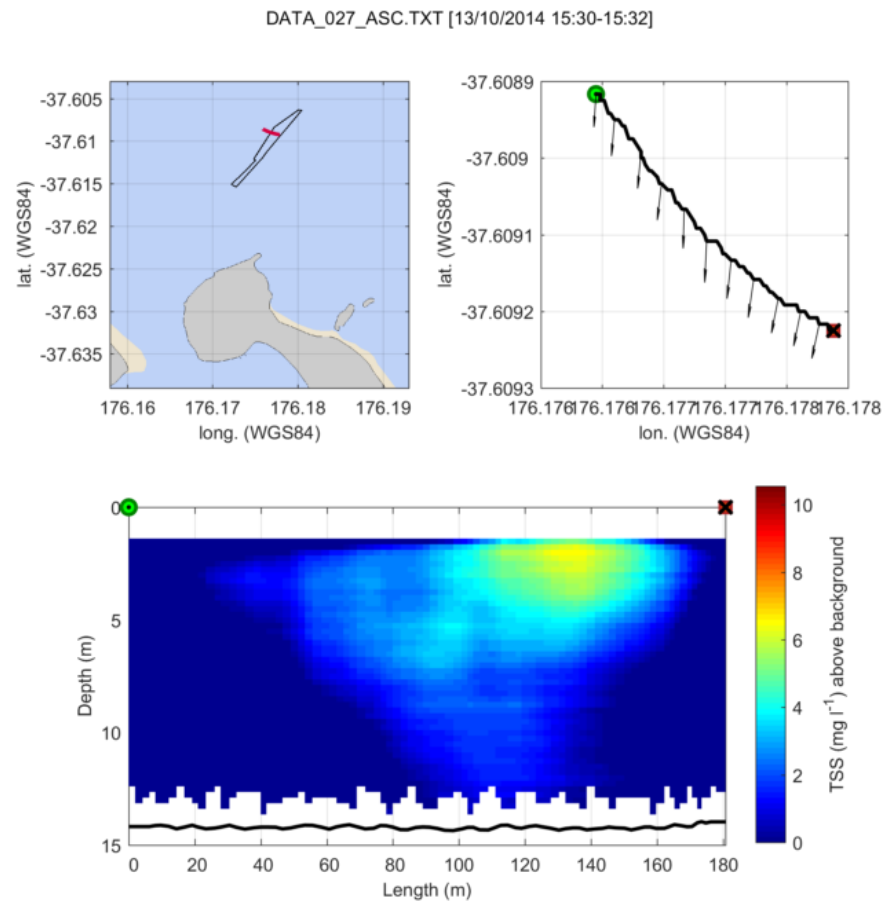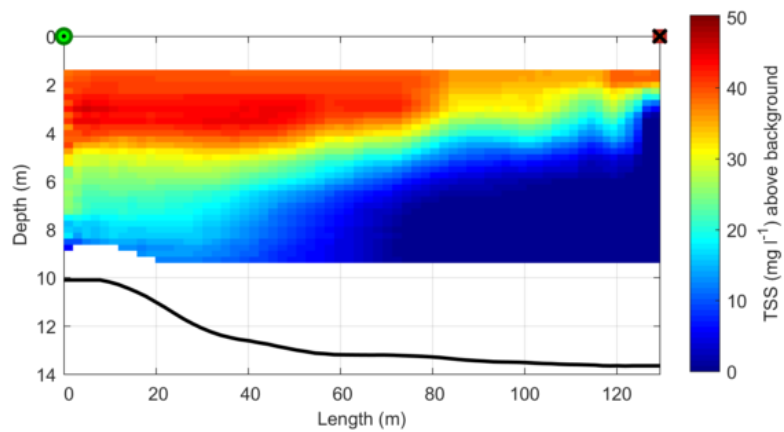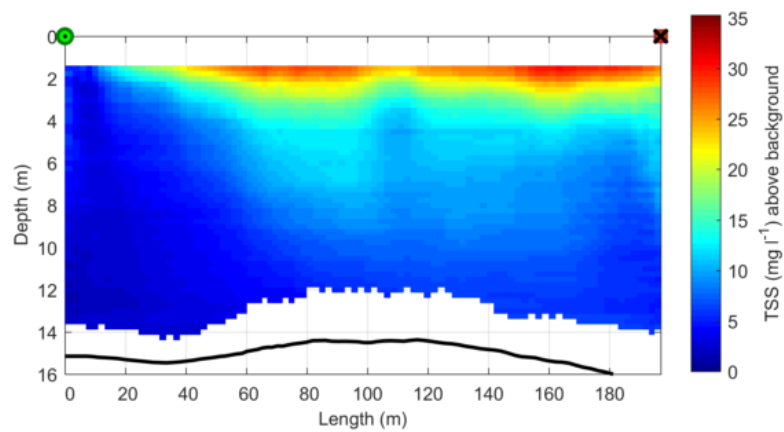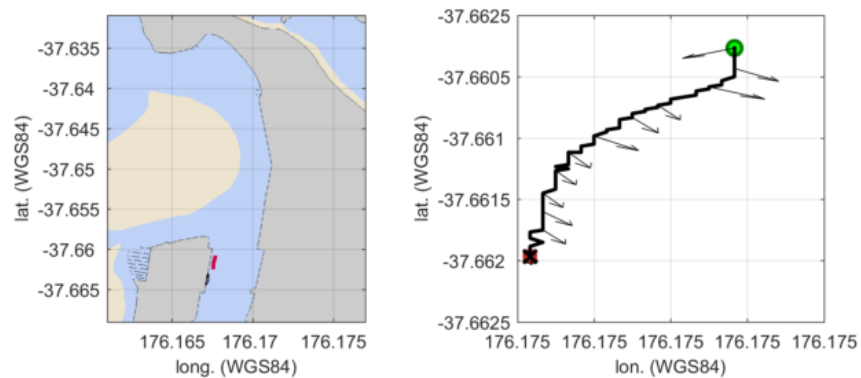
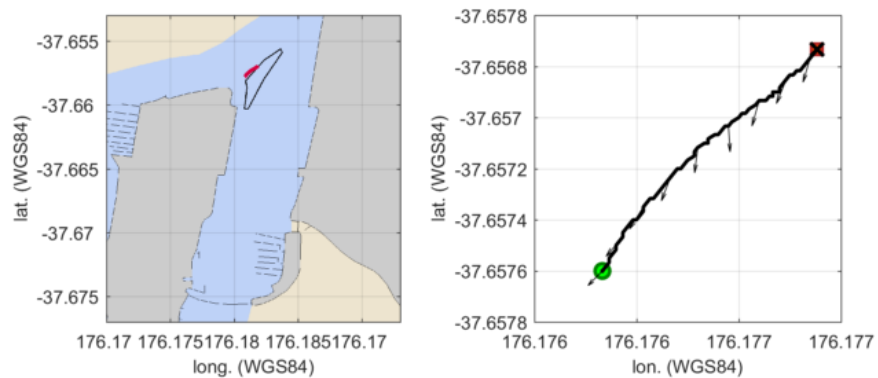(b) DATA_113_ASC.TXT [14/10/2014 14:24-14:27]

134

Figure C.3: Transects carried out during and after maintenance dredging at SP1 on the 14th October 2014. Top left map shows the location of transects (red line) and dredging area (black line) and top right map shows detailed transect position. Green circle is the start point and red square is the end point. Bottom profile shows TSS above background; white areas represent the bottom and bins not measured by the ADCP.

Dredging 15/10/2014 – Area H1 (H1_1)

A transect carried out at the beginning of dredging, detected a plume approximately 350 m long, with high TSS at the surface (< 4 m depth) and a gradient of TSS decreasing towards the bottom indicating settling of sediments from the plume (Figure C.4a). After 10 minutes, a transect depicts a plume formed by two peaks of TSS between 25 and 30 mg l^{-1}, at the surface and at the bottom, with TSS at surface slightly higher (Figure C.4b). Two transects carried out 10 and 15 minutes following the end of dredging, show highest TSS at the surface downstream of tide flow (flood tide, plume transported south of dredging area, Figure C.4c), and sediment settling in the transect carried out upstream (Figure C.4d). Southward movement of plume was revealed by transects running longitudinally to the channel 20 and 35 minutes after the dredging ended (Figure C.4e and f), and TSS decreased to background within the dredging area.

(a) DATA_145_ASC.TXT [15/10/2014 08:15-08:19]

(b) DATA_150_ASC.TXT [15/10/2014 08:27-08:30]
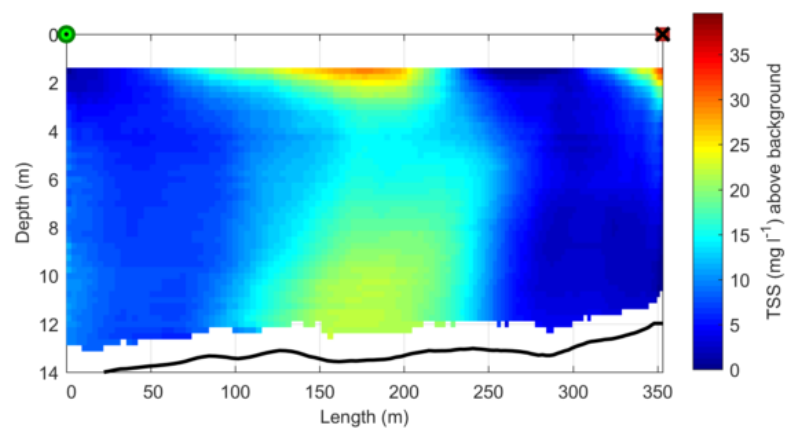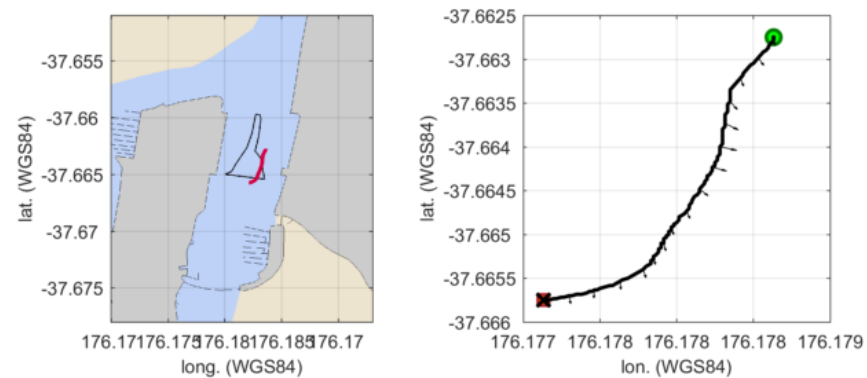
(c)

DATA_157_ASC.TXT [15/10/2014 08:56-08:57]
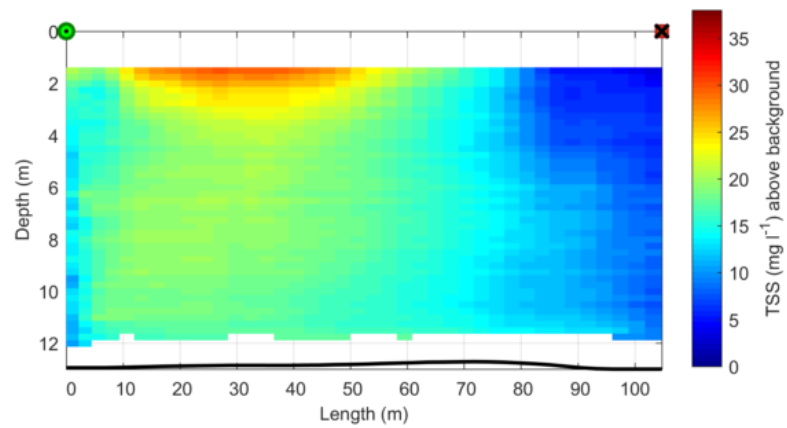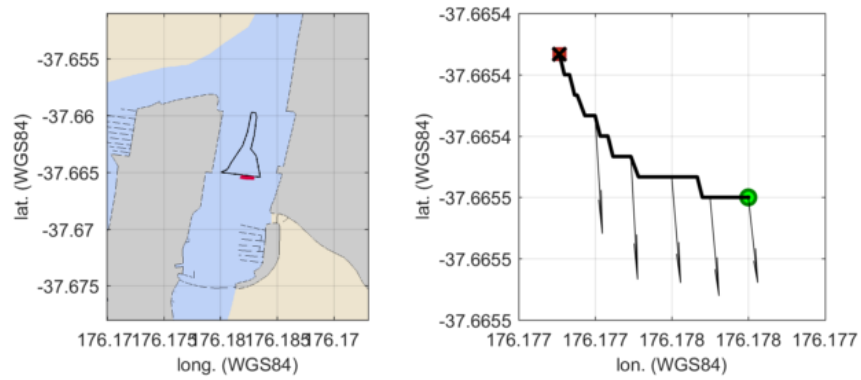
(d)

DATA_158_ASC.TXT [15/10/2014 08:58-09:00]
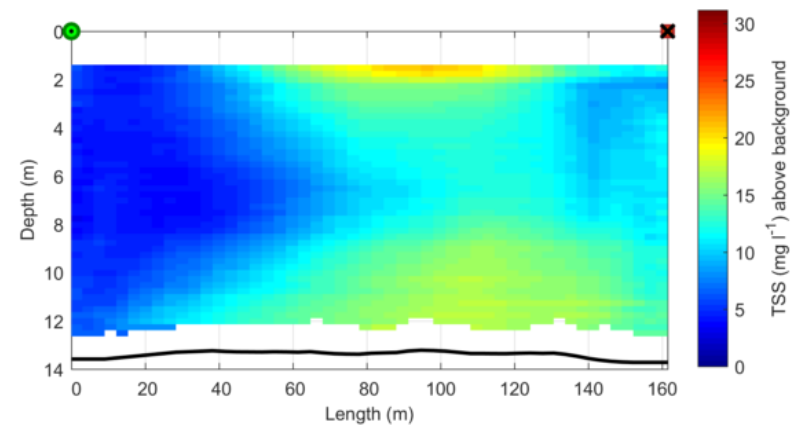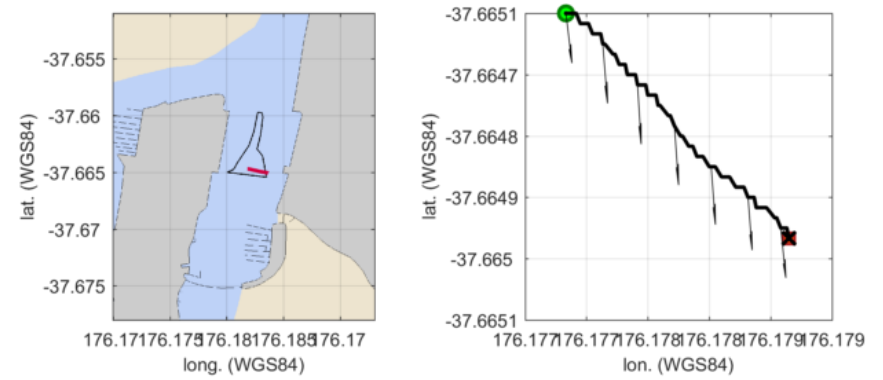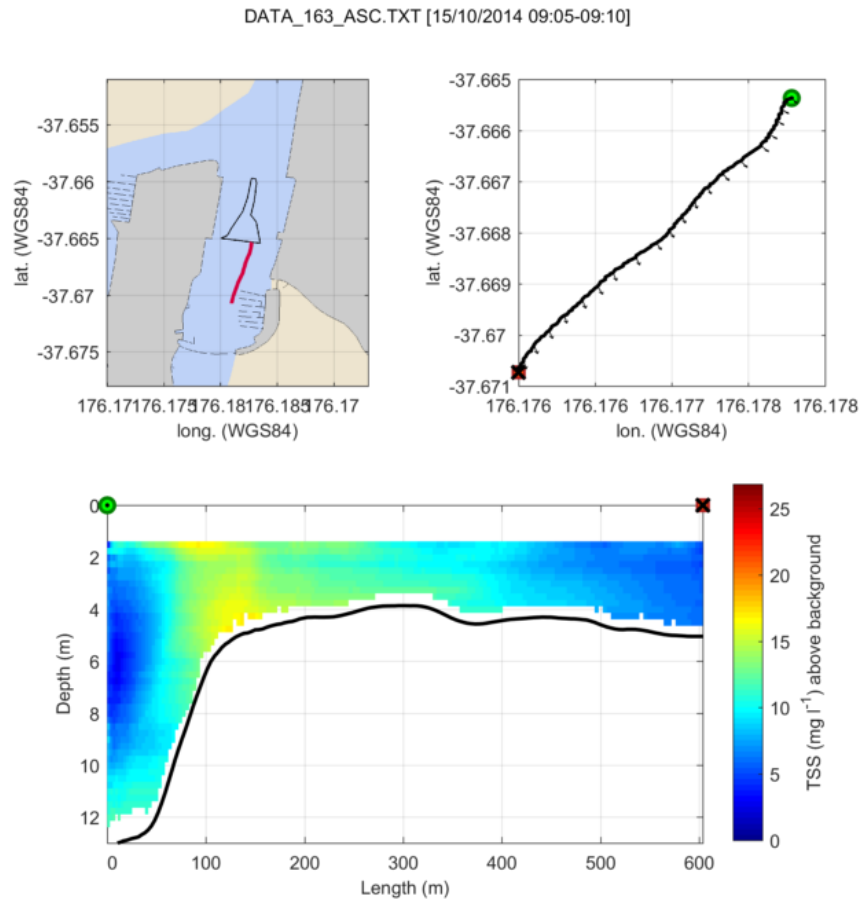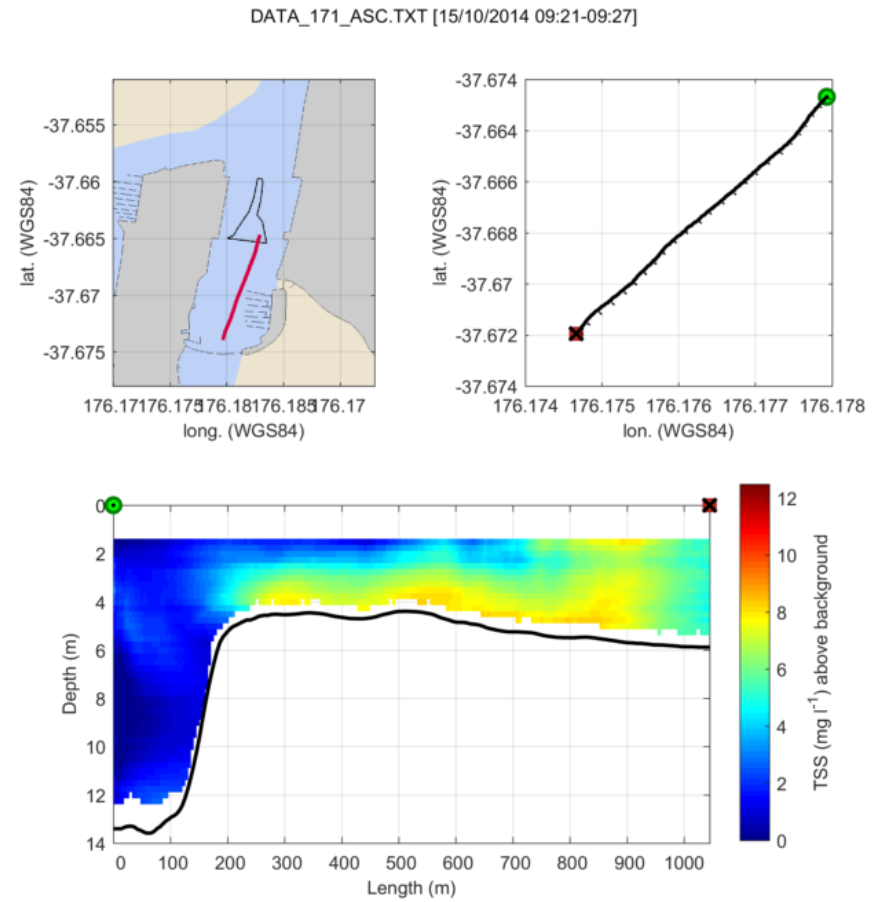
Figure C.4: Transects carried out during and after maintenance dredging at H1 (H1_1) on the 15th October 2014. Top left map shows the location of transects (red line) and dredging area (black line) and top right map shows detailed transect position. Green circle is the start point and red square is the end point. Bottom profile shows TSS above background; white areas represent the bottom and bins not measured by the ADCP.

Dredging 15/10/2014 – Area H7

TSS peaked at 49 mg l^{-1} during dredging monitoring at H7. Two ADCP transects show plume with maximum TSS around 40 mg l^{-1} after 30 and 40. The highest concentrations are visible down to depths of 4 to 5 m and TSS between 15 and 20 mg l^{-1} reaches depths between 7 and 10 m (Figure C.5a and b). After dredging, a transect carried out within the dredging area reveals a plume of lower TSS (between 5 and 8 mg l^{-1}) and sediment settling (Figure C.5c). A transect south of dredging area, following the current direction (flood tide), 35 minutes after dredging ended, show TSS as low as background indicating dissipation and settling of plume, with only a minor plume still detectable by ADCP.

(a) DATA_194_ASC.TXT [15/10/2014 10:38-10:45]
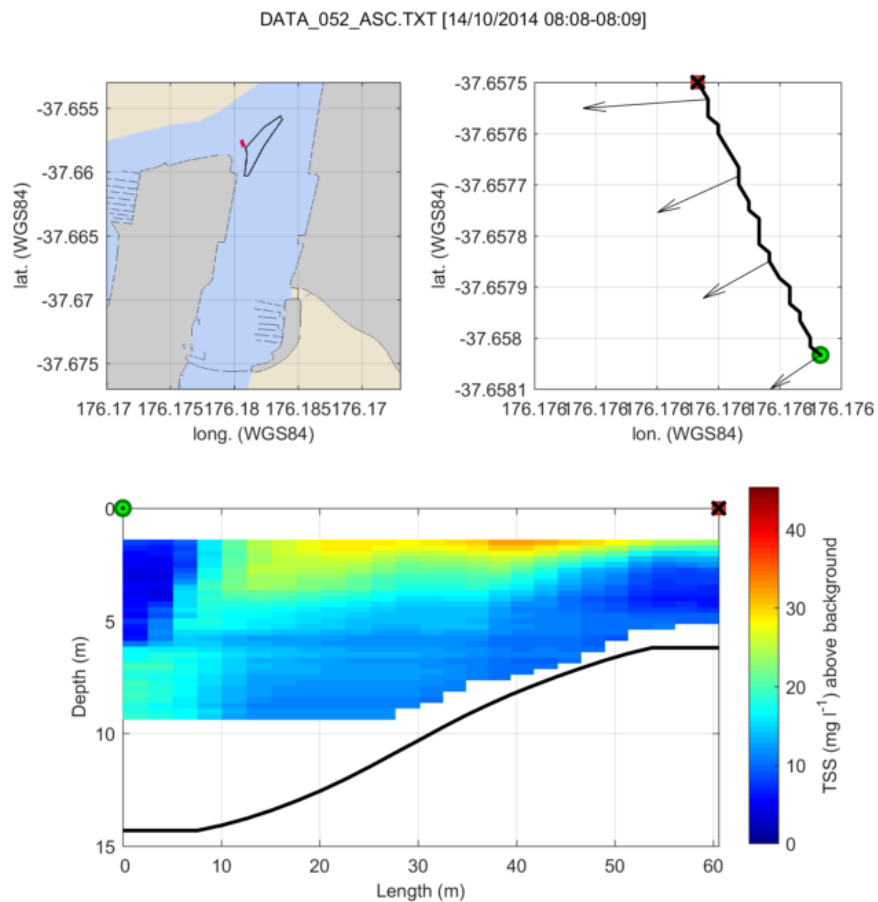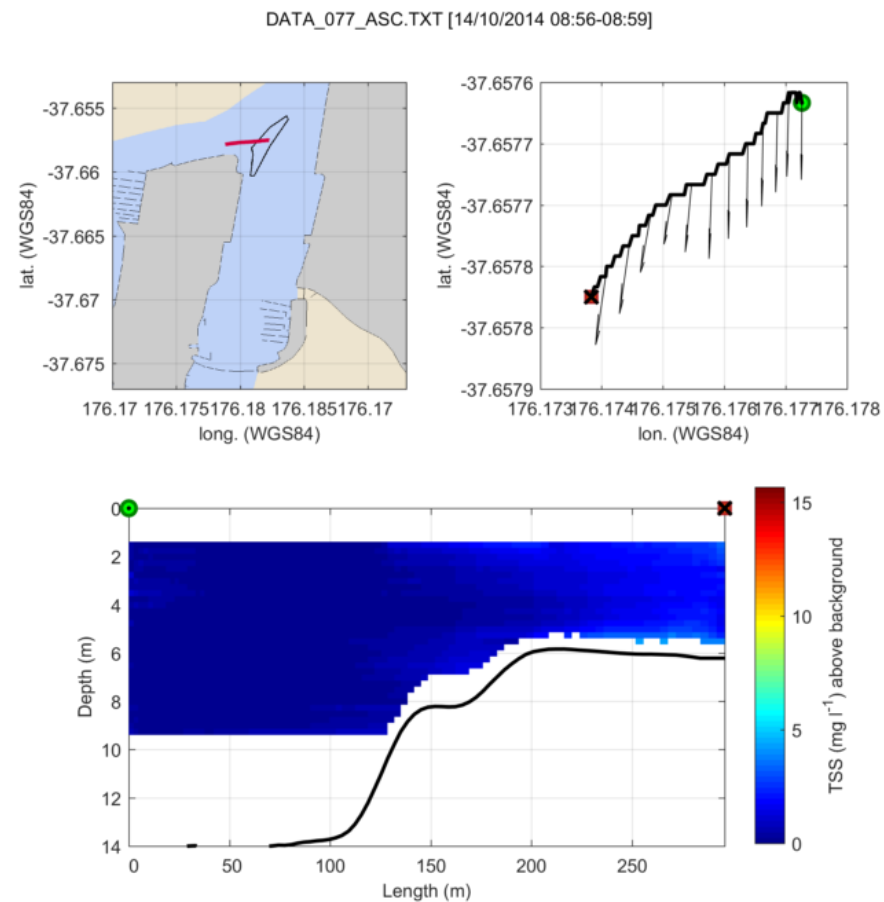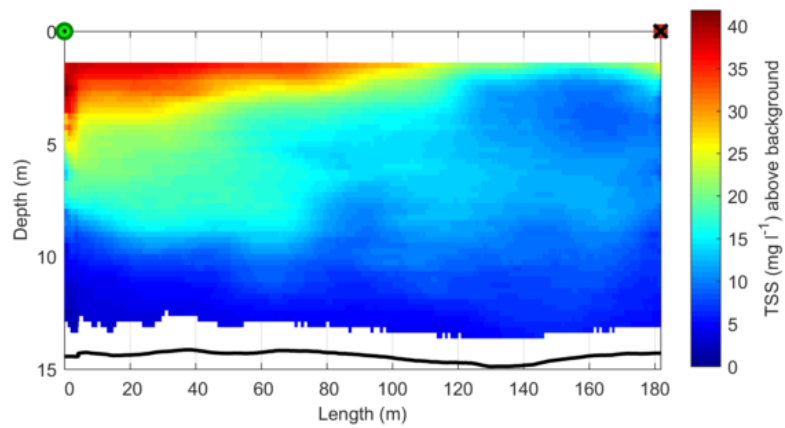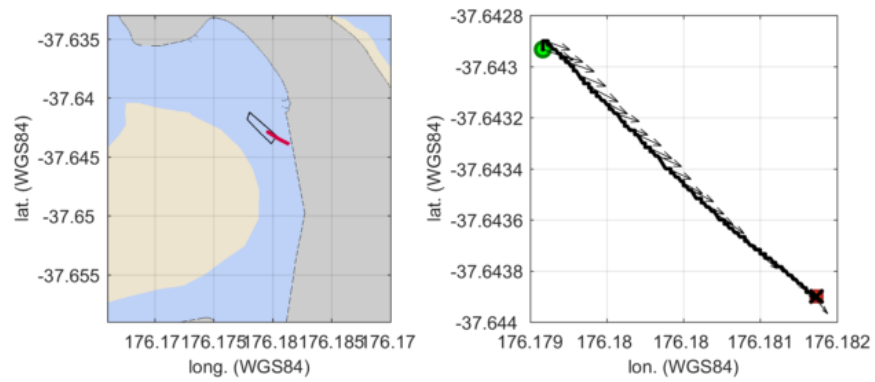
(b) DATA_196_ASC.TXT [15/10/2014 10:47-10:48]
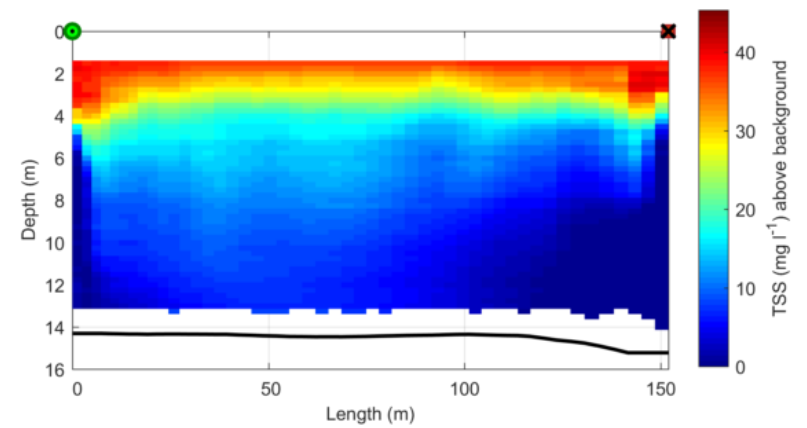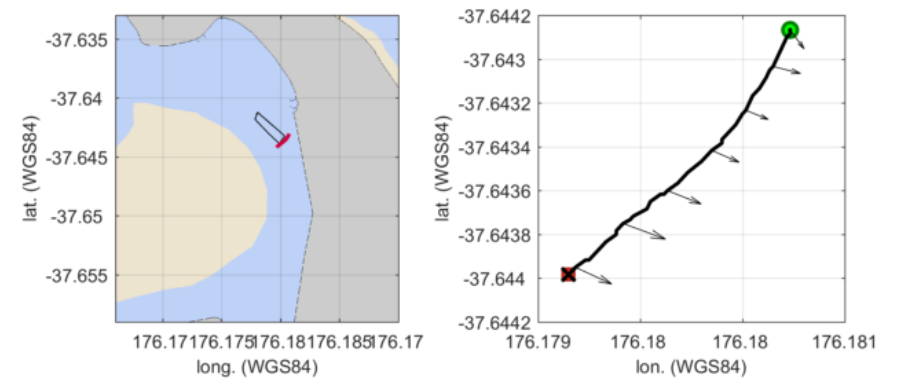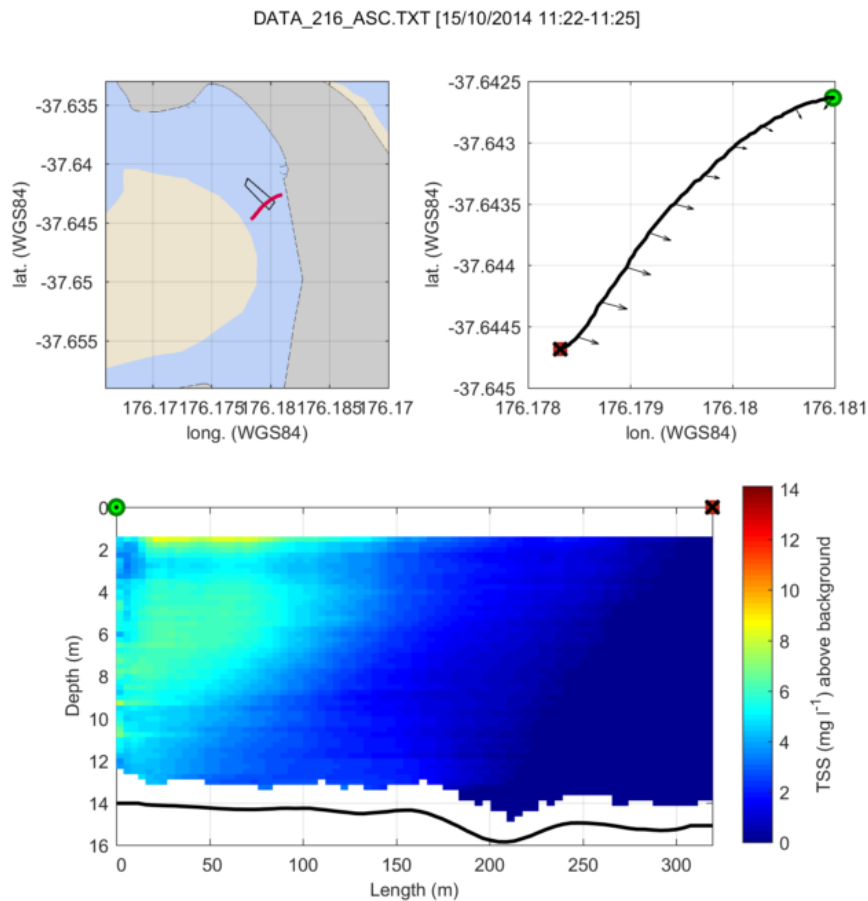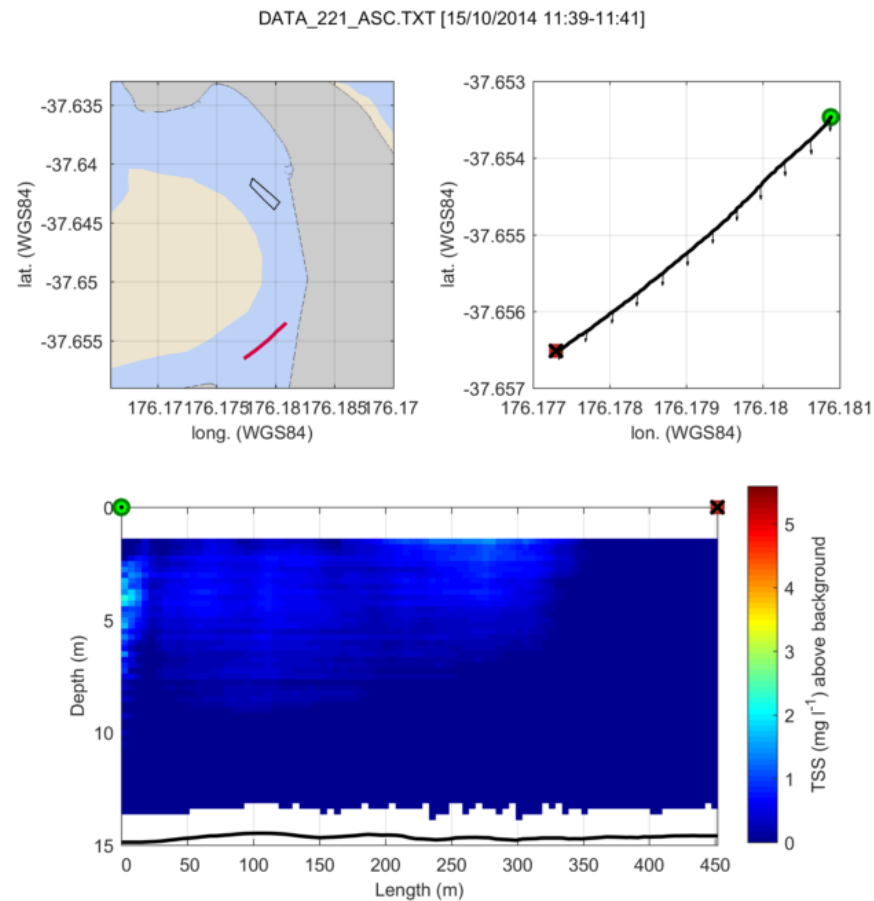
Figure C.5: Transects carried out during and after maintenance dredging at H7 on the 15th October 2014. Top left map shows the location of transects (red line) and dredging area (black line) and top right map shows detailed transect position. Green circle is the start point and red square is the end point. Bottom profile shows TSS above background; white areas represent the bottom and bins not measured by the ADCP.

Dredging 15/10/2014 – Area H1 (H1_2)

Figure C.6a, show a plume with TSS above 40 mg l^{-1} at the surface (< 3 m), and TSS of 20 mg l^{-1} at mid depths (between 4 and 8 m). After 30 minutes, a transect in the centre of dredging area (Figure C.6b) indicates there was a ~50 m long plume with TSS also higher at the surface, but those levels were lower compared with previous transect (max TSS ~ 17 mg l^{-1}). After dredging, two parallel transects made in the direction of flow show sediment settling and plumes with low TSS (< 12 mg l^{-1} and < 5 mg l^{-1}, Figure C.6c and d, respectively). A longitudinal transect carried out 30 minutes after dredging show plume is dissipating in the flow direction simultaneously with plume settling and decrease in max TSS (Figure C.6e). Figure C.6f shows transect that was conducted at similar location of transect in Figure C.6c 50 minutes later and show that TSS had reduced to background levels within and near the dredging area.

(a) DATA_230_ASC.TXT [15/10/2014 12:44-12:49]
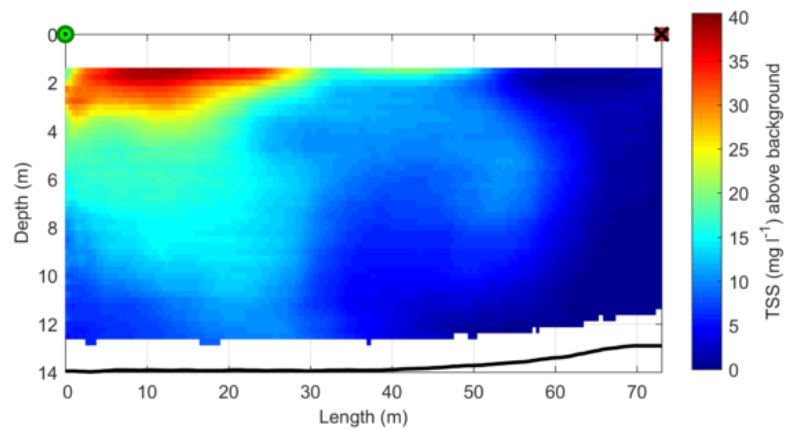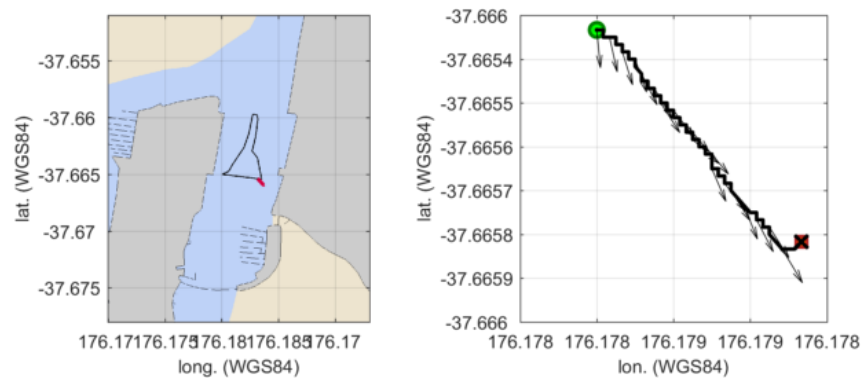
(b) DATA_234_ASC.TXT [15/10/2014 12:55-12:57]

144
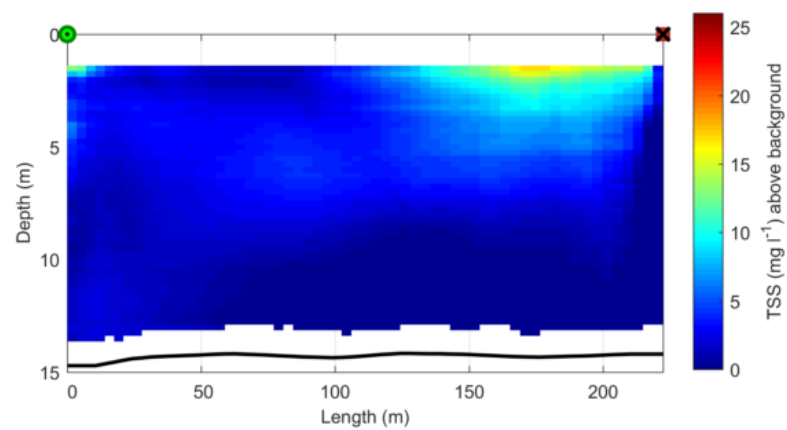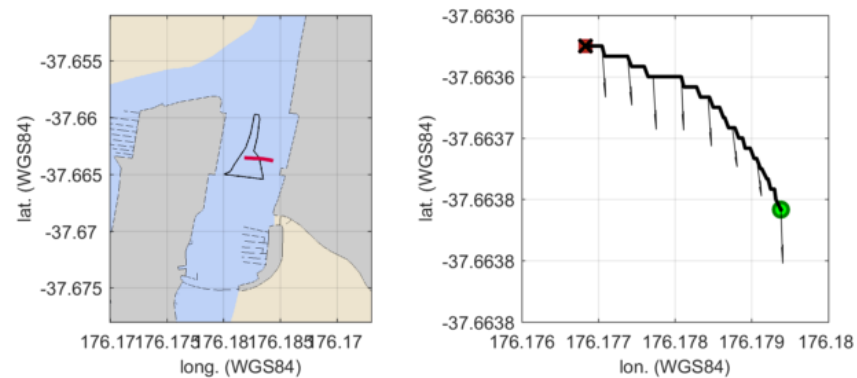
(c) DATA_248_ASC.TXT [15/10/2014 13:18-13:20]
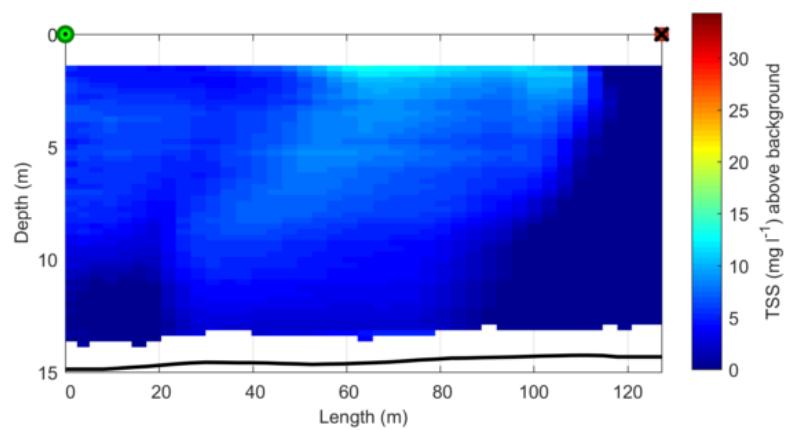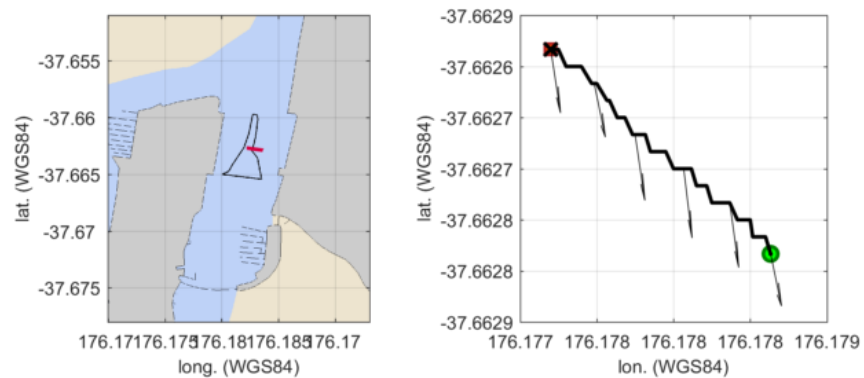
(d) DATA_257_ASC.TXT [15/10/2014 13:37-13:39]

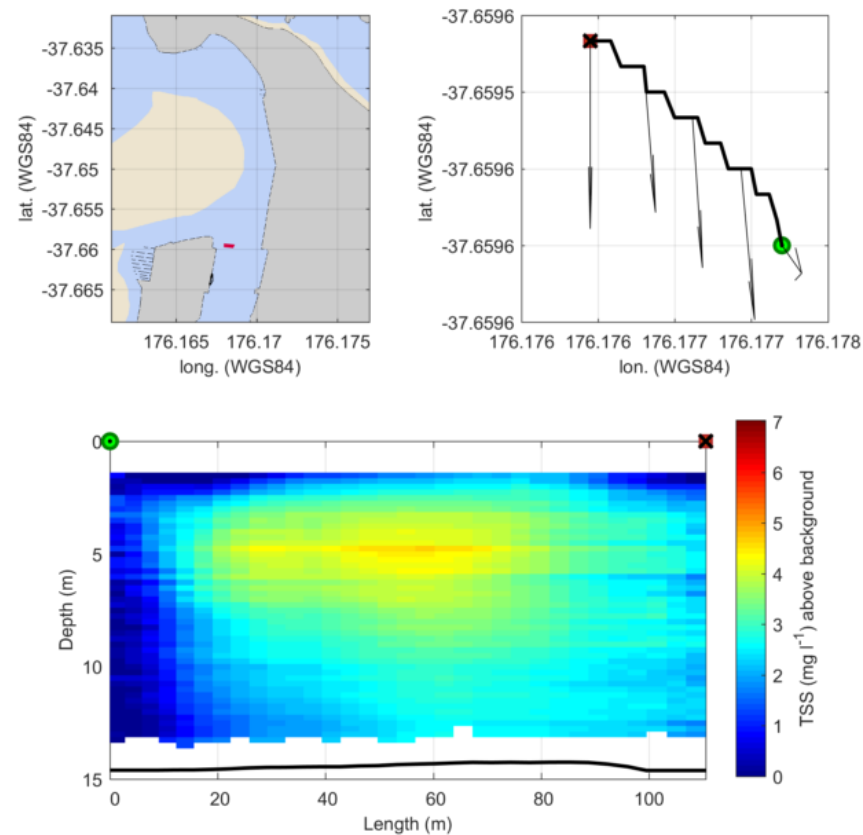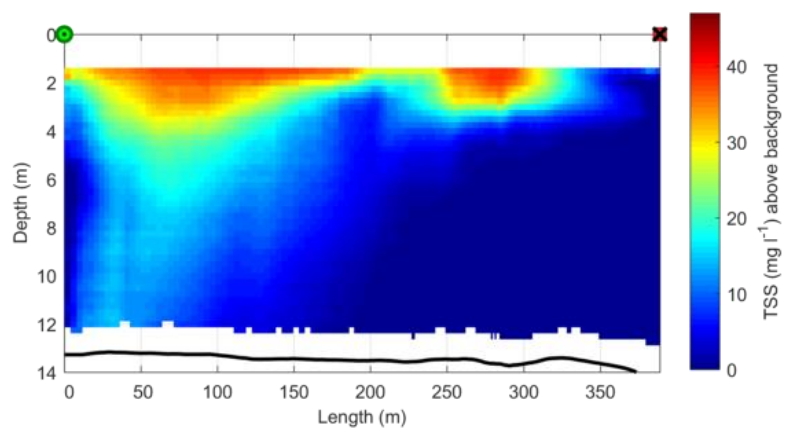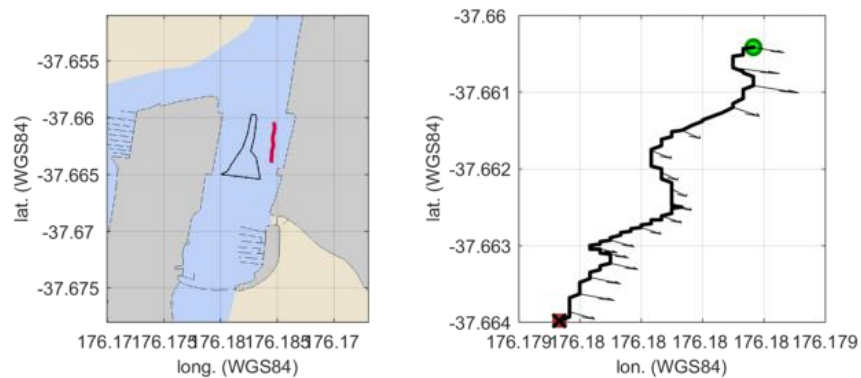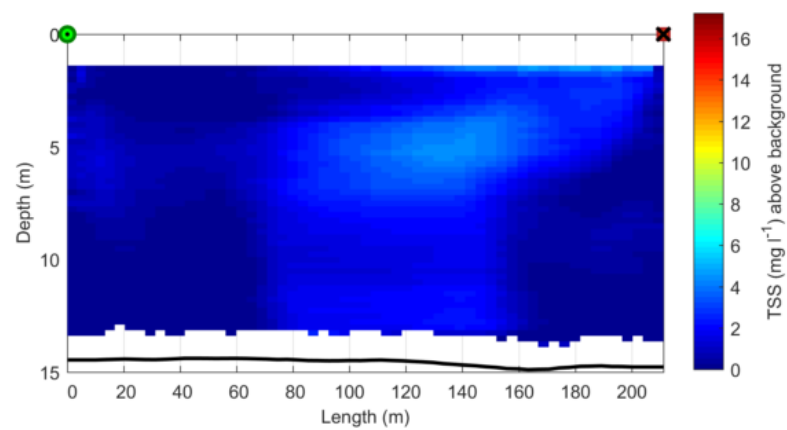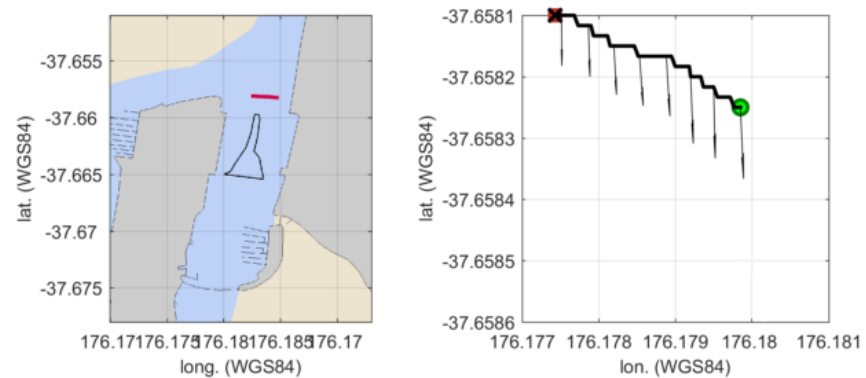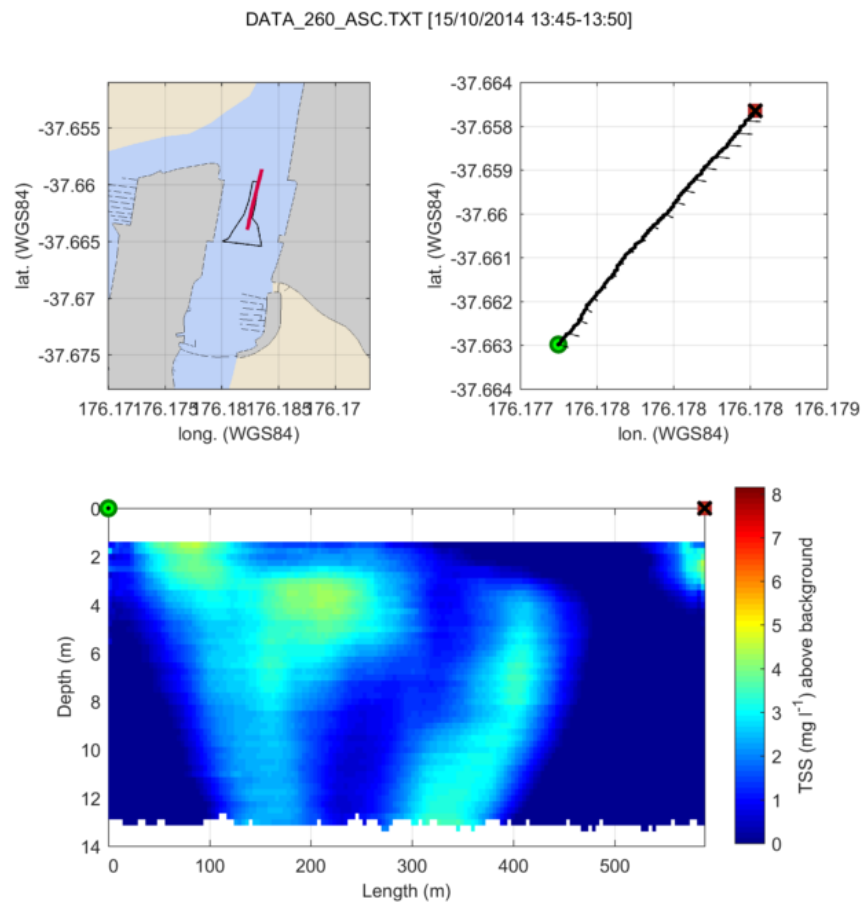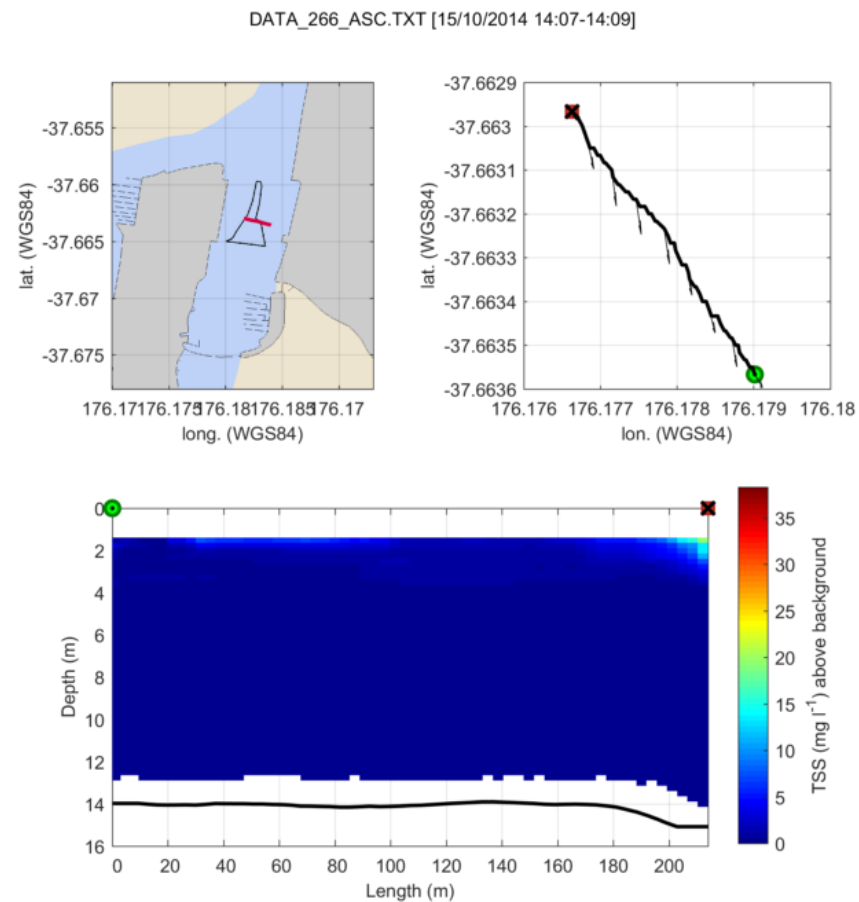Figure C.6: Transects carried out during and after maintenance dredging at H1 (H1_2) on the 15th October 2014. Top left map shows the location of transects (red line) and dredging area (black line) and top right map shows detailed transect position. Green circle is the start point and red square is the end point. Bottom profile shows TSS above background; white areas represent the bottom and bins not measured by the ADCP.

Dumping 16/10/2014 – Area Dump B

ADCP transects during dumping recorded the maximum backscatter signal that resulted in a TSS of 61 mg l^{-1} above background. However, TSS is reduced to 38 mg l^{-1} with further decreases afterwards. Dumping lasted 5 minutes and most part of transects were carried out afterwards. Figure C.7a show plume descended to the bottom with max TSS ~ 15 mg l^{-1} and sediment entrainment in the water column with lower TSS (~ 10 mg l^{-1}). Ten minutes after, a transect show that max TSS decreased to approximately 7 mg l^{-1} and remaining suspended sediments are in order of 2 to 4 mg l^{-1} detected from 6 to up to 3 m depth (Figure C.7b). Transect in Figure C.7c revealed part of the deposited mound of sediment, and depicts its edge which have likely not traversed the dumping area B. Subsequent transect reveals TSS similar of background levels and show that, 20 minutes after dumping, sediment plume and deposition is very localized within the dumping ground (Figure C.7d).

(a) DATA_295_ASC.TXT [16/10/2014 11:00-11:02]
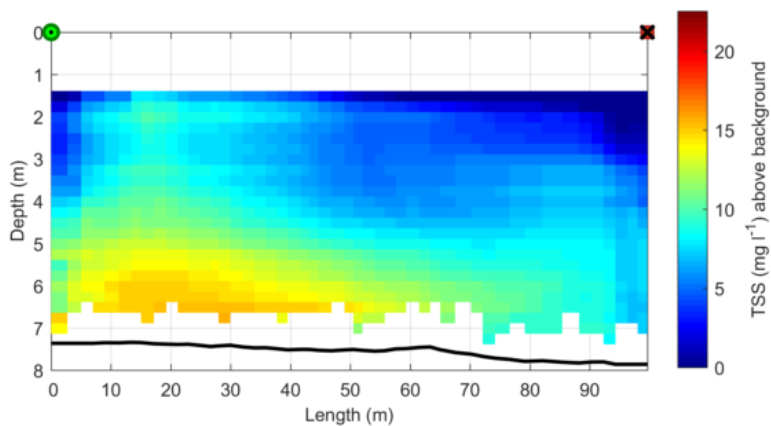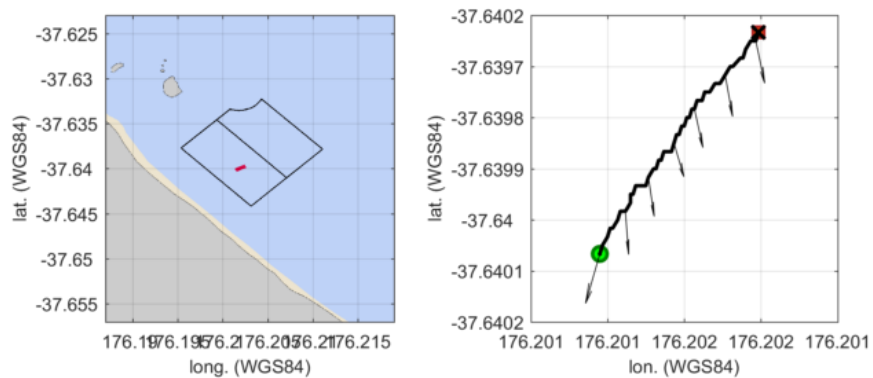
(b) DATA_302_ASC.TXT [16/10/2014 11:09-11:10]

148
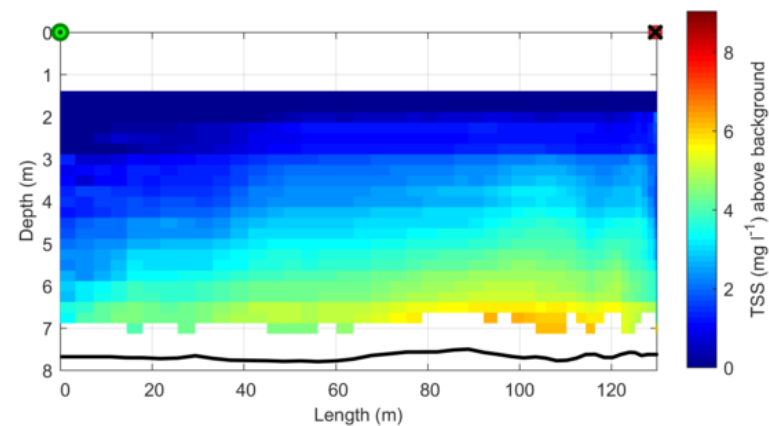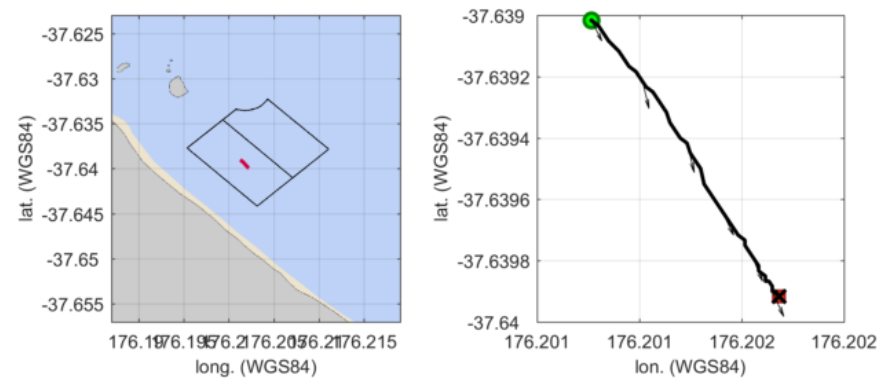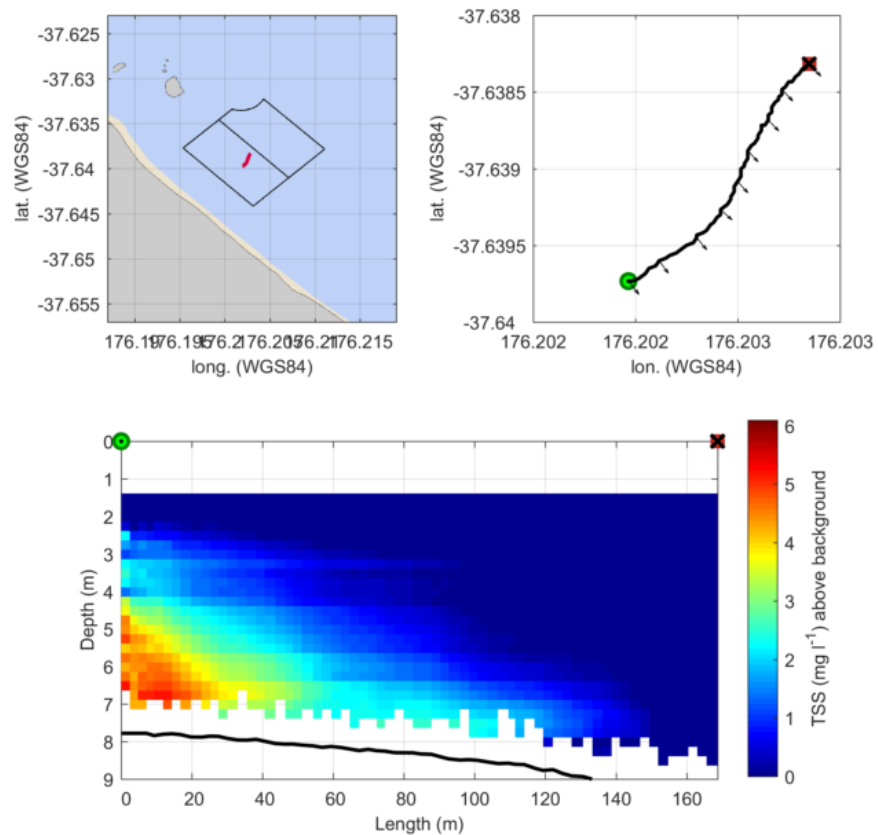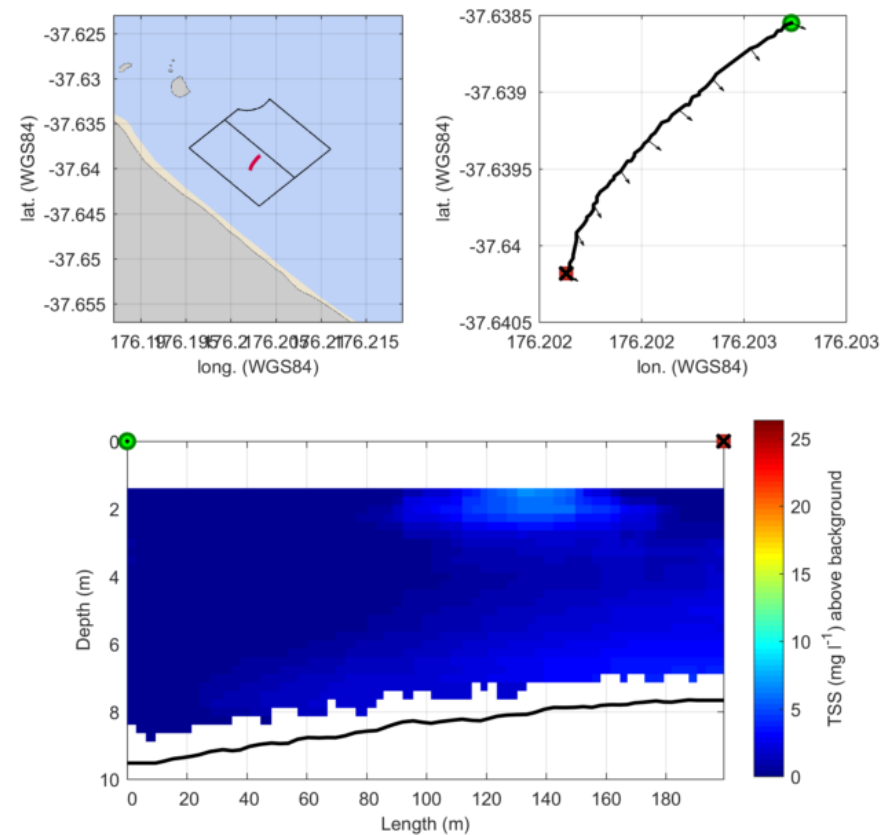
Figure C.7: Transects carried out after dumping at Dump B site on the 16th October 2014. Top left map shows the location of transects (red line) and dredging area (black line) and top right map shows detailed transect position. Green circle is the start point and red square is the end point. Bottom profile shows TSS above background; white areas represent the bottom and bins not measured by the ADCP.

APPENDIX D

HYDRODYNAMIC SIMULATION SETUP AND PARAMETERS
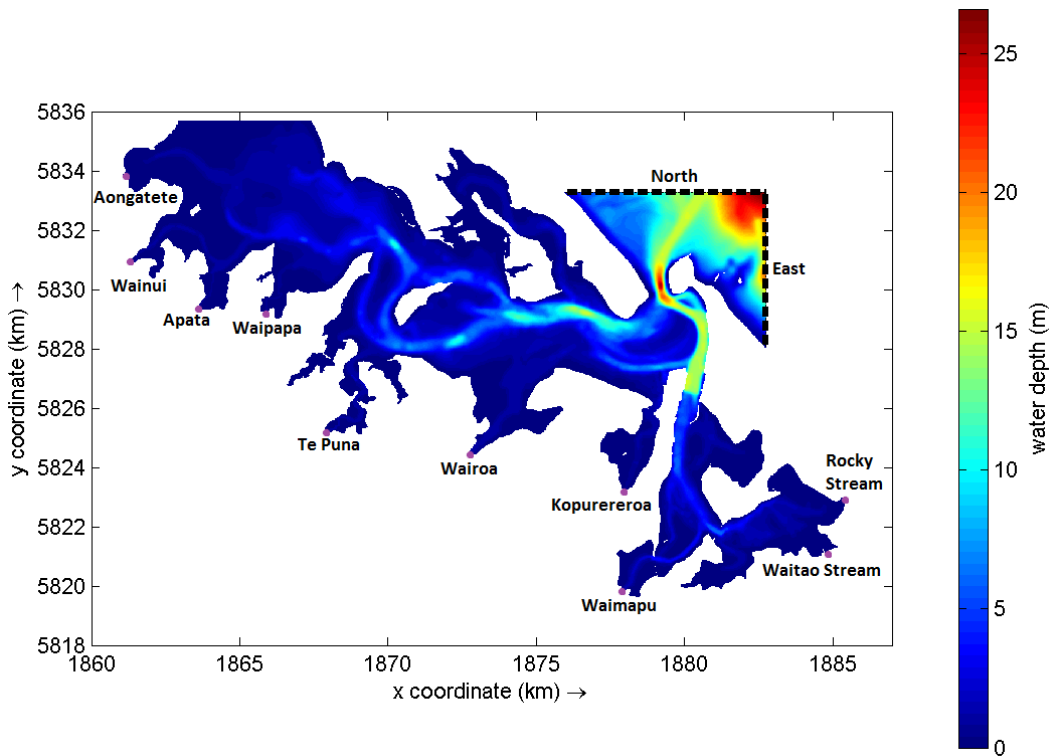
Figure D.1: Model domain, bathymetry (positive values are below mean sea level), open boundaries (dashed black line, 'North' and 'East'), and discharges points (purple dots).

Table D.1: Amplitude and phase of tidal constituents used as astronomic forcing for water level at the open boundaries. Phase is in Greenwich Mean Time (GMT). Source: Watson (2016).

Tidal Constituent	Amplitude (m)	Phase (º GMT)
M2	0.7480	189.70
S2	0.0983	262.99
N2	0.1672	154.42
K2	0.0186	266.91
K1	0.0506	180.74
P1	0.0160	174.87
Q1	0.0017	50.19
O1	0.0107	126.71

Table D.2: River and streams discharges used in the model. Source: Watson (2016).

Discharge point	Discharge (m^3 s^{-1})
Aongatete River	2.30
Wainui River	0.94
Apata Stream	0.21
Waipapa River	1.01
Te Puna Stream	0.69
Wairoa River	17.6
Kopurererua Stream	2.28
Waimapu River	3.34
Waitao Stream	1.03
Rocky Stream	1.09

Table D.3: Model parameters used in the hydrodynamic module. Modified from Watson (2016).

Parameter	Value
Time Step Interval	1 min
Simulation Period	13/10/2014 to 20/10/2014
Warm-up Period	3 days
Eddy Viscosity	10 m^2 s^{-1}
Threshold Depth	0.05 m
Bottom Roughness	Chezy (m$^{-1/2}$ s^{-1}) space-varying, from 1 to 65

APPENDIX E

HYDRODYNAMIC VALIDATION

Formulation

Statistical analyses (bias, accuracy and skill) were based on Sutherland et al. (2004). The equations follow:

$$\text{Bias} = \frac{1}{J}\sum_{j=1}^{J}\left(y_j - x_j\right) = \langle Y \rangle - \langle X \rangle \qquad \text{(Equation 3)}$$

where Y is a set of model results, X is a set of field data, J is the number of predictions and observations occurring at the same time and location. Angular brackets represent the mean.

Accuracy was determined by Mean Absolute Error (MAE) and by root-mean-square error (RMSE):

$$\text{MAE}(Y,X) = \frac{1}{J}\sum_{j=1}^{J}\left(y_j - x_j\right) = \langle |Y - X| \rangle \qquad \text{(Equation 4)}$$

where straight brackets represent the absolute value of the errors.

$$\text{RMSE}(Y,X) = \sqrt{\frac{1}{J}\sum_{j=1}^{J}\left(y_j - x_j\right)^2} = \sqrt{\langle (Y - X)^2 \rangle} \qquad \text{(Equation 5)}$$

$$\text{BSS} = 1 - \frac{MSE(Y,X)}{MSE(B,X)} = 1 - \frac{\langle (Y - X)^2 \rangle}{\langle (B - X)^2 \rangle} \qquad \text{(Equation 6)}$$

where B is a baseline prediction represented by the average of field data. BSS <0.0 is classified as 'bad', between 0.0 and 0.1 is 'poor', from 0.1 to 0.2 is 'reasonable/fair', between 0.2 and 0.5 is 'good', and from 0.5 to 1.0 is considered 'excellent' Sutherland et al. (2004).

Results
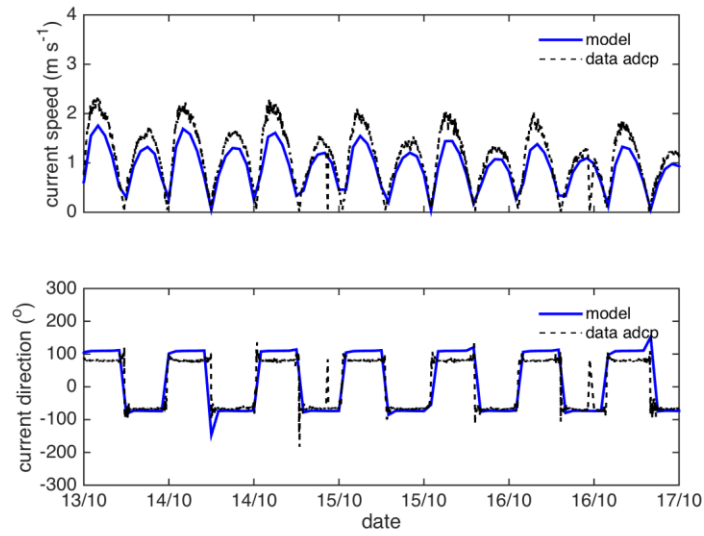
Figure E.1: Validation plots of measured (black dashed line) and modelled (blue solid line) current speed (m s-1) and direction (˚) during field deployment period at ADCP current meter (Figure 4.1).
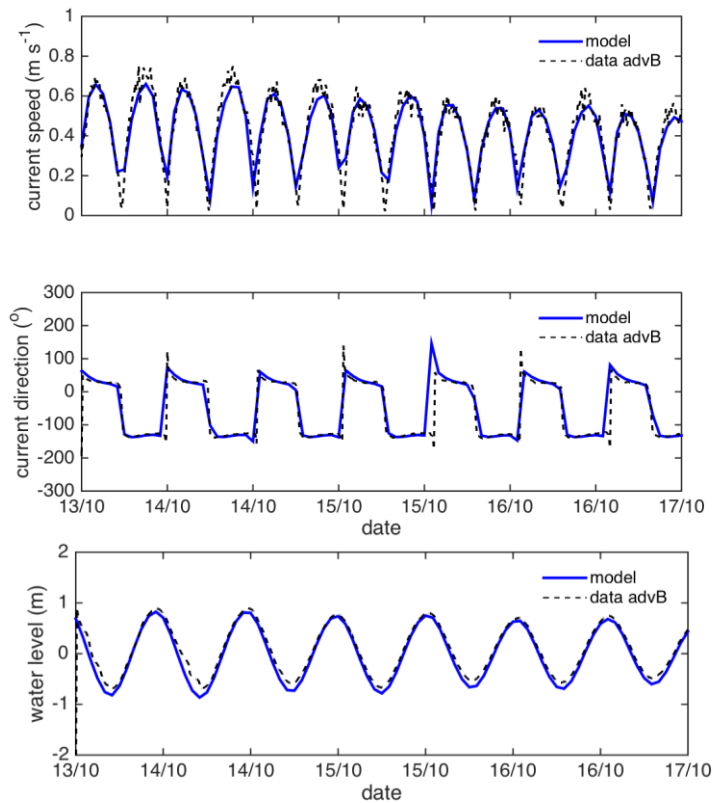
Figure E.2: Validation plots of measured (black dashed line) and modelled (blue solid line) current speed (m s-1) and direction (˚) and water level (m) during field deployment period at ADV B (Figure 4.1).
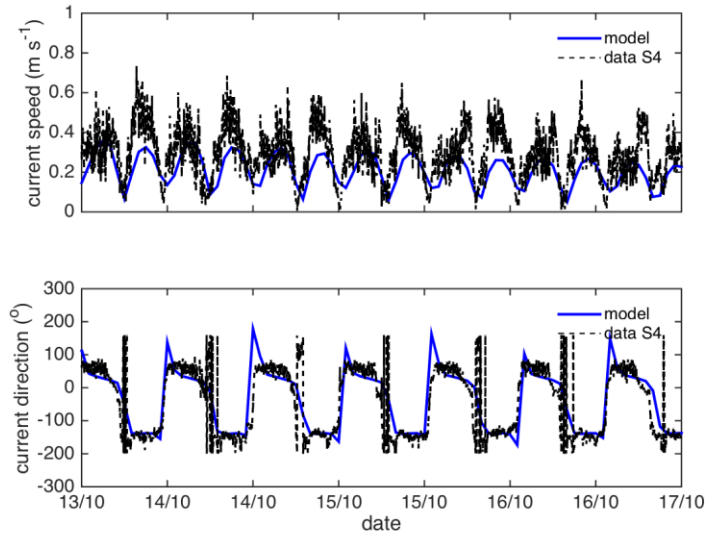
Figure E.3: Validation plots of measured (black dashed line) and modelled (blue solid line) current speed (m s-1) and direction (˚) during field deployment period at S4 current meter (Figure 4.1).
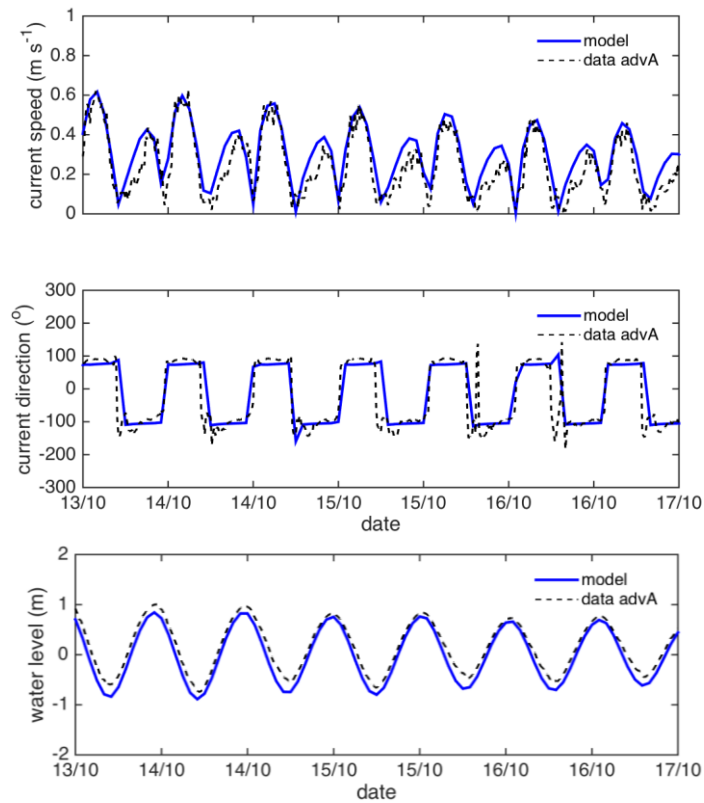
Figure E.4: Validation plots of measured (black dashed line) and modelled (blue solid line) current speed (m s-1) and direction (˚) and water level (m) during field deployment period at ADV A current meter (Figure 4.1).

154

APPENDIX F

Table F.1: Dredging duration and flow parameters used in simulation 5 (see Dredging Simulations Scenarios for more information). * represent the dredging areas included in simulation 6. All simulations had an initial sediment concentration of 300 kg m^3.

Area	Time dredging (min)	Flow (m³ s⁻¹)
E3	50	0.20
E4	50	0.24
* H4	65	0.16
* H4	45	0.18
E2	55	0.23
E5	50	0.19
* H4	80	0.15
E6	60	0.20
* H4	85	0.15
* SP2	20	0.45
* SP1	20	0.49
* H4	80	0.15
* H5	70	0.14
E6	60	0.21
* SP2	35	0.27
* SP1	25	0.39
* SP2	25	0.39
* SP1	20	0.48
* H4	80	0.07
* H4	90	0.13
* SP1	20	0.48
* H4	90	0.12
E3	45	0.25
* H1	30	0.38
* H7	60	0.20
* H1	30	0.35
E5	60	0.19
* H7	40	0.24
E4	50	0.22
E5	60	0.20
E4	45	0.24
E5	60	0.20
E4	55	0.22
E4	50	0.24
E4	55	0.21
E4	60	0.21
E4	55	0.23
* H8	80	0.14

APPENDIX G

Conference Paper: Australasian Coasts and Ports 2015

Cussioli, M.C., Bryan, K.R., Pilditch, C.A. and De Lange, W.P., 2015. Dispersal of dredging plumes in Tauranga Harbour, New Zealand: a field study. In Australasian Coasts and Ports 2015, Wellington, New Zealand. IPENZ, 222–228.

Dispersal of dredging plumes in Tauranga Harbour, New Zealand: A field study

Mariana C. Cussioli[1], Karin R. Bryan[1], Conrad A. Pilditch[1] and Willem P. De Lange[1]
[1] University of Waikato, Hamilton, New Zealand; mc204@students.waikato.ac.nz

Abstract

Water quality standards associated with dredging have become more stringent, requiring better monitoring and prediction. Here, we describe the dynamics and development of plumes generated during two dredging cycles and how they vary with respect to time and distance from the dredging activity. Backscatter signals were measured using a boat-mounted acoustic Doppler current profiler (ADCP) and total suspended solid concentrations (TSS) were determined from water samples. Results show that background TSS ranged from 7 to 9 mg l^{-1} whilst dredging plumes exhibited a vertical gradient of TSS ranging from 9 to 15 mg l^{-1} near the surface (0–2 m), and 24 to 70 mg l^{-1} near the bottom (10–12 m). ADCP transects conducted during and after dredging showed that the plume dissipated from the dredged area within 1 hour. Final transects (~1 hour after the dredging ended), revealed backscatter signals ranging from background levels to ~1.2 times greater than the background. Based on TSS concentrations and time for plume dispersion, previous studies indicated that a plume with duration of 1 to 2 hours and TSS concentration around 70 mg l^{-1} is below the threshold for causing serious impacts to the biota; therefore, only minor effects can be expected for the two dredging plumes monitored.

Keywords: Dredging, dredging plume, ADCP, backscatter signal, suspended solids concentration.

1. Introduction

In ports and harbours, routine dredging activity is needed to maintain and deepen navigation channels. Dredging can generate high quantities of suspended sediments, which are transported from dredged area by currents, and deposited on the seabed [19] [22] [23]. For example, a trailing suction hopper dredge (TSHD) can elevate turbidity close to the seabed by disturbing the bottom sediments by the draghead, and at the surface due to the overflow, whereby surplus water is discarded to increase hopper capacity. The dimensions and dispersal dynamics of a plume are determined by the dredging strategy (e.g. dredge volume, frequency, duration and method) and local sediment and hydrodynamic characteristics [6]. The complexity of these underlying factors and their potential interactions pose difficulties in predicting plume dynamics and behaviour.

Suspended sediments caused by dredge plumes and their potential impacts on marine flora and fauna are a key concern for environmental managers. For example, high suspended sediment concentrations (TSS) can reduce the feeding efficiency of filter feeding bivalves, and reduce light penetration thus affecting primary producers such as seagrasses [6] [10] [12] [15]. However, ecological effects are usually only considered significant when TSS caused by dredging is higher than the natural variation owing to storm events, wave-action, and river discharges [6]. Sediment plumes from maintenance dredging are usually of short duration, and most studies show that high TSS is mostly confined to the immediate environs of the dredging vessel and decays rapidly with time and distance from the dredge [5][16]. The rate of TSS reduction depends on the characteristics of the area being dredged, the spatial and temporal extent of the plumes and the areas of potential impact [17]. Given the transient nature of dredge plumes (which can disperse rapidly both vertically in the water column, and transversely across the harbour), the use of acoustic technologies, with high spatial and temporal resolution, for tracking plumes is an advance over the use of point sample measurements [19].

Through the application of the acoustic method, our aim was to track the plumes created during maintenance dredging in Tauranga Harbour, with the objective of describing their dynamics and development with time and distance from the dredging area and compare TSS values with background levels. Improving our understanding of dredge plume dynamics and dispersal will facilitate improvements to predictive models, dredge operation planning and reduce environmental impacts.

2. Study Area

Tauranga Harbour is an estuarine lagoon, located at 37˚40'S and 176˚10'E, on the east coast of New Zealand's North Island, comprising an area of about 200 km^2 [14]. Intertidal flats separate the lagoon into two main areas, the northern and the southern basins. It is predominantly a shallow harbour, with an average depth at low tide of 3 m [21]. The tides in Tauranga Harbour are semi-diurnal and have a tidal range of 1.62 m for spring tide and 1.24 m for neap tide [8] and 60% of the harbour is intertidal sandflats [14]. The Harbour has two tidal inlets, one at each end of Matakana Island. The more important inlet for navigation is the south-eastern end bounded by the rocky headland of Mt. Maunganui, where it is also the

1

entrance to the Port of Tauranga [3]. The Port of Tauranga was officially established in 1873 and dredging activities at the port started about 100 years afterwards, in 1968, and occurred until 1978, restarting in 1991. The main dredging projects were aimed at deepening and widening of the shipping channels. To maintain channel depths that are adequate for navigation, maintenance dredging was regularly carried out approximately every two years since 1992 [18] and presently, the Port undertakes it annually.
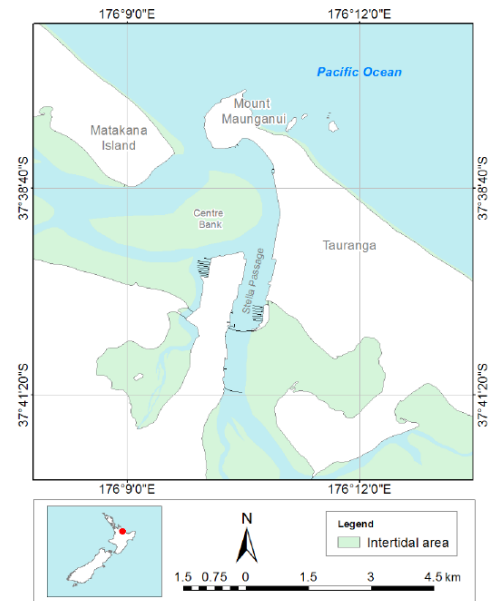
Figure 1   Map of New Zealand (small map) showing the location of the study area (red point) and a more detailed map of Tauranga Harbour (large map). The dredged area described in this paper is at south of Mount Maunganui, in the Stella Passage (176°10'37.665"E 37°39'54.72"S).

3.   Methods

A maintenance dredging event occurred in October 2014 and the sediment plumes generated by the dredging activities were monitored between 13th and 16th October 2014. In this paper we present two monitoring periods (dredging cycles) conducted on 15th October, Monitoring-1 and Monitoring-2 (hereafter M1 and M2, respectively), which tracked the dredging plume in the morning and afternoon, respectively (Table 1).

The dredging was carried out using the TSHD "Pelican" (Van Oord) which has a hopper capacity of 965 m^3, 63 m in length and 11 m in width. The draft when loaded is 3.7 m. During M1, dredging started at 08:15 and finished at 08:45 (Table 1). The sailing time to and from the dumping site was

45 and 30 minutes, respectively, and dumping duration was 5 minutes. In M2, the dredging time was from 12:25 to 13:15. However the dredging duration was 30 minutes so there was an operational delay of 20 minutes of the dredge. The sailing time to and from dumping site was 40 and 20 minutes, respectively, and dumping duration was also 5 minutes. Both dredging activities occurred in Stella Passage inside an area noted as H1 (Figure 3, thin black line).1,283 and 1,187 tons of material were dredged during M1 and M2 respectively. Both sediment types were composed mainly of sand. On 15th October, low tide was 0.2 m at 05:49 and high tide was 1.8 m at 12:15. Therefore, the M1 monitoring was conducted during flood tide and the M2 during ebb tide. The monitoring period covered the end of the spring tide.

Based on the method developed in [7], dredging plumes were tracked using backscatter signals measured by a boat-mounted acoustic Doppler current profiler – ADCP (Workhorse Teledyne RD Instruments 1200 kHz). Acoustic backscatter is proportional to the concentration of suspended particles in the water. Transects along and across the main current direction were made during and after dredging until the plume signal declined to background levels, and therefore difficult to detect, or until time or technical limits were imposed. Six and 9 transects were completed for M1 and M2, respectively. Plume backscatter signals were compared with averaged profiles of background values determined from transects conducted immediately before each dredging monitoring.

Additional measurements were carried out to complement the study: water temperature, salinity and suspended solids concentration. Temperature and salinity were measured using a CTD (SBE 19plus V2 SeaCAT) and casts carried out before dredging started for background conditions and at the end of each monitoring period. Water samples for total suspended solids concentration (TSS) were collected at the surface, mid-depth and bottom using a Schindler-Patalas trap and retained in 1 l bottles until filtering, which occurred less than 24 hours after sampling.

Table 1   Start and end time for measurements carried out during M1 and M2 in order to characterize the area before, during and after dredging. Times are in New Zealand Standard Time (NZST).

	Monitoring-1		**Monitoring-2**	
Time (NZST)	**Start**	**End**	**Start**	**End**
Monitoring	07:11	09:35	12:13	14:28
Background sampling				
CTD	07:13		12:16	
Water surface	07:25		12:17	
Water mid-depth	07:22		12:16	
Water bottom	07:20		12:14	
Transects	07:21	07:59	12:18	12:33

2

Plume sampling				
Dredging	08:15	08:45	12:25	13:15*
Transects	08:15	09:36	12:34	14:28
Water surface	08:30		12:45	
Water mid-depth	08:31		12:43	
Water bottom	08:35		12:41	
CTD	9:37		14:28	

* M2 dredging time was reduced to 30 minutes following an operational delay of 20 minutes.

TSS was determined according to the method described in [1]. The method consists in filtering known volumes of water using pre-rinsed and pre-weighed filters, drying samples in oven at 105°C for 18 hours minimum and reweighing them. The total TSS (mg l^{-1}) is given by the difference between the weight of the filter after and before filtering.

4. Results

4.1 Monitoring-1 (M1)

Surface temperature was ~1°C higher at the water surface than at the bottom, but there were no differences between CTD casts made before (07:13) and after (09:37) the dredging monitoring (Table 2). Before dredging monitoring, there was a vertical salinity gradient with slightly higher levels at the bottom compared with the surface, but differences were weaker at the end of the monitoring period. Thus, there was no strong evidence of water column stratification that could influence the distribution of the plume.

Table 2 Temperature and salinity for M1 and M2. Results from CTD casts conducted before dredging and after each monitoring.

	Temperature (°C)		Salinity	
Monitoring-1	**Before**	**After**	**Before**	**After**
Surface	16.6	16	32.3	33.3
Bottom	15.6	15.4	34	33.8
Monitoring-2				
Surface	15.2	15.4	34.4	34.5
Bottom	14.5	15.2	34.9	34.6
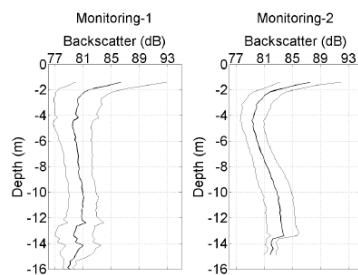
Figure 2 Averaged background backscatter profiles (thick line) ± standard deviation (thin lines) determined from transects conducted immediately before M1 (left) and M2 (right). Note the greater variability of backscatter at the surface.

Background backscatter for M1 (determined from transects conducted previous to the dredging monitoring) was highest (~84.4 dB ± 5.6) at the surface (<2 m depth) and was consistently lower (~80 dB ± 2) below this depth (Figure 2 – left). Background concentrations determined by TSS were 7 mg l^{-1} at the surface, 9.5 mg l^{-1} at mid-depth and 9 mg l^{-1} at the bottom. TSS concentrations were lower at the surface, thus was inconsistent with our ADCP transect data. During the dredging, the TSS concentration was 9, 13 and 70.3 mg l^{-1} at the surface, mid-depth and the bottom, respectively.

During dredging, ADCP measurements (Transect 1, Figure 3) detected an initial plume ~350 m long with a vertical gradient of backscatter ranging from 1.4 to 1.25 times greater than the background at the surface and the bottom, respectively (Figure 4a). After 10 minutes, in transect 2 the plume length at this position was >250 m with the highest relative backscatter (1.3) occurring at lower depths (below 8 m) compared to observations during transect 1 (Figure 4b).
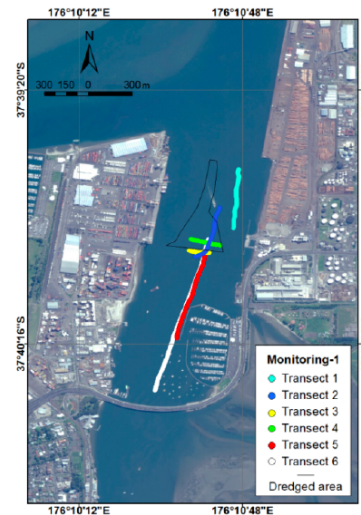
Figure 3 Map of the Stella Passage showing transects 1 to 6 conducted during and after dredging in M1. Thin black line delimits the dredged area.

Ten minutes following the end of the dredging, 2 parallel transects (3 and 4) revealed a plume >70 m in length with concentrations 1.35 to 1.30 times greater than background and higher concentrations at the surface. Diffuse areas of the plume (1.2 times greater than background) extended 30 m either side of the central plume area (Figure 4c and d).

3

Transects running longitudinally to the channel (5 and 6) 20 and 35 minutes after the dredging ended, revealed plume movement towards the south according to the direction of the currents and flood tide (Figure 4e and f). Along these transects, there was an abrupt change in the bathymetry, from a maximum of ~12 m to ~5 m depth. The plume presented maximum backscatter around 1.3 to 1.15 times the background as plume drifted from the deeper to the shallow area and measured ~600 m at the transect 5, and 800 m at transect 6. After 55 minutes of monitoring, the plume appeared to dissipate and was no longer detectable within the dredging area.
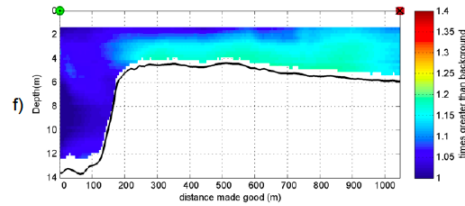
Figure 4   Profiles of Transects 1 to 6 conducted during and after dredging in M1 (Figure 3). Shading indicates backscatter greater than background and white areas represent the bottom and bins not measured by the ADCP. On top of each transect, a green circle is the start point and a red square is the end point, here described as geographic position (N – north, S – south, E – east and W – west). Start time, and start and end position for each transect follows (a) 08:15 N-S; (b) 08:27 N-S; (c) 08:56 E-W; (d) 08:58 W-E; (e) 09:05 N-S; and (f) 09:21 N-S.
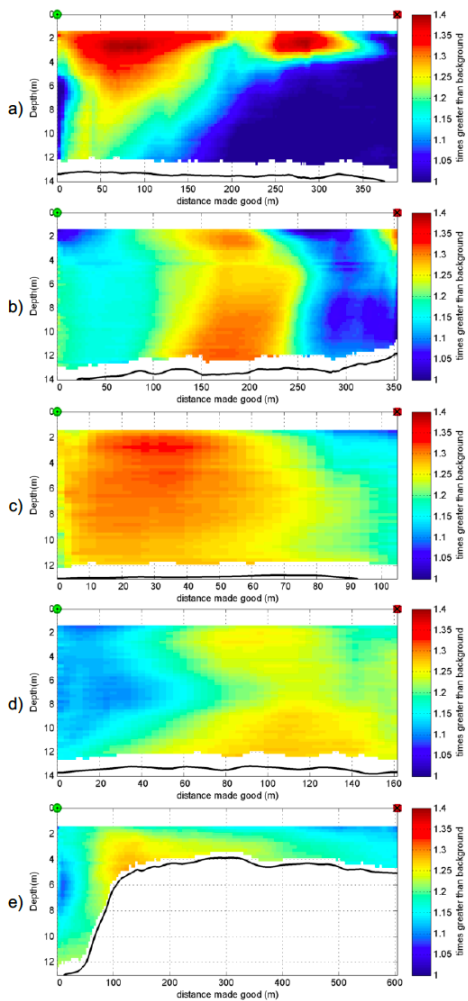
4.2   Monitoring-2 (M2)

Similar to M1, salinity and temperature did not vary noticeably through the water column or between CTD casts (Table 2) and background backscatter was also highest (~85.4 dB ± 3.4) at the surface (<2 m depth) and decreased towards the bottom (~80 ± 1.8) (Figure 2 – right); However, below a depth of 7 m, the background backscatter signal slightly increased (~82.5 ± 1.8). Background TSS concentrations were 6.7 mg l^{-1} at surface, 8.7 mg l^{-1} at mid-depth and 9.6 mg l^{-1} at the bottom, very similar to the M1 and also the opposite of the background ADCP profile (Figure 2 – right). Water samples collected during dredging produced TSS concentrations of 14.9, 21.6 and 24 mg l^{-1} at the surface, mid-depth and the bottom, respectively.

ADCP transect 1, at the beginning of the dredging, detected a plume with signal 1.35 to 1.4 times greater than background extending for ~60 m and a diffuse area of the plume 1.2 times greater than background extending ~30 m on the side of the central plume area. After 30 minutes, transects in the centre of the dredging area (2 and 3) showed a surface plume (< 6m) 1.15 to 1.2 times greater than background.

4
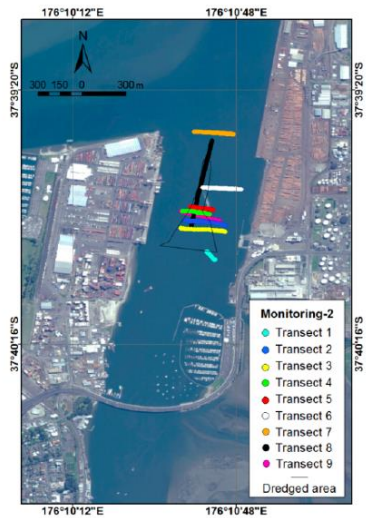
Figure 5 Map of the Stella Passage showing transects 1 to 9 conducted during and after dredging in M2. Thin black line delimits the dredged area.

After dredging finished, a series of parallel transects were made in the direction of flow, from transect 4 to transect 7, and showed plumes with maximum backscatter ranging from 1.4 (transect 4) to 1.15 (transect 7) times greater than the background with plumes usually measuring 100 m long. A longitudinal transect (8) made perpendicular to the previous transects showed backscatter similar to background levels. A comparison between one transect conducted just after dredging ended and another transect 50 minutes later (4 and 9) showed that levels had reduced to background levels within and near the dredging area.
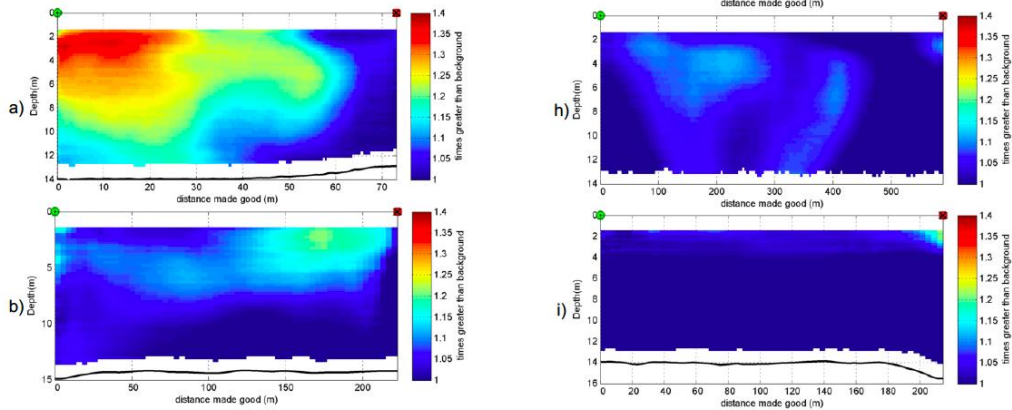
Figure 6 Profiles of Transects 1 to 9 conducted during and after dredging in M2 (Figure 5). Shade indicates backscatter greater than background and white areas represent the bottom and bins not measured by the ADCP. On top of each transect, a green circle is the start

5

point and a red square is the end point, here described as geographic position (N – north, S – south, E – east and W – west). Start time, and start and end position for each transect follows (a) 12:44 W-E; (b)12:55 E-W; (c)12:58 W-E; (d)13:16 W-E; (e)13:18 E-W; (f)13:25 W-E; (g)13:37 E-W; (h)13:45 S-N; and (i)14:07 E-W.

5. Discussion

Dredging plumes during M1 and M2 dissipated quickly, as shown by the rapidly-decaying backscatter signal during the first 10 minutes of dredging, which is in accordance with other studies [2] [20]. For example, [11] found a decrease of three orders of magnitude in suspended sediment concentration occurred in less than 3 minutes in a zone close to the dredging.

After dredging started, during M1, the plume was initially concentrated in the surface layers, but later descended in the water column, with deflections in backscatter signals in the direction of the current at the mid-depth ranges. These observations are indicative of material settling from the upper plume and the effect of currents on the plume motion. The plume was transported by the flood tide to the south of the dredging area; the abrupt change in bathymetry (from 12 m to 4 m), the shallow waters, and structures made it difficult to complete the survey and detect plume boundaries in this area. Furthermore, shipping traffic in the area added further complications. The turning and berthing of a large container ship generated a plume that was visibly evident in the area being monitored for the dredging plume. Therefore, the plume observed during the dredging monitoring potentially included not only the plume from the dredging but also from other contributors, such as ship movement disturbing the sediments. It was not possible to separate the ship effects from the dredging activity in the dredge plume data since the dredging was carried out very close to the berthing area. In M2, plume signals were easier to distinguish from the background and allowed a more comprehensive plume tracking. Manoeuvring of ships that were smaller than the one observed in M1 appeared to contribute less to the TSS concentrations. Transects conducted during dredging indicate that the plume drifted in the direction of the ebb tide currents and was more concentrated at surface and mid-depths.

After 1 hour, measurements obtained in the proximity of the dredged area, showed that the backscatter signal was close to the background levels for both monitoring periods. However, backscatter signals in profiles conducted within the plume track in M2 showed a more rapid reduction in concentrations compared to the plume from M1, suggesting a more rapid dissipation of the ebb tide plume. Just before the end of the monitoring, further away from the dredging area, the last observations collected showed that the plume from M2 shifted northward and backscatter signal was close to the background levels, whilst the plume from M1 was lower concentration but still detectable (1.15 to 1.2 greater than background) at ~1 km south. The estimation of the concentration of the residual plume could have been influenced by the fact that the background backscatter was measured in deeper areas, whilst the residual plume was detected in the shallow areas, thus potentially representing differences between background turbidity levels at the two locations.

The effects on biota were evaluated according to concentrations found in our TSS analysis and the time for plume dispersion detected in the transects. Other sources of contamination that could affect the biota, such as heavy metals and other possible dredge-related impacts were not considered in this study. Although studies have demonstrated negative effects caused by dredging plumes on the biota [13], our study suggests that the range of TSS and the duration of plume observed during the monitoring would have no adverse effects on key species in Tauranga Harbour such as bivalves: cockles (*Austrovenus stutchburyi*), pipis (*Paphies australis*) and seagrass (*Zostera muelleri*). Pipis, which are considered to be sensitive to increases in TSS, would only be negatively affected if exposed to concentrations of 150-200 mg l^{-1} for 5 days [9]. Seagrass can be moderately to severely impacted at TSS levels of > 75 mg l^{-1}; however, the duration of the plume resulting from dredging is unlikely to be long enough to adversely affect seagrass condition [4].

6. Conclusion

Backscatter signals during dredging showed concentrations up to 1.4 times greater than background and analysis of TSS for water samples collected in the dredging plume presented maximum concentration of 70 mg l^{-1}. However, it should be noted that discrete point samples cannot always represent the real concentrations due to the ephemeral nature of the plume. After dredging ceased, backscatter levels in the dredged area reduced to background levels in 1 hour or less, and our results suggest that the ebb tide plume dissipated faster than the flood tide plume. Previous studies indicated that a plume with duration of 1 to 2 hours and TSS concentration ~70 mg l^{-1} is below the threshold for causing serious impacts to the biota; therefore, only minor effects can be expected for plumes with the same characteristic of the two dredging plumes here described. Our preliminary results for Tauranga Harbour although the plume dissipated more quickly on the outgoing tide, and dredging on the outgoing tide only will provide the least likelihood of impacts, we also show that dredge operators should be able to continue working on both tides because the flood tide plume was also dissipated within an hour. This fast dissipation time is likely due to the strong flushing that occurs inside of the

6

162

entrance and the generally sandy sediments. Upcoming capital dredging may uncover a greater range of particle sizes, and so monitoring of the plume is ongoing with greater potential mitigation strategies in place should the plume dissipation rate decrease.

7.   Acknowledgements

8.   References

[1] APHA (1997). 2540 D Total suspended solids dried at 103-105°C.: American Public Health Association (APHA), American Water Works Association, Water Environment Federation.

[2] Bohlen, W.F.; Cundy, D.F., and Tramontano, J.M. (1979). Suspended material distributions in the wake of estuarine channel dredging operations. Estuarine and Coastal Marine Science, Vol. 9, No. 6, pp. 699–711.

[3] Davies-Colley R.J., Healy T.R. (1978). Sediment and hydrodynamics of the Tauranga entrance to Tauranga Harbour. New Zealand Journal of Marine and Freshwater Research, 12, pp. 225–236.

[4] Doorn-Groen, S.M. (2007). Environmental Monitoring and Management of Reclamations Works Close to Sensitive Habitats. Terra et Aqua, Vol. 108, pp. 3–18.

[5] Duclos, P.-A., Lafite, R., Le Bot, S., Rivoalen, E., and Cuvilliez, A. (2013). Dynamics of turbid plumes generated by marine aggregate dredging: an example of a macrotidal environment (the Bay of Seine, France). Journal of Coastal Research, Vol. 29, No. 6A, pp. 25–37.

[6] Erftemeijer, P.L.A., and Lewis, R.R.R. (2006). Environmental impacts of dredging on seagrasses: A review. Marine Pollution Bulletin, Vol. 52, pp. 1553–1572.

[7] Flaim, B.K. (2012). Sediment dispersion at the new Auckland marine disposal ground, Northeast New Zealand. Doctoral dissertation, University of Waikato, Hamilton, New Zealand.

[8] Heath, R.A. (1985) A review of the physical oceanography of the seas around New Zealand - 1982. New Zealand Journal of Marine and Freshwater Research, Vol. 19, No. 1, pp. 79–124.

[9] Hewitt, J. E., and Norkko, J. (2007). Incorporating temporal variability of stressors into studies: An example using suspension-feeding bivalves and elevated suspended sediment concentrations. Journal of Experimental Marine Biology and Ecology, Vol. 341, pp. 131–141.

[10] James, M., Probert, K., Boyd, R., and Sagar, P. (2009). Biological resources of Otago Harbour and offshore: assessment of effects of proposed dredging and disposal by Port Otago Ltd. Report prepared by NIWA for Port Otago Limited (NIWA Client Report: HAM2008-152; NIWA Project: POL08201).

[11] Nichols, M., Diaz, R.J. and Schaffner, L.C. (1990). Effects of hopper dredging and sediment dispersion, Chesapeake Bay. Environ. Geol. Water Sci. Vol. 15, No. 1, pp. 31–43.

[12] Nightingale, B., and Simenstad, C.A. (2001). Dredging activities: marine issues. Report prepared by Washington State Transportation Center for Washington State Transportation Commission (TRAC Technical Report WA-RD 507.1).

[13] Onuf, C.P. (1994). Seagrasses, dredging and light in Laguna Madre, Texas, U.S.A. Estuarine, Coastal and Shelf Science , Vol. 39, pp. 75–91.

[14] Park, S. (2004). Aspects of mangrove distribution and abundance in Tauranga Harbour. Report prepared by Stephen Park for Environment Bay of Plenty (Environmental Publication 2004/16).

[15] Park, S.G. (1999). Changes in abundance of seagrass (Zostera spp.) in Tauranga Harbour from 1959-96. Report prepared by S. G. Park for Environment Bay of Plenty (Environment BOP Environmental Report 99/30).

[16] Priestley, S.J. (1995). Measured environmental impacts of dredging operations. Transactions on the Built Environment, Vol 8.

[17] Puckette, T.P. (1998). Evaluation of dredged material plumes - physical monitoring techniques (No. TN DOER-E5). Vicksburg, MS: US Army Engineer Research and Development Center.

[18] Sinner, J., Clark, D., Ellis, J., Roberts, B., Jiang, W., Goodwin, E., Hale, L., Rolleston, S., Patterson, M., Hardy, D., Prouse, E., and Brown, S. (2011). Health of Te Awanui Tauranga Harbour (Manaaki Taha Moana Research Report No. 1; Cawthron Report No.1969).

[19] Smith, J.E., Friedrichs,C. (2011). Size and settling velocities of cohesive flocs and suspended sediment aggregates in a trailing suction hopper dredge plume. Continentl Shelf Research, Vol. 31, No. 10, pp. S50–S63.

[20] Smith, G.G.; Weitz, N.; Soltau, C.; Viljoen, A.; Luger, S., and Maartens, L. (2008). Fate of fine sediment from dredger-based mining in a wave dominated environment at Chameis Bay, Namibia. Journal of Coastal Research, Vol. 24, No. 1, pp. 232–247.

[21] Tay, H.W., Bryan, K.R., Pilditch, C.A., Stephen, P., and Hamilton, D.P. (2012). Variations in nutrient concentration at different time scales in two shallow tidally dominated estuaries. Marine and Freshwater Research, Vol. 63, pp. 95–109.

[22] USACE. (1983). Engineering and design: dredging and dredged material disposal (Engineer manual No. EM 1110-2-5025). Washington D.C.

[23] Wilber, D.H., and Clark, D.G. (2001). Biological effects of suspended sediments: a review of suspended sediment impacts on fish and shellfish with relation to dredging activities in estuaries. North American Journal of Fisheries Management, Vol. 21, No. 4, pp. 855–875.

APPENDIX H

New Zealand Coastal Society Newsletter

This appendix includes an article published in the New Zealand Coastal Society's newsletter which presents a modified version of the paper presented in Appendix G. The article is reproduced here with the permission of the NZ Coastal Society, www.coastalsociety.org.nz.

Cussioli, M., Bryan, K., Pilditch, C and de Lange, Willem. 2016. Dispersal of dredging plumes in Tauranga Harbour: A field study. *New Zealand Coastal Society Coastal News*, 62: 6-9.

Dispersal of dredging plumes in Tauranga Harbour: A field study

By Mariana Cussioli, Karin Bryan, Conrad Pilditch and Willem De Lange,
University of Waikato

In this issue we feature a summary of a paper presented at the 2015 Australasian Coasts and Ports conference. The full paper, including figures, references and acknowledgements, is available in the conference proceedings. Contact nzcoastalsociety@gmail.com for more information.

In ports and harbours, routine dredging activity is needed to maintain and deepen navigation channels. Dredging can generate high quantities of suspended sediments, which are transported from dredged area by currents and deposited on the seabed. The dimensions and dispersal dynamics of a plume are determined by the dredging strategy and local sediment and hydrodynamic characteristics. The complexity of these underlying factors and their potential interactions pose difficulties in predicting plume dynamics and behaviour.

Suspended sediments caused by dredge plumes and their potential impacts on marine flora and fauna are a key concern for environmental managers. For example, high suspended sediment concentrations (TSS) can reduce the feeding efficiency of filter-feeding bivalves and reduce light penetration thus affecting primary producers such as seagrasses. Ecological effects, however, are usually only considered significant when TSS caused by dredging is higher than the natural variation owing to storm events, wave-action, and river discharges.

Sediment plumes from maintenance dredging are usually of short duration, and most studies show that high TSS is mostly confined to the immediate environs of the dredging vessel and decays rapidly with time and distance from the dredge. The rate of TSS reduction depends on the characteristics of the area being dredged, the spatial and temporal extent of the plumes and the areas of potential impact.

Given the transient nature of dredge plumes, the use of acoustic technologies with high spatial and temporal resolution for tracking plumes is an advance over the use of point sample measurements.

Through the application of the acoustic method, our aim was to track the plumes created during maintenance dredging in Tauranga Harbour, with the objective of describing their dynamics and development with time and distance from the dredging area and comparing TSS values with background levels.

The harbour

Tauranga Harbour is an estuarine lagoon on the east coast of New Zealand's North Island, comprising an area of about 200 square kilometres. Intertidal flats separate the lagoon into two main areas, the northern and the southern basins. It is predominantly a shallow harbour, with an average depth at low tide of three metres. The tides in Tauranga Harbour are semi-diurnal and have a tidal range of 1.62 metres for spring tide and 1.24 metres for neap tide, and 60 percent of the harbour is intertidal sandflats. The harbour has two tidal inlets, one at each end of Matakana Island. The more important inlet for navigation is the south-eastern end bounded by the rocky headland of Mt Maunganui, where it is also the entrance to the Port of Tauranga.

The Port of Tauranga was officially established in 1873 and dredging activities at the port started about 100 years afterwards, in 1968, and occurred until 1978, restarting in 1991. The main dredging projects were aimed at deepening and widening of the shipping channels. To maintain channel depths that are adequate for navigation, maintenance dredging was regularly carried out approximately every two years since 1992. Presently, the port undertakes it annually.

Monitoring a maintenance dredging event

A maintenance dredging event occurred in October 2014, and the sediment plumes generated by the dredging activities were monitored between 13 and 16 October 2014. In this article we present two monitoring periods (dredging cycles) conducted on 15 October, Monitoring-1 and Monitoring-2 (hereafter M1 and M2, respectively), which tracked the dredging plume in the morning and afternoon.

The dredging was carried out using the TSHD *Pelican* (Van Oord) which has a hopper capacity of 965 cubic metres, 63 metres in length and 11 metres in width. The draft when loaded is 3.7 metres.

Dredging activities occurred in Stella Passage with 1283 and 1187 tons of material dredged during M1 and M2, respectively. Both sediment types were composed mainly of sand. On 15 October, low tide was 0.2 metres at 05:49 and high tide was 1.8 metres at 12:15. The M1 monitoring was conducted during flood tide and the M2 during ebb tide. The monitoring period covered the end of the spring tide.

TSHD Pelican. *Photo: Mariana Cussioli.*

165

Dredging plumes were tracked using backscatter signals measured by a boat-mounted acoustic Doppler current profiler – ADCP (Workhorse Teledyne RD Instruments 1200 kHz). Transects along and across the main current direction were made during and after dredging until the plume signal declined to background levels, and therefore difficult to detect, or until time or technical limits were imposed. Six and nine transects were completed for M1 and M2, respectively. Plume backscatter signals were compared with averaged profiles of background values determined from transects conducted immediately before each dredging monitoring.

Additional measurements were carried out to complement the study: water temperature, salinity and suspended solids concentration. Temperature and salinity were measured using a CTD (SBE 19 plus V2 SeaCAT) and casts carried out before dredging started for background conditions and at the end of each monitoring period. Water samples for total suspended solids concentration (TSS) were collected at the surface, mid-depth and bottom using a Schindler-Patalas trap and retained in bottles until filtering, which occurred less than 24 hours after sampling.

	Monitoring-1		Monitoring-2	
	Start	End	Start	End
Time (NZST)				
Monitoring	07:11	09:35	12:13	14:28
Background sampling				
CTD	07:13		12:16	
Water surface	07:25		12:17	
Water mid-depth	07:22		12:16	
Water bottom	07:20		12:14	
Transects	07:21	07:59	12:18	3
Plume sampling				
Dredging	08:15	08:45	12:25	13:15*
Transects	08:15	09:36	12:34	14:28
Water surface	08:30		12:45	
Water mid-depth	08:31		12:43	
Water bottom	08:35		12:41	
CTD	9:37		14:28	

* M2 dredging time was reduced to 30 minutes following an operational delay of 20 minutes.

Table 1. Start and end time for measurements carried out during M1 and M2 to characterise the area before, during and after dredging. Times are in New Zealand Standard Time (NZST).

Results for M1

Surface temperature was ~1˚C higher at the water surface than at the bottom, but there were no differences between CTD casts made before (07:13) and after (09:37) the dredging monitoring. Before dredging monitoring, there was a vertical salinity gradient with slightly higher levels at the bottom compared with the surface, but differences were weaker at the end of the monitoring period. Thus, there was no strong evidence of water column stratification that could influence the distribution of the plume.

Tauranga Port from the Coastal Marine Group's research vessel Tai Rangahau. Photo: Mariana Cussioli.

Background backscatter for M1 (determined from transects conducted previous to the dredging monitoring) was highest (~84.4 dB ± 5.6) at the surface (<2 metres depth) and was consistently lower (~80 dB ± 2) below this depth. Background concentrations determined by TSS were 7 mg l^{-1} at the surface, 9.5 mg l^{-1} at mid-depth and 9 mg l^{-1} at the bottom. TSS concentrations were lower at the surface, thus was inconsistent with our ADCP transect data. During the dredging, the TSS concentration was 9, 13 and 70.3 mg l^{-1} at the surface, mid-depth and the bottom, respectively.

During dredging, ADCP measurements detected an initial plume ~350 metres long with a vertical gradient of backscatter ranging from 1.4 to 1.25 times greater than the background at the surface and the bottom, respectively. After 10 minutes, in transect 2 the plume length at this position was >250 metres with the highest relative backscatter occurring at lower depths (below 8 metres) compared to observations during transect 1.

Ten minutes following the end of the dredging, two parallel transects (3 and 4) revealed a plume >70 metres in length with concentrations 1.35 to 1.30 times greater than background and higher concentrations at the surface. Diffuse areas of the plume (1.2 times greater than background) extended 30 metres either side of the central plume area.

Transects running longitudinally to the channel (5 and 6) 20 and 35 minutes after the dredging ended, revealed plume movement towards the south according to the direction of the currents and flood tide. Along these transects, there was an abrupt change in the bathymetry, from a maximum of ~12 metres to ~5 metres depth. The plume presented maximum backscatter around 1.3 to 1.15 times the background as plume drifted from the deeper to the shallow area and measured ~600 metres at transect 5, and 800 metres at transect 6. After 55 minutes of monitoring, the plume appeared to dissipate and was no longer detectable within the dredging area.

Results for M2

Similar to M1, salinity and temperature did not vary noticeably through the water column or between CTD casts and background backscatter was also highest (~85.4 dB ± 3.4) at the surface (<2 metres depth) and

166

decreased towards the bottom (~80 ± 1.8). However, below a depth of seven metres, the background backscatter signal slightly increased (~82.5 ± 1.8). Background TSS concentrations were 6.7 mg l^{-1} at surface, 8.7 mg l^{-1} at mid-depth and 9.6 mg l^{-1} at the bottom, very similar to the M1 and also the opposite of the background ADCP profile. Water samples collected during dredging produced TSS concentrations of 14.9, 21.6 and 24 mg l^{-1} at the surface, mid-depth and the bottom, respectively.

ADCP transect 1, at the beginning of the dredging, detected a plume with signal 1.35 to 1.4 times greater than background extending for ~60 metres and a diffuse area of the plume 1.2 times greater than background extending ~30 metres on the side of the central plume area. After 30 minutes, transects in the centre of the dredging area (2 and 3) showed a surface plume (< 6 metres) 1.15 to 1.2 times greater than background.

After dredging finished, a series of parallel transects were made in the direction of flow, from transect 4 to transect 7, and showed plumes with maximum backscatter ranging from 1.4 (transect 4) to 1.15 (transect 7) times greater than the background with plumes usually measuring 100 metres long. A longitudinal transect (8) made perpendicular to the previous transects showed backscatter similar to background levels. A comparison between one transect conducted just after dredging ended and another transect 50 minutes later (4 and 9) showed that levels had reduced to background levels within and near the dredging area.

Analysing the results

Dredging plumes during M1 and M2 dissipated quickly, as shown by the rapidly decaying backscatter signal during the first 10 minutes of dredging.

After dredging started, during M1, the plume was initially concentrated in the surface layers, but later

Tauranga Port from the Coastal Marine Group's research vessel Tai Rangahau. *Photo: Mariana Cussioli.*

descended in the water column, with deflections in backscatter signals in the direction of the current at the mid-depth ranges. These observations are indicative of material settling from the upper plume and the effect of currents on the plume motion. The plume was transported by the flood tide to the south of the dredging area; the abrupt change in bathymetry, the shallow waters and structures made it difficult to complete the survey and detect plume boundaries in this area. Shipping traffic in the area added further complications. The plume observed during the dredging monitoring potentially included not only the plume from the dredging but also from other contributors, such as ship movement disturbing the sediments. It was not possible to separate the ship effects from the dredging activity in the dredge plume data since the dredging was carried out very close to the berthing area. In M2, plume signals were easier to distinguish from the background and allowed a more comprehensive plume tracking. Manoeuvring of ships that were smaller than the one observed in M1 appeared to contribute less to the TSS concentrations. Transects conducted during dredging indicate that the plume drifted in the direction of the ebb tide currents and was more concentrated at surface and mid-depths.

After one hour, measurements obtained in the proximity of the dredged area showed that the backscatter signal was close to the background levels for both monitoring periods. However, backscatter signals in profiles conducted within the plume track in M2 showed a more rapid reduction in concentrations compared to the plume from M1, suggesting a more rapid dissipation of the ebb tide plume. Just before the end of the monitoring, further away from the dredging area, the last observations collected showed that the plume from M2 shifted northward and backscatter signal was close to the background levels, whilst the plume from M1 was lower concentration but still detectable (1.15 to 1.2 greater than background) at ~1 kilometre south. The estimation of the concentration of the residual plume could have been influenced by the fact that the background backscatter was measured in deeper areas, whilst the residual plume was detected in the shallow areas, thus potentially representing differences between background turbidity levels at the two locations.

The effects on biota were evaluated according to concentrations found in our TSS analysis and the time for plume dispersion detected in the transects.

Other sources of contamination that could affect the biota, such as heavy metals and other possible dredge-related impacts, were not considered in this study. Although studies have demonstrated negative effects caused by dredging plumes on the biota, our study suggests that the range of TSS and the duration of plume observed during the monitoring would have no adverse effects on key species in Tauranga Harbour such as bivalves: cockles (*Austrovenus stutchburyi*), pipis (*Paphies australis*) and seagrass (*Zostera muelleri*). Pipis, which are considered to be sensitive to increases in TSS, would only be negatively affected if exposed

to concentrations of 150-200 mg l^{-1} for five days. Seagrass can be moderately to severely impacted at TSS levels of > 75 mg l^{-1}; however, the duration of the plume resulting from dredging is unlikely to be long enough to adversely affect seagrass condition.

Our preliminary results for Tauranga Harbour show that although the plume dissipated more quickly on the outgoing tide, and dredging on the outgoing tide only will provide the least likelihood of impacts, we also show that dredge operators should be able to continue working on both tides because the flood tide plume was also dissipated within an hour. This fast dissipation time is likely due to the strong flushing that occurs inside of the entrance and the generally sandy sediments. Upcoming capital dredging may uncover a greater range of particle sizes, and so monitoring of the plume is ongoing with greater potential mitigation strategies in place should the plume dissipation rate decrease.

Update on dredging

Since this presentation was given, the port has almost finished the major dredging campaign and has had no complaints about turbidity to date. In part, this is attributed to management of the dredging to mix silty sediment with non-silty sediment in the hopper, and also to a "green" valve that adjusts the rate and amount of overflow from the hopper.

There are plans to incorporate the green valve technology in the replacement dredge for the port's ongoing maintenance dredging requirements.
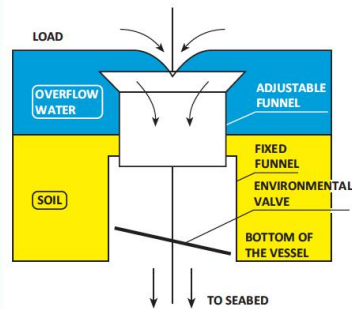
Image shows the structure of the discharge funnel from the hopper including the "green" or environmental valve. The purpose of the valve is to reduce the amount of air being discharged with the sediment, allowing the sediment to sink to the seabed faster, which reduces turbidity. Image: Willem de Lange.

(Top image) This image shows the entrainment of air, which creates bubbles. At the top is an adjustable funnel that can be released and lowered to vary the rate of discharge, which also reduces the turbidity. Photo: Willem de Lange.

(Left image) View looking down on the discharge funnel. Photo: Willem de Lange.

Contributing to Coastal News

We always welcome contributions for forthcoming issues of Coastal News. Please contact the Editor, Shelly Farr Biswell, at shelly@biswell.net if you'd like to submit a news in brief, article, or have content suggestions. The submission deadline for the next issue is 14 October 2016.

168

REFERENCES

Aarninkhof, S.G.J., 2008. The day after we stop dredging: A world without sediment plumes? *Terra et Aqua*, 110: 15–25.

Abal E.G., Loneragan N., Bowen P., Perry C.J., Udy J.W. and Dennison W.C., 1994. Physiological and morphological responses of the seagrass *Zostera capricorni* Aschers. to light intensity. *Journal of Experimental Marine Biology and Ecology*, 178(1): 113–129.

ANZECC 2000. Australian and New Zealand Guidelines for Fresh and Marine Water Quality - Volume One: the guidelines, Australian and New Zealand Environment and Conservation Council and Agriculture and Resource Management Council of Australia and New Zealand.

APHA, 1997. 2540 D Total suspended solids dried at 103-105°C.: American Public Health Association (APHA), American Water Works Association, Water Environment Federation.

Asmus, H. and Asmus, R.M., 1993. Phytoplankton-mussel bed interactions in intertidal ecosystems. In: Dame, R.F. (Ed.). Bivalve filter feeders in estuarine and coastal ecosystem processes, Springer-Verlag, Berlin, 57–84.

Bacon, G.S., MacDonald, B.A., Ward, J.E., 1998. Physiological responses of infaunal (*Mya arenaria*) and epifaunal (*Placopecten magellanicus*) bivalves to variations in the concentration and quality of suspended particles I. Feeding activity and selection. *Journal of Experimental Marine Biology and Ecology*, 219: 105–125.

Barbier, E.B., Hacker, S.D., Kennedy, C., Koch, E.W., Stier, A.C. and Silliman, B.R., 2011. The value of estuarine and coastal ecosystem services. *Ecological Monographs*, 81(2): 169–193.

Barillé, L., Prou, J., Héral, M., and Razet, D., 1997. Effects of high natural seston concentrations on the feeding, selection, and absorption of the oyster

Crassostrea gigas. Journal of Experimental Marine Biology and Ecology, 212: 149–172.

Barker M. and Larcombe M., 1976. Aspects of the ecology of Tauranga Harbour. Bioresearchers Ltd, Auckland, New Zealand.

Bayne, B.L., Iglesias, J.I.P., Hawkins, A.J.S., Navarro, E., Héral, M., Deslous-Paoli, J.M., 1993. Feeding behaviour of the mussel, *Mytilus edulis* L.: responses to variations in both quantity and organic content of seston. *Journal of the Marine Biological Association of the United Kingdom*, 73: 813–829.

Bayne, B.L. and Newell, R.C., 1983. Physiological energetics of marine molluscs. In: Wilbur, K.M. and Saleuddin, A.S. (Eds.). The Mollusca, Vol4, Academic Press, New York, 407–515.

Benham, C.F., Beavis, S.G., Hendry, R.A. and Jackson, E.L., 2016. Growth effects of shading and sedimentation in two tropical seagrass species: Implications for port management and impact assessment. *Marine Pollution Bulletin*, 109: 461–470.

Bohlen, W.F.; Cundy, D.F., and Tramontano, J.M., 1979. Suspended material distributions in the wake of estuarine channel dredging operations. *Estuarine and Coastal Marine Science*, 9(6): 699–711.

Brabec, E., Schulte, S. and Richards, P., 2002. Impervious surfaces and water quality: A review of current literature and its implications for watershed planning. *Journal of Planning Literature*, 16(4): 499–514.

Bricelj, V.M. and Malouf, R.E., 1984. Influence of algal and suspended sediment concentrations on the feeding physiology of the hard clam *Mercenaria mercenaria*. *Marine Biology*, 84: 155–165.

Bricelj, V.M., Malouf, R.E. and de Quillfeldt, C., 1984. Growth of juvenile *Mercenaria mercenaria* and the effect of resuspended bottom sediments. *Marine Biology*, 84: 167–173.

Brunschwiler, N.R., 2015. *Dispersal and mixing of stormwater run-off plumes in the Port of Tauranga, New Zealand*. MSc thesis, University of Waikato, New Zealand.

Bryan, K.R., Douglas, E., Pilditch, C.A. and Cussioli, M.C., 2014. Setting water quality limits and monitoring turbidity for the Port of Tauranga. Part A: Preliminary Investigation. ERI report number: ERI025. Environmental Research Institute, Hamilton, New Zealand.

Bulmer, R.H., Kelly, S. and Jeffs, A.G., 2016. Light requirements of the seagrass, *Zostera muelleri*, determined by observations at the maximum depth limit in a temperate estuary, New Zealand. *New Zealand Journal of Marine and Freshwater Research*, 50 (2): 183–194.

Cabaço, S., Santos, R. and Duarte, C.M., 2008. The impact of sediment burial and erosion on seagrasses: A review. *Estuarine, Coastal and Shelf Science*, 79: 354–366.

Campbell, M.L., 2016. Burial duration and frequency influences resilience of differing propagule types in subtidal seagrass, *Posidonia australis*. *PLoS ONE*, 11(8): e0161309.

Campbell, S.J., McKenzie, L.J., 2004. Flood related loss and recovery of intertidal seagrass meadows in southern Queensland, Australia. *Estuarine Coastal and Shelf Science*, 60: 477–490.

Carder, K. L., Steward, R. G., Harvey, G. R. and Ortner, P. B., 1989. Marine humic and fulvic acids. Their effect on remote sensing of ocean chlorophyll. *Limnology and Oceanography*, 34(1): 68–81.

Chartrand, K.M., Rasheed, M., Petrou, K. and Ralph, P., 2012. Establishing tropical seagrass light requirements in a dynamic port environment. Proceedings of the 12th International Coral Reef Symposium, Cairns, Australia.

Clarke, D. and Wilber, D., 2008. Compliance monitoring of dredging-induced turbidity: Defective designs and potential solutions. Paper presented at the Western Hemisfere's Annual Dredging Conference, Missouri.

Close, D., Bates, A., Morelissen, R. and Roche, C., 2013. Dredging and disposal at Lough Foyle, Northern Ireland. *Terra et Aqua*, 130: 10–19.

Coles, R., McKenzie, L., Campbell, S., 2003. The seagrasses of Eastern Australia. In: E.P. Green, F.T. Short (eds.) *World Atlas of Seagrasses*, Prepared by the UNEP World Conservation Monitoring Centre. University of California Press, Berkeley, USA, p. 119–133.

Cook, S. de C., 2010. New Zealand Coastal Marine Invertebrates 1. Canterbury University Press. 640 pp.

Cooper, K.M., Curtis, M., Wan Hussin, W.M.R., Barrio Froján, C.R.S., Defew, E.C., Nye, V. and Paterson, D.M., 2011. Implications of dredging induced changes in sediment particle size composition for the structure and function of marine benthic macrofaunal communities. *Marine Pollution Bulletin*, 62: 2087–2094.

Costanza, R., d'Arge, R., de Groot, R., Farber, S., Grasso, M., Hannon, B., Limburg, K., Naeem, S., O'Neall, R.V., Paruelo, J., Raskin, R.G., Sutton, P. and Van den Belt, M., 1997. The value of the world's ecosystem services and natural capital. *Nature*, 387: 253–260.

Cummings, V.J., and Thrush, S.F., 2004. Behavioural response of juvenile bivalves to terrestrial sediment deposits: implications for post-disturbance recolonisation. *Marine Ecology Progress Series*, 278: 179–191.

Cussioli, M.C., Bryan, K.R., Pilditch, C.A. and De Lange, W.P., 2015. Dispersal of dredging plumes in Tauranga Harbour, New Zealand: a field study. In Australasian Coasts and Ports 2015, Wellington, New Zealand. IPENZ, 222–228.

Cussioli, M.C., Bryan, K.R., Pilditch, C.A., de Lange, W.P., and Bischof, K., (submitted). Modulation of photosynthetically active radiation (PAR) in a well-flushed channelized temperate estuary, Tauranga Harbour, New Zealand: implications for seagrass growth and dredging.

Cutroneo L., Castellano M., Pieracci A., Povero P., Tucci S. and Capello M., 2012. The use of a combined monitoring system for following a turbid plume

generated by dredging activities in a port. *Journal of Soils and Sediments*, 12: 797–809.

Cutroneo, L., Castellano, M., Ferranti, M.P., Povero, P., Tucci, S. and Capello, M., 2013. Use of optical and acoustic instruments to study the turbid plumes generated by three different types of dredges during dredging activities inside and outside of a port. *Journal of Soils and Sediments*, 13: 1645–1654.

Dame, R.F., 1993. The role of bivalve filter feeder material fluxes in estuarine ecosystems. In: Dame, R.F. (ed.). *Bivalve filter feeders in estuarine and coastal ecosystem processes*, Springer-Verlag, Berlin, p. 245–269.

Davies-Colley, R.J. and Close, M.E., 1990. Water colour and clarity of New Zealand rivers under baseflow conditions. *New Zealand Journal of Marine and Freshwater Research*, 24(3): 357–365.

Davies-Colley, R.J. and Healy, T.R., 1978. Sediment and hydrodynamics of the Tauranga entrance to Tauranga Harbour. *New Zealand Journal of Marine and Freshwater Research*, 12(3): 225–236.

Davies-Colley, R.J. and Smith, D.G., 2001. Turbidity, suspended sediment, and water clarity: a review. *Journal of the American Water Resources Association*, 37(5): 1085–1101.

Davies-Colley, R.J. and Vant, W.N., 1987. Absorption of light by yellow substance in freshwater lakes. *Limnology and Oceanography*, 32(2): 416–425.

Davies-Colley, R.J., Vant, W.N. and Smith, D.G., 1993. Colour and clarity of natural waters. Science and management of optical water quality. Ellis Horwood, Chichester, U.K.

Davis, R.A. and Healy T.R., 1993. Holocene coastal depositional sequences on a tectonically active setting: southeastern Tauranga Harbour, New Zealand. *Sedimentary Geology*, 84: 57–69.

de Lange, W.P. and Healy, T.R., 1990. Renourishment of a flood- tidal delta adjacent beach, Tauranga Harbour, New Zealand. *Journal of Coastal Research*, 6(3): 627–640.

de Lange, W.P., Moon, V.G., and Fox, B.R.S., 2014. Distribution of silty sediments in the shallow subsurface of the shipping channels of Tauranga Harbour. *Environmental Research Institute Report No. 28*. Client report prepared for Port of Tauranga. Environmental Research Institute, Faculty of Science and Engineering, University of Waikato, Hamilton. 76 pp.

Del Barrio, P., Ganju, N.K., Aretxabaleta, A.L., Hayn, M., García, A., Howarth, R.W., 2014. Modeling future scenarios of light attenuation and potential seagrass success in a eutrophic estuary. *Estuarine, Coastal and Shelf Science*, 149: 13–23.

Dennison, W.C., 1987. Effects of light on seagrass photosynthesis, growth and depth distribution. *Aquatic Botany*, 27: 15–26.

Devlin, M.J, Barry, J., Mills, D.K., Gowen, R.J., Foden, J., Sivyer, D., Tett, P., 2008. Relationships between suspended particulate material, light attenuation and Secchi depth in the UK marine waters. *Estuarine, Coastal and Shelf Science*, 79: 429–439.

Dennison, W.C., 1987. Effects of light on seagrass photosynthesis, growth and depth distribution. *Aquatic Botany*, 27: 15–26.

Dennison, W.C., Orth, R.J., Moore, K.A., Stevenson, J.C., Carter, V., Kollar, S., Bergstrom, P.W., Batiuk, R.A., 1993. Assessing water quality with submersed aquatic vegetation. *BioScience*, 43(2): 86–94.

Do, V.T, Montaudouin, X., Blanchet, H. and Lavesque, N., 2012. Seagrass burial by dredged sediments: Benthic community alteration, secondary production loss, biotic index reaction and recovery possibility. *Marine Pollution Bulletin*, 64: 2340–2350.

Doorn-Groen, S.M., 2007. Environmental monitoring and management of reclamations works close to sensitive habitats. *Terra et Aqua*, 108: 3–18.

Duarte, C.M., 1991. Seagrass depth limits. *Aquatic Botany*, 40: 363–377.

Duarte, C.M., 2002. The future of seagrass meadows. *Environmental Conservation*, 29(2): 192–206.

Duclos, P.-A., Lafite, R., Le Bot, S., Rivoalen, E., and Cuvilliez, A., 2013. Dynamics of turbid plumes generated by marine aggregate dredging: an example of a macrotidal environment (the Bay of Seine, France). *Journal of Coastal Research*, 29(6A): 25–37.

Durand, M. D. and Olson, R. J., 1996. Contributions of phytoplankton light scattering and cell concentration changes to diel variations in beam attenuation in the equatorial Pacific from flow cytometric measurements of pico-, ultra- and nanoplankton. *Deep Sea Research Part II: Tropical Studies in Oceanography*, 43(4–6): 891–906.

Elliott, S., Parshotam, A. and Wadhwa, S., 2010. Tauranga Harbour sediment study: catchment model results. NIWA Client Report: HAM2009–046, National Institute of Water & Atmospheric Research Ltd, Hamilton, New Zealand.

Ellis, J., Clark, D., Hewitt, J., Taiapa, C., Sinner, J., Patterson, M., Hardy, D., Park, S., Gardner, B., Morrison, A., Culliford, D., Battershill, C., Hancock, N., Hale, L., Asher, R., Gower, F., Brown, E. and McCallion, A., 2013. Ecological Survey of Tauranga Harbour. Prepared for Manaaki Taha Moana, Manaaki Taha Moana Research Report No. 13. Cawthron Report No. 2321.

Environmetrics Australia Pty. Ltd., 2007. Turbidity monitoring. Environmental NTU limits for seagrass monitoring.

EPA, 2011. Environmental Assessment Guideline for Marine Dredging Programs EAG7. Environmental Protection Authority (EPA), Perth, Western Australia, p. 36.

Erftemeijer, P.L.A. and Lewis, R.R.R., 2006. Environmental impacts of dredging on seagrass: A review. *Marine Pollution Bulletin*, 52: 1553–1572.

Eyre, B.D. and Ferguson, A.J.P., 2002. Comparison of carbon production and decomposition, benthic nutrient fluxes and denitrification in seagrass, phytoplankton, benthic microalgae- and macroalgae- dominated warm-temperate Australian lagoons. *Marine Ecology Progress Series*, 229: 43–59.

Fahey, B.D., Coker, R.J., 1992. Sediment production from forest roads in Queen Charlotte forest and potential impact on marine water quality, Marlborough

Sounds, New Zealand. *New Zealand Journal of Marine and Freshwater Research*, 26: 187–195.

Flaim, B.K., 2008. The continental shelf as a site for dredged material disposal, northeast New Zealand. MSc Thesis, University of Waikato, Hamilton, New Zealand.

Flaim, B.K., 2012. Sediment dispersion at the new Auckland marine disposal ground, Northeast New Zealand. PhD Thesis, University of Waikato, Hamilton, New Zealand.

Fourqurean, J.W., Duarte, C.M., Kennedy, H., Marbà, N., Holmer, M., Mateo, M.A., Apostolaki, E.T., Kendrick, G.A., Krause-Jensen, D., McGlathery, K.J. and Serrano, O., 2012. Seagrass ecosystems as a globally significant carbon stock. *Nature Geoscience*, 5: 505–509.

Frost-Christensen, H. and Sand-Jensen, K., 1992. The quantum efficiency of photosynthesis in macroalgae and submerged angiosperms. *Oecologia*, 91(3): 377–384.

Fujiki, T., Taguchi, S., 2002. Variability in chlorophyll a specific absorption coefficient in marine phytoplankton as a function of cell size and irradiance. *Journal of Plankton Research*, 24: 859–874.

Gajewski, L.S. and Uscinowicz, S., 1993. Hydrologic and Sedimentologic Aspects of Mining Aggregate from the Slupsk Bank (Baltic Sea). *Marine Georesources & Geotechnology*, 11: 229–244.

Gardner, J.P.A., 2002. Effects of seston variability on the clearance rate and absorption efficiency of the mussels *Aulacomya maoriana*, *Mytilus galloprovincialis* and *Perna canaliculus* from New Zealand. *Journal of Experimental Marine Biology and Ecology*, 268: 83–101.

Gartner, J.W., 2004. Estimating suspended solids concentrations from backscatter intensity measured by acoustic Doppler current profiler in San Francisco Bay, California. *Marine Geology*, 211: 169–187.

GESAMP, 1990. The state of marine environment. Report prepared by IMO/FAO/Unesco/WMO/WHO/IAEA/UN/UNEP Joint Group of Experts on the Scientific Aspects of Marine Pollution. Reports and Studies No. 39.

Gibbs, M. and Hewitt, J., 2004. Effects of sedimentation on macrofaunal communities: a synthesis of research studies for ARC. Report prepared by NIWA for Auckland Regional Council. ARC Technical Publication 264.

Giesen, W.B.J.T., van Katwijk, M.M. and den Hartog, C., 1990. Eelgrass condition and turbidity in the Dutch Wadden Sea. *Aquatic Botany*, 37: 71–85.

Green, E.P. and Short, F.T., 2003. World Atlas of Seagrasses. Prepared by the UIMEP World Conservation Monitoring Centre. University of California Press, Berkeley, USA.

Green, M.O., 2006. New Zealand's estuaries: how they work and the issues that affect them. *NIWA Information Series* No. 59.

Green, M.O. and Coco, G., 2007. Sediment transport on an estuarine intertidal flat: Measurements and conceptual model of waves, rainfall and exchanges with a tidal creek. *Estuarine, Coastal and Shelf Science*, 72: 553–569.

Hach, C.C., Vanous, R.D. and Heer, J.M., 1982. Understanding turbidity measurements. Hach Technical Information Series, Booklet No. 11. 11 pp. Ames, IOWA.

Hawkins, A.J.S., Smith, R.F.M., Bayne, B.L. and Héral, M., 1996. Novel observations underlying the fast growth of suspension-feeding shellfish in turbid environments: *Mytilus edulis*. *Marine Ecology Progress Series*, 131: 179–190.

Hawkins, A.J.S., Bayne, B.L., Bougrier, S., Héral, M., Iglesias, J.I.P., Navarro, E., Smith, R.F.M. and Urrutia, M.B., 1998a. Some general relationships in comparing the feeding physiology of suspension-feeding bivalve molluscs. *Journal of Experimental Marine Biology and Ecology*, 219: 87–103.

Hawkins, A.J.S., Smith, R.F.M., Tan, S.H. and Yasin, Z.B., 1998b. Suspension-feeding behaviour in tropical bivalve molluscs: *Perna viridis*, *Crassostrea belcheri*,

Crassostrea iradelei, *Saccostrea cucculata* and *Pinctada margarifera*. *Marine Ecology Progress Series*, 166: 173–185.

Hawkins, A.J.S., James, M.R., Hickman, R.W., Hatton, S. and Weatherhead, M., 1999. Modelling of suspension-feeding and growth in the green-lipped mussel *Perna canaliculus* exposed to natural and experimental variations of seston availability in the Marlborough Sounds, New Zealand. *Marine Ecology Progress Series*, 191: 217–232.

Hayes, M.O., 1975. Morphology of sand accumulation in estuaries. In Cronin, L.E. (ed.), *Estuarine Research*, Vol II. Academic Press, INC. New York, pp. 3-22.

Healy T. and Tian F., 1999. Report on the dredging and disposal monitoring programme for Pine Harbour Marina–1998. Coastal Marine Group, Department of Earth Sciences, University of Waikato, p. 42.

Healy, T.R., Cole, R. and De Lange W., 1996. Geomorphology and ecology of New Zealand shallow estuaries and shorelines. In: Nordstrom, K.F. and Roman, C.T., (Eds.). Estuarine Shores, John Wiley & Sons, England, 115–154.

Healy, T., Mehta, A., Rodriguez, H. and Tian, F., 1999. Bypassing of dredged littoral muddy sediments using a thin layer dispersal technique. *Journal of Coastal Research*, 15(4): 1119–1131.

Heath, R.A., 1976. Broad classification of New Zealand inlets with emphasis on residence times. *New Zealand Journal of Marine and Freshwater Research*, 10: 429–444.

Heath, R.A., 1985. A review of the physical oceanography of the seas around New Zealand - 1982. *New Zealand Journal of Marine and Freshwater Research*, 19(1): 79–124.

Hendrick, V.J., Hutchison, Z.L. and Last, K.S., 2016. Sediment Burial Intolerance of Marine Macroinvertebrates. *PLoS ONE*, 11(2): e0149114.

Hewitt, J., Hatton, S., Safi, K. and Craggs, R., 2001. Effects of suspended sediment levels on suspension-feeding shellfish in the Whitford Embayment. Report

prepared by NIWA for Auckland Regional Council. ARC Technical Publication: 159.

Hewitt, J.E. and Norkko, J., 2007. Incorporating temporal variability of stressors into studies: An example using suspension-feeding bivalves and elevated suspended sediment concentrations. *Journal of Experimental Marine Biology and Ecology*, 341: 131–141.

Hewitt, J.E. and Pilditch, C.A., 2004. Environmental history and physiological state influence feeding responses of *Atrina zelandica* to suspended sediment concentrations. *Journal of Experimental Marine Biology and Ecology*, 306: 95–112.

Hitchcock, D.R. and Bell, S., 2004. Physical impacts of marine aggregate dredging on seabed resources in coastal deposits. *Journal of Coastal Research*, 20(1): 101–114.

Hitchcock, D.R. and Drucker, B.R., 1996. Investigation of benthic and surface plumes associated with marine aggregates mining in the United Kingdom. In: *The Global Ocean-Towards Operational Oceanography* Volume 2. Proceedings of the Oceanology International Conference.

Hoitink, A.J.F. and Hoekstra, P., 2005. Observations of suspended sediment from ADCP and OBS measurements in a mud-dominated environment. *Coastal Engineering*, 52: 103–118.

Holdaway, G.P., Thorne, P.D., Flatt, D., Jones, S.E., Prandle, D., 1999. Comparison between ADCP and transmissometer measurements of suspended sediment concentration. *Continental Shelf Research*, 19: 421– 441.

Hooker, S.H., 1997. Larval and postlarval development of the New Zealand pipi, *Paphies australis* (Bivalvia: Mesodesmatidae). *Bulletin of Marine Science*, 61(2): 225–240.

HR Wallingford Ltd and Dredging Research Ltd, 2003. Protocol for the field measurement of sediment release from dredgers. Vereniging van Waterbouwers in Bagger-Kust en Oeverwerken, VBKO.

Hughes, A.O., Davies-Colley, R.J., and Elliott, A.H., 2015. Measurement of light attenuation extends the application of suspended sediment monitoring in rivers, Proceedings of IAHS, 367: 170–176.

Iglesias, J.I.P., Navarro, E., Alvarez Jorna, P. and Armentia, I., 1992. Feeding, particle selection and absorption in cockles *Cerastoderma edule* (L.) exposed to variable conditions of food concentration and quality. *Journal of Experimental Marine Biology and Ecology*, 162: 177–198.

Iglesias, J.I.P., Urrutia, M.B., Navarro, E. and Ibarrola, I., 1998. Measuring feeding and absorption in suspension-feeding bivalves: an appraisal of the biodeposition method. *Journal of Experimental Marine Biology and Ecology*, 219: 71–86.

James, M., Probert, K., Boyd, R. and Sagar, P., 2009. Biological resources of Otago Harbour and offshore, assessment of effects of proposed dredging and dispersal by Port Otago Ltd. NIWA Client Report: HAM2008–152, National Institute of Water & Atmospheric Research Ltd, Hamilton, New Zealand.

Je, C.H. and Hayes, D.F., 2004. Development of a two-dimensional analytical model for predicting toxic sediment plunges due to environmental dredging operations. *Journal of Environmental Science and Health, Part A*, 39(8): 1935–1947.

Je, C.H., Hayes, D.F. and Kim, K.S., 2007. Simulation of resuspended sediments resulting from dredging operations by a numerical flocculent transport model. *Chemosphere*, 70(2): 187–195.

Jones, H., 2008. Coastal sedimentation: what we know and the information gaps. Environment Waikato Technical Report 2008/12, Document #1305126.

Jorgensen, C.B., 1996. Bivalve filter feeding revisited. *Marine Ecology Progress Series*, 142: 287-302.

Kirk, J.T.O., 1976. Yellow substance (Gelbstoff) and its contribution to the attenuation of photosynthetically active radiation in some inland and coastal South-Eastern Australian waters. *Australian Journal of Marine and Freshwater Research*, 27: 61–71.

180

Kirk, J.T.O., 1977. Attenuation of light in natural waters. Australian *Journal of Marine and Freshwater Research*, 28: 497–508.

Kirk, J.T.O., 2011. *Light and photosynthesis in aquatic ecosystems*. Cambridge University Press, Cambridge, U.K.

Kohlmeier, D., 2016. *Light acclimation in intertidal seagrass – spatial and diurnal variations and the role of suspended sediment*. PhD thesis, University of Bremen, Germany.

Komar, P.D., 1996. The budget of littoral sediments: Concepts and applications: *Shore and Beach*, 64(3): 18–26.

Kowalczuk, P., 1999. Seasonal variability of yellow substance absorption in the surface layer of the Baltic Sea. Journal of Geophysical Research, 104(C12): 30,047–30,058.

Kuo, A.Y. and Hayes, D.F., 1991. Model for turbidity plume induced by bucket dredge. *Journal of Waterway, Port, Coastal, and Ocean Engineering*, 117(6): 610–623.

Kuo, A.Y., Welch, C.S. and Lukens, R.J., 1985. Dredge induced turbidity plume model. *Journal of Waterway, Port, Coastal, and Ocean Engineering*, 111(3): 476–494.

Lee, R.W. and Rast, W., 1997. Light attenuation in a shallow, turbid reservoir, Lake Houston, Texas. Water-Resources Investigations Report 97–4064.

Lewis, R.R., 1976. Impact of dredging in the Tampa Bay estuary, 1876–1976. In: Pruitt, E.L. (ed.) *Time-stressed Coastal Environments: Assessment and Future Action*. The Coastal Society, Arlington, Virginia (USA), p. 31–55.

Longstaff, B.J., 2003. *Investigating into the light requirements of seagrass in northeast Australia*. PhD thesis, University of Queensland, Australia.

Longstaff, B.J., Loneragan, N.R., O'Donohue, M.J. and Dennison, W.C., 1999. Effects of light deprivation on the survival and recovery of the seagrass *Halophila ovalis* (R.Br.) Hook. *Journal of Experimental Marine Biology and Ecology*, 234(1): 1–27.

Lotze, H.K., Lenihan, H.S., Bourque ,B.J., Bradbury, R.H., Cooke, R.G., Kay, M.C., Kidwell, S.M., Kirby, M.X., Peterson, C.H., and Jackson, J.B.C., 2006. Depletion, degradation, and recovery potential of estuaries and coastal seas. *Science*, 312(5781): 1806–1809.

Luger, S.A., Schoonees, J.S., G P Mocke, G.P. and Smit, F., 1998. Predicting and evaluating turbidity caused by dredging in the environmentally sensitive Saldanha Bay. 26th International Conference on Coastal Engineering, Copenhagen, Denmark.

Lund-Hansen, L.C., 2004. Diffuse attenuation coefficients K_d(PAR) at the estuarine North Sea–Baltic Sea transition: time-series, partitioning, absorption, and scattering. *Estuarine, Coastal and Shelf Science*, 61: 251–259.

MacDonald, B.A., Bricelj, M. and Shumway, S.E., 2006. Physiology: Energy Acquisition and Utilisation. In Scallops: Biology, Ecology and Aquaculture. Shumway, S.E. and Parsons, G.J. (Eds.), Elsevier B.V., 417–489.

MacDonald, B.A., Bacon, G.S. and Ward, J.E., 1998. Physiological responses of infaunal (*Mya arenaria*) and epifaunal (*Placopecten magellanicus*) bivalves to variations in the concentration and quality of suspended particles II. Absorption efficiency and scope for growth. *Journal of Experimental Marine Biology and Ecology*, 219: 127–141.

Macdonald, R.K., Ridd, P.V., Whinney, J.C., Larcombe, P. and Neil, D.T., 2013. Towards environmental management of water turbidity within open coastal waters of the Great Barrier Reef. *Marine Pollution Bulletin*, 74: 82–94.

Mamat, N. Z, 2010. Nutrition and Broodstock Conditioning of the New Zealand Pipi, *Paphies australis*. Master of Applied Science, Auckland University of Technology, 133 pp.

Mamat, N.Z. and Alfaro, A.C., 2014. Evaluation of microalgal and formulated diets for the culture of the New Zealand pipi clam *Paphies australis*. *International Aquatic Research*, 6:2.

Marbà, N., Duarte, C.M., 1994. Growth response of the seagrass *Cymodocea nodosa* to experimental burial and erosion. *Marine Ecology Progress Series*, 107: 307–311.

Matheson, F. E., and Schwarz, A.-M., 2007. Growth responses of *Zostera capricorni* to estuarine sediment conditions. *Aquatic Botany,* 87: 299–306.

Matheson, F.E., Reed, J., Dos Santos, V.M., Mackay, G. and Cummings, V.J., 2017. Seagrass rehabilitation: successful transplants and evaluation of methods at different spatial scales. *New Zealand Journal of Marine and Freshwater Research*, 51(1): 96–1097.

Maxwell, P.S., Pitt, K.A., Burfeind, D.D., Olds, A.D., Babcock, R.C., and Connolly, R.M., 2014. Phenotypic plasticity promotes persistence following severe events: physiological and morphological responses of seagrass to flooding. *Journal of Ecology*, 102(1): 54–64.

MEMG, 2003. Group Co-ordinating Sea Disposal Monitoring. Final Report of the Dredging and Dredged Material Disposal Monitoring Task Team, Science Series Aquatic Environment Monitoring Report, CEFAS, Lowestoft, 55, p. 1–52.

Møhlenberg, F. and Riisgård, H.U., 1978. Efficiency of particle retention in 13 species of suspension feeding bivalves. *Ophelia*, 17: 239–246.

Navarro, E., Iglesias, J.I.P., Perez Camacho, A., Labarta, U. and Beiras, R., 1991. The physiological energetics of mussels (*Mytilus galloprovincialis* Lmk) from different cultivation rafts in the Ria de Arosa (Galicia, N.W. Spain). *Aquaculture*, 94: 197–212.

Navarro, E., Iglesias, J.I.P. and Ortega, M.M., 1992. Natural sediment as a food source for the cockle *Cerastoderma edule* (L.): effect of variable particle concentration on feeding, digestion and the scope for growth. *Journal of Experimental Marine Biology and Ecology*, 156: 69–87.

Navarro, E. and Iglesias, J.I.P., 1993. Infaunal filter-feeding bivalves and the physiological response to short-term fluctuations in food availability. In:

Dame, R.F. (Ed.). Bivalve filter feeders in estuarine and coastal ecosystem processes, Springer-Verlag, Berlin, 25–56.

Navarro, E., Iglesias, J.I.P., Ortega, M.M. and Larretxea, X., 1994. The basis for a functional response to variable food quantity and quality in cockles *Cerastoderma edule* (Bivalvia Cardiidae). *Physiological Zoology*, 67: 468-496.

Navarro, J. M. and Widdows, J., 1997. Feeding physiology of *Cerastoderma edule* in response to a wide range of seston concentrations. *Marine Ecology Progress Series*, 152: 175–186.

Netzband, A. and Adnitt, C., 2009. Dredging management practices for the environment: a structured selection approach. *Terra et Aqua*, 114: 3–8.

Newcombe, C.P. and MacDonald, D.D., 1991. Effects of Suspended Sediments on Aquatic Ecosystems. *North American Journal of Fisheries Management*, 11: 72–82.

Newell, C.R. and Shumway, S.E., 1993. Grazing of natural particulates by bivalve molluscs: a spatial and temporal perspective. In: Dame, R.F. (Ed.). Bivalve filter feeders in estuarine and coastal ecosystem processes, Springer-Verlag, Berlin, 85–148.

Newell, R.C., Seiderer, L.J. and Hitchcock, D.R., 1998. The impact of dredging works in coastal waters: a review of the sensitivity to disturbance and subsequent recovery of biological resources on the sea bed. *Oceanography and Marine Biology: an Annual Review*, 36: 127–78.

Newell, R.I.E., 2004. Ecosystem influences of natural and cultivated populations of suspension-feeding bivalve molluscs: a review. *Journal of Shellfish Research*, 23(1): 51–61.

Newell, R.I.E. and Koch, E.W., 2004. Modeling seagrass density and distribution in response to changes in turbidity stemming from bivalve filtration and seagrass sediment stabilization. *Estuaries*, 27(5): 793–806.

Nichols, M., Diaz, R.J. and Schaffner, L.C., 1990. Effects of hopper dredging and sediment dispersion, Chesapeake Bay. *Environmental Geology and Water Sciences*, 15(1): 31–43.

Nicholls, P., Hewitt, J. and Halliday, J., 2009. Effects of suspended sediment concentrations on suspension and deposit feeding marine macrofauna. Report prepared by NIWA for Auckland Regional Council. ARC Technical Report 2009/117.

Nightingale, B. and Simenstad, C.A., 2001. Dredging activities: marine issues. Technical Report WA–RD 507.1. Washington State Transportation Centre, Seattle, USA.

Norkko, A., Thrush, S.F., Hewitt, J.E., Cummings, V.J., Norkko, J., Ellis, J.I., Funnell, G.A., Schultz, D. and MacDonald, I., 2002. Smothering of estuarine sandflats by terrigenous clay: the role of wind-wave disturbance and bioturbation in site-dependent macrofaunal recovery. *Marine Ecology Progress Series*, 234: 23–41.

Norkko, J., Hewitt, J.E., Thrush, S.F., 2006. Effects of increased sedimentation on the physiology of two estuarine soft-sediment bivalves, *Austrovenus stutchburyi* and *Paphies australis*. *Journal of Experimental Marine Biology and Ecology*, 333: 12–26.

Norkko, J., Pilditch, C. A., Thrush, S. F. and Wells, R. M. G., 2005. Effects of food availability and hypoxia on bivalves: the value of using multiple parameters to measure bivalve condition in environmental studies. *Marine Ecology Progress Series*, 298: 205–218.

Onuf, C.P., 1994. Seagrasses, Dredging and Light in Laguna Madre, Texas, U.S.A. *Estuarine, Coastal and Shelf Science*, 39: 75–91.

Orpin, A.R., Ridd, P.V., Thomas, S., Anthony, K.R.N., Marshall, P. and Oliver, J., 2004. Natural turbidity variability and weather forecasts in risk management of anthropogenic sediment discharge near sensitive environments. *Marine Pollution Bulletin*, 49:602–612.

Orth, R.J., Carruthers, T.J.B., Dennison, W.C., Duarte, C.M., Fourqurean, J.W., Heck Jr., K.L., Hughes, A.R., Kendrick, G.A., Kenworthy, W.J., Olyarnik, S., Short, F.T., Waycott, M., And Williams, S.L., 2006. A Global Crisis for Seagrass Ecosystems. *BioScience*, 56(12): 987–996.

Park, S., 1998. Bay of Plenty coastal water quality 1996–1997. Environmental Report 98/5, Environment Bay of Plenty, New Zealand.

Park, S.G., 1999. Change in abundance of seagrass (*Zostera spp.*) in Tauranga Harbour from 1959–96. Environmental Report 99/30, Environment Bay of Plenty, New Zealand.

Park, S., 2004. Aspects of Mangrove Distribution and Abundance in Tauranga Harbour. Environmental Publication 2004/16, Environment Bay of Plenty, New Zealand.

Park, S., 2016. Extent of seagrass in the Bay of Plenty in 2011. Environmental publication 2016/03. Bay of Plenty Regional Council, New Zealand.

Pauly, D. and Christensen, V., 1995. Primary production required to sustain global fisheries. *Nature*, 374: 255–257.

Pedersen, T.M., Gallegos, C.L. and Nielsen, S.L., 2012. Influence of near-bottom re-suspended sediment on benthic light availability. *Estuarine, Coastal and Shelf Science*, 106: 93–101.

Pennekamp, J.G.S, Epskamp, R.J.C., Rosenbrand, W.F., Mullié, A., Wessel, G.L., Arts, T. and Deibel, I.K., 1996. Turbidity Caused by Dredging; Viewed in Perspective. *Terra et Aqua*, 64: 10–17.

Pfannkuche, J., 2002. Optical properties of the Otago Shelf waters: South Island New Zealand. *Estuarine, Coastal and Shelf Science*, 55: 613–627.

Port of Melbourne Corporation (PoMC), 2008. Turbidity-Detailed Design. CDP_ENV_MD_024 REV 2. Port of Melbourne Corporation, Melbourne, Victoria.

Port of Tauranga, 2013. Welcoming the future (Annual Report). Retrieved from http://www.port-tauranga.co.nz/.

186

Puckette, T.P., 1998. Evaluation of dredged material plumes—Physical monitoring techniques. DOER Technical Notes Collection (TN DOER-E5), U.S. Army Engineer Research and Development Center, Vicksburg, MS.

Ramli, A.Y., 2016. The Impact of Dredging on the Stability of the Matakana Banks Ebb-Tidal Delta. PhD Thesis, University of Waikato.

Reine, K. J., Clarke, D. G. and Dickerson, C., 2002. Acoustic characterization of suspended sediment plumes resulting from barge overflow. DOER Technical Notes Collection (ERDC TN-DOER-E15), U.S. Army Engineer Research and Development Center, Vicksburg, MS.

Ren, J.S., Ross, A.H., Schiel, D.R., 2000. Functional descriptions of feeding and energetics of the Pacific oyster *Crassostrea gigas* in New Zealand. *Marine Ecology Progress Series*, 208: 119–130.

Richmond, H.E., Hrabik, T.R. and Mensinger, A.F., 2004. Light intensity, prey detection and foraging mechanisms of age 0 year yellow perch. Journal of Fish Biology, 65: 195–205.

Ridley Thomas, W.N., Hale, R.E., and Land, J.M., 1998. Suspended sediment measurement in Hong Kong. *Hydro International*, 2(6): 61–63.

Robertson, B.M. and Stevens, L., 2012. Tasman Coast: Waimea Inlet to Kahurangi Point, habitat mapping, risk assessment and monitoring recommendations. Prepared for Tasman District Council. 167p.

Robins, P.E., Skov, M.W., Lewis, M.J., Gimenez, L., Davies, A.G., Malham, S.K., Neill, S.P., McDonald, J.E., Whitton, T.A., Jackson, S.E. and Jago, C.F., 2016. Impact of climate change on UK estuaries: A review of past trends and potential projections. *Estuarine, Coastal and Shelf Science*, 169: 119–135.

Ruiz, J.M. and Romero, J., 2003. Effects of disturbances caused by coastal constructions on spatial structure, growth dynamics and photosynthesis of the seagrass *Posidonia oceanica*. *Marine Pollution Bulletin*, 46(12): 1523–1533.

Ruiz-Frau, A., Gelcich, S., Hendriks, I.E., Duarte, C.M. and Marbà, N., 2017. Current state of seagrass ecosystem services: Research and policy integration. *Ocean & Coastal Management*, 149: 107–115.

Schaffner, L.C., Dellapenna, T.M., Hinchey, E.K., Friedrichs, C.T., Neubauer, M.T., Smith, M.E. and Kuehl, S.A., 2001. Physical energy regimes, seabed dynamics, and organism-sediment interactions along an estuarine gradient. In: J.Y. Aller et al. (eds.), *Organism-Sediment interactions*. USC Press, p. 161–182.

Scholes, P., 2015. NERMN Estuary Water Quality Report 2014. Environmental Publication 2015/01. Bay of Plenty Regional Council.

Schwarz, A–M., 2004. Contribution of photosynthetic gains during tidal emersion to production of Zostera capricorni in a North Island, New Zealand estuary. *New Zealand Journal of Marine and Freshwater Research*, 38: 809–818.

Schwarz, A–M., Morrison, M., Hawes, I. and Halliday, J., 2006. Physical and biological characteristics of a rare marine habitat: sub-tidal seagrass beds of offshore islands. *Science for Conservation*, 269.

Seo, J.Y., Ha, H.K, Im, J., Hwang, J.H., Choi, S.M., Won, N-I, Kim, Y., 2018. Impact of seasonal vertical stratification on the dispersion patterns of dredging plumes off the south coast of Korea. *Marine Geology*, 395: 14–21.

Shao, D., Purnama, A. and Sun, T., 2015. Modeling the Temporal Evolution of Dredging-Induced Turbidity in the Far Field. *Journal of Waterway, Port, Coastal, and Ocean Engineering*, 10.1061/(ASCE)WW.1943-5460.0000295.

Sheahan, D., Maud, J., Wither, A., Moffat, C. and Engelke, C., 2013. Impacts of climate change on pollution (estuarine and coastal). *Marine Climate Change Impacts Partnership: Science Review*, 244–251.

Short, F.T., Coles, R., Fortes, M.D., Victor, S., Salik, M., Isnain, I., Andrew, J. and Seno, A., 2014. Monitoring in the Western Pacific region shows evidence of seagrass decline in line with global trends. *Marine Pollution Bulletin*, 83: 408–416.

Short, F.T., Polidoro, B., Livingstone, S.R., Carpenter, K.E., Bandeira, S., Bujang, J.S., Calumpong, H.P., Carruthers, T.J.B., Coles, R.G., Dennison, W.C., Erftemeijer, P.L.A., Fortes, M.D., Freeman, A.S., Jagtap, T.G., Kamal, A.H.M., Kendrick, G.A., Kenworthy, W.J., La Nafie, Y.A., Nasution, I.M., Orth, R.J., Prathep, A., Sanciangco, J.C., van Tussenbroek, B., Vergara, S.G., Waycott, M. and Zieman, J.C., 2011. Extinction risk assessment of the world's seagrass species. *Biological Conservation*, 144: 1961–1971.

Sieburth, J.McN. and Jensen, A., 1968. Studies on algal substances in the sea. I. Gelbstoff (humic material) in terrestrial and marine waters. *Journal of Experimental Marine Biology and Ecology*, 2: 174–189.

Silva, J., Barrote, I., Costa, M.M., Albano, S., and Santos, R., 2013. Physiological responses of *Zostera marina* and *Cymodocea nodosa* to light-limitation stress. *PLoS ONE*, 8(11): e81058.

Sinner, J., Clark, D., Ellis, J., Roberts, B., Jiang, W., Goodwin, E., Hale, L., Rolleston, S., Patterson, M., Hardy, D., Prouse, E. and Brown, S., 2011. Health of Te Awanui Tauranga Harbour. Manaaki Taha Moana Research Report No. 1; Cawthron Report No.1969.

Smaal, A.C. and Prins, T.C., 1993. The uptake of organic matter and the release of nutrients by bivalve suspension feeder beds. In: Dame, R.F. (Ed.). Bivalve filter feeders in estuarine and coastal ecosystem processes, Springer-Verlag, Berlin, 271–298.

Smith, J.E. and Friedrichs, C., 2011. Size and settling velocities of cohesive flocs and suspended sediment aggregates in a trailing suction hopper dredge plume. *Continental Shelf Research*, 31(10): S50–S63.

Smith, G.G., Weitz, N., Soltau, C., Viljoen, A., Luger, S. and Maartens, L., 2008. Fate of fine sediment from dredger-based mining in a wave-dominated environment at Chameis Bay, Namibia. *Journal of Coastal Research*, 24(1): 232–247.

Sofonia, J.J. and Unsworth, R.K.F., 2009. Development of water quality thresholds during dredging for the protection of benthic primary producer habitats. *Journal of Environmental Monitoring*, 12: 159–163.

Storlazzi, C.D., Norris, B.K., and Rosenberger, K.J., 2015. The influence of grain size, grain color, and suspended-sediment concentration on light attenuation: Why fine-grained terrestrial sediment is bad for coral reef ecosystems. *Coral Reefs*, DOI 10.1007/s00338-015-1268-0

Strickland J.D.H. and Parsons, T.R., 1972. *A practical handbook of seawater analysis*. Fisheries Research Board of Canada, Ottawa, Canada.

Sutherland, J., Peet, A.H. and Soulsby, R.L., 2004. Evaluating the performance of morphological models. *Coastal Engineering*, 51(8–9): 917–939.

Syvitski, J.P.M., Vörösmarty, C.J., Kettner, A.J. and Green, P., 2005. Impacts of humans on the flux of terrestrial sediment to the global coastal ocean. Science, 308: 376–380.

Tay, H.W., Bryan, K.R., Pilditch, C.A., Park, S. and Hamilton, D., 2012. Variations in nutrient concentrations at different time scales in two shallow tidally dominated estuaries. *Marine and Freshwater Research*, 63: 95–109.

Tay, H.W., Bryan, K.R., de Lange, W.P. and Pilditch, C.A., 2013. The hydrodynamics of the southern basin of Tauranga Harbour. *New Zealand Journal of Marine and Freshwater Research*, 47(2): 249–274.

Teaioro, I., 1999. The Effects of Turbidity on Suspension Feeding Bivalves. Master Thesis in Biological Science. University of Waikato. Hamilton, New Zealand.

Thrush, S.F., Hewitt, J.E., Cummings, V.J., Ellis, J.I., Hatton, C., Lohrer, A. and Norkko, A., 2004. Muddy waters: elevating sediment input to coastal and estuarine habitats. *Frontiers in Ecology and the Environment*, 2(6): 299–306.

Tian, F., Healy, T.R. and Davies-Colley, R.J., 1994. Light absorption by yellow substance in storm runoff from log handling area at a timber export port, Tauranga, New Zealand. *Journal of Coastal Research*, 10(4): 803–808.

Tubman, M.W. and Corson, W.D., 2000. Acoustic monitoring of dredging-related suspended-sediment plumes. DOER Technical Notes Collection (ERDC TN-DOER-E7), U.S. Army Engineer Research and Development Center, Vicksburg, MS.

Turner S.J. and Schwarz A.M., 2006. Management and conservation of seagrass in New Zealand: an introduction. *Science for Conservation*, 264.

Udelhoven, T. and Symader, W., 1995. Particle characteristics and their significance in the identification of suspended sediment sources. Tracer Technologies/or Hydrological Systems (Proceedings of a Boulder Symposium, July 1995). IAHS Publ. no. 229.

Urrutia, M.B., Iglesias, J.I.P. and Navarro, E., 1997. Feeding behaviour of *Cerastoderma edule* in a turbid environment: physiological adaptations and derived benefit. *Hydrobiologia*, 355: 173–180.

van Maren, D.S., van Kessel, T., Cronin, K. and Sittoni, L., 2015. The impact of channel deepening and dredging on estuarine sediment concentration. *Continental Shelf Research*, 95:1–14.

van Raalte, G., Dirks, W., Minns, T., van Dalfsen, J., Erftemeijer, P., Aarninkhof, S. and Otter, H., 2007. Building with nature: creating sustainable solutions for marine and inland water constructions. New research initiative towards a Centre of Excellence. Proceedings of the 18th World Dredging Congress (WODCON XVIII), Florida, USA, p. 637–648.

Vant, W.N., 1990. Causes of light attenuation in nine New Zealand estuaries. *Estuarine, Coastal and Shelf Science*, 31: 125–137.

Vlasblom, W.J., 2007. Trailing suction hopper dredger. In: Designing Dredging Equipment, wb3408B. pp.109.

Watson, H.M., 2016. Potential impacts of wharf extensions on the hydrodynamics of Stella Passage and upstream regions of Tauranga Harbour, New Zealand. MSc Thesis, University of Waikato.

Waycott, M., Longstaff, B.J., and Mellors, J., 2005. Seagrass population dynamics and water quality in the Great Barrier Reef region: a review and future research directions. Marine Pollution Bulletin, 51: 343–350.

Waycott, M., Duarte, C.M., Carruthers, T.J.B., Orth, R.J., Dennison, W.C., Olyarnik, S., Calladine, A., Fourqurean, J.W., Heck, Jr., K.L., Hughes, A.R., Kendrick, G.A., Kenworthy, W.J., Short, F.T. and Williams, S.L., 2009. Accelerating loss of seagrasses across the globe threatens coastal ecosystems. *Proceedings of the National Academy of Science*, 106(30): 12377–12381.

Wentworth, C.K., 1922. A scale of grade and class terms of clastic sediments. *Journal of Geology*, 30: 377–392.

Wheatcroft, R., Sommerfield, C., Drake, D., Borgeld, J., and Nittrouer, C., 1997. Rapid and widespread dispersal of flood sediment on the northern California margin. *Geology*, 25: 163–166.

Whitehead, P.G., Wilby, R.L., Battarbee, R.W., Kernan, M. and Wade, A.J., 2009. A review of the potential impacts of climate change on surface water quality. *Hydrological Sciences–Journal–des Sciences Hydrologiques*, 54(1): 101–123.

Wilber, D.H. and Clark, D.G., 2001. Biological effects of suspended sediments: a review of suspended sediment impacts on fish and shellfish with relation to dredging activities in estuaries. *North American Journal of Fisheries Management*, 21(4): 855–875.

Wilber, D.H., Brostoff, W., Clarke, D.G. and Ray, G.L., 2005. Sedimentation: Potential biological effects from dredging operations in estuarine and marine environments. DOER Technical Notes Collection (ERDC TNDOER-E20), U.S. Army Engineer Research and Development Center, Vicksburg, MS.

Wong, W.H., Cheung, S.G., 1999. Feeding behaviour of the green mussel, *Perna viridis* (L.): Responses to variation in seston quantity and quality. *Journal of Experimental Marine Biology and Ecology*, 236: 191–207.

Wong, W.H., Cheung, S.G., 2001. Feeding rhythms of the green-lipped mussel, *Perna viridis* (Linnaeus, 1758) (Bivalvia: Mytilidae) during spring and neap tidal cycles. *Journal of Experimental Marine Biology and Ecology*, 257: 13–36.

Woodin, S.A., Wethey, D.S., Hewitt, J.E. and Thrush, S.F., 2012. Small scale terrestrial clay deposits on intertidal sandflats: Behavioral changes and productivity reduction. *Journal of Experimental Marine Biology and Ecology*, 413: 184–191.

Wu, G.F., de Leeuw, J., Skidmore, A.K., Prins, H.H.T. and Liu, Y.L., 2007. Concurrent monitoring of vessels and water turbidity enhances the strength of evidence in remotely sensed dredging impact assessment. *Water Research*, 41(15): 3271–3280.